Meiotic prophase regulation and achiasmate chromosome segregation in *Caenorhabditis elegans*

By

Christina Marie Glazier

A dissertation submitted in partial satisfaction of

the requirements for the degree of

Doctor of Philosophy

in

Molecular and Cell Biology

in the

Graduate Division

of the

University of California, Berkeley

Committee in Charge:

Professor Abby Dernburg, Chair
Professor Georjana Barnes
Professor Rebecca Heald
Professor Marvalee Wake

Spring 2015

Abstract

Meiotic prophase regulation and achiasmate chromosome segregation in *Caenorhabditis elegans*

by

Christina Marie Glazier

Doctor of Philosophy in Molecular and Cell Biology

University of California, Berkeley

Professor Abby Dernburg, Chair

Meiosis is the specialized cell division by which sexually reproducing organisms produce haploid gametes. In order to reduce the chromosome complement by half, chromosomes must undergo pairing, synapsis, and crossover formation, followed by two rounds of chromosome division. All of these mechanisms depend on the proper establishment, maintenance, and remodeling of sister chromatid cohesion. Sister chromatid cohesion is mediated by cohesin complexes, which associate with newly replicated sister chromatids. Cohesion is required for all major aspects of meiosis: formation of the synaptonemal complex, induction of DNA double-strand breaks, and the repair of breaks to form crossovers, in addition to the regulated release of cohesion to enable segregation. During meiosis, cohesin complexes incorporate specialized subunits and are subject to different regulation, compared to mitotically dividing cells. The functions and regulation of cohesion during meiosis remain poorly characterized, and a major goal of my thesis work has been to address these important questions.

Wapl is a widely conserved regulator of cohesin. It has been implicated in antagonizing the association of cohesin complexes with DNA to facilitate cohesin removal during mitosis. However, its role in meiotic chromosome dynamics has not been investigated in any detail. To better understand the roles and regulation of sister chromatid cohesion in meiosis, I have focused on the *Caenorhabditis elegans* Wapl homolog, WAPL-1. I found that *C. elegans* WAPL-1 promotes faithful mitotic chromosome segregation, as in other organisms. I also found that WAPL-1 affects cohesin dynamics during meiosis, contributes to DNA double-strand break repair, and is regulated by the meiosis-specific kinase, CHK-2.

A second component of my thesis work examines the behavior of achiasmate chromosomes during meiosis. When early meiotic events fail to establish the requisite crossovers, the resulting achiasmate chromosomes often missegregate, or nondisjoin. Chromosome nondisjunction can result in aneuploid gametes, which has disastrous consequences for the developing embryo. To accurately detect autosomal nondisjunction in single embryos, I developed a *f*ragment *l*ength *p*olymorphism (FLP) assay. I used this approach to analyze chromosome segregation in oocyte meiosis in wildtype animals at different ages, and in mutants with elevated frequencies of achiasmate chromosomes. I found that nondisjunction occurred asymmetrically, yielding a higher frequency of monosomic than trisomic embryos. I also found evidence that germline apoptosis protects *C. elegans* hermaphrodites from increased nondisjunction as they age. Together, the results of these studies further illuminate meiotic prophase regulation and achiasmate chromosome segregation.

.

Dedicated to those who imparted on me
four pieces of advice
required for the successful completion of this dissertation.

To my father,
who, through his own actions and
stories of my Nana and Papa,
reminds me to work hard.

To my mother,
who teaches me to stand up for others,
as well as myself.

To my sweet brother,
who reminds me to be kind.

And to my Lola and Lolo,
who taught me that happiness is sadness.

Table of Contents

List of Tables

List of Figures

Acknowledgements

I would like to thank all past and present members of the Dernburg Lab, including Yumi Kim, Ofer Rog, Nora Kostow, Baris Avsaroglu, Keith Cheveralls, Hoang Pham, Simone Kohler, Liangyu Zhang, Josh Bayes, Gilbert Garcia, Clara Wang, Jilian Cabornay, Christina Whittle, Chitra Kotwaliwale, Andrea Dose, Jonathan Debebe, Dinara Azimova, Daniel He, Regina Rillo, Nicola Harper, Dave Wynne, Jacqueline Chretin, Roshni Kasad, and Aya Sato.

I would like to give a special thanks to Yumi Kim, Nora Kostow and Simone Kohler for specific help with the WAPL-1 project. Simone Kohler helped with image analysis by Fiji and RNA-seq analysis of *wapl-1*. Nora Kostow constructed the *gfp:wapl-1* strain using CRISPR/Cas9, aided in the purification of recombinant WAPL-1, and took part in many helpful conversations about the WAPL-1 project. Yumi Kim purified active CHK-2 kinase, trained me using radiation for the *in vitro* kinase assay, and was also part of countless conversations about WAPL-1 and CHK-2. I would like to give additional thanks to Ofer Rog and Keith Cheveralls for training and advice concerning use of the spinning-disc confocal microscope.

For use of their LI-COR imager and helpful comments on the project, I would like to thank Gloria Brar, Elçin Ünal, and the Brünal lab. For the mass spectrometry analysis, I would like to thank Lori Kohlstaedt, Nathalie Quintero, and the Vincent J. Coates Proteomics/Mass Spectrometry Laboratory. For helpful conversations about Wapl, I would like to thank Vinny Guacci, Thomas Eng, and the Koshland Lab. For reagents, helpful advice concerning the FLP project, and help with the irradiator, I would like to thank Aaron Severson, Ed Ralston, and the Meyer Lab.

Thanks to Abby Dernburg for her mentorship, training, and support over the past five years. To my thesis and qualifying exam committee members, Georjana Barnes, Rebecca Heald, Marvalee Wake, Doug Koshland, and Rachel Brem, thank you all for your comments and advice.

I would also like to thank Thomas Burke of the Portnoy Lab. As my classmate in the Molecular and Cell Biology department, he aided me in the use of the LI-COR imager for visualization of Western blots, immunoprecipitation methodology, Adobe Illustrator, problems arising in PCR and cloning, protein purification protocols, preparation of samples for mass spectrometry and reagents. As my partner for the past four years, Thomas brought me many laughs, much comfort, and a great deal of motivation. Between Triple Rock, Barker Lawn, the Joy of Cooking, Cal sports, the A's, the big hill(s), softball, kickball, starting cultures at midnight, camping, morning walks to work, River, case studies, 290s, karaoke, and all of his scientific help in the completion of this dissertation, graduate school would not have been nearly as productive or enjoyable without him. Well, possibly as productive, but not nearly as much fun.

Chapter 1: Introduction

1.1 Meiosis, a specialized cell division

Meiosis is the specialized cell division by which sexually reproducing organisms produce haploid gametes. During mitosis, cells divide and produce daughter cells containing the same number of chromosomes as the mother cell. Additionally, the genetic information in the daughter cells will be identical in sequence to the mother cell since mitosis segregates exact copies of its chromosomes. Meiosis is fundamentally different in that this process halves the number of chromosomes in the resulting cells, known as gametes. The reduction of chromosome number is necessary so that upon fertilization, or gamete fusion, diploidy will be restored in the resulting progeny (Figure 1.1a). Proper meiosis is absolutely essential for the propagation of a species, the inheritance of genetic information through generations, and the developmental success of an individual.

The meiotic program is a series of complex and specialized steps that result in the production of haploid gametes. First, meiosis is preceded by S phase, during which chromosomes replicate and sister chromatid cohesion is initially established. Sister chromatid cohesion in both mitosis and meiosis is mediated by the cohesin complex, although these two different cell division programs show differences in cohesin components and regulation of cohesion. Upon completing replication, chromosomes enter meiotic prophase, a prolonged G2-like period, during which chromosomes must pair, synapse, and undergo crossover formation. The first stage of meiotic prophase is leptotene, where homologous chromosomes must find each other and pair. During the second stage, zygotene, synapsis stabilizes the association of homologous chromosomes. This is mediated by formation of the synaptonemal complex, a proteinaceous structure. Proper pairing and synapsis enable crossover recombination to occur between homologous chromosomes, which is completed during the stage of meiotic prophase known as pachytene. Crossover recombination begins with the induction of programmed DNA double-strand breaks (DSBs). These DSBs can then be repaired using the nearby homolog as a template, leading to “simple” gene conversions and crossovers. These homologous recombination events have two primary benefits. The first is that they mix information between the maternal and paternal copies of each chromosome. Thus, they produce “recombinant” chromosomes that give rise to genetic diversity among the progeny. In addition, crossover recombination is necessary for meiosis because it creates physical links between homologs called chiasmata, which allow homologs to bi-orient on the meiotic spindle. During the fourth stage of meiotic prophase, diplotene, chromosomes begin to condense and the synaptonemal complex relocalizes or disappears. In the final step, diakinesis, chromosomes condense in preparation to undergo the meiotic chromosome segregations (Figure 1.1b).

After pairing, synapsis, and crossover recombination take place during meiotic prophase, the cell enters the first division, during which homologs segregate away from one another. This reductional division is called Meiosis I. In metazoans, the nuclear envelope is disassembled. Homologs bi-orient on the bipolar microtubule spindle, meaning that one homolog attaches to one pole and its partner attaches to the opposite pole. During anaphase I, the cohesion between homologous chromosomes is released and they segregate away from one another. Chromosomes

then undergo the second meiotic division, known as Meiosis II. In this division, sister chromatids attach to opposite poles of the meiotic spindle and segregate away from one another, similar to a mitotic division (Figure 1.2a).

During oocyte meiosis, following Meiosis I, one of the two daughter nuclei is extruded through the membrane surrounding the egg to form an inert "polar body", while the other daughter nucleus undergoes the second division. Only one of these products forms a nucleus that will be inherited, known as the female pronucleus, and the other is also extruded to form the second polar body. During spermatogenesis, both products of Meiosis I undergo a second division, leading to the production of four gametes.The single female meiotic product is referred to as an egg. Male gametes mature to form sperm. Sperm are motile and contain very little besides one copy of the genome and protein complexes called centrosomes, which are required for subsequent mitotic divisions. In mammalian females, fertilization of the egg by sperm takes place at metaphase II. In humans, since Meiosis I take place during fetal development *in utero* and fertilization might take place in a woman's 20s or 30s, it can be decades before an egg finally completes meiosis. In males, the entire meiotic program takes place to produce sperm, which only then can go on to fertilize an egg. Male and female meiosis differs in other ways as well. For example, in males, one meiosis produces four haploid gametes. In females, however, one meiosis produces only a single gamete. The production of a single gamete by one meiosis is due to polar bodies. During both female meiotic segregations, half of the chromatin segregates not into another cell, but into a small, cell-like structure called a polar body. These polar bodies do not go on to develop any further. As a result, female meiosis produces a single gamete.

Meiosis continues to be investigated due to its key role in sexual reproduction, its dynamic and specialized nature, and its significance in evolution. Here, we will probe further into two different aspects of meiosis. First, we will explore the events that must take place during meiotic prophase to ensure proper chromosome segregation. Second, we will examine what happens when chromosome segregation is perturbed. Through the study of these two aspects of meiosis, a broader understanding of meiosis will be reached.

1.2 Early meiotic processes ensure proper chromosome segregation

Proper meiotic chromosome segregation is vital for embryonic development, the perpetuation of a species, and the introduction of genetic diversity into a population. In order to ensure that chromosomes segregate properly during Meiosis I and II, a number of biological processes must take place. These processes include the loading and establishment of sister chromatid cohesion, the pairing of homologous chromosomes, the physical association of homologous chromosomes through synapsis, and the formation of chiasmata between homologous chromosomes by crossover recombination (Figure 1.1B).

Sister chromatid cohesion

Sister chromatid cohesion is the biological process by which newly replicated sister chromatids are held together during mitosis and meiosis. Sister chromatid cohesion is essential for the proper segregation of chromosomes in both mitosis and meiosis. During mitosis, sister chromatid cohesion holds sister chromatids together as they bi-orient on the mitotic spindle.

Sister chromatid cohesion is then removed so that sister chromatids can separate. During meiosis, sister chromatid cohesion is required to hold sister chromatids together and to mediate chiasmata. Due to the two meiotic segregation steps, sister chromatid cohesion must be removed in a two-step process. During Meiosis I, sister chromatid cohesion between homologous chromosomes and/or at chiasmata must be removed. At Meiosis II, sister chromatid cohesion between sister chromatids is removed in a division similar to mitosis. As a result, sister chromatid cohesion is essential for proper chromosome segregation in both mitosis and meiosis (reviewed in Marston, 2014; Nasmyth and Haering, 2005; Onn et al., 2008; Peters et al., 2008).

In addition to holding sister chromatids, sister chromatid cohesion has been implicated in post-replicative repair of DNA double-strand breaks (DSBs). In budding yeast, cohesin mutants display defects in DNA DSB repair. Also, *S. pombe* Scc1 and *S. cerevisiae* Wapl were first identified in yeast screens to identify mutants hypersensitive to DNA damage (Birkenbihl and Subramani, 1992; Game et al., 2003; Sjogren and Nasmyth, 2001). It is also known that new cohesion is generated following DNA damage and that cohesin subunits are phosphorylated in response to DNA damage (Strom et al., 2007; Unal et al., 2007) (reviewed in Peters et al., 2008). It is still unclear the molecular mechanism underlying how cohesin functions in DNA DSB repair, whether cohesin functions to direct repair off of the homolog during meiosis, or whether cohesin subunits interact with other repair machinery proteins.

Given the importance of sister chromatid cohesion, much research has been done to understand the proteins underlying the process. The highly conserved cohesin complex mediates sister chromatid cohesion. The cohesin complex is a tripartite ring structure. It is made up of two structural maintenance of chromosome (Smc) proteins, SMC-1 (Smc1) and SMC-3 (Smc3) (Larionov et al., 1985; Michaelis et al., 1997). Smc proteins fold over onto themselves, forming an ATP-binding head domain through interaction of the N- and C-terminals. Anti-parallel coiled coil domains then lead to the hinge domain. The hinge domain allows for dimerization between Smc proteins. In the cohesin complex, Smc1 and Smc3 interact at their hinge domains forming a V-shape. A third cohesin subunit, the kleisin, binds the ATPase domains of Smc1 and Smc3, thus completing the tripartite ring structure (Guacci et al., 1997).

The kleisin family of proteins include a number of different classes, and it is the α-kleisin class that binds to the Smc1/Smc3 heterodimer to form the cohesin complex. Within the α-kleisin class, a number of further specialized proteins exist. During mitosis, the α-kleisin Rad21/Scc1/Mcd1 binds to Smc1 and Smc3. During meiosis, it is the α-kleisin Rec8 that binds to Smc1 and Smc3. Interestingly, more recent studies have described additional α-kleisins in higher eukaryotes that bind to Smc1 and Smc3 and facilitate specialized roles for the cohesin complex (Watanabe and Nurse, 1999) (reviewed in Stoop-Myer and Amon, 1999). In Arabidopsis, for example, SYN3 was characterized as a second meiotic kleisin that is required for normal synapsis (Yuan et al., 2012). In vertebrates, the α-kleisin Rad21L was found to be specifically expressed in meiotic cells, localized to chromosomes from leptotene to mid-pachytene, and thought to be involved in synapsis initiation and crossover recombination (Gutierrez-Caballero et al., 2011; Lee and Hirano, 2011).

In conclusion, sister chromatid cohesion is a conserved biological process that is essential during mitosis and meiosis. Sister chromatid cohesion is mediated through the cohesin complex and its associated proteins. The cohesin complex functions in holding sister chromatids together during mitosis and meiosis, mediating crossovers during meiosis, and is implicated in the repair of DNA DSBs.

Sister chromatid cohesion in *C. elegans*

Investigation into the *C. elegans* cohesin homologs has revealed a conserved function for the cohesin complex in the nematode. *C. elegans* appears to be similar to higher eukaryotes in that it possesses a number of α-kleisins. In *C. elegans,* SCC-1, COH-1, REC-8, COH-3 were identified as α-kleisins based on their sequence similarity to Rad21. Based on localization and characterization after protein depletion, SCC-1 and COH-1 were first classified as mitotic α-kleisins and REC-8 and COH-3 as meiotic α-kleisins (Pasierbek et al., 2001). A few years later, a paralog of COH-3 was identified and named COH-4. Due to the fact that COH-3 and COH-4 act redundantly and share high sequence similarity, they are often referred to as COH-3/4. Similar to what has been seen in other higher eukaryotes, recent studies have demonstrated that REC-8 and COH-3/4 have specialized functions and regulation during meiosis. For example, during diakinesis when homologous chromosomes have condensed around the chiasma, COH-3/4 is localized at the short axis and REC-8 is localized to the long axis. This led to a model in which COH-3/4 cohesin complexes are removed at Meiosis I to allow homologous chromosome to segregate, followed by the disassociation of REC-8 at Meiosis II to allow sister chromatids to segregate (Severson et al., 2009; Severson and Meyer, 2014).

It also appears that cohesin complexes containing COH-3/4 are regulated differently than cohesin complexes containing REC-8. In the germline, immunofluorescence shows REC-8 localization through the germline, including the mitotic zone, while COH-3/4 does not appear until meiotic entry. This suggested that COH-3/4 and REC-8 experience differential temporal regulation.

COH-3/4 and REC-8 were also assayed for localization and cohesiveness in the germline. Loading of COH-3/4 onto meiotic chromosome axes was dependent on the meiosis-specific kinase CHK-2, but REC-8 localization was independent of CHK-2. Cohesiveness of COH-3/4, but not REC-8, required programmed DNA DSBs and the DNA damage kinases ATM/ATR. Additionally, the loading of REC-8 onto meiotic chromosome axes was contingent on the axial element protein HTP-3, but not the loading of COH-3/4. Interestingly, while REC-8 and COH-3/4 appear to have specialized functions and differential regulation, they do act somewhat redundantly to hold chromosomes together. The loss of both REC-8 and COH-3/4 is required for complete loss of cohesion and the visualization of ~24 DAPI-staining bodies at diakinesis. In either a *rec-8* or *coh-4coh-3* mutant, 12 DAPI-staining bodies can be visualized suggesting that sister chromatids are still being held together (Severson et al., 2009; Severson and Meyer, 2014). Taken together, COH-3/4 localization, axis loading, and cohesiveness is regulated differently than REC-8.

Although SCC-1 and COH-1 were first characterized as mitotic α-kleisins, a recent investigation of SCC-1 suggested that SCC-1 may play a role during meiotic prophase. When sister chromatid cohesion was assayed during pachytene for separation of sister chromatids in meiotic α-kleisin triple mutants (*rec-8;coh-4coh-3*), sister chromatids were held together in 45% of nuclei. This means that meiotic cohesion was mediated by cohesin complexes containing a non-meiotic α-kleisin. Indeed, when SCC-1 was depleted from meiotic α-kleisin triple mutants, sisters were held together in only 12% of nuclei (Severson and Meyer, 2014). This suggested that either SCC-1 functions during meiosis or that SCC-1 can substitute as the α-kleisin in the absence of the meiotic α-kleisins. A similar phenotype for the mitotic α-kleisin has been seen in budding yeast. In budding yeast, persistent sister chromatid cohesion has been shown to be

dependent on Rad21/Scc1, suggesting that the mitotic α-kleisin may play a role during meiosis (Yokobayashi et al., 2003).

While research has demonstrated that SCC-1, REC-8 and COH-3/4 have different functions and regulation, much is still unknown about how such similar proteins can be regulated differently and perform different functions. In *C. elegans*, the gonad contains a zone of mitotically proliferating nuclei that populates the gonad. Presumably, the mitotic α-kleisins SCC-1 and COH-1 act here. At the mitosis-to-meiosis transition, where nuclei stop mitotically proliferating and start the meiotic program, the meiotic α-kleisins REC-8 and COH-3/4 must load and establish cohesion, each through a different regulatory mechanism. It is currently unknown how the mitotic α-kleisins are regulated at the mitosis-to-meiosis transition and the different regulatory pathways governing the meiotic α-kleisins, REC-8 and COH-3/4.

Sister chromatid cohesion is absolutely vital for human health and human reproduction. Defects in the proteins that mediate sister chromatid cohesion are implicated in cancers and responsible for chromosomal disorders like Cornelia de Lange Syndrome and Roberts Syndrome. In the case of Roberts Syndrome, development of bilateral symmetry, the head, and limbs can be severely stunted. As a result, mortality is high among those affected by Roberts Syndrome (Deardorff et al., 1993; Losada, 2014; Vega et al., 2005). Defects in sister chromatid cohesion during meiosis causes chromosome missegregation (described in its own section), which negatively affects fertility and embryonic development. By investigating the mechanisms, functions, and regulation of sister chromatid cohesion, we will be better suited to treat and prevent such afflictions.

Wapl antagonizes sister chromatid cohesion

In addition to proteins making up the cohesin tripartite ring, a number cohesin and cohesin-associated proteins are required for the loading and maintenance of sister chromatid cohesion. The α-kleisin binds to the fourth and last cohesin core component. In yeast, this protein is called Scc3 and in vertebrates it the stromal antigen (SA) protein. In higher eukaryotes, there are three characterized stromal antigen proteins. SA1 and SA2 act during mitosis, while SA3 acts during meiosis (Hopkins et al., 2014). The α-kleisin and SA proteins associate with additional, cohesin-associated proteins, including Pds5 (Marston, 2014; Peters et al., 2008). In 2006, Jan-Michael Peters' lab identified a protein in a human cohesin immunoprecipitation previously unidentified as a cohesin-associated protein. This protein was named Wapl and found to interact with Pds5, the α-kleisin, and SA-1/2 (Kueng et al., 2006).

Wapl was originally named in humans due to its homology to the *Drosophila w*ings *ap*art-*l*ike protein (Oikawa et al., 2004). In *Drosophila,* like in mice, Wapl is required for viability. Characterization of the *wapl* mutants found that they suffered late larval lethality and abnormal chromosome morphology. Characterization of the *wapl* mutant found that *wapl* functions in chromatin morphology. In metaphase spreads of *wapl* mutants, rather than chromosomes displaying the normal X- or V-shaped morphology, sister chromatids appeared H-shaped, with sister chromatids aligned parallel to one another. Additionally, while the fourth chromosome normally appeared as just one dot, it appeared as two distinct dots in the *wapl* mutant. The authors concluded that *wapl* functioned to hold sister chromatids together, specifically within heterochromatic regions (Verni et al., 2000).

In human cells, Kueng *et al.* showed that Wapl specifically interacts with the cohesin complex and controls the dynamicity of the cohesin complex on chromosomes. Research has shown that Wapl interacts with cohesin through interaction with the α-kleisin SCC-1 and the cohesin-associated SA1/SA2 proteins. Wapl is present in nuclei from telophase until the next mitotic prophase. During interphase, Wapl protein is present in nuclei and tightly associated with chromatin, as determined by the fact that Wapl protein is insensitive to extraction by detergent. During interphase, Wapl antagonizes the loading of mitotic cohesin complexes onto chromatin. In the absence of Wapl during interphase, chromatin appears more condensed, cohesin complex loading onto chromatin is increased, and cohesin association with chromatin is less dynamic. During mitotic prophase, Wapl protein is still present, but is sensitive to extraction by detergent, suggesting a weaker association with chromatin. During mitotic prophase and metaphase, Wapl acts to antagonize cohesin complexes and disassociates these complexes from chromosomes. In mammals, the bulk of cohesion is removed from chromosome arms during prophase in the so-called "prophase pathway", a process that is now known to be mediated by Wapl (Gandhi et al., 2006; Kueng et al., 2006; Tedeschi et al., 2013).

The discovery of Wapl as a cohesin-associated protein and antagonist of sister chromatid cohesion in humans helped illuminate the role of Wapl in other organisms. In budding yeast, loss of the Wapl homolog Wpl1, originally named Rad61 due to its sensitivity to irradiation, was found to suppress the lethality of the essential protein, Eco1 (Ctf7) (Rowland et al., 2009; Sutani et al., 2009). Eco1 is an acetyltransferase that is not required for the loading of cohesin onto chromosomes, but is required to generate cohesion. Wapl's function in mammalian cells led to a model in which Eco1 counteracts the cohesion-destabilizing activity of Wpl1. Studies using FRAP to measure cohesin dynamicity showed that Wpl1 does promote turnover of cohesin on chromosomes and that this cohesin dynamicity is counteracted by Eco1. Strangely, budding yeast without Wpl1 display cohesion defects and reduced levels of cohesin on chromosomes. It is currently unclear why this is, but it is suspected that it might be due to overall lower levels of nuclear cohesin (Chan et al., 2012; Lopez-Serra et al., 2013).

While recent studies have provided a better understanding of Wapl's regulation in these organisms, much is still unknown. In mammals, Wapl must be at least partially inhibited after DNA replication to allow for cohesin to become more stably associated with chromatin. Upon DNA replication and acetylation of Smc3, a protein called Sororin becomes recruited to chromatin-bound cohesin complexes. Sororin then displaces Wapl from its association with the cohesin complex, thus allowing cohesin to become more stably associated with chromatin (Nishiyama et al., 2010). During mitotic prophase, Wapl must be activated in order to remove the bulk of cohesin from chromosome arms during the "prophase pathway". In mammalian cells, phosphorylated Sororin cannot dissociate Wapl from cohesin complexes. Additionally, Sororin is phosphorylated in a Cyclin-dependent kinase 1 (Cdk1)- and Aurora B-dependent manner during mitosis of the cell cycle. This has led to a model in which phosphorylation of Sororin releases its inhibition of Wapl, allowing Wapl to act on cohesin (Nishiyama et al., 2010; Nishiyama et al., 2013). Since *Drosophila* contains a Sororin homolog that is required for sister chromatid cohesion, it is thought that this model is conserved within vertebrates. Since Sororin homologs do not exist outside of vertebrates, it is unclear how these organisms regulate Wapl. It is known, though, that budding yeast Wpl1 cannot act on cohesin after Smc3 acetylation by Eco1 (Chan et al., 2012; Lopez-Serra et al., 2013). Therefore, in both yeast and mammals, Wapl inhibition is linked to Smc3 acetylation.

Although Wapl has clearly been shown to play a role in mitosis, it is unclear whether Wapl functions during meiosis. In *Arabidopsis thaliana*, WAPL is required during meiosis to remove cohesin from chromosome axes, but does not function during mitosis (De et al., 2014). As a result, WAPL in *Arabidopsis* may not be analogous to Wapl in mammals and yeast. In budding yeast, the absence of Wpl1 does not affect spore viability, suggesting that Wapl is not required for proper chromosome segregation during meiosis (Lopez-Serra et al., 2013). In *Drosophila,* Wapl is implicated in heterochromatin pairing during meiosis, but it is unclear whether this is related to Wapl's cohesion-antagonism function (Verni et al., 2000). In mice, Wapl has been seen colocalized with the synaptonemal complex along meiotic chromosomes. This localization to meiotic chromosome axes occurred in both male pachytene spermatocytes and female pachytene oocytes (Kuroda et al., 2005; Zhang et al., 2008). While evidence from mice and *Drosophila* suggests that Wapl could function during meiosis, additional research will have to be done to determine whether this is truly the case.

Wapl is a conserved protein that antagonizes cohesin complexes, making cohesin association with chromatin more dynamic. Although a great deal of research on Wapl has characterized its function in a variety of organisms, many questions still remain. It is still not completely understood how Wapl is regulated, whether is functions during meiosis, or whether the *C. elegans* Wapl homolog has a conserved function.

Pairing, synapsis, and crossover recombination ensure proper meiosis

In addition to the establishment of sister chromatid cohesion, other events must occur to ensure proper chromosome segregation during meiosis. During meiotic prophase, homologous chromosomes must pair, synapse, and undergo crossover recombination (Figure 1.1b).

The pairing of homologous chromosomes is essential for the proper completion of meiosis; however, pairing remains a mysterious process in many organisms. In *C. elegans*, homologous chromosome pairing requires pairing center proteins HIM-8, ZIM-1, -2, and -3. The pairing center proteins bind to chromosome pairing centers, discrete DNA sequences at one end of each chromosome. HIM-8 binds to the X chromosome, ZIM-1 binds to chromosomes II and III, ZIM-2 binds to chromosome V, and ZIM-3 binds to chromosome I and. The pairing centers promote pairing by tethering chromosomes to the nuclear envelope and facilitating dynein-dependent chromosome motion IV (MacQueen et al., 2005; Phillips and Dernburg, 2006; Phillips et al., 2005). The tethering of chromosomes to the nuclear envelope also requires the SUN/KASH proteins SUN-1 and ZYG-12 (Sato et al., 2009). Loss of a pairing center results in a lack of pairing between the chromosomes to which it should normally bind.

During zygotene of meiotic prophase, synapsis stabilizes the association of chromosomes. Synapsis is mediated by the synaptonemal complex, a tripartite, proteinaceous structure. More specifically, the synaptonemal complex is made up of axial elements that localize along the lengths of meiotic chromosomes and the central elements, which bridge the axial elements holding the homologous chromosomes together. In *C. elegans,* the axial element proteins are HTP-3, HTP-1/2, and HIM-3 and the central elements are SYP-1, -2, -3, and -4. In diplotene and diakinesis, the synaptonemal complex relocalizes around the site of the crossover on the long and short axes (reviewed in Schvarzstein et al., 2010).

If synapsis has proper aligned homologous chromosomes, then crossover recombination can take place during pachytene. In addition to swapping genetic information between homologs,

crossover recombination forms a physical linkage between homologous chromosomes. These linkages are called chiasmata. Crossover recombination is initiated by the formation of programmed double-strand breaks (DSBs) by the highly conserved enzyme Spo11. The DSB is resected in the 5'-3' direction by the MRN complex, which is composed of Mre11, Rad50, and Nbs1. 5'-3' resection forms 3' single-stranded DNA overhangs, onto which either Rad51 or DMC1 localizes. The localization of these proteins to the DNA allows for strand invasion, where the DNA invades either the sister chromatid or homolog. If repair occurs off of the homolog, genetic information is swapped between homologs and a chiasma is formed. Chiasma are physical linkages between homologous chromosomes mediated by sister chromatid cohesion (reviewed in Keeney and Neale, 2006; Marston, 2014; Neale and Keeney, 2006).

After the formation of crossovers, meiotic chromosomes condense and synaptonemal complex proteins relocalize to prepare chromosomes for segregation. In *C. elegans*, chromosomes condense around the site of the crossover. In doing so, chromatin takes on a cross-like shape called the cruciform. Relocalization of synaptonemal complex proteins and cohesin also happens around the site of the crossover. Chromosome condensation and relocalization of proteins results in the formation of two axes – a long and short axis (Schvarzstein et al., 2010). REC-8 localizes to the long axis and will align parallel with the Meiosis I spindle. COH-3/4 localizes to the short axis and will align perpendicular to the Meiosis I spindle. This localization has led to a model in which COH-3/4 is removed during Meiosis I to allow homologous chromosomes to separate, followed by removal of REC-8 during Meiosis II to allow sister chromatids to separate (Severson and Meyer, 2014).

1.3 Chromosome nondisjunction and its affects on human health

After meiotic prophase, chromosomes are prepared to undergo the two segregation steps. During the Meiosis I, homologous chromosomes segregate away from one another in what is known as the reductional division. During Meiosis II, sister chromatids segregate away from one another in the equational division. If at any point during meiosis sister chromatid cohesion, pairing, synapsis, crossover formation, or the meiotic segregations do not proceed correctly, chromosome missegregation can occur. Chromosome missegregation, or nondisjunction, is hugely detrimental as it leads having an extra copy or lacking a copy of a chromosome, a cellular state called aneuploidy.

Chromosome nondisjunction can occur at either Meiosis I, during the first division, or Meiosis II, the second division. If a chromosome fails to form a crossover during meiotic prophase, then the unpaired chromosomes are called achiasmate. Achiasmate chromosomes are simply sister chromatids and will nondisjoin at Meiosis I. Normally, paired homologous chromosomes move away from one another, with one segregating to one pole and one segregating to the other pole. If homologs are achiasmate, then they will act separately during Meiosis I. This means that both homologs could move to the same pole and the other pole will receive no copies of the chromosome. During Meiosis II, the achiasmate chromosomes are now properly suited for chromosome segregation. One sister chromatid can move to one pole and one sister chromatid to the other pole. However, nondisjunction at Meiosis I causes a problem in the chromosome copy number in the gametes. In males, for example, two of the four sperm produced now contain an extra copy of the chromosome while the other two sperm lack a copy of the chromosome. In females, due to segregation of chromosomes into polar bodies, the one

resulting egg will have either an extra copy of the chromosome or lack a copy of the chromosome (Figure 1.2b). The gamete, which should be uniploid, is considered either diploid or euploid. If the gamete is fertilized by a uniploid gamete, then the resulting embryo is aneuploidy because it holds either an extra copy or lacks a copy of a chromosome. Aneuploidy is hugely detrimental for the health of the embryo (Fragouli et al., 2013; Hassold and Hunt, 2001).

Aneuploidy is well studied due to the ramifications of aneuploidy on human health. Embryonic aneuploidy is thought to affect at like 4% of all clinical pregnancies. Due to the inability of the embryo to withstand an improper number of chromosomes, the vast majority of embryonic aneuploidy end in spontaneous abortion (Hassold and Hunt, 2001). Additionally, research now suggests that the rates of aneuploidy are much higher than 4% at fertilization and that aneuploidy negatively affects early development and implantation, primary stages that are not included in clinical pregnancy numbers (Delhanty et al., 1997; Wells and Delhanty, 2000). In the few pregnancy cases where an aneuploid embryo is not miscarried, the children born suffer from developmental defects. For example, Down syndrome patients have an extra copy of chromosome 21. Due to this aneuploidy, patients have mental impairment, stunted physical development and a higher frequency of health issues (Fragouli et al., 2013; Hassold and Hunt, 2001).

It is currently unclear why humans have such a high rate of embryonic aneuploidy and what are the primary molecular causes of embryonic aneuploidy. Unfortunately, rates of aneuploidy do increase in mothers of advanced age, suggesting a breakdown of active mechanisms that normally act to ensure proper chromosome segregation. Given the trend of women to wait longer until having children, it is critical that we gain a better understanding of embryonic aneuploidy and its causes (Johnson, 2007).

1.4 The model organism Caenorhabditis elegans

Caenorhabditis elegans is a small, free-living nematode that can be found in bacteria-rich soil environments. First introduced to researchers in 1974, *C. elegans* has emerged as a fantastic model organism due to the wide arrange of techniques available to *C. elegans* researchers – genetics, genomics, microscopy and biochemistry. Due to its power as a model organism, *C. elegans* has been used to study cell lineage, development, programmed cell death, RNA interference, aging, and cell division.

In 1974, Sydney Brenner published *The Genetics of* Caenorhabditis Elegans. Here, he described the isolation of the worm and the mapping of over one hundred genes. Brenner discussed the benefits of biological study using *C. elegans*. In addition to its small size and rapid life cycle, *C. elegans* can generally be found as self-fertilizing hermaphrodites. This means a single hermaphrodite can give rise to hundreds of genetic clones. If researchers would like to perform a cross, males can be produced as a result of missegregation of the X chromosome. Additionally, Brenner mapped visible genetic markers like *unc* and *rol,* allowing for complementation and mapping of other genes. Even in 1974, one of *C. elegans'* key strengths was its genetic tractability (Brenner, 1974).

Since the first years of *C. elegans* research, the genetics and genomics tools available to researchers have increased dramatically. In 1998, *C. elegans* became the first multicellular organism to have its whole genome sequenced (The C. elegans Consortium, 1998). In that year, Fire *et al.* published their work on genetic interference by RNA, providing both a broader

understanding of gene regulation and additional genetic tools (Fire et al., 1998). In the past six years, *C. elegans* has experienced a revolution in genome editing. From bombardment, where DNA sequences were randomly integrated into the worm by microparticle bombardment, to MosDel and MosSci, transposon-based systems to delete or introduce DNA sequences (Lo, 2001) (Frokjaer-Jensen et al., 2008). More recently, Crispr/Cas9 has emerged as a way tag, delete, or introduce point mutations into endogenous genes (Chiu et al., 2013; Dickinson et al., 2013; Friedland et al., 2013).

In addition to the genetic and genomic tools available in *C. elegans*, the worm's transparent body makes it an excellent model organism for microscopy. Differential interference contrast (DIC) microscopy allows for the live examination of nuclei, nucleoli, and other large cellular structures. Fluorescent microscopy, either through fluorescent dyes, fluorescently labeled antibodies, or fluorescently tagged proteins, allows for the study of cell biology in *C. elegans.* Chromosome morphology can be assayed with dyes like DAPI. The localization of proteins can be determined with fluorescently labeled antibodies. With fluorescently tagged proteins, proteins can be studied in both live and fixed images (Shaham, 2006). Along with other microscopy techniques not listed here, there are many options available to researchers for fixed and live imaging of *C. elegans*.

In addition to genetics and microscopy, researchers have also developed a number of biochemical techniques for use in *C. elegans*. Immuno-affinity precipitation of endogenous or transgenic proteins from worm lysates, followed by mass spectrometry or immunoblotting, allows researchers to identify protein interactors and post-translational modifications (Walhout and Boulton, 2006; Zanin et al., 2011). The preparation of worm lysate is possible because *C. elegans* can be grown in large numbers using liquid cultures. Additionally, the range of antibodies and tagged-proteins available means there are a few possible ways in which a protein or complex can be affinity purified.

Given the wide range of biological methods available to researchers, *C. elegans* has become a fantastic model organism with which to study meiosis. Not only can researchers use genetics, genomics, microscopy, and biochemistry, but the *C. elegans* physiology makes it uniquely tractable for meiotic studies. The gonad itself is very large and takes up almost the entire volume of the 1 mm worm. Additionally, the nuclei within the gonad are arranged spatially and temporally. Nuclei in the far distal end of the gonad proliferate mitotically. Nuclei then switch from proliferating mitotically and begin the meiotic program. Progression of nuclei through leptotene, zygotene, pachytene, diplotene, and diakinesis can be easily viewed and assessed for defects (Greenstein, 2005).

Taken together, *C. elegans* is a model organism with which researchers can study a variety of cellular processes using an assortment of biological techniques. Here, we explore both the regulation of early meiosis and meiotic chromosome segregation using *C. elegans.*

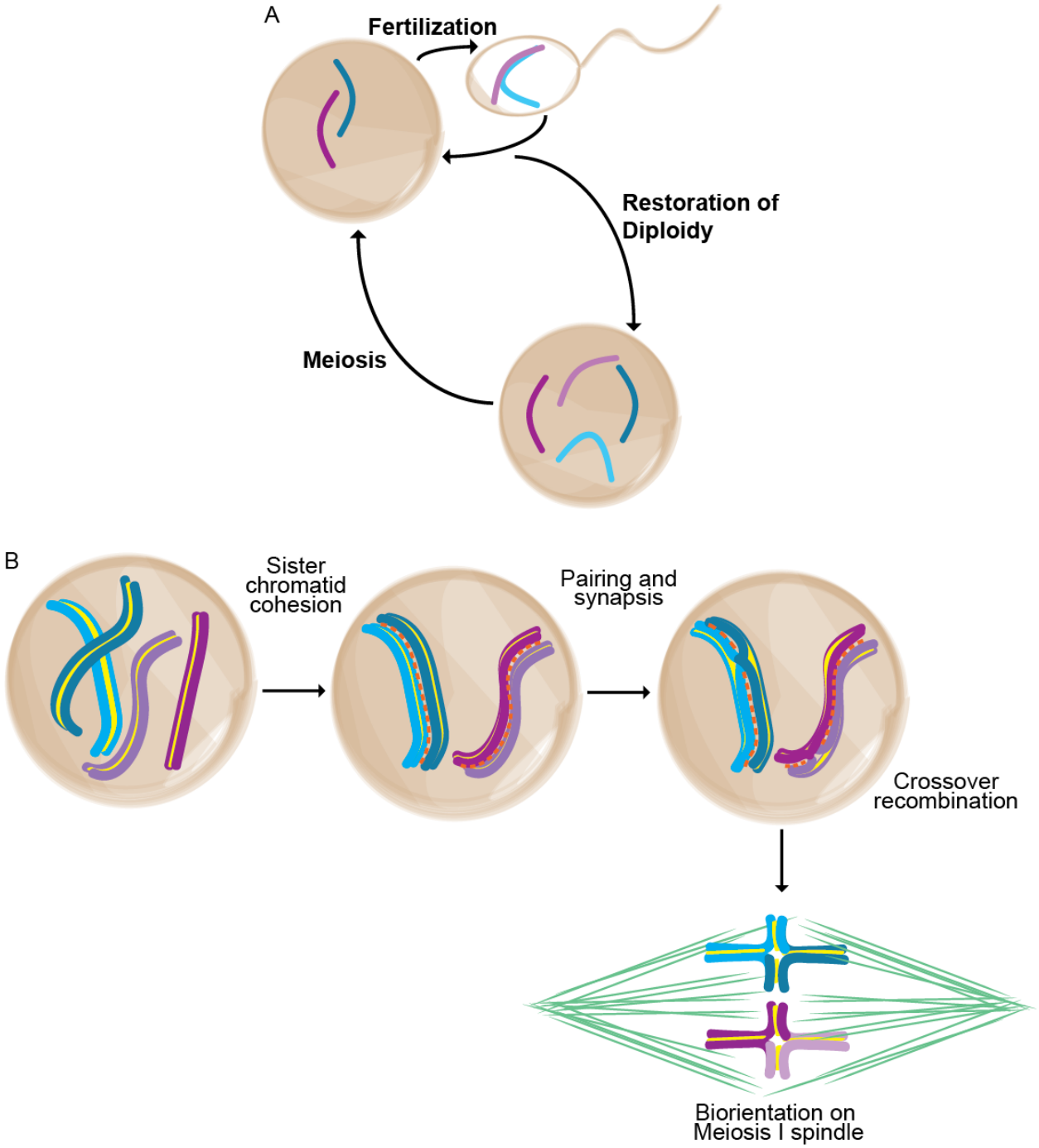

Figure 1.1 Fertilization of a haploid egg by a haploid sperm restores diploidy in the resulting progeny, which then undergoes meiosis to halve its chromosome numbers (A). Sister chromatid cohesion, pairing and synapsis, and crossover formation are events that must occur in order to allow homologous chromosomes to bi-orient on the metaphase I spindle (B).

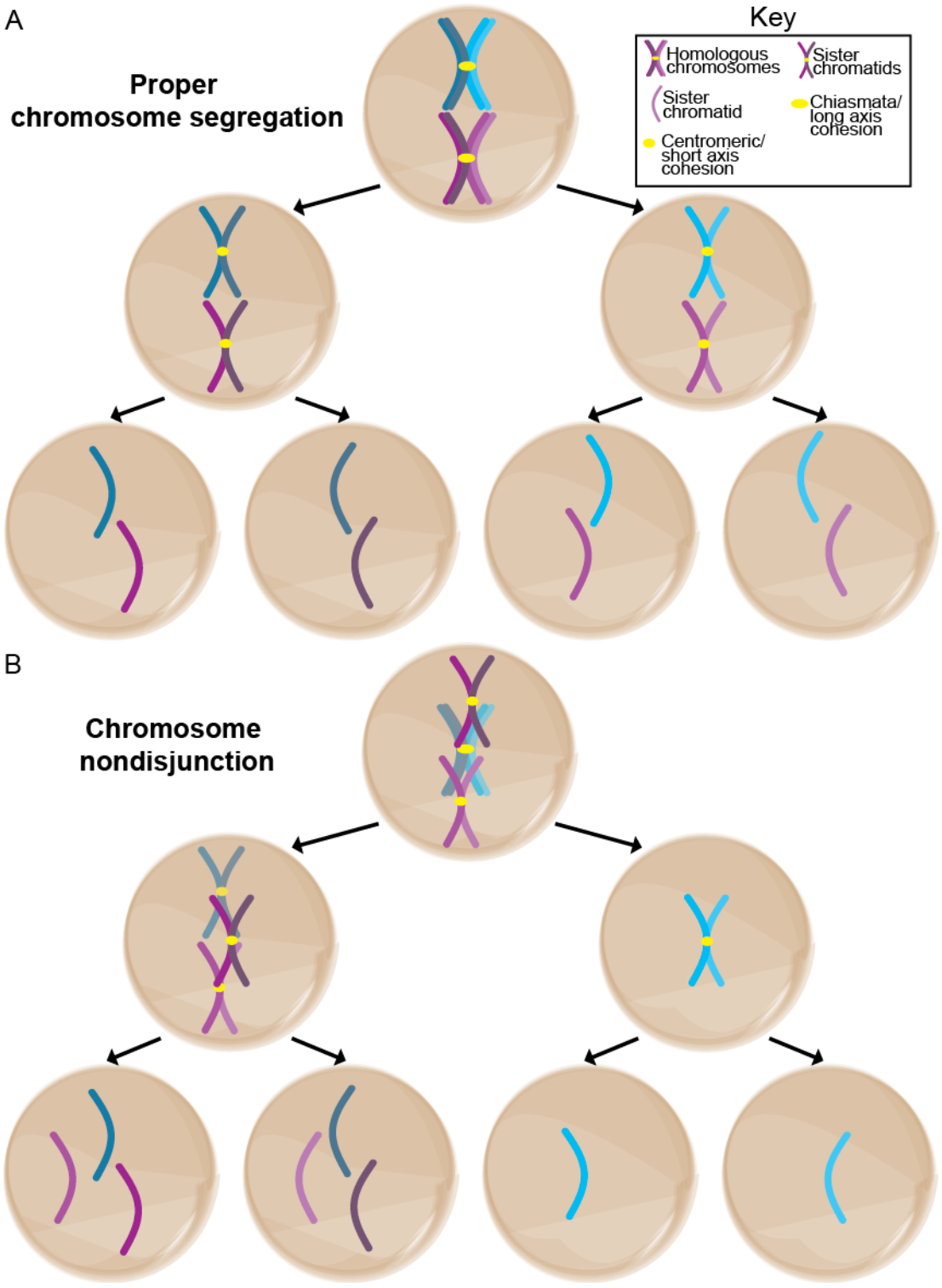

Figure 1.2 During Meiosis I, homologous chromosomes segregate away from one another, followed by Meiosis II, during which sister chromatids segregate away from one another (A). Chromosome nondisjunction during Meiosis I is the segregation of both homologous chromosomes to the same pole (B).

Chapter 2: WAPL-1 is regulated by the meiotic kinase, CHK-2, during meiotic prophase

2.1 Introduction and summary of results

Meiosis is the specialized cell division by which sexually reproducing organisms produce haploid gametes. In order to reduce the chromosome complement by half, a number of events must occur so that homologous chromosomes can segregate away from one another at Meiosis I (Figure 1.1b). The first of these events is the loading and establishment of sister chromatid cohesion. During meiosis, cohesion is required to hold sister chromatids together and mediate chiasmata, the physical linkages that hold homologous chromosomes together. The establishment of sister chromatid cohesion during *C. elegans* requires the loading of axial element proteins along chromosomes. The second process that must take place is the pairing and synapsis of homologous chromosomes. In *C. elegans,* pairing requires pairing center proteins to localize at distinct sequences on chromosome ends and attach chromosomes to the nuclear envelope through a SUN-KASH protein complex. Attachment allows for dynein-mediated chromosome motion, which pairs homologous chromosomes. Synapsis then stabilizes the physical association of homologs through the synaptonemal complex, a proteinaceous structure that localizes along the length of chromosomes. The third process that must take place to ensure proper meiotic chromosome segregation is the formation of chiasmata through crossover recombination. During this process, programmed DNA double-strand breads (DSB) are mediated by the enzyme SPO-11. DNA DSBs are then repaired through a highly regulated process that involves, among other proteins, MRE-11 and RAD-50. DNA DSBs can be repaired using sequence from the homologous chromosome pair (Rose, 2014; Sato et al., 2009; Schvarzstein et al., 2010). This type of repair can result in a physical link between homologous chromosomes called chiasma.

As these events must take place to ensure a proper meiotic division, regulation of each process is key. In some cases, regulation is mediated through timing. In this case, one process will not start until another is finished. Synapsis requires the loading of the axial elements, which in turn requires the loading of sister chromatid cohesion. Since each process requires another process, no process is skipped during meiotic prophase. In another case, regulation might occur through an outside, regulatory protein. CHK-2 is a meiosis-specific regulator of early meiotic events. This serine/threonine kinase regulates processes like pairing through direct phosphorylation of key substrates (Kim et al., unsubmitted; Schvarzstein et al., 2010; Severson et al., 2009).

The regulation of sister chromatid cohesion has fascinated researchers for decades. Sister chromatid cohesion is a highly conserved biological process that is mediated by the cohesin complex. The cohesin complex is made up of two structural maintenance of chromosome proteins, SMC-3 (Smc3) and HIM-1 (Smc1), and a third subunit, the kleisin. These three proteins form a ring structure that holds sister chromatids together. In order to segregate chromosomes, either during meiosis or mitosis, sister chromatid cohesion must be abolished. The release of the cohesin complex requires the kleisin. Since mitosis and meiosis requires different and specialized cohesin release, there exist mitosis- and meiosis-specific kleisins. In mitosis, SCC-1 (Rad21/Mcd1/Scc1) and COH-1 (Rad21 homolog) are the two currently annotated mitotic kleisins. During meiosis, REC-8 (Rec8) and COH-3/4 (Rec8 homologs) are the kleisins. Recent work has shown that, not only are there multiple *C. elegans* meiotic kleisins, but cohesin complexes containing these kleisins are regulated differently and perform different functions. During meiotic prophase, REC-8 cohesin complexes require the axial element protein HTP3,

while COH-3/4 cohesin complexes require CHK-2 (Pasierbek et al., 2001; Severson et al., 2009; Severson and Meyer, 2014). While recent work has described some regulatory and functional differences between REC-8 and COH-3/4 cohesin complexes, much is still unknown.

In 2006, the Wapl protein was described as a mediator of sister chromatid cohesion. Pulled down in an immunoprecipitation of cohesin subunits, *Wapl(RNAi)* in mitotically-dividing HeLa cells showed sister chromatid arms being held together. Further studies demonstrated that Wapl is in fact an antagonist of sister chromatid cohesion. In mammalian cells, the bulk of cohesin is removed from chromosome arms during mitotic prophase. This gives results in the arms of sister chromatids flayed out like Xs when visualized by metaphase spreads. Studies in other organisms, such as yeast, demonstrated that Wapl is a conserved protein with roles in chromatin structure and cohesin dynamicity. While it was clear that Wapl played a role in mitosis, it was unclear whether it functioned during meiosis. Additionally, studies to explore the regulation of Wapl describe a complex process. In mammals, Wapl is regulated by competition with the protein Sororin; however, Sororin homologs do not exist in invertebrates. Additionally, Wapl appears to function in a number of capacities and undergoes a number of changes between interphase, prophase, and the mitotic divisions (Kueng et al., 2006; Marston, 2014; Nishiyama et al., 2010).

Here, we demonstrate the *C. elegans* Wapl homolog, WAPL-1, plays a functionally conserved role during mitosis. Taking advantage of the protracted *C. elegans* meiotic prophase, we directly assay what role, if any, WAPL-1 plays during meiotic prophase. Through directly visualization, we found that WAPL-1 antagonizes the formation of SCC-1 cohesin complexes during meiotic prophase. Additionally, WAPL-1 may play a role in DNA DSB repair. Through a combination of live imaging and immunofluorescence, it was also found that WAPL-1 undergoes a change in localization. In the mitotic zone, WAPL-1 appears brightly localized to interphase nuclei and is insensitive to extraction by detergent, suggesting tight association with chromatin. Upon meiotic entry, WAPL-1 remains localized in nuclei, but undergoes a change. In meiotic prophase, WAPL-1 is now sensitive to detergent, suggesting a less tight association with chromatin. Given the role of WAPL-1 during meiotic prophase and its change in form at the mitosis-to-meiosis transition, we hypothesized that WAPL-1 was tightly regulated. A candidate screen identified the meiosis-specific kinase, CHK-2, as a regulator of WAPL-1. In *chk-2* germlines, WAPL-1 remained tightly associated with chromatin and caused defects in the loading of COH-3/4 cohesin complexes. Taken together, we show that WAPL-1 does function during meiosis and is differentially regulated by a meiosis-specific kinase.

2.2 Results

WAPL-1 is the *C. elegans* homolog of Wapl/Wpl1

Based on sequence similarity, R08C7.10 was previously identified as the *C. elegans* homolog of the widely conserved protein, Wapl/Wpl/Wapal. Five WAPL-1 isoforms are annotated on WormBase. Isoforms A and B are the two longest isoforms at 746 and 748 amino acids, respectively. Their lengths differ due to a six basepair addition at the beginning of exon 3. Isoforms C and D are C-terminal truncations of isoforms A and B and are 613 and 615 amino acids long, respectively, and annotated based on RNASeq data. The fifth and last isoform,

isoform E, is the shortest isoform at 102 amino acids and is an exact duplication of the last 102 amino acids of isoforms A and B. Isoform E was annotated due to an SL1 site (Figure 2.1a).

We utilized RNASeq data from the germline to determine transcriptional levels of *wapl-1*. FPKM levels of isoform A, isoform B, and isoforms C/D revealed that isoform A was the primary transcribed isoform, isoform B with lower transcription, and negligible transcription of isoforms C/D. As isoform E is annotated as a direct duplication of the c-terminal region of isoforms A/B, FPKM levels cannot be determined; however, overall reads of the *wapl-1* area did not display any increase in the area of *wapl-1* that would be transcribed for isoform E (Figure 2.2b). Based on this, we determined that isoform A is the primary transcribed *wapl-1* isoform.

In order to check for protein translation by western blot analysis, WAPL-1 polyclonal antibodies were raised against the first 644 amino acids of WAPL-1 isoform A. These antibodies should, therefore, recognize isoforms A/B/C/D. Specificity could be tested against *wapl-1(tm1814)*, an allele from the National BioResource Project that includes an indel spanning the *wapl-1* start codon. Western blot analysis of wildtype and *wapl-1(tm184)* lysate revealed WAPL-1-specific, detectable protein at a size consistent with isoforms A/B (Figure 2.1c). Based on this, we concluded that isoform A is the primary transcribed and translated WAPL-1 isoform. From this point onwards, any mention of WAPL-1 refers to isoform A and all *wapl-1* loss-of-function analysis was performed using the *tm1814* allele.

Given the high sequence conservation of WAPL-1 and its homologs, we utilized the *P*rotein *H*omology/analog*Y* *R*ecognition *E*ngine V 2.0 to predict the 3-dimensional structure of WAPL-1. Phyre2 analysis revealed very strong structural similarity between WAPL-1 and the two Wapl solved crystal structures, HsWapl and BmWapl. WAPL-1 primarily consists of eight HEAT domains, which are made up of anti-parallel alpha helices. HEAT containing proteins are often involved in cargo transport and known to bind Ran-GTP. In yeast and mammalian cells, the HEAT domains have been shown to interact with the cohesin subunits Scc1 and Smc1 by immunoprecipitation and cross-linking. Previous work crystalizing the HsWapl heat domains described a flexible axis dividing the HEAT domains, allowing them some flexibility to move relative to one another. This axis was located between HEAT domains 3 and 4, dividing these domains into an N-lobe consisting of HEAT domains 1-3 and a C-lobe consisting of HEAT domains 4-8. Like HsWapl, eight clear HEAT domains could be seen within WAPL-1. Additionally, Phyre2 predicted a long, unstructured region at the far N-terminal of WAPL-1. This region is structurally conserved in other Wapl homologs and thought to interact with the cohesin adaptor protein, Pds5 in both humans and yeast.

Based on this data, we concluded that WAPL-1 is the *C. elegans* homolog of Wapl/Wpl/Wapal by sequence and structural similarity.

WAPL-1 localizes to chromatin during interphase, but not during mitosis

To examine the localization of WAPL-1 in *C. elegans*, western blot analysis was performed on various genetic mutants. In order to test whether WAPL-1 is present in somatic cells, the *glp-1* mutant was used. *glp-1*, which encodes an N-glycosylated transmembrane protein that comprises one of the Notch family receptors. In *C. elegans*, GLP-1 is required for formation of the germline. In order to test for the presence of WAPL-1 in non-embryonically dividing tissues, western blot analysis was performed on L4 larva as at this stage, worms have somatic tissues and a meiotic germline, but no embryos. When analyzed, *glp-1* and L4 lysate revealed

robust WAPL-1 protein levels, suggesting WAPL-1 is present in somatic tissues (data not shown).

To gain further insight into the localization of WAPL-1, immunofluorescence against WAPL-1 was performed on embryos and the germline. In the developing embryo, WAPL-1 was present in interphase nuclei as a cloud surrounding chromatin. By anaphase of mitosis, WAPL-1 was not present on or surrounding the chromatin (Figure 2.2a). In the germline, WAPL-1 is present in the mitotic zone, a region of mitotically proliferating nuclei near the gonad's distal tip (Figure 2.2b). Upon meiotic entry, which can be determined by the appearance of crescent-shaped chromosome morphology and the formation of axial element filaments, WAPL-1 abruptly disappears (Figure 2.2d). Closer examination of nuclei in the mitotic zone revealed that WAPL-1 is present in interphase nuclei, but disappears by mitotic anaphase (Figure 2.2c). These results agree with previously published work showing Wapl is present and tightly bound to chromatin during interphase of the cell cycle and not present during mitosis.

In order to gain a more comprehensive understanding of WAPL-1 localization in the germline, a gfp-tagged transgene of *wapl-1* was constructed. Imaging of GFP:WAPL-1 in live worms showed bright nuclear staining. At the distal arm of the gonad, visualization of GFP-WAPL-1 and the meiotic entry/transition zone marker, SUN-1:mRuby, showed that nuclear WAPL-1 becomes brighter through the mitotic zone, then abruptly decreases in intensity upon meiotic entry (Figure 2.3a). Surprisingly, visualization of GFP:WAPL-1 revealed nuclear WAPL-1 throughout meiotic prophase. Coincident with meiotic entry, GFP:WAPL-1 signal decreased, but did not disappear. GFP:WAPL-1 signal then increased gradually through meiotic prophase, always localized within nuclei (Figure 2.3b).

Immunofluorescence on the *gfp:wapl-1* strain using α-WAPL-1 and α-GFP antibodies showed GFP:WAPL-1 localized to nuclei in the mitotic zone followed by abrupt disappearance of staining (Figure 2.3c). Based on this localization, we concluded that WAPL-1 in meiotic prophase is sensitive to the immunofluorescence procedure, most likely the detergent used to permeabilize the specimen. To test this, *gfp:wapl-1* worms were imaged live with or without the addition of detergent. GFP:WAPL-1 signal in the portion of the germline that is consistent with meiosis was more sensitive to treatment with detergent than GFP:WAPL-1 in the mitotic zone. The presence of detergent-sensitive WAPL-1 in meiotic prophase is similar to what has been seen in HeLa cells. In these cells, Wapl was sensitive to extraction by detergent during mitotic prophase, but not interphase (data not shown). Taken together, we concluded that WAPL-1 in the mitotic zone is tightly associated with chromatin. Upon meiotic entry, WAPL-1 changes to a state in which it is less tightly associated with chromatin and therefore more sensitive to extraction by detergent.

WAPL-1 could also be seen by immunofluorescence and live imaging localized in gut nuclei and gonadal sheath cells, meaning that WAPL-1 appears tightly associated with chromatin (Figure 2.2b). This is consistent with western blot analysis on *glp-1* and wildtype L4 lysate. Unlike developing embryos, however, these nuclei are terminally differentiated. It is unknown whether WAPL-1 functions in these cells.

wapl-1 phenotypes are consistent with a role for WAPL-1 during mitosis

In order to understand the function of WAPL-1, *wapl-1* worms were analyzed for defects. For these assays, *wapl-1* worms were maintained as heterozygotes and balanced over nT1. When

an experiment required *wapl-1* worms, *wapl-1* homozygotes were picked plates maintained by picking *wapl-1/nT1* hermaphrodites. wapl-*1* worms displayed defects in embryonic viability as compared to wildtype (Figure 2.4a). Progeny of *wapl-1* hermaphrodites that did not survive to the L4 stage or adulthood could be seen on plates having died as embryos or at earlier larval stages. In contrast, *wapl-1* worms analyzed for male self-progeny, which can arise from nondisjunction of the X chromosome, displayed a mild phenotype as compared to wildtype worms (Figure 2.4a). These results suggest that the decreased embryonic viability of *wapl-1* worms was not due to meiotically introduced aneuploidy, but rather in defects during development.

When wildtype and *wapl-1* worms were followed over time to assay adult survival, *wapl-1* worms died prematurely due to bagging, a phenotype in which the worm's eggs are not properly laid and hatch inside the adult worm, killing it in the process (Figure 2.4b). Bagging can result from defects in vulval development of the worm. Consistent with a vulval development defect, adult *wapl-1* worms displayed a number of other developmental defects, including immobility (*unc*), defective tail formation, and protruding gonad.

The *wapl-1* germline was also analyzed for defects. While *wapl-1* germlines displayed no obvious meiotic defects as will be described later, *wapl-1* germlines appeared shorter than wildtype germlines (Figure 2.4c). Measurements of the distal gonad and the mitotic zone lengths as defined by chromosome morphology revealed *wapl-1* worms to have a significantly shorter gonad (Figure 2.4d). This phenotype can arise due to defects in the mitotic zone and an inability to populate the gonad with wildtype numbers of nuclei.

Given that *wapl-1* displayed phenotypes consistent with a role in mitosis, we performed live-imaging of embryonic mitotic divisions to assess where WAPL-1 may function during mitosis. Live-imaging by DIC and GFP:Histone2B during the first, second, and third embryonic mitotic divisions in *gfp:h2b* and *gfp:h2b;wapl-1* worms at 20°c revealed no anaphase brides, lagging chromosomes, defects in metaphase plate congression, or an inability to complete mitosis. We hypothesized that stressing the embryos with higher temperature could reveal mitotic defects in the *wapl-1* background previously unseen. Growing worms at 25°c for at least two days and imaging at 25°c did result in the appearance of anaphase brideges, lagging chromosomes, defects in metaphase plate congression, and premature anaphase onset. There did not, however, exist a difference in the number of defects seen between control and *wapl-1* worms (data not shown). We concluded that if mitotic defects exist in *wapl-1* worms, they occurr at low enough frequency so as not to be detectable by live-imaging or were subtle enough so as not to be detectable by DIC or fluorescently-tagged histone H2B.

Based on the *wapl-1* phenotypes, in addition to the localization of WAPL-1, we concluded that WAPL-1 is a nonessential protein that functions during mitosis to ensure proper mitotic divisions.

wapl-1 displays defects in germline DNA repair

We utilized the spatio-temporal organization of meiotic prophase and direct visualization to probe *wapl-1* worms for defects in meiotic prophase. DAPI-staining of *wapl-1* gonads revealed the presence of distinct chromatin morphology indicative of the mitotic zone, transition zone, pachytene, diplotene, and diakinesis (Figure 2.4c). This demonstrated normal progression through meiotic prophase. Immunofluorescence against the protein HIM-8, which localizes as

foci at the ends of the X chromosomes, revealed no defects in pairing of *wapl-1* worms (Figure 2.6a). Staining of a synaptonemal complex component, SYP-1, showed no defects in synapsis (Figure 2.6b). At diakinesis, *wapl-1* worms showed six DAPI-staining bodies, corresponding to six homologous chromosomes, suggesting no defects in crossover formation (Figure 2.6c).

The number and kinetics of DNA double-strand breaks (DSBs) in meiotic prophase were assayed with immunofluoresce against RAD-51, a protein that localizes to DNA at the sites of DSBs. *wapl-1* worms displayed an increase in the number of RAD-51 foci (Figure 2.6d). To quantify this phenotype, the region of meiotic prophase with RAD-51 foci was divided into five equal zones and the mean number of RAD-51 foci per nucleus determined for each zone. This quantification revealed that *wapl-1* mutants have a greater number of RAD-51 foci than wildtype (Figure 2.6e). The length of the entire RAD-51 zone was also quantified and found to be significantly longer in *wapl-1* worms (Figure 2.6f). This increase in RAD-51 foci number could be due to an increase in overall DSB number or a defect in DNA DSB repair. In order to gain further insight, wildtype and *wapl-1* adults were treated with γ-irradiation. Germline nuclei of irradiated worms were assayed for embryonic viability to test their ability to withstand DNA DSBs. Concurrent with a defect in DSB repair, *wapl-1* germlines demonstrated a dose-dependent sensitivity to γ-irradiation (Figure 2.6g); however, as the entire adult worm was treated, it is unclear whether the sensitivity to γ-irradiation is due to defects in DSB repair in the germline mitotic zone or meiotic prophase. We concluded that although present in meiotic prophase nuclei, WAPL-1 is not required for proper meiotic chromosome segregation, but may play a role in DSB repair.

WAPL-1 interacts with mitotic cohesin components

In other organisms, WAPL-1 is a known cohesin adaptor protein and involved in cohesin dynamicity. In order to determine if WAPL-1 plays a similar role in *C. elegans*, a WAPL-1 immunoprecipitation was performed to identify interacting proteins. To pull down WAPL-1, affinity purified α-WAPL-1 antibody raised in guinea pig was coupled to dynabeads and incubated with wildtype whole worm lysate. To identify proteins non-specifically binding to the tube and dynabeads, wildtype lysate was also incubated with dynabeads coupled to normal guinea pig IgG. Mass spectrometry of proteins eluting with WAPL-1 identified all mitotic cohesin components, including SMC-3 (Smc3), HIM-1 (Smc1), SCC-1 (Rad21/Scc1/Mcd1), COH-1 (Rad21 homolog), and SCC-3 (STAG-family protein) (Figure 2.5a).

WAPL-1 appeared to interact with mitosis-specific cohesin components, as the *C. elegans* meiosis-specific cohesins REC-8 and COH-3/4 were not identified by mass spectrometry. Additionally, REC-8 and COH-3/4 were identified by western blot to be in the flow through and not in the eluate of the WAPL-1 immunoprecipitation (Figure 2.5b). In addition to the cohesin subunits, mass spectrometry also identified MRE-11 (Mre11) and RAD-50 (Rad50) was WAPL-1 interacts (Figure 2.5a). MRE-11 and RAD-50 are components of the MRN complex, which is required for the initial processing of DSB repair. Identification of MRE-11 and RAD-50 as interactors of WAPL-1 lends further evidence that WAPL-1 may play a role in DSB repair. Casein kinase 1 and casein kinase 2 were also identified by mass spectrometry as WAPL-1 co-eluting proteins (Table 2.1). The family of casein kinase proteins have been identified in other organisms as regulators of cohesion through direct phosphorylation of cohesin

components. Based on this data, we concluded that WAPL-1 plays a conserved role in mitosis through interaction with the cohesin complex.

WAPL-1 acts during meiosis to inhibit mitotic cohesin

We took advantage of the protracted meiotic prophase in *C. elegans* to better understand the role, if any, WAPL-1 plays in establishing proper meiotic cohesion. The presence of six DAPI-staining bodies during diakinesis in *wapl-1* already suggested no defects in cohesion. To assay whether cohesin was loaded in a wildtype manner, germline immunofluorescence was performed on cohesin components. Immunofluorescence against SMC-3 showed normal loading of cohesin axes along chromosomes. To gain further insight into each class of meiotic cohesin, immunofluorescence was also performed against the meiotic kleisins, REC-8 and COH-3/4 (data not shown). No defects were detected in REC-8 or COH-3/4 loading in *wapl-1* worms, providing further evidence that WAPL-1 does not directly regulate meiotic cohesin complexes.

Since COH-1 was identified as a WAPL-1 interacting protein by immunoprecipitation, we performed COH-1 immunofluorescence on wildtype and *wapl-1* germlines. We stained with four antibodies raised against two different COH-1 epitopes in wildtype and *wapl-1* germlines. It is unclear whether or not the COH-1 antibody is specific or recognizing COH-1 *in vivo*; however, no differences were detected in COH-1 localization between wildtype and *wapl-1*. The SDIX Rabbit-α-COH-1 Q0809 antibody stained gut nuclei, sheath cells, the distal tip cell, and within diplotene and diakinesis nuclei in wildtype worms. There was no staining in the mitotic zone, the transition zone and most of pachytene as nuclei. Localization was similar in *wapl-1* worms and there was no staining in the mitotic zone or transition zone. The SDIX Rabbit-α-COH-1 Q0812 antibody stained all germline nuclei and appeared nucleoplasmic. In the mitotic zone, a nucleus that appeared to be at metaphase had COH-1 brightly around the chromosomes. It was unclear whether it was excluded or on chromatin. COH-1 also stained the distal tip cell, sheath nuclei, and gut nuclei. In *wapl-1* germlines, COH-1 appeared as in wildtype. More specifically, COH-1 did not form axes in the mitotic zone or during meiotic prophase. It did look like it was somewhat staining DAPI bodies during diakinesis, but it is unclear whether this could be repeated. The SDIX SDIX Rabbit-α-COH-1 Q3160 did not stain in the germline in wildtype worms and looked the same in *wapl-1*. The SDIX Rabbit-α-COH-1 Q3162 had no staining in wildtype germlines except for the distal tip cell, but did appear to form axes in late pachytene and on DAPI staining bodies during diakinesis. It should be noted that this type of staining seen in *wapl-1* germlines was the staining described for COH-1 in Pasierbek et al., 2001. Overall, since COH-1 did not appear drastically different between wildtype and *wapl-1* germlines, these experiments were not repeated.

As we had also identified SCC-1 in the WAPL-1 immunoprecipitation and because it had been shown to weakly stain meiotic prophase chromosomes, we assayed SCC-1 loading in *wapl-1* germlines. In *wapl-1*, SCC-1 formed robust axes along meiotic prophase chromosomes. This SCC-1 localization contrasted with SCC-1 localization in wildtype germlines, which is often weak or not present at all (Figure 2.7a). It was surprising to see mislocalization of SCC-1 on meiotic chromosomes because most most meiotic processes proceed normally in *wapl-1* worms. It appears that mislocalization of SCC-1, but not COH-1, to chromosome axes does not disrupt the function of cohesin complexes containing meiotic kleisins. Based on this data, we concluded

that WAPL-1 antagonizes the loading of cohesin complexes containing the mitotic kleisin SCC-1 during meiotic prophase.

Candidate screen reveals CHK-2 as WAPL-1 meiotic prophase regulator

Based on WAPL-1's role in antagonizing cohesin loading during meiotic prophase and its change in form upon meiotic entry, we hypothesized that WAPL-1 is tightly regulated at the mitosis to meiosis transition. We performed a small candidate screen to identify regulators of WAPL-1. CHK-2, the meiosis-specific serine/threonine kinase and *C. elegans* homolog of Chk2, displayed a clear defect in WAPL-1 localization during meiotic prophase. Rather than disappearing, WAPL-1 remained at chromatin throughout meiotic prophase. Since *chk-2* worms do not activate DNA DSBs, we assayed WAPL-1 localization in the *spo-11* background, as worms lacking SPO-11 cannot make programmed DSBs. WAPL-1 localized normally to the mitotic zone in *spo-11,* demonstrating that WAPL-1 regulation is independent of programmed DSBs. As known early meiotic regulators and cohesion regulators, PLK-1/2 were tested and found to have normal WAPL-1 localization. Additionally, the *htp-3* mutant, which is defective in a number of early meiotic events including REC-8 loading, displayed wildtype WAPL-1 localization (Figure 2.8a).

We also tested known mitosis to meiosis transition regulators for defects in WAPL-1 localization. *prom-1*, which encodes an F-box protein, results in a delay of meiotic entry. WAPL-1 localization to chromatin was extended and concurrent with the extension of the mitotic zone of *prom-1* germlines. GLD-1 is a mitosis-to-meiosis transition regulator. In *gld-1* germlines, germlines contain a mixture of mitotic and meiotic nuclei. In *gld-1* germlines, chromatin-associated WAPL-1 was seen in some nuclei, but not others. This phenotype is consistent with a model in which WAPL-1 was localized to chromatin in the mitotic nuclei. Lastly, *gld-3;nos-3* germlines were assayed for WAPL-1 localization. As mitosis-to-meiosis regulators, GLD-3 and NOS-3 are required for entry into meiosis. In *gld-3;nos-3* germlines, nuclei never enter meiosis and WAPL-1 was localized in nuclei throughout the germline. Consistent with CHK-2 regulating WAPL-1, CHK-2 activity as assayed by phosphoHIM-8 staining was delayed in *prom-1*, patchy in *gld-1*, and absent in *gld-3;nos-3* (data not shown).

Crossing the *gfp:wapl-1* transgene into the *chk-2* background differed from the wildtype background as now GFP:WAPL-1 displayed no change in signal intensity at meiotic entry (Figure 2.8b). *C. elegans* CHK-2 is a meiosis specific kinase, suggesting that WAPL-1 is uniquely regulated during meiotic prophase. Additionally, this regulation activates WAPL-1, allowing it to antagonize the loading of mitotic cohesin during meiosis prophase.

WAPL-1 may or may not be a substrate of CHK-2

Given CHK-2's kinase activity, we wondered whether CHK-2's regulation of WAPL-1 could be due to direct phosphorylation of WAPL-1. Western blot analysis of WAPL-1 on wildtype lysate run on standard SDS-Page gel revealed no phosphoshift or difference in the WAPL-1 protein band as compared with *chk-2* lysate. We hypothesized that the lack of a phosphoshift could be due to the large size of WAPL-1. To determine whether a phosphoshift could be detected by another method, we tried two different methods. The first method was to

use phosTag gels, which slow the migration of phosphorylated proteins. No phosphoshift was identified with the phosTag gels, although it was unclear whether that was due to the lack of phosphorylated WAPL-1 or due a defect in the phosTag gels. The second method to test for the presence of a phosphoshift was to chemically cleave the WAPL-1 protein. 2-nitro-5-thiocyanatobenzoic acid (NTCB) is a chemical that selectively cyanylates cysteine residues and, under alkaline conditions, this is followed by chain cleavage at the modified residues. As WAPL-1 contains ten cysteines, we hypothesized the cleavage of NTCB into smaller, reproducible fragments would allow for the visualization of phosphoshifts on one or many of the small fragments. To test for the visualization of phosphoshifts, NTCB was used to cleave recombinant WAPL-1 that was previously incubated with CHK-2 enzymatically active kinase. Visualization by western blot analysis using WAPL-1 polyclonal antibodies raised against 654 of 746 amino acids of WAPL-1 revealed no phosphoshift in cleaved fragments previously incubated with CHK-2 (data not shown). As we could not visualize a WAPL-1 phosphoshift, we turned to testing the phosphorylation of WAPL-1 by CHK-2 with recombinant proteins.

To further investigate CHK-2's regulation of WAPL-1, enzymatically active CHK-2 and kinase dead CHK-2 were purified from insect cells. Recombinant WAPL-1 was purified from *E. coli*. Incubation of CHK-2 and WAPL-1 revealed *in vitro* phosphorylation of WAPL-1 by CHK-2 that was specific to CHK-2's kinase activity (Figure 2.10a). To identify the CHK-2 phosphorylation sites on WAPL-1, mass spectrometry was performed on recombinant WAPL-1 that had been incubated with CHK-2. Forty-six different serines and threonines were identified as having been phosphorylated (Table 2.2). This was surprising given that WAPL-1 has only 110 serines and threonines. Of the 46 phosphorylated serines/threonines identified, one site (pS371) was present in a CHK-2 consensus motif (RXXS/T). p371 was located in the helical insert of HEAT 3 and found to be conserved in yeast and *Drosophila*. The other 45 sites of phosphorylation were found throughout the entire length of WAPL-1 in the N-extension, N-lobe, and C-lobe and had various levels of conservation. No clear characteristic (conservation, protein domain, consensus motif) was shared between all 46 sites. Given the substantial phosphorylation of WAPL-1 by CHK-2 *in vitro* and previously identified CHK-2 substrates, it is possible that CHK-2 phosphorylated WAPL-1 promiscuously and that the sites identified by mass spectrometry were not indicative of *in vivo* phosphorylation.

Given the massive phosphorylation throughout WAPL-1 by CHK-2 *in vitro*, we wondered whether we could identify regions of WAPL-1 that were preferentially phosphorylated by CHK-2. We set out to purify three truncations of WAPL-1 that were based on WAPL-1's Phyre2 predicted protein domains. The first truncation was to be the unstructured, N-extension. The second truncation was the N-lobe, containing HEAT domains 1-3. The last and third truncation was to be the C-lobe, containing HEAT domains 4-8. Surprisingly, expression of the WAPL-1 N-extension and WAPL-1 C-lobe could not be expressed in bacterial cells. The N-lobe, however, expressed very well in bacterial cells at levels similar to what had previously been seen during purification of full-length WAPL-1. Purification of various WAPL-1 truncations revealed that only truncations containing the WAPL-1 N-lobe could be expressed in bacterial cells. While it is unclear why the N-lobe is important, it may be due to the H3 helical insert located in HEAT domain 3. Deletion of the H3 helical insert of HsWapl completely destabilized the protein in human cells. Due to poor expression of the WAPL-1 truncations, we turned to other assays to probe CHK-2 regulation of WAPL-1.

Based on other CHK-2 substrates, we hypothesized that CHK-2 phosphorylates WAPL-1 within its four CHK-2 consensus motifs and that phosphorylation results in the differential

WAPL-1 localization visualized at meiotic entry. The serines located in the four CHK-2 consensus motifs were mutated to alanine and introduced into the *C. elegans* genome as a transgene by MosSci. The integrated transgene was then crossed into the *wapl-1* background to ensure that the *gfp:wapl-1(4SA)* transgene provided the only WAPL-1 present in the worm. Immunofluorescence against WAPL-1 in *gfp:wapl-1(4SA)* worms displayed wildtype localization of WAPL-1. While the 4SA mutations revealed no change to WAPL-1 during meiotic prophase, phosphorylation by CHK-2 *in vitro* was reduced by nearly 30% (Figure 2.10b and c). Given the wildtype WAPL-1 localization of the 4SA mutant, a number of possibilities exist. The first is that WAPL-1 is not a direct substrate of CHK-2. The second is that WAPL-1 is a direct substrate of CHK-2, but CHK-2 does not phosphorylate WAPL-1 within the canonical CHK-2 consensus motifs. Lastly, WAPL-1 is a direct substrate of CHK-2 and does phosphorylate WAPL-1 at CHK-2 consensus motifs, but that this phosphorylates is not enough to change the localization of WAPL-1. This could be due to the fact that other substrates must be phosphorylated or that other sites within WAPL-1 must be phosphorylated to affect WAPL-1 localization.

In an effort to identify *in vivo* phosphorylation of WAPL-1, endogenous WAPL-1 purified from wildtype worm lysate was analyzed for post-translational modifications by mass spectrometry. Mass spectrometry identified eight phosphorylated amino acids (Table 2.3). Seven of the eight phosphorylated amino acids were serine or threonines, while one phosphorylated amino acid was a tyrosine. None of the eight phosphorylated amino acids resided within a CHK-2 consensus motif. Of the eight amino acids, four were located in the N-extension, two were located in the N-lobe, and two were located in the C-lobe. Of the eight phosphorylated amino acids, three had also been been shown to be phosphorylated *in* vitro by CHK-2. These three sites were located in the N- and C-lobes. Of the seven phosphorylated serines/threonines, T159 was found to lie in a casein kinase 2 consensus motif. While mass spectrometry identified casein kinases 1 and 2 as a co-eluted protein in the WAPL-1 immunoprecipitation, these kinases were also identified in immunoprecipitations of axial element proteins (Yumi Kim and Nora Kostow, personal communication). Therefore, it is unclear whether the casein kinases are true cohesin interactors.

Misregulation of WAPL-1 during meiotic prophase results in cohesin loading defects

After identifying CHK-2 as a regulator of WAPL-1, we wondered what the affect on meiosis would be if WAPL-1 was misregulated during meiotic prophase. *chk-2* worms suffer from a variety of meiotic defects, including defects in pairing, synapsis and crossover formation. As a result, *chk-2* worms have a severe embryonic viability and high incidence of males phenotype. *chk-2* worms are also defective in loading cohesin complexes containing COH-3/4, but not REC-8. To test whether any of these phenotypes could be a result of misregulation of WAPL-1, a *wapl-1;chk-2* double was constructed.

We examined *wapl-1;chk-2* worms for rescue of any *chk-2* phenotypes. To test pairing, immunofluorescence against pairing center proteins was performed. *wapl-1;chk-2* displayed two pairing center protein foci per nucleus, demonstrating no rescue of pairing. To test synapsis, immunofluorescence against a synaptonemal complex was performed. This staining showed long, robust synaptonemal complex axes along chromosome lengths. To test for rescue of crossover formation, DAPI-staining bodies during diakinesis were analyzed. *wapl-1;chk-2*

worms displayed 12 DAPI-staining bodies at diakinesis, so no rescue of crossover formation. *chk-2* worms do not activate the formation of DNA DSBs. To test whether this was due to WAPL-1 mislocalization, we performed immunofluorescence against RAD-51 in *wapl-1;chk-2* worms. *wapl-1;chk-2* worms displayed no RAD-51 foci, demonstrating a lack of DNA DSBs (data not shown).

Although *wapl-1;chk-2* worms did not exhibit a rescue of pairing, synapsis, crossover formation, or programmed DSBs, loading of COH-3/4 axes during meiotic prophase was clearly improved. In *chk-2* worms, COH-3/4 appears weakly around chromatin and produces a robust signal only at short stretches where synapsis has occurred. Over meiotic prophase, COH-3/4 loading was improved immediately in early meiotic prophase. Long stretches of COH-3/4 axes could clearly be visualized even when synapsis had not occurred. As meiotic prophase continued, robust axes of COH-3/4 continued to be seen along chromosomes (Figure 2.9a). Based on this data, it appears that regulation of WAPL-1 is required for proper loading of cohesin complexes containing COH-3/4.

2.3 Discussion

WAPL-1 plays a conserved role during mitosis in *C. elegans*

WAPL-1 was first identified and named as the *C. elegans* Wapl/Wpl/Wapal homolog based on sequence similarity. In order to determine whether WAPL-1 was also structurally and functionally conserved, analyses of WAPL-1 structure, localization, function, and interactors were performed.

To gain an understanding of where in the worm WAPL-1 functions, we visualized WAPL-1 by immunofluorescence. WAPL-1 localized to nuclei in developing embryos and in nuclei of the mitotic zone. Based on chromosome morphology, we noted that WAPL-1 was present surrounding chromatin during interphase, but dissipated during mitosis. This localization was similar to what had been seen in HeLa cells, in which WAPL-1 could be visualized during interphase, but disappeared by mitotic anaphase. This localization was due to the fact that WAPL-1 functioned primarily during interphase and prophase to regulate chromatin structure during interphase and the removal of cohesin from chromosome arms during prophase. Based on this data, WAPL-1 localization was consistent with a conserved role in mitotically-dividing cells.

To test whether the function of WAPL-1 was conserved in *C. elegans,* we analyzed the *wapl-1(tm1814)* allele for various mitotic and meiotic phenotypes. *wapl-1* worms displayed a number of developmental defects. First, *wapl-1* showed a clear defect in embryonic viability as compared to wildtype, but without a concurrent increase in males. This suggested that the decrease in embryonic viability was not due to aneuploidy resulting from meiotic nondisjunction, but from defects during development. Additionally, *wapl-1* worms demonstrated a number of developmental defects, including bagging, defective tail formation, immobility, and protruding gonad. As wildtype development requires proper cell division, the *wapl-1* developmental defects were consistent with a WAPL-1 function during mitosis.

Further evidence of WAPL-1 functioning during mitosis came during analysis of *wapl-1* germlines. DAPI-staining of fixed gonads revealed that the distal gonad of *wapl-1* worms was, on average, significantly shorter than the distal gonad of wildtype worms. Given that the

germline is populated by nuclei through mitotic proliferation in the mitotic zone, the shorter *wapl-1* gonads provided further evidence that WAPL-1 functions during mitosis.

To further probe WAPL-1's function, immunoprecipitation of WAPL-1 was performed to identify protein interactors. Immunoprecipitation, followed by mass spectrometry, identified all of the mitotic cohesin complex subunits, including both mitosis-specific kleisins, SCC-1 and COH-1. Taking the data together, we concluded that WAPL-1 is a nonessential protein that plays a conserved function during mitosis through interaction with the cohesin complex.

WAPL-1 functions during meiotic prophase in DNA double-strand break repair and mitotic cohesin antagonism

While Wapl's role during mitotis has clearly been shown in a number of organisms, it is unclear whether Wapl plays a role during meiosis. Given that Wapl primarily functions during mitotic prophase, we hypothesized that Wapl could function during meiotic prophase. The *C. elegans* gonad is spatially and temporally organized in a way that makes visualization of meiotic prophase relatively simple. We therefore took advantage of the *C. elegans* protracted meiotic prophase to determine whether WAPL-1 functions during meiosis.

During meiotic prophase, homologous chromosomes must pair, synapse, and undergo crossover formation to ensure proper meiosis. Live-imaging of GFP:WAPL-1 during meiotic prophase demonstrated that WAPL-1 was present during meiotic prophase, though not tightly associated with chromatin as in interphase. Immunofluorescence against pairing center proteins and a component of the synaptonemal complex demonstrated proper pairing and synapsis. The presence of six DAPI-staining bodies during diakinesis was consistent with proper crossover formation during prophase. Given WAPL-1's known interaction with cohesin components, meiotic cohesin complexes were assessed by immunofluorescence and found to load normally. Based on this data, we concluded that WAPL-1 was not required for meiotic prophase.

Since WAPL-1 was shown to interact with mitotic cohesin subunits, we stained for the mitosis-specific kleisin subunits in the *wapl-1* germline. While SCC-1 was barely visible in wildtype meiotic nuclei, SCC-1 localized robustly along meiotic chromosome axes in *wapl-1*. Based on this, we concluded that WAPL-1 does function during meiotic prophase to antagonize mitotic cohesin complexes from loading onto meiotic chromosomes.

Given that DNA double-strand breaks (DSBs) are highly regulated during meiotic prophase, we stained for the DNA DSB marker RAD-51. *wapl-1* germlines had a greater number of RAD-51 foci per nucleus, as well as an extended RAD-51 zone. We wondered whether this increase in DSBs was due to an increase in programmed DSBs or defects in DSB repair. To test this, we γ-irradiated adult worms, allowed for the irradiated germline nuclei to proceed through meiosis, then analyzed embryonic viability. If *wapl-1* worms were defective in DNA DSB repair, then they would show greater sensitivity to γ-irradiation than wildtype worms. Interestingly, *wapl-1* germlines were more sensitive to γ-irradiation suggesting a defect in DNA DSB repair.

Based on this data, we concluded that although not required for meiotic prophase, WAPL-1 does function during meiotic prophase to antagonize mitotic cohesin complex loading and the repair of DNA DSBs.

WAPL-1 is regulated by the meiosis-specific kinase, CHK-2

WAPL-1 displays an abrupt disappearance upon meiotic entry by immunofluorescence and live imaging of GFP:WAPL-1 reveals a change in WAPL-1 signal intensity upon meiotic entry. Based on this, we hypothesized that WAPL-1 was regulated at the mitosis-to-meiosis transition. Performance of a candidate screen to identify regulators of WAPL-1 identified the meiosis-specific kinase, CHK-2, as a regulator of WAPL-1. In *chk-2*, WAPL-1 remained localized to chromatin throughout the entire germline.

Given that CHK-2 is a serine/threonine kinase, we hypothesized that WAPL-1 could be a substrate of CHK-2. While CHK-2 can phosphorylate WAPL-1 *in vitro* and endogenous WAPL-1 was found to be phosphorylated by mass spectrometry, we found no direct evidence that WAPL-1 phosphorylated by CHK-2 *in vivo*. Nevertheless, regulation of WAPL-1 by CHK-2 suggests that during meiotic prophase, WAPL-1 is regulated at the mitosis-to-meiosis transition through a meiosis-specific pathway.

After identifying CHK-2 as a regulator of WAPL-1, we wondered what negative affects might arise due to misregulation of WAPL-1 during meiotic prophase. Since *chk-2* worms exhibit a number of meiotic defects, we constructed a *wapl-1;chk-2* strain to determine whether any of the *chk-2* defects were due to the misregulation of WAPL-1. Pairing, synapsis, crossover formation, and DSB formation were not rescued in the *wapl-1;chk-2*. In addition to these defects, *chk-2* germlines also have defects in loading of COH-3/4 cohesin complexes, but not REC-8 cohesin complexes. In *wapl-1;chk-2* germlines, loading of COH-3/4 cohesin complexes was much improved. While COH-3/4 cohesin loading is dependent on proper WAPL-1 regulation, it is unclear whether it is due to direct antagonism of COH-3/4 cohesin complexes by WAPL-1 or through another mechanism.

Based on our data, we concluded that WAPL-1 is the *C. elegans* functional homolog of Wapl/Wpl/Wapal. WAPL-1 functions primarily during mitosis to ensure proper cell division through interaction with the cohesin complex. WAPL-1 also functions during meiotic prophase, during which it antagonizes loading of mitotic cohesin complexes containing SCC-1 and plays a role in DNA DSB repair. In addition to a role during meiosis, WAPL-1 is regulated through a meiosis-specific pathway mediated by the CHK-2 kinase.

2.4 Materials and Methods

C. elegans *mutations and strains*

Unless otherwise stated, all animals were cultured under standard conditions at 20°c. The wildtype strain was N2 Bristol. One deletion of allele of *wapl-1* was generated by the Japanese National BioResource for the Nematode (*tm1814*). This allele is described as a complex substitution at the N-terminus of *wapl-1*. *wapl-1(tm1814)* was maintained as a heterozygote over the nT1 balancer and all assays were performed on homozygous animals derived from heterozygous parents.

To construct the *wapl-1:gfp(4SA)* transgene, MosSci was used. The *wapl-1* genomic sequence, including 1000 basepairs upstream and 1000 basepairs downstream of the coding region, was inserted into pCFJ350. A coding sequence of Emerald GFP (*C. elegans* codon-optimized) and a 12 amino acid linker were inserted into pCFJ350 before the *wapl-1* first exon by isothermal assembly to generate a repair template. Q5 site-directed mutagenesis^{TM} (NEB) was performed to generate the 4SA mutations, which was verified by sequencing. ttTi5605 animals

were injected with either wildtype or 4SA mutant donor template. Homozygous insertions were confirmed by stable rescue of *unc-119(ed3)*, the lack of mCherry signal in worms, and PCR. These insertions were then crossed into *wapl-1(tm1814)* and assayed by immunofluorescence for expression of WAPL-1. A *wapl-1:gfp* wildtype control was constructed in parallel using the same protocol as was used for the 4SA mutant.

To construct the *gfp:wapl-1* transgene, *wapl-1* and its surrounding regions was cloned into pCR-BLUNT. The coding sequence for Emerald GFP and a 12 amino acid linker was clonsed by isothermal assembly into the N-terminus of *wapl-1*. The PAM sequence was then mutated by Q5 site-directed mutagenesis (NEB) so that Cas9 would not cut the repair template. pDD162 (Addgene) with an added sgRNA target sequence was used as the Cas9/sgRNA plasmid. N2 worms were injected with 50 ng/µl repair template, 50 ng/µl pDD162 Cas9/sgRNA plasmid, 10 ng/µl pGH8, 5 ng/µl pCFJ104, and 2.5 ng/µl pCFJ90 in 1X injection buffer. All red F1s were screened by PCR. If PCR demonstrated successful insertion into an F1, then the progeny of that F1 were checked for 2 or more generations using PCR.

For a full list of strains and alleles used, see tables 4.1 and 4.2.

Immunoblot

150-200 adult hermaphrodites were picked, washed with M9 and 0.5% Tween-20, and boiled in 40 µl of sample buffer. Protein samples were separated by by SDS-PAGE, transferred to nitrocellulose membrane, and probed with WAPL-1 (SDIX, Novus Biologicals and guinea pig described below) and DM1A (anti-tubulin, Sigma).

C. elegans *egg count and survival assays*

To score egg viability and male progeny, L4 hermaphrodites were picked onto individual plates and transferred to new plates every 12 hours for a total of ~4 day laying periods. Eggs were counted immediately after each laying period and surviving progenies were scored when worms reached adult stage. To assay survival, L4 hermaphrodites were picked onto plates containing OP50. Adults were counted every 12 hours for a total of ~4 days.

Antibodies and cytological assays

WAPL-1 polyclonal antibodies were raised in guinea pigs against a 6XHIS-tagged 544 amino acid recombinantly purified portion of WAPL-1 and affinity purified against recombinant full-length WAPL-1. Rabbit antibodies against COH-1, SCC-1, and amino acids 2-102 of WAPL-1 were generated by SDIX using Genomic Antibody Technology™ and are commercially available through Novus Biologicals. Polyclonal antibodies against the following antigens have previously been described: GFP (Roche), HTP-3 (MacQueen *et al*., 2005), HIM-8 (Phillips *et al*., 2005), COH-3/4 (Kim *et al.,* 2014), REC-8 (Kim *et al.,* 2014), SMC-3 (Millipore AB3914) and SYP-1.

Immunofluorescence was performed as previously described. Briefly, L4 hermaphrodites were picked 24 hours before dissection to age-match worms. Young adult hermaphrodites were dissected in egg buffer containing tetramisole and 0.1% Tween-20 and fixed for 4 minutes in 1% formaldehyde in the same buffer. Worms were then squeezed between a Histobond slide and siliconized coverslip and frozen on dry ice. Worms were then freeze-cracked by the swift removal of the coverslip. Slides were immediately transferred to -30°c methanol for 1 minute. Slides were then transferred to PBST (PBS with 0.1% Tween-20) for three washes at 10 minutes each. Slides were blocked for 1 hour in Roche blocking agent and stained with primary

antibodies for at least 2 hours. Secondary antibodies labeled with Alexa 488, FITC, Cy3, or Cy5 were purchased from Invitrogen or Jackson Immunoresearch and used to label specimens. Following immunostaining, slides were stained in 0.5 μg/ml DAPI, destained in PBST, and mounted in ProlongGold (Invitrogen). Slides were dried overnight with minimal light exposure before acquisition of images.

All images were acquired using a DeltaVision RT system (Applied Precision) equipped with a 100X N.A. 1.4 oil-immersion objective (Olympus). 3D image stacks were collected at 0.5 μm Z-spacing and processed by constrained, iterative deconvolution with SoftWoRx software package (Applied Precision). Image projection was performed with Fiji software using a maximum-intensity algorithm of 3D stacks. Composite image assembly, image scaling, and false coloring were performed with Adobe Photoshop.

Time-lapse and live imaging

For time-lapse imaging of mitosis, 16 hours post-L4 adults (grown at either 20°c or 25°c) were dissected and immobilized on freshly made 2% agarose pads in a drop of M9. A 0.17 mm coverslip was applied without sealing and images were collected at 20°c or 25°c. Confocal microscopy was performed using a spinning-disk confocal digital microscopy workstation (Marianas; Intelligent Imaging Innovations) equipped with a spinning disk (CSU-X1; Yokogawa), EM CCD camera (Evolve; Photometrics), 63X or 20X, 1.4 NA Plan Apochromat objectives (Carl Zeiss), and a sphermical aberration correction module. Images were acquired using SlideBook software (Intelligent Imaging Innovations). For 3D confocal imaging, stacks of 20 optical sections with 0.6 μm spacing were acquired. For 2D confocal imaging, 50-100 ms exposures in each channel were acquired every 2 seconds or 50 ms exposures in Max488 channel was acquired every 100 ms. Some false coloring was performed in Adobe Photoshop.

Purification and immunoprecipitation of endogenous WAPL-1 from C. elegans *lysate*

Immunoprecipitation of WAPL-1 as previously described. Briefly, wildtype *C. elegans* were synchronized by bleaching and grown in liquid culture at 20°c until worms reached the young adult stage. Animals were harvested by sucrose flotation, frozen, and disrupted using a mixer mill. Soluble WAPL-1 was purified using affinity purified WAPL-1 antibody from guinea pig coupled to Dynabeads Protein A. Immunoprecipitated proteins were separated by SDS-Page gel, stained with Coomassie, and IgG heavy and light chains cut out and removed. Remaining in-gel sample was trypsin-digested and analyzed for protein identification and post-translational modifications by MudPIT. Immunoprecipitation with normal guinea pig IgG in place of WAPL-1 IgG was performed in parallel using the same protocol.

Feeding RNAi

RNAi targeting of *plk-1* and *wapl-1* was described previously. Briefly, RNAi against *plk-1* and *wapl-1* was performed with a clone from the Ahringer laboratory. Bacterial cultures were grown in LB with antibiotics overnight and spread on 60mm NGM plates with 1 mM IPTG and antibiotics. Double-stranded RNA production was induced for 8-24 hours at 37°c. L4 animals were placed on NGM plates without bacteria and allowed to crawl around for 1 hour to clean worms of OP50 bacteria. Animals were then placed on freshly prepared RNAi plates and transferred to new RNAi plates after several hours to minimize carryover of OP50. Animals were dissected for cytological analysis after 44-48 hours on RNAi plates. Efficacy of *plk-1* RNAi was

confirmed by aneuploidy in the mitotic zone. Efficacy of *wapl-1* RNAi was confirmed by loss of WAPL-1 immunofluorescence in the germline mitotic zone.

Purification of recombinant WAPL-1 and CHK-2

wapl-1 cDNA was amplified from a *C. elegans* cDNA library using primers `agtggctagcATGTCGTCGGATGCTAATTCGG` and `tagcctcgagCTCGAGCCGCTCGAGGTA`. Amplified *wapl-1* cDNA was for isoform A as determined by sequencing. *wapl-1* cDNA was cloned into pET23c protein expression vector so as to contain a 6XHIS tag and sequenced to verify the correct sequence (pNIN32). pNIN32 was transformed into XL10-Gold competent cells. XL10-Gold cells were grown in LB with antibiotics until OD_{600} 0.8 was reached. Protein expression was then induced with 1 mM IPTG for 2 hours. After induction, cells were pelleted and freeze/thawed 3 times. Cell pellet was thawed on ice and resuspended in lysis buffer (25 mM Tris-HCl pH8.0, 300 mM NaCl, 2 mM $MgCl_2$, 0.5 mM EDTA, 1 mM DTT, and 20 mM imidazole, pH8.0, filter sterilized). Lysozyme was added to lysate for a final concentration of and incubated on ice for 30 minutes. Benzonase was added to lysate and incubated at 37°c for 30 minutes. Lysate was cleared by centrifugation at 10,000xg for 30 minutes at 4°c.

Cleared lysate was incubated with washed Ni-NTA agarose (Qiagen) for 60 minutes at 4°c with gentle shaking. Agarose was spun down and flow-through collected. Agarose was washed with 20 volumes wash buffer (lysis buffer without EDTA). Protein was eluted with elution buffer (25 mM Tris-HCl pH 8.0, 300 mM NaCl, 2 mM $MgCl_2$, 1 mM DTT, 250 mM Imidazole, pH 8.0, filter sterilized), snap-frozen in 30% glycerol, and stored at -80°c.

In vitro *phosphorylation assay*

Recombinant WAPL-1, enzymatically active CHK-2, and kinase dead CHK-2 were purified as described previously. WAPL-1 was incubated for one hour with either CHK-2 or kinase dead CHK-2 in the presence of 50 μCi/ml γ-^{32}P ATP, 10mM MgATP, and kinase buffer (HEPES pH 7.5, 25 mM KCl, 1 mM $MgCl_2$, 1 mM DTT) at room temperature. After incubation, the reaction stopped by the addition of sample buffer and run on an SDS-Page gel, stained with Coomassie for 1 hour, and destained in 10% glacial acetic acid and 50% methanol overnight. The gel was then dried onto Whatman paper and imaged by Typhoon. Band intensity was quantified using Fiji.

NTCB cleavage

Recombinant WAPL-1 was incubated with or without active CHK-2 protein in the presence of 50 μCi/ml γ-^{32}P ATP, 10mM MgATP, and kinase buffer (HEPES pH 7.5, 25 mM KCl, 1 mM $MgCl_2$, 1 mM DTT) at room temperature. For NTCB cleavage, 0.3 volumes of 0.5 M CHES pH 10.5) and 0.2 volumes of NTCB (7.5 mM in H_2O, Sigma Aldrich) were added and samples incubated over night at room temperature. The following day, 1 volume of 2X sample buffer with 0.5X Phosphatase Inhibitor Cocktail 3 (Sigma Aldrich) was added. Immunoblotting analysis was performed by SDS-PAGE protein separation and transfer to nitrocellulose membrane. Immunoblotting against WAPL-1 was performed using rabbit and guinea pig polyclonal antibodies raised against WAPL-1 amino acids 2-646

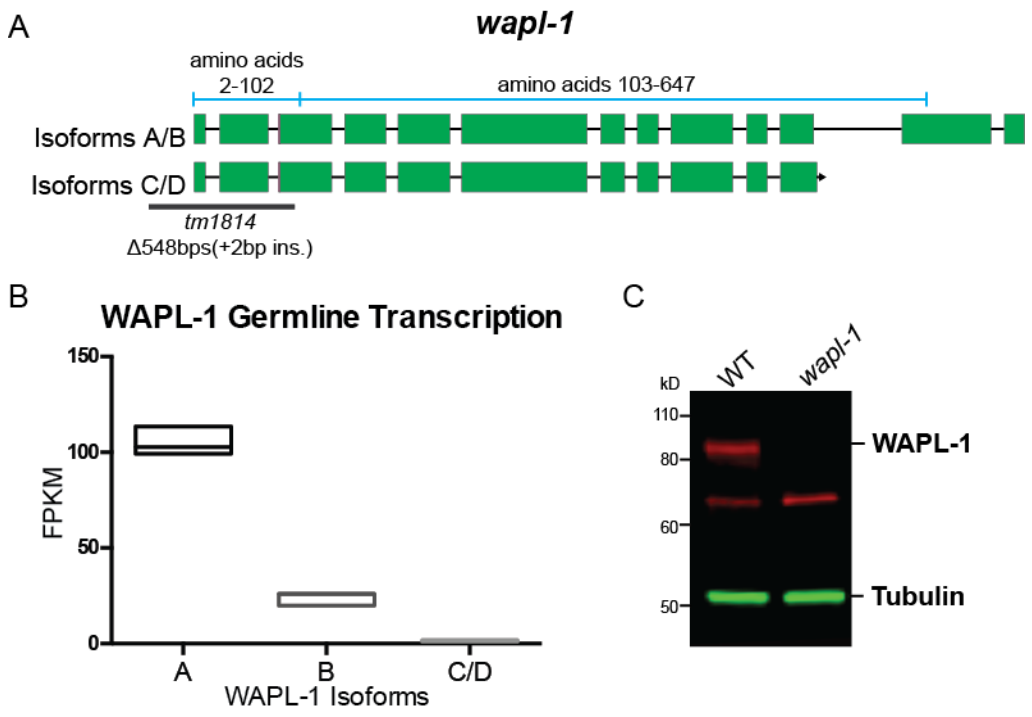

Figure 2.1 cDNA data predicts four *wapl-1* isoforms. Isoforms A and B differ by the addition of two amino acids at the beginning of the third exon. Isoforms C and D are C-terminal truncations of isoforms A and B (A). RNA-Seq data from the germline displays transcriptional levels from isoforms A, B, and C/D (B). A combination of WAPL-1 antibodies raised different regions of WAPL-1 in guinea pig and rabbit display specific recognition of a WAPL-1 at a size corresponding to either isoforms A or B (C). A lower non-specific band at ~70kD is recognized only by the guinea pig antibody, but not the rabbit (data not shown).

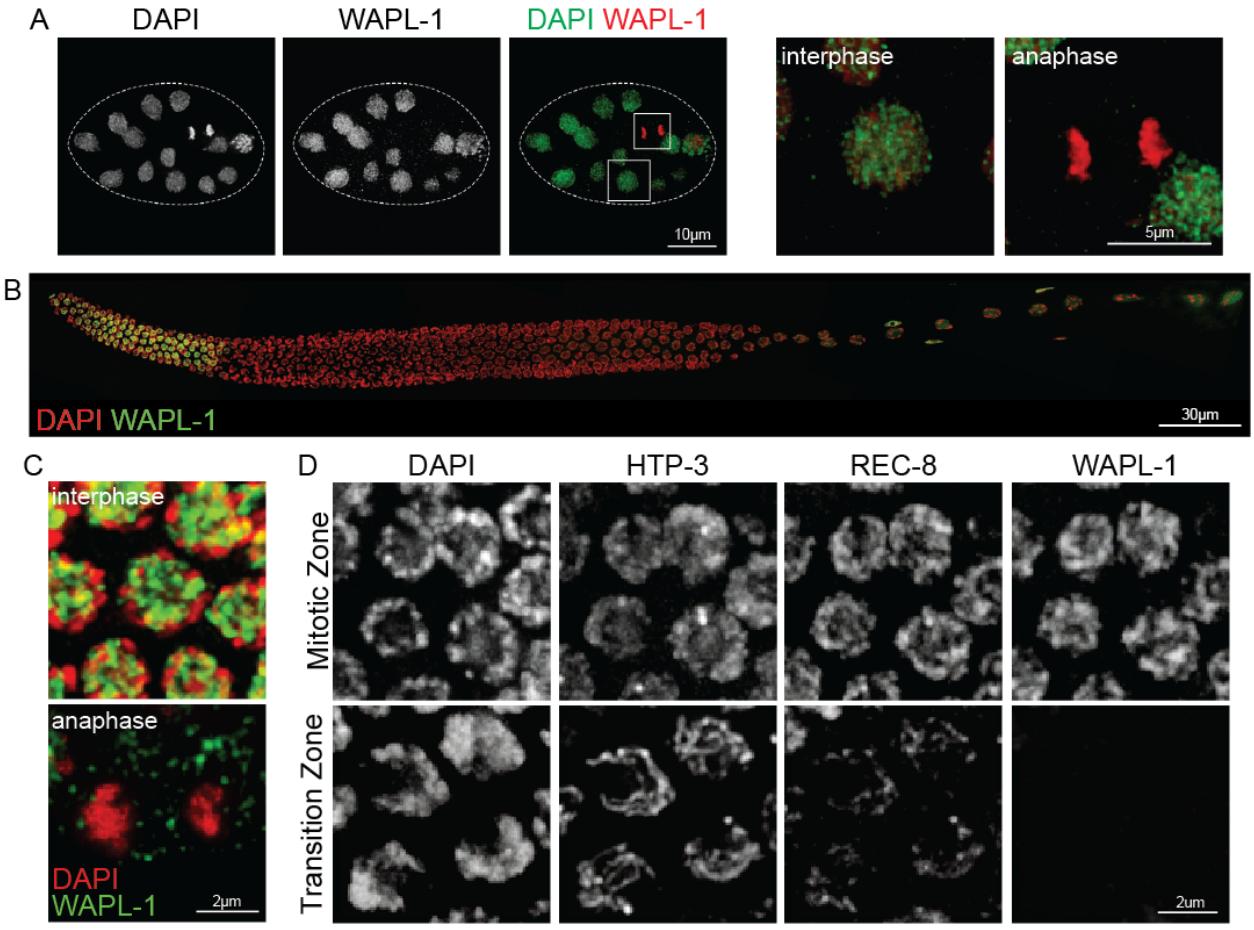

Figure 2.2 WAPL-1 localizes to nuclei in mitotically-dividing cells. In embryos, WAPL-1 is present during interphase. By anaphase, WAPL-1 is no longer present (A). In the germline, WAPL-1 localizes to the mitotic zone, disappears upon meiotic entry, but then returns within nuclei at diakinesis. WAPL-1 is also seen in the somatic sheath cells (B). Within the mitotic zone, WAPL-1 is present on chromatin at interphase, but dissipates by anaphase (C). The disappearance of WAPL-1 is coincident with meiotic entry as determined by HTP-3 and REC-8, which form axes upon meiotic entry (D).

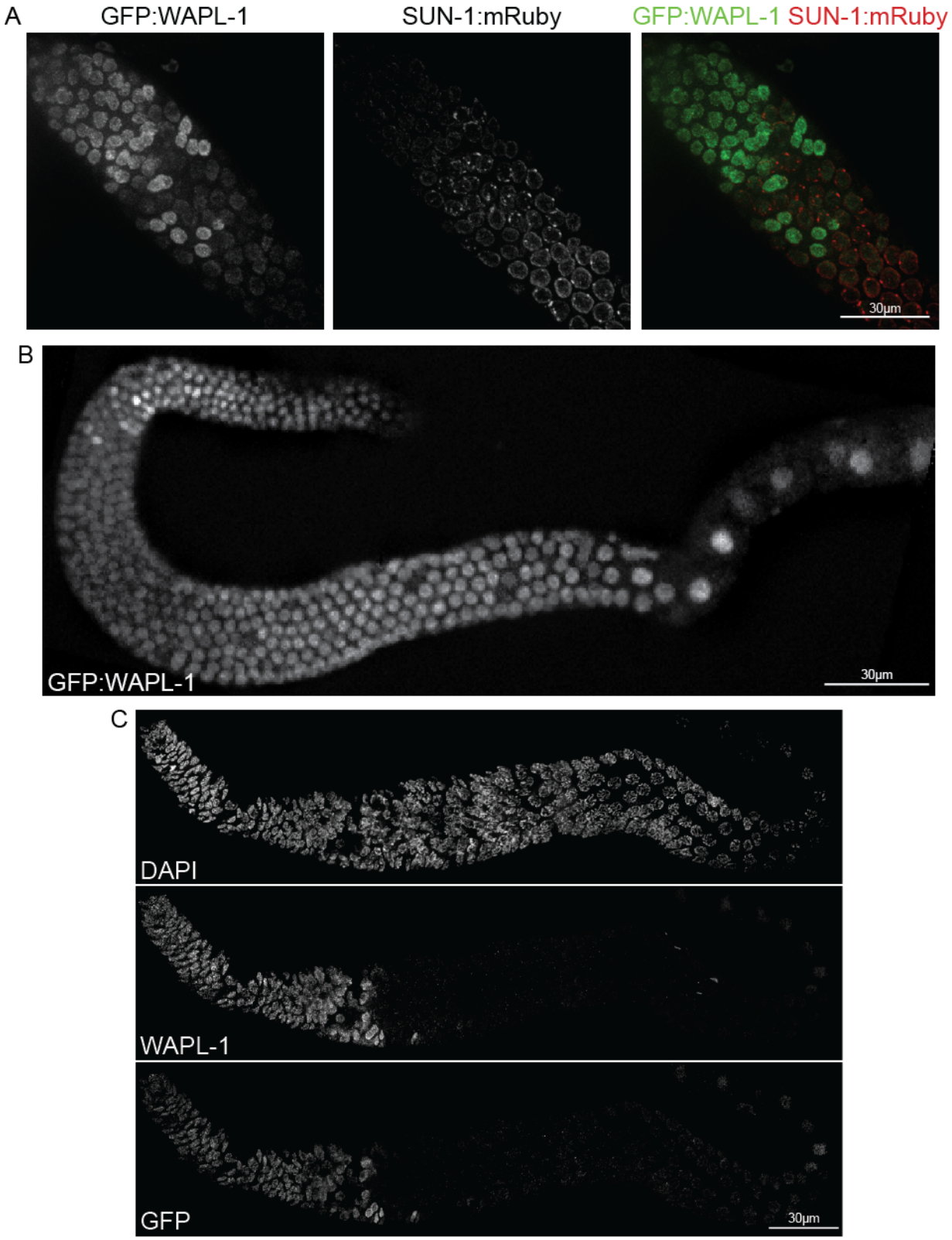

Figure 2.3 GFP:WAPL-1 is bright in the mitotic zone, but reduces in intensity upon meiotic entry as determined by SUN-1:mRuby foci (A). GFP:WAPL-1 is present throughout meiotic prophase (B). GFP:WAPL-1 in meiotic prophase is sensitive to immunofluorescence (C).

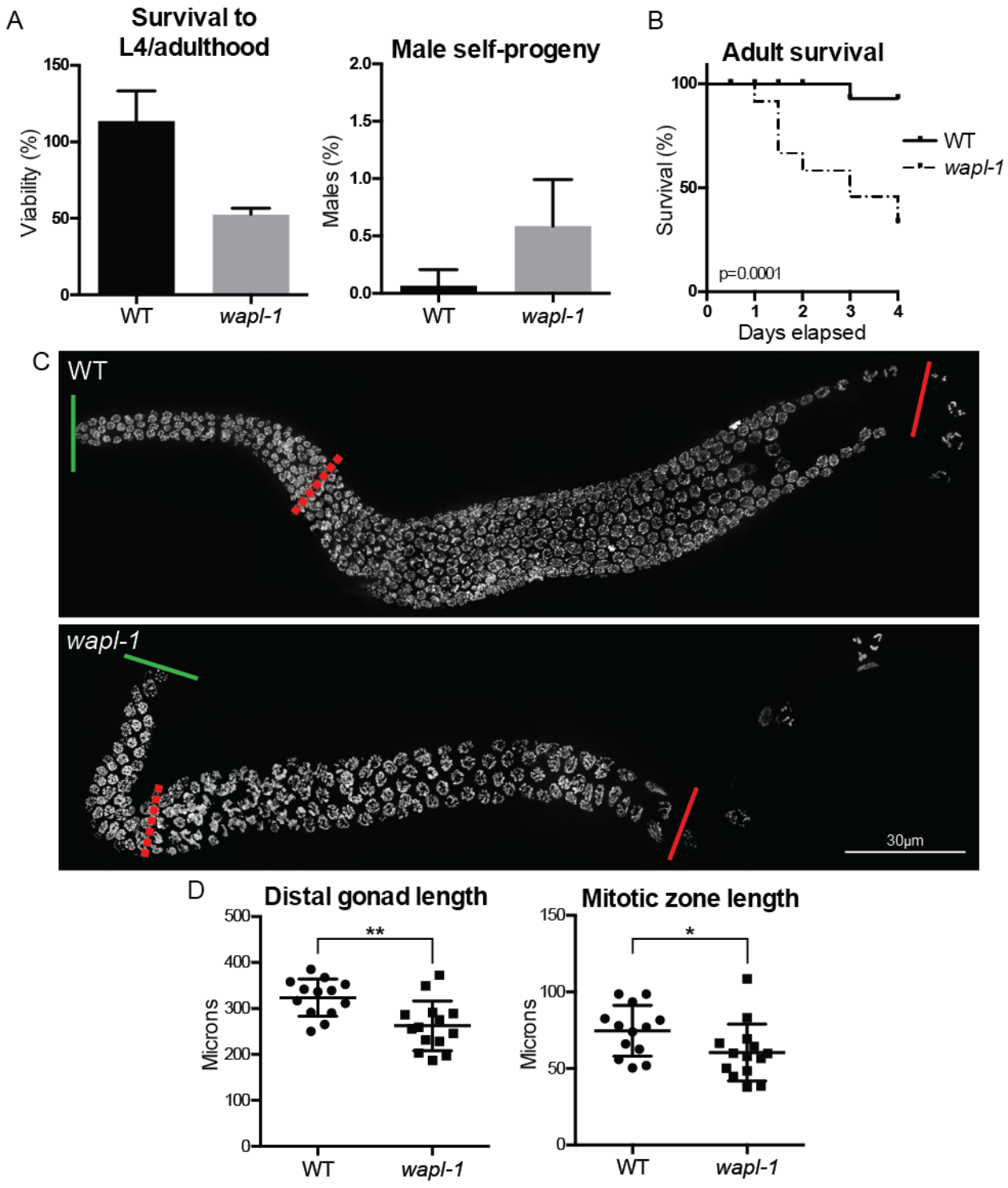

Figure 2.4 *wapl-1* display defects in embryonic viability, but only a mild increase in the incidence of males (A). *wapl-1* hermaphrodites have reduced survival due to bagging (B). *wapl-1* germlines are significantly shorter than wildtype, as is the length of the mitotic zone (C and D).

A

		Seq. cov.(%)
Cohesin	WAPL-1	60.30
	SMC-3	66.90
	HIM-1(Smc1)	66.10
	COH-1	42.40
	SCC-1	6.80
	SCC-3	45.00
DNA Repair	MRE-11	23.10
	RAD-50	14.90

B

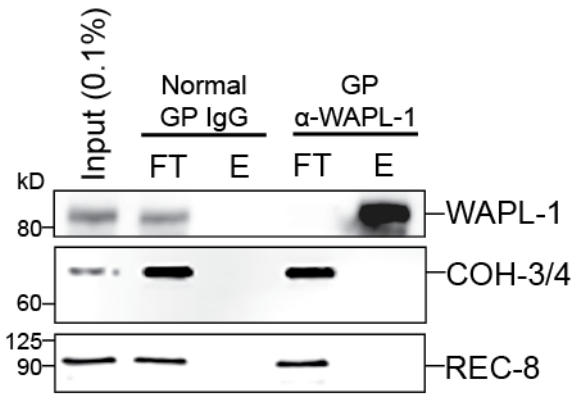

Figure 2.5 Immunoprecipitation of WAPL-1 followed by mass spectrometry identified the mitotic cohesin complex proteins and two proteins required for DNA damage repair (A). Immunoblot of immunoprecipitation with normal IgG and WAPL-1 identifies WAPL-1 in the elution, but not the meiotic kleisins. FT, flow through; E, eluate (B).

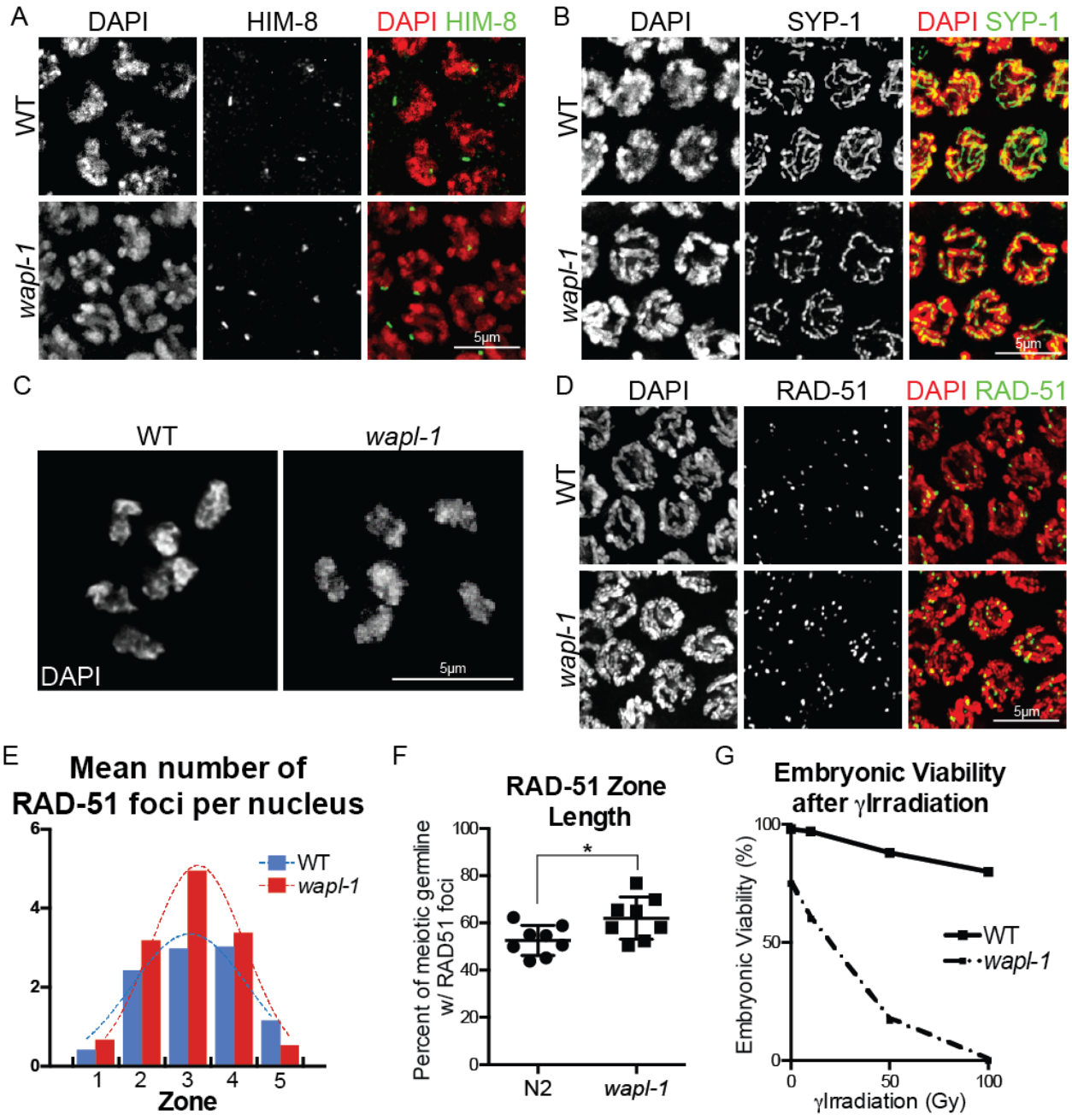

Figure 2.6 *wapl-1* displays no defects in pairing as assessed by the pairing center protein, HIM-8, which shows one focus per nucleus in wildtype and *wapl-1* (A). *wapl-1* displays no defects in synapsis when stained with the synaptonemal complex central element protein, SYP-1 (B). *wapl-1* worms have six DAPI-staining bodies at diakinesis corresponding to six homologous chromosomes (C). *wapl-1* displays an increase in DNA double-strand breaks as shown by RAD-51, which localizes to sites of double-strand breaks (D). Quantification of the average number of RAD-51 foci per nucleus over the entire RAD-51 positive zone displays an increase of breaks in *wapl-1* (E). The average length of the RAD-51 positive zone is significantly longer in *wapl-1* (F). *wapl-1* germlines are sensitive to γ-irradiation (G).

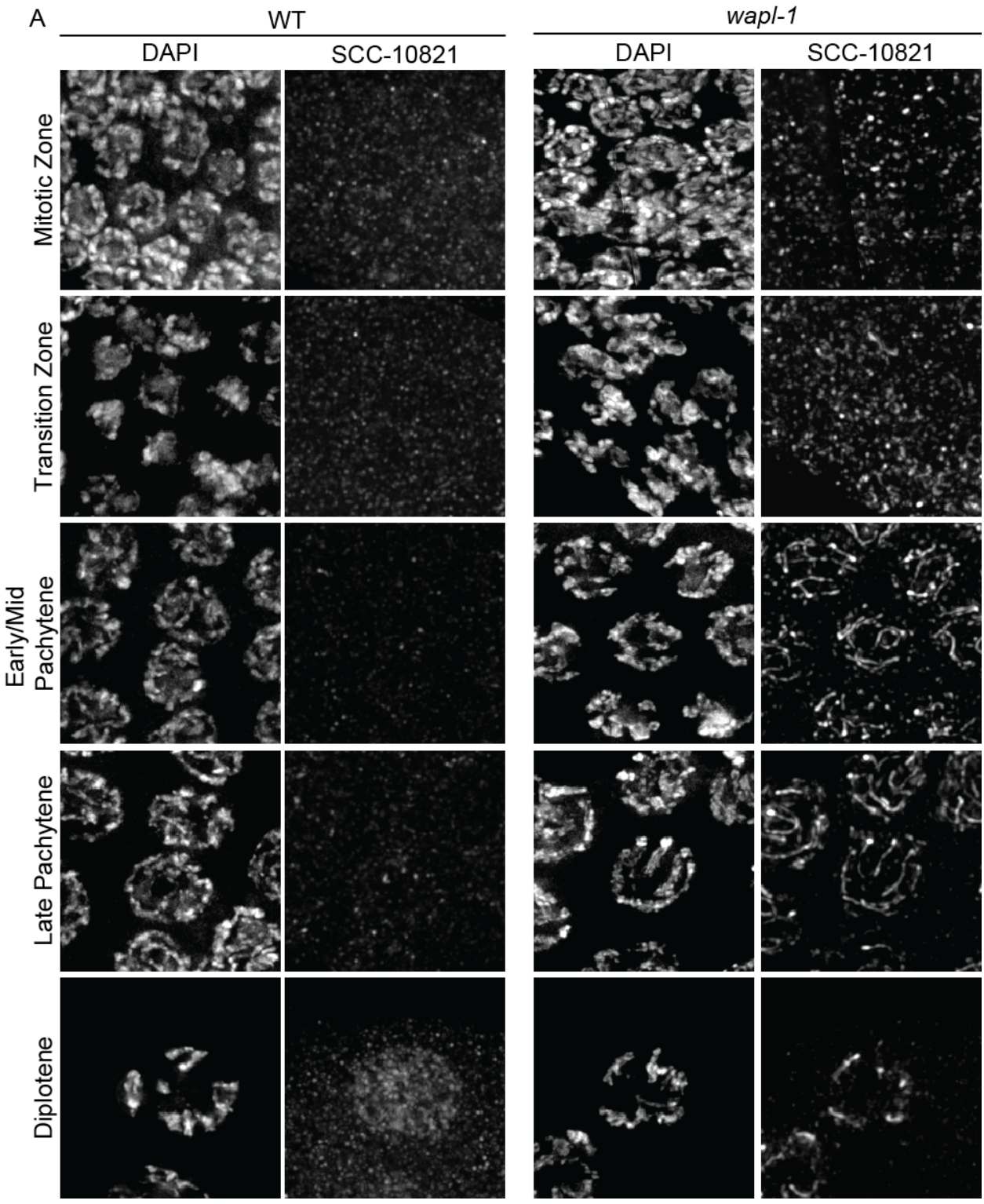

Figure 2.7 In wildtype, SCC-1 localization to chromosomes is faint, if present at all. In *wapl-1*, SCC-1 localizes robust to meiotic chromosome axes during pachytene and diplotene (A).

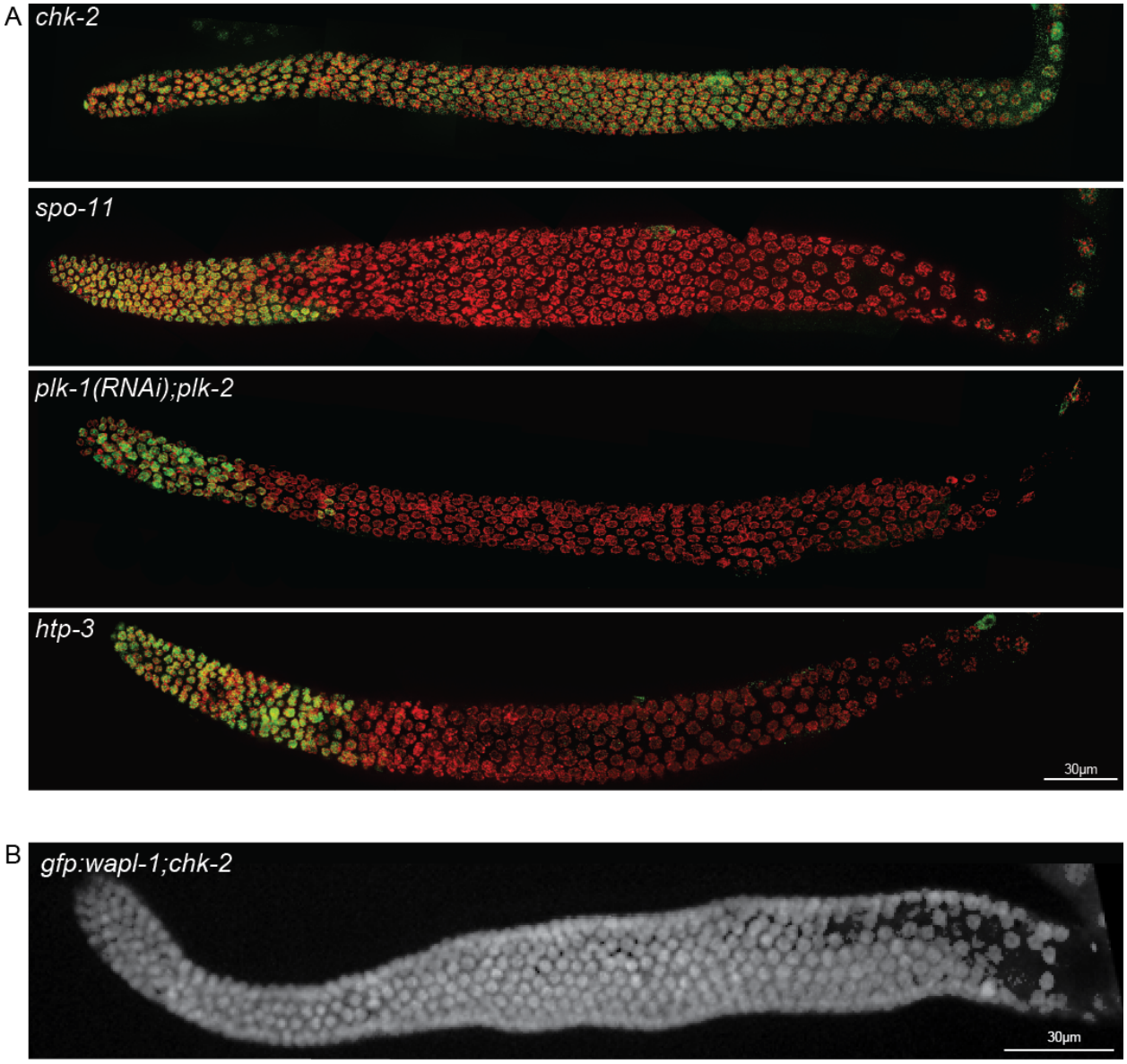

Figure 2.8 A candidate screen of known meiotic regulators identifies CHK-2 as being required for the regulation of WAPL-1 at the mitosis to meiosis transition (A). GFP:WAPL-1 in the *chk-2* background displays bright signal throughout the germline and no decrease in intensity upon meiotic entry (B).

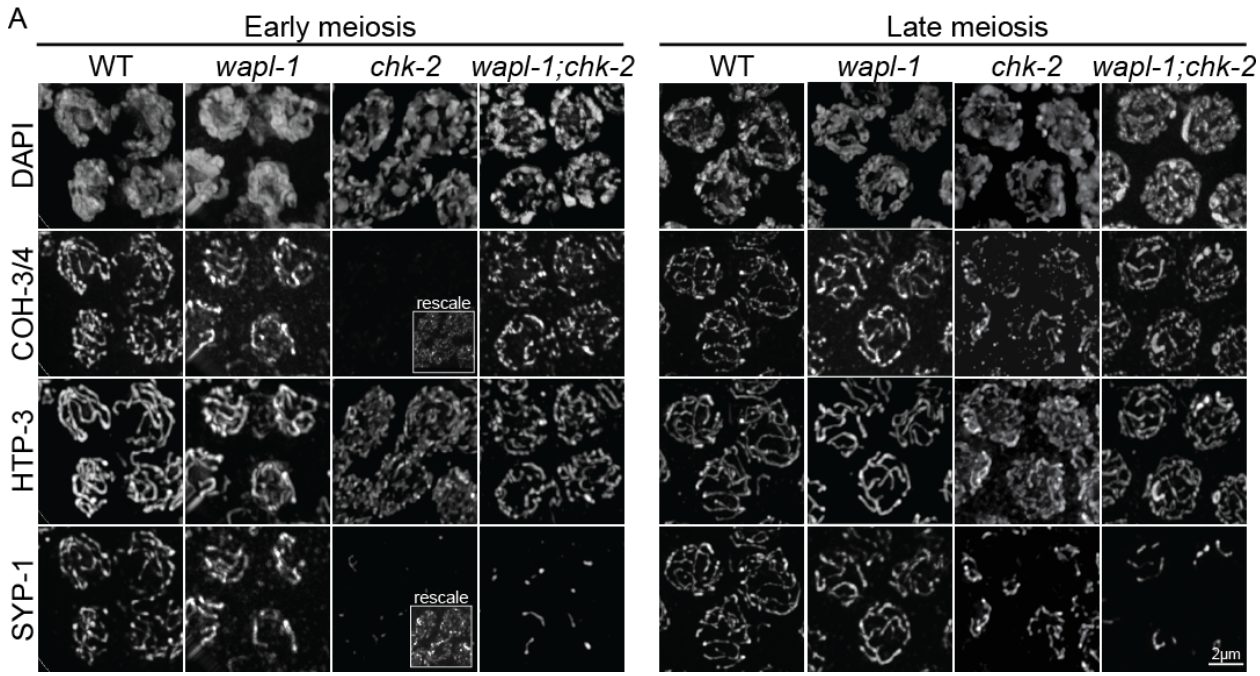

Figure 2.9 In early meiosis, *chk-2* displays defects in COH-3/4 loading, while HTP-3 loads normally. COH-3/4 axes are faint and only present where synapsis (SYP-1) has occurred. In late meiosis, COH-3/4 loading is more robust, but still located at sites where synapsis has occurred. In *wapl-1;chk-2*, COH-3/4 loads robustly in early meiosis, even at sites where synapsis has not occurred. At late meiosis, COH-3/4 loading is still robust.

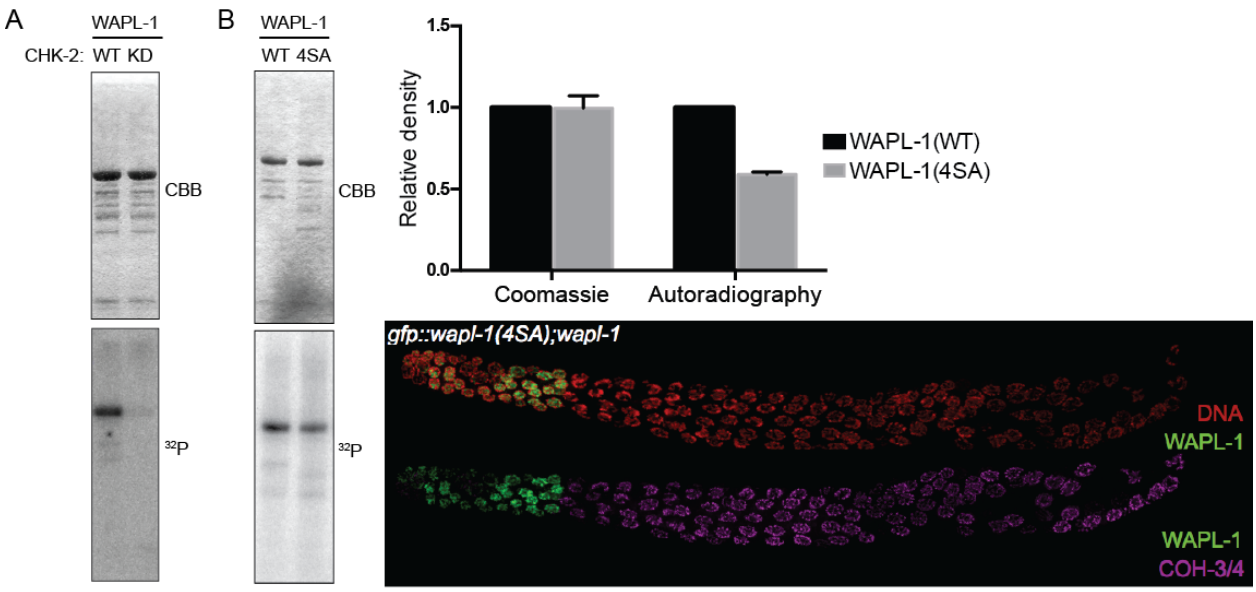

Figure 2.10 WAPL-1 is phosphorylated by enzymatically active CHK-2 *in vitro* (A). Mutation of serines in CHK-2 consensus motifs decreases phosphorylation of WAPL-1 by CHK-2 (B). Introduction of *gfp:wapl-1(4SA)* as the only copy of *wapl-1* displays wildtype localization in the germline and wildtype loading of COH-3/4 cohesin complexes (C).

Chapter 3: Achiasmate chromosome segregation

3.1 Introduction and summary of results

Mendelian genetics is composed of two laws. The first, the principle of segregation, states that two members of a gene pair segregate away from each other during the formation of gametes. The second is the principle of independent assortment, and states that genes for different traits assort independently of one another. These laws are based on the physical properties of the specialized cell division called meiosis.

During meiosis, homologous chromosome pairs must undergo crossover recombination in order to form physical linkages called chiasmata. These chiasmata allow for homologs to then bi-orient on the metaphase I microtubule spindle before the first meiotic chromosome segregation. During anaphase I, homologs segregate away from one another. The resulting sister chromatids then realign along the metaphase plate and undergo another segregation event. This time, sister chromatids segregate away from one another in a mitotic-like division. The result of meiosis is a gamete, or sex cell, which contains a single copy of the organism's genome.

When there is a defect in meiosis, chromosome missegregation can occur. Chromosome missegregation, or nondisjunction (NDJ), can occur for a variety of reasons. If homologous chromosomes fail to make a chiasma, they will enter Meiosis I as unpaired univalents and can be described as achiasmate. At the metaphase I plate, each univalent will act independently of the other and could be pulled to either pole of the microtubule spindle. As a result, both univalents could segregate to the same pole (Figure 1.2b). In fact, the laws of Mendelian genetics would state that the one homolog, now acting separately from the other homolog, has an equal change of moving to either pole. Since the other homolog experiences the same probability, Mendel's law states predicts a 50% chance of the univalent moving to opposite poles, a 25% chance of both moving to one of the poles, and a 25% chance of both moving to the other pole. In the cases when the homologs both move to the same pole, the resulting gamete is either diploid, containing two copies of the chromosome, or euploid, containing no copies of the chromosome. A progeny from such a gamete would, if combined with a wildtype gamete through fertilization, be aneuploid for that chromosome. Aneuploidy means that the cell or organism contains an extra copy or lacks a copy of a chromosome. Aneuploidy can be further differentiated as a monosmic, containing a single copy of a chromosome, or trisomic, containing three copies of a chromosome.

An interesting example of chromosome nondisjunction occurs in *C. elegans* due to the fact that it utilizes an XO sex determination system. A *C. elegans* population is primarily composed of self-fertilizing hermaphrodites (XX), which contain two copies of the sex (X) chromosome. Males (XO), which develop as a result of having a single copy of the X chromosome, can spontaneously arise in a population due to missegregation of the X chromosome and a euploid gamete. Triplo-X hermaphrodites (XXX), which contain three copies of the X chromosome, could also arise due to missegregation of the X chromosome and a diploid gamete. As a result, the *C. elegans* males and triplo-X hermaphrodites are examples of chromosomal aneuploidy. Interestingly, males and triplo-X hermaphrodites can be visually differentiated from XX hermaphrodites, allowing for rates of males and triplo-X hermaphrodites can be quantified to gauge X chromosome nondisjunction.

In the 1979 Genetics paper by Hodgkin *et al.,* the authors utilized the XO sex determination system to perform a screen identifying genetic mutants in which meiosis was

disrupted. This screen was named the HIM screen for *h*igh *i*ncidence of *m*ales. While quantifying the rates of males and triplo-X hermaphrodites during the screen, Hodgkin *et al.* noticed that males arose more frequently in a *C. elegans* population than triplo-X hermaphrodites. This excess of males over triplo-X hermaphrodites was true for the wildtype strain, as well as mutants which produced a *h*igh *i*ncidence of *m*ales (HIM) phenotype. By using X chromosome-linked genetic markers, Hodgkin *et al.* asserted that the excess of males over hermaphrodites was due to an excess of euploid over diploid gametes that. Based on their crosses, they also asserted that this excess was due to X chromosome nondisjunction at Meiosis I (Hodgkin et al., 1979).

Hodgkin *et al.* hypothesized that the excess of euploid over diploid eggs was due to an inherent difference between male and female meiosis. Male and female meiosis differs in that male meiosis produces four functional gametes and female meiosis produces only one. In the case of female meiosis, each segregation event results in half of the chromatin mass segregating into a polar body. Polar bodies are small, cell-like structures that do not develop into an organism and are eventually destroyed. Due to this process, one copy of each chromosome ends up in the polar body and will not be inherited by the progeny and one copy ends up in the egg and will be inherited. If achiasmate chromosomes preferentially segregated to the polar body, rather than the egg during Meiosis I, then an excess of euploid gametes would result. Interestingly, similar phenomena have been described in other organisms, including humans and mice.

In mice, it had long been observed that XO female mice gave rise to more XX daughters than XO daughters. It was ultimately demonstrated that these mice demonstrated preferential segregation of the achiasmate X chromosome to the oocyte rather than the polar body during Meiosis I. The frequency of this bias could explain the excess of XX daughters over XO daughters (LeMaire-Adkins and Hunt, 2000). Additionally, due to interest in screening oocytes to be used for *in vitro* fertilization, researchers have used comparative genomic hybridization on polar bodies to assess the ploidy of the oocyte. These studies have shown an excess of trisomy over monosomy in aneuploidy oocytes (Fragouli et al., 2011). Although the cases of skewed nondisjunction in mice and humans display an excess of trisomy over monosomy and not monosomy over trisomy as is seen in *C. elegans*, it does suggest that asymmetry during nondisjunction could be due to a conserved mechanism.

Which leads us to an interesting idea. Based on Mendel's laws, the probabilities of an achiasmate chromosome segregating to the polar body versus the oocyte are the same. However, if a chromosome or allele could preferentially segregate to the egg rather than the polar body, it could increase its frequency in the population more than what Mendel's laws of genetics would predict. In this chapter, I explore achiasmate chromosome segregation in the nematode *Caenorhabditis elegans* and whether or not there exists a case of nonMendelian chromosome segregation.

We hypothesized that if asymmetric chromosome segregation did exist during meiosis, it was most likely due to a conserved and active mechanism. Such a mechanism would act globally on all chromosomes, not just the X chromosome, and not be due to heterozygosity between homologs. In order to test this hypothesis and gain greater insight into chromosome segregation, the *f*ragment *l*ength *p*olymorphism (FLP) assay was developed. The FLP assay allows for chromosome copy number to be determined in single embryos in a high-throughput manner. In this assay, each copy of chromosome II was tagged with a DNA barcode. This barcode produced, by the polymerase chain reaction (PCR), a DNA fragment of a particular length. DNA from a single embryo can be prepared, PCR performed, and the presence of a tagged chromosome determined. The assay revealed asymmetric inheritance of autosomes in both wildtype and HIM

mutant backgrounds and the clear excess of monosomic over trisomic nondisjunction. Fluorescent tagging of chromosomes and direct visualization of female meiosis revealed achiasmate chromosomes segregating together to the polar body more often than the egg.

Upon concluding that asymmetric nondisjunction occurred for autosomes as well as the X chromosome, we set out to identify whether this asymmetry was a result achiasmate chromosomes segregating to the polar body more often than the oocyte. In order to do this, we tagged chromosome V and directly visualized the embryo after Meiosis I segregation. Through this process, we revealed that chromosome V more often segregates to the polar body than the oocyte.

Due to the sensitivity and robustness of the FLP assay, we embarked on a second analysis to test aged worms for meiotic defects. Many organisms experience a weakening of meiotic fidelity over time. This biological phenomenon is more commonly known as the meiotic age-effect. The meiotic age-effect has been characterized in a variety of organisms, including humans. In humans, the meiotic age-effect is characterized by both a decrease in overall fertility and an increase in the incidence of chromosome disorders. These chromosome disorders include Downs syndrome, which results from trisomy of chromosome 21. The increase in aneuploidy-based disorders drove research into meiotic fidelity over time. The FLP assay allowed sensitive and accurate detection of chromosome nondisjunction in aged worms. The assay revealed that *C. elegans* displays almost no meiotic age-effect and that the fidelity of chromosome segregation in aged worms was maintained in part by the apoptotic pathway.

3.2 Results

Development of the *f*ragment *l*ength *p*olymorphism assay

In order to detect autosomal nondisjunction, the assay used was required to have three characteristics. First, the assay would have to be incredibly sensitive and able to be performed on single *C. elegans* embryos. Second, since we suspected autosomal nondisjunction to occur at very low rates, results from a single embryo would have to be accurate and unambiguous. Third, the assay would have to be high-throughput as testing of nondisjunction rates would be done on large populations.

In their 2009 paper, Severson *et al.* devised a way in which to tag individual homologs and determine whether or not the particular homolog was inherited by an embryo. Since the assay tagged individual homologs, it could also show how many copies of the chromosome was present in the embryo. To tag homologs, Severson *et al.* found previously characterized alleles of the gene, *sup-9*. These alleles introduced restriction fragment length polymorphisms – in one allele, a restriction site existed, while in the other it did not. As a result, amplification of the region containing the allele and restriction digestion would result in one of two possible DNA fragment sizes. Loss of *sup-9,* which encodes one of forty-four potassium channel subunits, does not result in any fertility, developmental, or locomotion phenotypes. In theory, the alleles could be used and chromosome segregation monitored without any affect on chromosome segregation (Severson et al., 2009).

Three issues complicated use of the RFLP assay to detect asymmetric chromosome segregation. First, PCR amplification of the region surrounding the *sup-9* alleles was inconsistent. Only occasionally did the PCR reaction result in a robust amplification product,

most likely due to the small amount of DNA in the embryo. Second, restriction digestion after PCR reaction was both time-consuming and introduced another error-prone step that reduced the efficiency of the assay. Lastly, the RFLP assay revealed that embryos inherited one of the *sup-9* alleles more often than the allele. This strange observation, which conflicted with Mendel's law of genetics, was also in contrast to our hypothesis that the mechanism causing asymmetric chromosome segregation acted globally on all achiasmate chromosomes and was not due to heterozygosity between homologs. To circumvent these issues, we set out to redesign the RFLP assay.

We made two changes to the RFLP assay. The first change to the RFLP assay replaced the *sup-9* alleles with engineered DNA "barcodes". The barcodes are actually short, engineered DNA sequences. Each barcode is 359 basepairs long and made up of random DNA sequence that does not encode regulatory elements or open reading frames. Each barcode contains the same primer binding sequence that binds the same primer; however, in each barcode the primer binding sequence is moved so as to produce a different sized PCR product (Figure 3.1a). Due to this change, the RFLP assay was renamed the *f*ragment *l*ength *p*olymorphism (FLP assay).

The second change was to replace the single PCR reaction with nested PCR. Nested PCR, in which a second PCR reaction is performed using the first PCR product as a template, reliably produced a robust PCR product from a single embryo. Now, the FLP barcodes individually tagging a chromosome could be "read" by two PCR reactions and the results "printed" by DNA gel electrophoresis (Figure 3.1a). The strength of the nested PCR reactions did introduce a complication, which was that if any contaminating DNA existed in the reaction, bright non-specific bands would appear in the DNA gel. As a result, care was taken to sterilize tools and reagents by inactivation of contaminating DNA using UV irradiation.

The FLP assay required three DNA barcodes. These DNA barcodes were constructed and named FLP1, FLP2, and FLP3. Within each sequence, the primer binding sequence is underlined.

>FLP1
CTCGAGTCGCTCAGGCGCAATCACGAATGAATAACGGTTTGGTTGATGCGAGTGATTTTGATGA
CGAGCGTAATGGCTGGCCTGTTGAACAAGTCTGGAAAGAAATGCATAAACTTTTGCCATTCTCA
CCGGATTCAGTCGTCACTCATGGTGATTTCTCACTTGATAACCTTATTTTTGACGAGGGGAAAT
TAATAGGTTGTATTGATGTTGGACGAGTCGGAATCGCAGACCGATACCAGGATCTTGCCATCCT
ATGGAACTGCCTCGGTGAGTTTTCTCCTTCATTACAGAAACGGCTTTTTCAAAAATATGGTATT
GATAATCCTGATATGAATAAATTGCAGTTTCAACTAGT

>FLP2
CTCGAGGCATAAACTTTTGCCATTCTCACCGGATTCAGTCGTCACTCATGGTGATTTCTCACTT
GATAACCTTATTTTTGACGAGGGGAAATTAATAGGTTGTATTGATGTTGGACGAGTCGGAATCG
CAGACCGATACCAGGATCTTGCCATCCTATGGAACTGCCTCGGTGAGTTTTCTCCTTCATTACA
GAAACGGCTTTTTCAAAAATATGGTATTGATAATCCTGATATGAATAAATTGCAGTTTCATTTG
ATGCTCGATGAGTTTTTCTAATCAGAATTGGTTAATTGGTTGTAACACTGGCAGAGCATTACGC
TGACTTGACGGGACGGCGCAAGCTCATGACCAACTAGT

>FLP3
CTCGAGGATGTTGGACGAGTCGGAATCGCAGACCGATACCAGGATCTTGCCATCCTATGGAACT
GCCTCGGTGAGTTTTCTCCTTCATTACAGAAACGGCTTTTTCAAAAATATGGTATTGATAATCC
TGATATGAATAAATTGCAGTTTCATTTGATGCTCGATGAGTTTTTCTAATCAGAATTGGTTAAT

TGGTTGTAACACTGGCAGAGCATTACGCTGACTTGACGGGACGGCGCAAGCTCATGACCAAAAT
CCCTTAACGTGAGTTACGCGTCGTTCCACTGAGCGTCAGACCCCGTAGAAAAGATCAAAGGATC
TTCTTGAGATCCTTTTTTTCTGCGCGTAATCTACTAGT

Barcodes were introduced into the *C. elegans* genome using the transposon-based integration system, MosSci. By using the MosSci system, barcodes could theoretically be integrated into any of the six *C. elegans* chromosomes. For our purposes of monitoring segregation of an autosome, we began by integrating the barcodes into chromosome II.

The *f*ragment *l*ength *p*olymorphism assay

The *f*ragment *l*ength *p*olymorphism (FLP) assay is a sensitive, accurate, and high throughput test that can detect if an embryo received one, both, or neither copy of a chromosome from one of its parents. Detection of a chromosome is possible through DNA barcodes that produce PCR products of unique lengths and a specific mating scheme.

To begin the assay, the homozygous FLP1 strain is crossed to the homozygous FLP3 strain, producing transheterozygous FLP1/FLP3 progeny. A transheterozygous FLP1/FLP3 animal is then crossed to a homozygous FLP2 animal. Single embryos from this cross can be analyzed for chromosome inheritance by lysing the embryo, performing nested PCR, and running the PCR product on an agarose gel. If the cross took place, the PCR will produce a gel band corresponding to FLP2. The FLP2 gel band acts as an internal control and shows that the PCR reaction worked. If the chromosome containing FLP1 was inherited, another gel band corresponding to FLP1 will be produced. If the chromosome containing FLP3 was inherited, yet another gel band corresponding to FLP3 will be produced. If a nondisjunction event took place in the heterozygous animal and a diploid gamete with two copies of the chromosome was produced, the PCR reaction will produce bands corresponding to both FLP1 and FLP3, in addition to FLP2. If a nondisjunction event produced a euploid gamete containing neither copy, then the PCR reaction will produce only a single band corresponding to FLP2 (Figure 3.1b).

A number of variations can easily be introduced to the FLP assay. For example, chromosome segregation can be assayed in either males or hermaphrodites without any additional crosses. Additionally, the barcodes can be crossed into mutant backgrounds to test for changes in chromosome segregation as compared to wildtype. Lastly, temperature, age, food source, and any number of environmental changes can be made to the experimental setup.

While the FLP assay is a powerful tool, care must be taken to ensure accurate results. A trisomic false positive can be introduced if two embryos are accidentally assayed together. Since this assay is often performed on an entire brood, single embryos can be picked into single wells of a 96-well plate. If two embryos are picked into the same well and one embryo inherited FLP1 while the other inherited FLP3, then the subsequent PCR reaction will identify the well as containing a trisomic embryo. While such false positives can be detrimental, these errors can be minimized by vigilant sample preparation.

Autosomal nondisjunction results in an excess of monosomy over trisomy

In *C. elegans,* it has long been known that nondisjunction of the X chromosome results in an excess of males (XO) over triplo-X (XXX) hermaphrodites. We hypothesized that this bias

was due to a global mechanism acting on all achiasmate chromosomes to cause asymmetric nondisjunction. If true, then autosomal nondisjunction would also produce an excess of monosomy over trisomy events. To test this hypothesis, we used the FLP assay to monitor chromosome segregation of chromosome II in the hermaphrodite.

We expected that the FLP assay, performed under standard laboratory conditions and without the introduction of additional genetic mutations, would detect very few nondisjunction events. This was based on the fact that the wildtype laboratory *C. elegans* strain produces very few males (<0.1%), which arise from X chromosome nondisjunction, and few dead eggs (<0.1%), which arise from autosomal nondisjunction. As expected, the FLP assay identified very few (14/1282) nondisjunction events, for a nondisjunction rate of 1% (Figure 3.2a). While this rate is greater than expected, it is most likely due to oversampling of embryos from aged worms and will be explained later. Ultimately, the rate of detectable nondisjunction demonstrated that trisomy false positives were negligible. Also, the FLP assay revealed equal inheritance of FLP1 and FLP3 demonstrating that neither barcode introduced a chromosome segregation defect.

A very low nondisjunction rate means comparing monosomy and trisomy is difficult and error-prone, since a single false positive can dramatically skew rates of trisomy. To bypass this problem, we genetically increased the number of nondisjunction events. *zim-1* encodes the pairing center protein required for pairing of chromosomes II and III (Phillips and Dernburg, 2006). Based on the number of DAPI bodies during diakinesis, it is expected that the chromosome II and III will enter the meiotic segregations as achiasmate chromosomes at a rate of 60-90%. In the *zim-1* mutant background, 48% (197/408) of embryos inherited either FLP1 or FLP3 from the hermaphrodite (Figure 3.2a). Conversely, 52% (211/408) of embryos inherited either both FLP1 and FLP3, or neither FLP1 nor FLP3. In the cases of proper segregation, FLP1 and FLP3 were inherited at equal rates suggesting no synthetic chromosome segregation defects due to combining the barcodes with *zim-1* (Figure 3.2b). Given the rates of proper segregation and nondisjunction, we can extrapolate that essentially all copies of chromosome II entered the first meiotic segregation as achiasmate chromosomes.

In order to assay asymmetric chromosome segregation, we looked specifically at the cases of nondisjunction. In these cases, 77% (163/211) of embryos inherited neither FLP1 nor FLP3, while 23% (48/211) of embryos inherited both FLP1 and FLP3 (Figure 3.2c). The excess of chromosome II monosomy over trisomy as detected by the FLP assay is similar to the excess of X chromosome monosomy (males) over trisomy (triplo-X hermaphrodites). Based on this data, we concluded that autosomes experience the same asymmetric nondisjunction first described of the X chromosome. Such evidence supports a model in which a global mechanism acts on all chromosomes to bias missegregation of chromosomes.

We hypothesized that the asymmetric nondisjunction identified by the FLP assay was due to the preferential segregation of achiasmate chromosomes to the polar body rather than the egg during the first meiotic segregation. If such a bias existed, then there would be a higher percentage of euploid embryos than diploid embryos after nondisjunction, which would then explain the excess of monosomy over trisomy. In order to test this hypothesis, we set out to directly visualize achiasmate chromosomes at the first meiotic segregation and determine whether a bias towards the polar body over the egg existed.

In order to directly visualize achiasmate chromosomes, we required a system with which to tag chromosomes. We turned to the LacI/LacO system. In this system, Lac operator DNA repeats are integrated into the genome and can bind the LacI protein. The LacI protein can be fused to a fluorescent protein like GFP, or visualized by immunofluorescence with an antibody

recognizing the LacI protein (Aaron Severson, personal communication). We began by testing *C. elegans* strains in which 256 LacO repeats were integrated into a chromosome and a *lacI-gfp* expressing transgene was integrated into the genome. Unfortunately, due to low expression of the transgene coupled with the size of the LacO integration, we could not visualize by live imaging or immunofluorescence the LacI/LacO tag. To solve this issue, we took advantage of a *C. elegans* strain in which a large LacO array had been integrated into chromosome V. While the array was of an undetermined size and its location on the chromosome not known, its size made visualization by fluorescence microscopy possible. Next, rather than using a *lacI-gfp* transgene, we turned to a system in which fixed tissues are treated with recombinant LacI-GFP protein. The LacI-GFP protein binds to LacO repeats in the fixed tissue and can, in turn, be visualized with antibody recognizing GFP. By combining the LacO array and recombinant LacI-GFP protein, we were able to reproducibly tag chromosome V and visualize tagged chromosomes in the germline and embryos (Figure 3.3a).

To follow the segregation of chromosome V during Meiosis I, the visualization of the meiotic segregations was required. Since the LacO/LacI-GFP system required fixed specimens, we decided to analyze embryos at Meiosis II for segregation of chromosome V at Meiosis I. Meiosis II can easily be identified in *C. elegans* as DAPI-staining should reveal a small, dense DAPI mass located in the polar body, and another mass of sister chromatids within the embryo. These sister chromatids may be aligned along the metaphase II in the characteristic rosette pattern, or segregating away from one another as in anaphase II. In either case, the location of chromosome V homologs can be determined by the location of LacI-GFP foci. If homologs segregated properly, then one LacI-GFP focus will be located in the polar body and another located on a sister chromatid in the embryo (Figure 3.3a). If nondisjunction occurred, one focus or two foci will be seen either in the polar body or the embryo (Figure 3.3b). Additionally, the existence of asymmetric nondisjunction can be scored. Nondisjunction of chromosomes to the polar body would produce a euploid gamete and monosomic embryo, while nondisjunction of chromosomes to the embryo would produce a diploid gamete and trisomic embryo.

Chromosome V segregation was first analyzed using the LacO/LacI-GFP without any additional genetic mutants. As expected, analysis of 22 embryos revealed no nondisjunction events (Figure 3.3c). In order to increase the rate of nondisjunction, the use of a genetic mutant was used. *zim-2,* like *zim-1*, encodes a pairing center protein that is required for pairing of a particular chromosome. In the *zim-2* background, chromosome V homologs cannot pair. Based on our knowledge of *zim-2* and the number of DAPI-staining bodies during diakinesis, we expected at least 70% of chromosome V homologs would enter meiosis as achiasmate chromosomes (Phillips and Dernburg, 2006). In the *zim-2* background, analysis of 75 embryos revealed 11 nondisjunction events, or a nondisjunction rate of 15% (Figure 3.3c). A nondisjunction rate of <50% suggests that, as expected based on DAPI-staining bodies, a certain percentage of chromosome V homologs were able to pair and form crossovers. Even so, a nondisjunction rate of 15% is lower than expected as it implies that only 30% of chromosome V homologs lacked a crossover, which is much lower than DAPI-staining bodies would suggest. The low rate of nondisjunction could be explained by a mistake in the quantification of DAPI-staining bodies, a mechanism that segregates achiasmate chromosomes, or a systematic error in our assay to identify all nondisjunction events.

Nevertheless, the 11 nondisjunction events were scored for nondisjunction to the polar body or to the embryo. As our hypothesis predicted, nondisjunction to the polar body occurred at a greater frequency than nondisjunction to the embryo. The 64% frequency of nondisjunction to

the polar body would produce an excess of euploid gametes over diploid gametes, and ultimately an excess of monosomy over trisomy (Figure 3.3d).

The LacO/LacI-GFP system does have limitations. The first limitation is that, while care was taken to score Meiosis II embryos and properly identify the polar body, it is possible that a polar body could be mislabeled as no markers existed to unambiguously label the polar body. Second, it is possible that if LacI-GFP tagging of either the polar body or embryo failed, then a nondisjunction event would be erroneously counted; however, the lack of nondisjunction in the wildtype background suggests that LacI-GFP tagging was efficient. Third, since cytokinesis was not validated, it is possible that a nondisjunction event could theoretically be corrected as lagging or late chromosomes can be visualized during meiosis. If this occurred, then the nondisjunction events would be artificially inflated. Nevertheless, taking the FLP data together with direct visualization of chromosome V nondisjunction, we concluded that asymmetric nondisjunction does exist in *C. elegans*. Our data supports a model in which an active mechanism preferences nondisjunction to the polar body and that this mechanism acts globally on all achiasmate chromosomes.

Apoptosis maintains meiotic fidelity and oocyte quality in aged worms

In order to assay asymmetric nondisjunction, we increased the number of nondisjunction by utilizing a genetic background that would prevent the formation of crossovers on chromosome II. We wondered if there were other, non-genetic ways in which to increase the nondisjunction rate. Our interest moved to the meiotic age-effect. The meiotic age-effect is the biological phenomenon in which women experience a decrease in fertility as they age. This decrease in fertility is accompanied by increases in the probability of spontaneous abortion in the mother and chromosomal disorders in the children. As a result, many researchers hypothesize that the meiotic age-effect is due, at least in part, to an increase in meiotic defects.

We hypothesized that the meiotic age-effect was a conserved phenomenon and could be identified in *C. elegans* given a tool sensitive and flexible enough to test progeny from aged worms. Additionally, previous research had described age-related meiotic defects in *C. elegans* and suggested that *C. elegans* could be used to study the meiotic age-effect (Luo et al., 2010). Given the development of the FLP assay, we set out to assay chromosome nondisjunction in aged worms to test whether the meiotic age-effect existed in *C. elegans* and, if so, whether the nondisjunction would still demonstrate an asymmetric bias towards monosomy over trisomy.

To test chromosome segregation in aged worms, age-matched FLP1/FLP3 hermaphrodites were crossed to young FLP2 males. After two days, the FLP2 males were removed from plates. The hermaphrodites were followed over time and embryos gathered every day until the hermaphrodite stopped producing embryos. In general, hermaphrodites laid fertilized embryos for seven to eight days. Over this time, the rate of laid embryos decreased, which meant there were many more embryos laid by young hermaphrodites than old. In order to accurately compare chromosome segregation from young and old hermaphrodites, we over-sampled embryos laid by older hermaphrodites. To simplify analysis, embryos laid were placed into one of three bins based on the age of the hermaphrodite. The bins were ‘early’ (days 1-2), ‘middle’ (days 3-5), and ‘late’ (days 6-8).

In the FLP strains, the FLP assay revealed a very low nondisjunction rate in early (0.58%), middle (1.04%), and late (1.92%) embryos (Figure 3.4a). Interestingly, although the

rates were very low, there was a slight increase over time in the nondisjunction rate. Based on this data, we concluded that while *C. elegans* show a subtle trend towards chromosome nondisjunction over time, that the rates were low enough so as not to be considered a true meiotic age-effect. Given the very small number of nondisjunction events in early (n=3), middle (n=4), and late (n=7) embryos, as well as the possibility of error generating false positives, we determined that it would not be biologically relevant to compare the rates of monosomy and trisomy in these embryos.

Given the low nondisjunction rate in the aged FLP strains, we analyzed chromosome nondisjunction in aged *zim-1* worms since the rate of nondisjunction would be greater. Following the same protocol as before, embryos were collected from *zim-1* hermaphrodites every day until the hermaphrodite stopped laying fertilized eggs. Like in the FLP strains without additional genetic mutants, *zim-1* hermaphrodites laid fertilized eggs for seven to eight days. As a result, embryos were binned into early (days 1-2), middle (days 3-5), and late (days 6-8), as before. In the *zim-1* background, the nondisjunction rate did not increase over time (Figure 3.4a). Based on our data and knowledge of *zim-1*, there are two potential reasons why the nondisjunction rate did not increase. The first reason is that the very slight increase in chromosome nondisjunction seen in the FLP strains is just too low to be detected by the assay in the *zim-1* background. The second reason is that the very slight increase in chromosome nondisjunction seen in the FLP strains is due to a slight increase in achiasmate chromosomes and, since in the *zim-1* background essentially all copies of chromosome II are achiasmate, there is no way to increase more.

After the FLP assay revealed little to no age-effect, we utilized a second assay to measure whether a meiotic age-effect really existed in *C. elegans*. To do this, we stained chromosomes in diakinesis with DAPI. During diakinesis, if meiotic prophase has proceeded normally, six DAPI-staining bodies can be seen corresponding to the six paired homologous chromosomes of *C. elegans*. If crossover formation failed to take place, then more than six DAPI-staining bodies will be counted at diakinesis. We hypothesized that if a meiotic age-effect existed, then aged germlines will be defective in pairing, synapsis, and crossover formation. This would then result in more than six DAPI-staining bodies in aged germlines. To test this hypothesis, we compared diakinesis DAPI-staining bodies from early (1-day post-L4) and late (7-day post-L4) hermaphrodites. Comparison between the timepoints revealed only a slight increase in the percentage of nuclei with 7 or more DAPI-staining bodies. Based on this data and results from the FLP assay, we concluded that there existed little to no meiotic age-effect in *C. elegans* hermaphrodites.

Given the severity of the meiotic age-effect in other organisms and previous data on the meiotic age-effect in *C. elegans*, we were surprised that the FLP assay detected little to no increase of nondisjunction in aged worms. Given that *C. elegans* experiences many other phenotypes of aging, we hypothesized that a mechanism existed to specifically protect meiosis from aging.

It has been shown that apoptosis, or programmed cell death, is present in the *C. elegans* germline to cull defective nuclei (Bhalla and Dernburg, 2005; Gartner et al., 2008). This model is based on research demonstrating that triggering of meiotic checkpoints by defects in meiosis increases germline apoptosis. Based on this, we hypothesized that apoptosis protects the meiotic program from defects associated with aging. To test this hypothesis, we performed the FLP assay in a genetic background that abrogates apoptosis. If our hypothesis was correct, the FLP assay should reveal an increase in nondisjunction in aged worms.

To abolish apoptosis, we utilized the *ced-4* genetic background, as it has previously been shown that *ced-4* encodes a protein that is required for the *C. elegans* apoptotic pathway. *ced-4* hermaphrodites containing FLP1 and FLP3 barcodes were crossed to wildtype FLP2 males. After two days, the FLP2 males were removed from the hermaphrodite as had been done previously. Embryos were collected every day for FLP analysis until the hermaphrodite stopped laying fertilized embryos. Introduction of the *ced-4* genetic background resulted in a shortening of days in which hermaphrodites laid fertilized embryos. Rather than seven or eight days, *ced-4* hermaphrodites laid eggs for five to six days. As a result, embryos were binned into early (days 1-2), middle (days 3-4), and late (days 5-6). The FLP assay revealed that, as *ced-4* hermaphrodites aged, the rate of nondisjunction increased (Figure 3.4a). Based on this data, we concluded that apoptosis does protect aged worms from experiencing high levels of nondisjunction and a meiotic age-effect.

We were curious as to whether the increase in nondisjunction rates over the reproductive lifespan of the worm was due to defects in crossover formation or another factor. To determine whether *ced-4* mutants displayed defects in crossover formation, diakinesis nuclei were examined for the number of DAPI-staining bodies. First, we compared the number of DAPI-staining bodies between wildtype and *ced-4* hermaphrodites. Consistent with *ced-4* hermaphrodites having defects in crossover formation, a greater number of diakinesis nuclei had 7 or more DAPI bodies in *ced-4* mutants than in wildtype worms (Figure 3.4b). Second, we compared the number of DAPI-staining bodies in early (1-day post-L4) and late (5-day post-L4) *ced-4* hermaphrodites. These counts displayed a mild increase over the reproductive lifespan of the worm (Figure 3.4b). Given that the percentage of *ced-4* nuclei with greater than 7 DAPI-staining bodies could not account for the nondisjunction rates seen in *ced-4* mutants as determined by the FLP assay, we hypothesized that another factor was affecting nondisjunction.

It had previously been shown that apoptosis was required to maintain oocyte quality in *C. elegans* (Andux and Ellis, 2008). While performing the FLP assay, we noticed that in the *ced-4* genetic background, there was an increase in the number of misshapen embryos (Figure 3.4c). These embryos had clearly been fertilized, as they were reflective and not dull in color; however, rather than being large and oval, they were small and round shaped. Additionally, the rate of misshapen embryos increased in aged *ced-4* worms. We wondered whether the other genetic backgrounds had also produced misshapen embryos. Analysis of the wildtype and *zim-1* FLP strains revealed that while they both produced a very low rate of misshapen embryos and wildtype, but not *zim-1* showed an increase in misshapen embryos in aged worms (Figure 3.4c). It is unclear why *zim-1* did not display an increase in misshapen embryos over time. It could be due to the fact that with the small percentage of misshapen embryos, too few embryos were assayed.

We wondered whether a causative link existed between chromosome nondisjunction and misshapen embryos since the rate of both was increased in aged worms. To test this, we analyzed misshapen embryos for chromosome segregation using the FLP assay. In order to have a large sampling of misshapen embryos, we performed the FLP assay in the *ced-4* background, in addition to the wildtype and *zim-1* backgrounds. Analysis revealed that the rate of nondisjunction in misshapen embryos was 50% compared to a nondisjunction rate of 10% overall. The nondisjunction rates were also higher in misshapen embryos than the overall nondisjunction rates in wildtype and *zim-1* (Figure 3.4d). Given the rate of nondisjunction in misshapen embryos, we concluded that while there may be a correlation between chromosome nondisjunction and oocyte morphology, chromosome nondisjunction is not the sole cause of misshapen embryos. Therefore,

without protection from apoptosis, *C. elegans* would suffer from two aspects of the meiotic age effect, an increase in chromosome nondisjunction and defects in embryo morphology.

3.3 Discussion

The *f*ragment *l*ength *p*olymorphism assay is high-throughput, sensitive and accurate

In order to reliably identify autosomal nondisjunction rates and to differentiate between the rates of monosomy and trisomy, a sensitive, accurate, and high-throughput assay was required. While the previously developed RFLP assay was indeed a powerful assay, it had a number of limitations. The first limitation was the fact that PCR amplification from single embryos was inconsistent and not robust. The second limitation was the additional restriction digestion step, which was both time-consuming and error prone. Lastly, the third limitation was the nonMendelian inheritance of one of the *sup-9* alleles over the other. Considering that the aim of the assay was to accurately identify chromosome segregation, it was a problem that the RFLP assay demonstrated an inexplicable chromosome segregation bias.

The limitations of the RFLP led us to introduce three changes to the assay. The first change was to use nested PCR in place of the traditional PCR reaction used in the RFLP assay. Nested PCR allowed for robust and consistent amplification of the target region, even from very low amounts of starting genomic DNA. The second change was the removal of the restriction digestion step. By removing a step in the protocol, time and error were reduced; however, in order to remove this step, the assay needed a tag that did not utilize restriction fragment length polymorphisms. This led us to the third and final major change, which was the replacement of the *sup-9* alleles with DNA barcodes. These engineered barcodes, FLP1, FLP2, and FLP3, introduced PCR fragment length polymorphisms. This meant that the barcodes could be read simply with PCR and did not require the additional restriction digestion step. The barcode system had the additional benefit of reliably displaying proper, non-biased wildtype chromosome segregation.

In practice, the FLP assay reliably calculated chromosome nondisjunction. When performed without the addition of any additional genetic mutations, the FLP assay revealed a very low nondisjunction rate, as expected. Additionally, chromosomes tagged with FLP barcodes segregated at equal rates as detected by the FLP assay, demonstrating that the FLP barcodes did not introduce any chromosome segregation defects. Taken together, the FLP assay proved a high-throughput, sensitive and accurate assay with which to follow chromosome segregation.

C. elegans displays asymmetric chromosome nondisjunction during Meiosis I

Hodgkin *et al.* first described asymmetric chromosome nondisjunction in 1979 when they calculated the rates of males (XO) and triplo-X hermaphrodites (XXX) in wildtype and genetic mutants. Their data demonstrated that *C. elegans* X chromosome nondisjunction resulted in an excess of monosomy (XO) over trisomy (XXX). This was surprising considering that Mendel's laws of genetics predict that rates of monosomy should equal rates of trisomy. We posited that current technology could demonstrate that asymmetric chromosome nondisjunction occurs at Meiosis I and that the bias of monosomy over trisomy was due to achiasmate chromosomes missegregating more often to the polar body than the oocyte.

We hypothesized that the X chromosome achiasmate chromosome nondisjunction was mediated by a global mechanism that acts on all chromosomes. If true, then autosomes should also exhibit achiasmate chromosome nondisjunction. In order to test this hypothesis, we utilized the FLP assay to monitor chromosome segregation of chromosome II. The FLP assay demonstrated that autosomes did in fact demonstrate achiasmate chromosome nondisjunction in both wildtype and *zim-1* backgrounds. We concluded, therefore, that achiasmate chromosome nondisjunction was mediated by a global mechanism that acted on all chromosomes, not just the sex (X) chromosome.

After identifying autosomal achiasmate chromosome nondisjunction in *C. elegans*, we hypothesized that the bias of monosomy over trisomy was due to preferential nondisjunction to the polar body over the oocyte at Meiosis I. To test this hypothesis, we directly tagged chromosome V with fluorescent protein and quantified chromosome nondisjunction in fixed embryos. By quantifying chromosome V segregation to the polar body and oocyte, it was revealed that the achiasmate chromosome V segregated to the polar body more often than the oocyte. This was consistent with a model in which a global mechanism preferentially segregates achiasmate chromosomes to the polar body.

Apoptosis protects *C. elegans* from the meiotic age-effect

With the development of the FLP assay, we wondered whether the sensitivity of the assay could be used to investigate the meiotic age-effect in *C. elegans*. Previous researchers had hypothesized that, like other organisms, *C. elegans* experienced the meiotic age effect. Their work postulated that fertility defects in aged worms was due to the diminishment of meiotic fidelity. To test this hypothesis, we utilized the FLP assay and DAPI body counts in aged worms. If the meiotic age-effect did exist in *C. elegans*, then these assays would reveal an increase in nondisjunction and DAPI-staining bodies in aged worms. Surprisingly, we detected little to no meiotic defects in aged worms. Taken together, we concluded that *C. elegans* does not suffer from a meiotic age-effect.

Considering that *C. elegans* displays a number of other aging phenotypes and that so many other organisms experience the meiotic age effect, we hypothesized that a mechanism must be in place to protect *C. elegans* from the meiotic age effect and that apoptosis could be this mechanism. To test this hypothesis, we performed the FLP assay in a *ced-4* background. The *ced-4* FLP assay revealed an increase in nondisjunction over the lifetime of the worm. This suggested that apoptosis did, in fact, protect *C. elegans* from a meiotic age effect. We wondered whether this age effect was due to only to a previously described diminishment of oocyte quality, or additionally by an increase in chromosome nondisjunction. While performing the FLP assay, we had noticed an age-dependent increase in small, misshapen oocytes. We used the FLP assay to specifically examine misshapen oocytes for chromosome nondisjunction. We found that misshapen oocytes had a 50% chromosome nondisjunction rate, which was higher than the overall nondisjunction rate. Based on this, we concluded that while oocyte quality and chromosome nondisjunction are correlated in the *ced-4* background, there is no causative link.

C. elegans meiosis faithfully segregates chromosomes to produce haploid gametes. In a departure from Mendelian genetics, achiasmate chromosomes display a preferential segregation to the hermaphrodite polar body over the oocyte. This preference results in an excess of monosomic progeny over trisomic progeny, no matter whether the achiasmate chromosomes

were autosomes or sex chromosomes. Additionally, our research demonstrated that the accurate segregation of chromosomes in maintained through protective mechanisms. In aged worms, apoptosis protects the germline from chromosome segregation defects.

3.4 Materials and Methods

C. elegans *mutations and strains*

Unless otherwise stated, all animals were cultured under standard conditions at 20°c. The wildtype strain was N2 Bristol. *zim-1(tm1813)IV*, *zim-2(tm574)IV*, and *ced-4(n1162)III* were used to assay chromosome II nondisjunction, chromosome V nondisjunction, and the affect of apoptosis on nondisjunction.

Strains containing FLP1, FLP2, and FLP3 were constructed using MosSci. FLP1, FLP2, and FLP3 were amplified from the pDONR221 vector backbone. A donor template was constructed by inserting either FLP1, FLP2, or FLP3 into pCFJ350. Donor template and mCherry co-injection markers were injected into the MosSci insertion strain *ttTi5605* provided by the CGC. NonUnc and nonRFP insertions were identified in the F_1 and F_2 generations of injected P_0 worms. Successful insertion was verified by PCR and strains were outcrossed three times to *unc-119(ed3)*.

FLP assay

Single embryos were mouth pipetted with 5-6 µl of cold 1X ThermoPol buffer + Proteinase K into individual wells of a 96-well plates. After 1600 µJoules of UV irradiation to sterilize from nuclei acid contamination, samples were freeze/thawed three times in liquid nitrogen. Genomic DNA was released during the lysis protocol (1 hour at 55°c, followed by Proteinase K deactivation at 95°c for 15 minutes) performed in the thermocycler.

Nested PCR was performed on genomic DNA. The first PCR reaction required the entire embryo lysate. The second PCR reaction required only a drop of the first PCR reaction as the DNA template. Both PCR reactions were performed with VentR DNA polymerase and the standard VentR protocol. Primers for the first PCR reaction were `CCTTCCCCTTCCCCTTCTCATGTTCAATGCATTCCT` and `TTGAATTTGGCTTGTAACGCGGAATCACTACGTGCG`. Primers for the second PCR reaction were `GGACGAGTCGGAATCGCAGACCGATACCAGGATCTTGCC` and `GGTCACGGGCAGGAAACAGCTATGACCATGATTACGCCAAGC`. The second PCR reaction was run on a 1.5% TBE gel to visualize bands.

Cytological assays

LacI-GFP recombinant protein was expressed from a LacI-GFP expression vector in which the LacO sites were deleted to allow for robust LacI-GFP expression. LacI-GFP was expressed in BL21 cells and purified on a Nickel column. LacI-GFP was stored at -80°c in a Hepes, low imidazole buffer. Mouse monoclonal antibody against GFP was obtained commercial by Roche/Life Sciences.

LacI-GFP immunostaining was performed as previously described (Yuen *et al.,* 2011). Briefly, embryos were dissected from young adult worms into egg buffer. Worms and embryos were squeezed between a Histobond slide and coverslip, and frozen on dry ice. The coverslip was quickly and embryos were fixed using a 20 minute cold methanol incubation. Afterwards, slides were transferred to PBST (PBS containing 0.1% Tween-20) for rehydration. Recombinant

LacI-GFP protein was added to the fixed embryos for 90 minutes and then crosslinked in 3% formaldehyde for 15 minutes. The rest of the protocol was the same as the standard immunofluorescence protocol previously described (Phillips *et al.* 2009). Briefly, slides were blocked with Roche blocking agent and stained with primary antibodies for at least 2 hours. Secondary antibodies labeled with Alexa 488, Cy3, or Cy5 were purchased from Invitrogen or Jackson Immunoresearch. Following immunostaining, slides were stained in 0.5 μg/ml DAPI, destained in PBST, and mounted in glycerol-based mounting medium containing n-propyl gallate.

All images were acquired using a DeltaVision RT system (Applied Precision) equipped with a 100X N.A. 1.4 oil-immersion objective (Olympus). 3D image stacks were collected at 0.5 μm Z-spacing and processed by constrained, iterative deconvolution with SoftWoRx software package (Applied Precision). Image projection was performed with Fiji software using a maximum-intensity algorithm of 3D stacks. Composite image assembly, image scaling, and false coloring were performed with Adobe Photoshop.

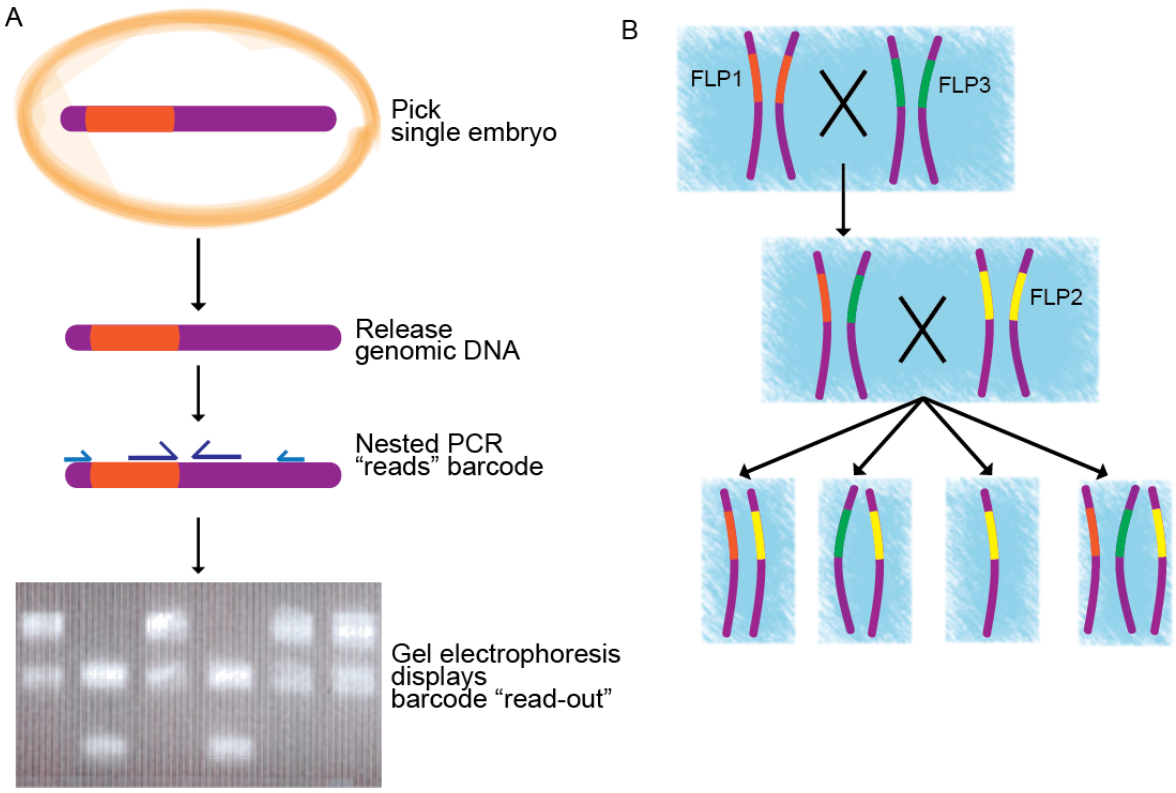

Figure 3.1 The *f*ragment *l*ength *p*olymorphism (FLP) can be performed on a single embryo. Worm lysis releases genomic DNA. Nested PCR “reads” the FLP barcodes and amplifies a unique fragment size corresponding to the barcode (A). In order for the FLP assay to determine chromosome copy number, a particular mating scheme must be set up. Homozygous FLP1 and FLP3 strains are crossed to produce a FLP1/FLP3 transheterozyote. This worm is crossed to the FLP2 strain. Resulting embryos from this cross are collected for the FLP assay (B).

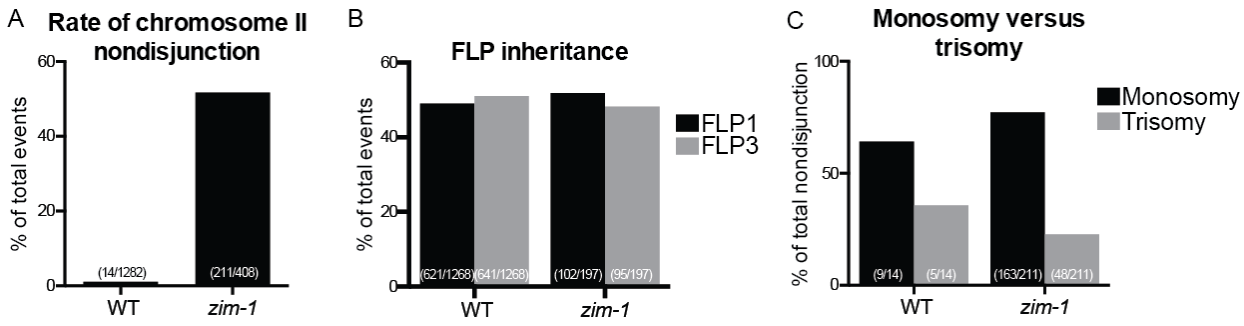

Figure 3.2 As expected, the FLP assay identifies a very low nondisjunction rate in wildtype animals and high nondisjunction rate in *zim-1* (A). Chromosomes containing the FLP1 and FLP3 barcodes are inherited at equal rates in wildtype and *zim-1* (B). In both wildtype and *zim-1*, the rates of monosomy are greater than the rates of trisomy (C).

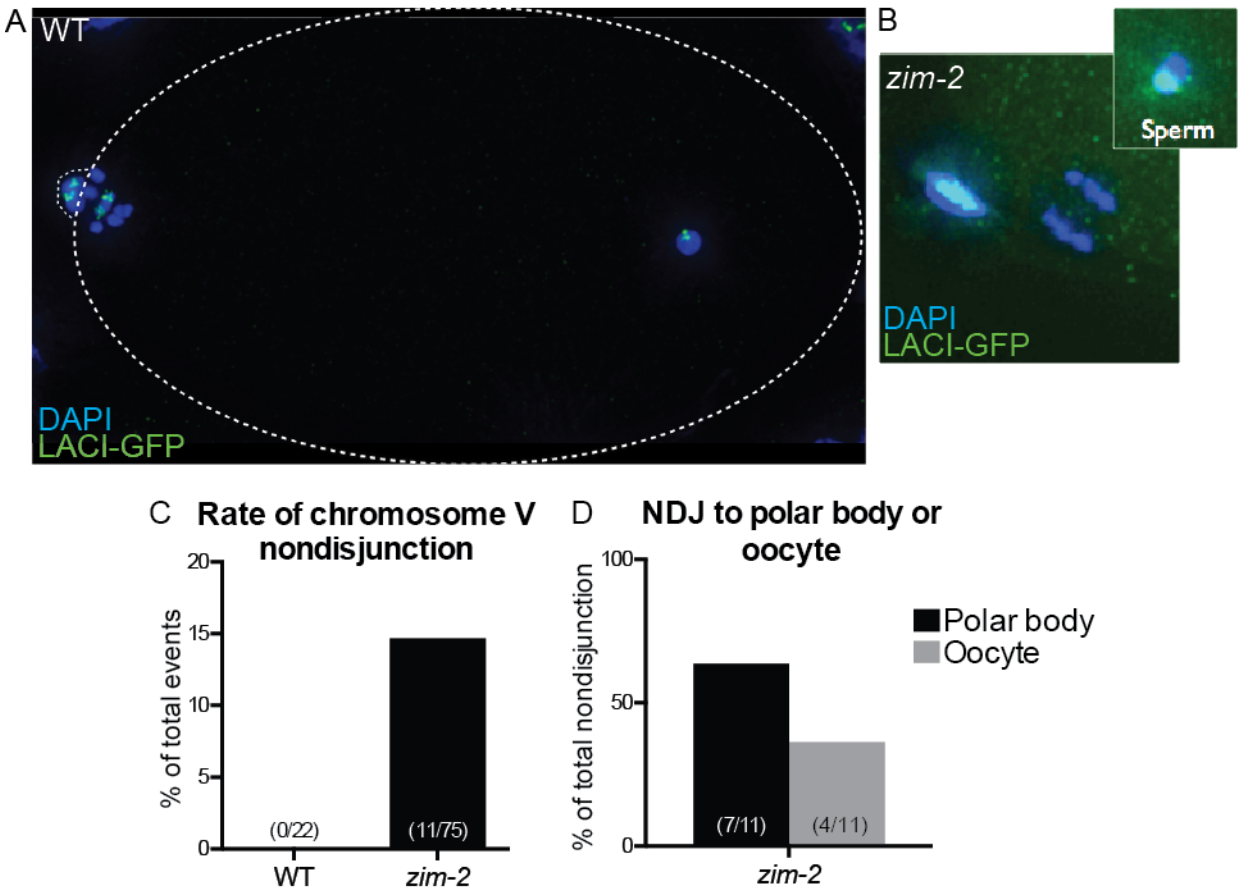

Figure 3.3 Fixed embryos with a LacO array integrated in chromosome V are treated with recombinant LacI-GFP. Based on the location of the LacI-GFP foci, these embryos can be scored for chromosome V nondisjunction (A). The LacO array strain was crossed into *zim-1* in order to increase the nondisjunction rate of chromosome V (B). As expected, chromosome V nondisjunction rates were higher in *zim-2* (C). The frequency of nondisjunction to the polar body was slightly higher than nondisjunction to the oocyte (D).

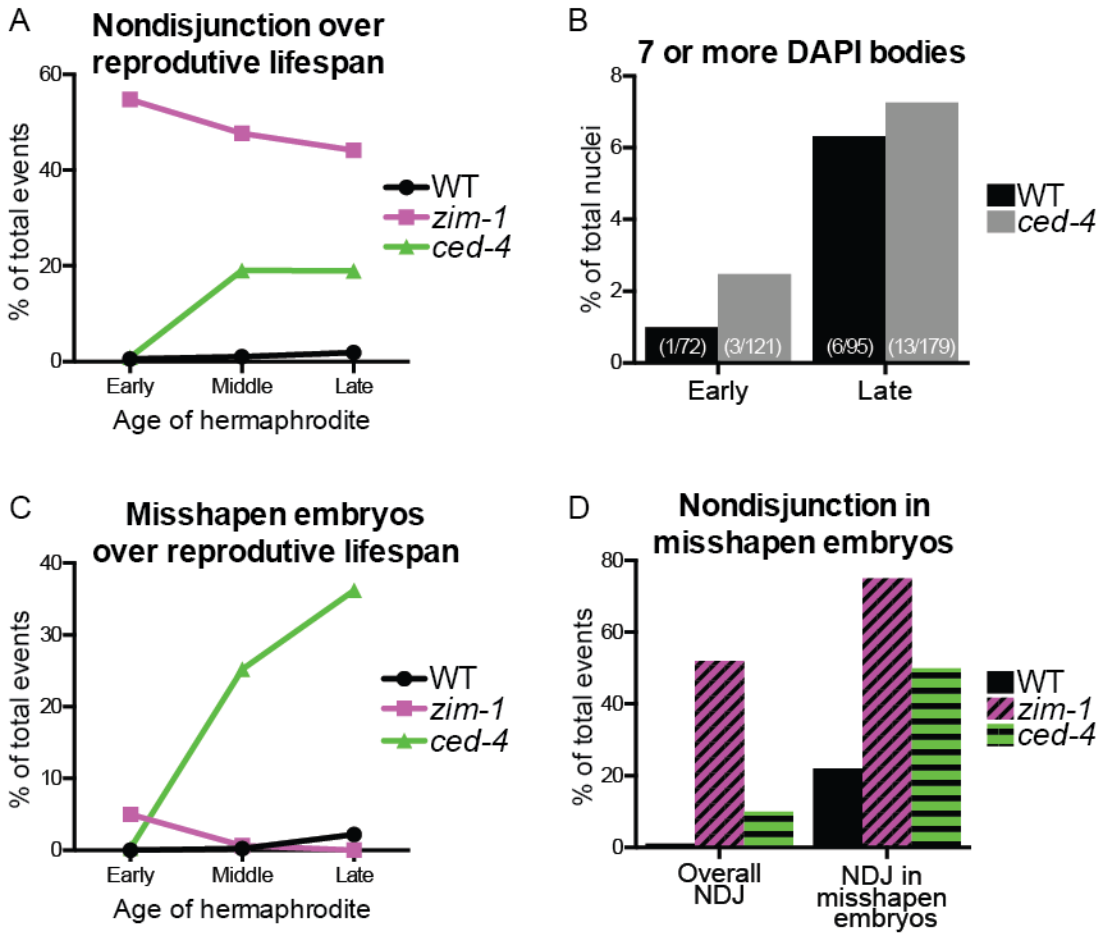

Figure 3.4 The rate of nondisjunction over the reproductive lifespan of wildtype worms increases only slightly. In *zim-1*, the rate of nondisjunction over time actually decreases. In *ced-4*, the rate of nondisjunction increase over time (A). Germlines of older wildtype and *ced-4* animals display a slight increase in the percentage of nuclei with seven of more DAPI-staining bodies (B). The frequency of misshapen embryos increases slightly over the reproductive lifespan of wildtype animals. The frequency of misshapen embryos in *zim-1* does not increase over time. The frequency of misshapen embryos increases over time in *cec-4* (C). The rate of nondisjunction is greater in misshapen embryos than overall (D).

Chapter 4: Concluding remarks and future perspectives

4.1 Review of findings

WAPL-1 is regulated during meiotic prophase by the meiosis-specific kinase, CHK-2

During meiotic prophase, homologous chromosome must pair, synapse, and form crossovers in order to ensure proper chromosome segregation at Meiosis I. Sister chromatid cohesion, the biological process that holds sister chromatids together, is required for these events to properly take place. Sister chromatid cohesion is mediated by the cohesin complex, which entraps DNA to both hold sister chromatids together, function in DNA double-strand break (DSB) repair, and mediate crossovers. Here, we described the characterization of the conserved cohesin-associated protein, WAPL-1 during meiotic prophase.

We show that, like its homologs in yeast and vertebrates, WAPL-1 functions primarily during mitosis. Although WAPL-1 was not required for mitosis and live-imaging of early mitotic divisions displayed no defects, worms lacking WAPL-1 displayed a number of developmental defects associated with improper mitotic cell divisions. Immunoprecipitation of WAPL-1 followed by mass spectrometry identified all of the cohesin complex components, the mitotic α-kleisins, and the two *C. elegans* components of the MRN complex. Based on this, we concluded that WAPL-1 is a nonessential protein that functions primary during mitosis as a cohesin-associated protein.

As studies in other organisms have been unable to closely assess whether Wapl/Wpl functions during meiotic prophase, we performed a detailed investigation of WAPL-1 during meiotic prophase. We showed that while WAPL-1 is not required for accurate chromosome segregation, the lack of WAPL-1 did display two meiotic phenotypes. First, we showed that WAPL-1 is required to antagonize the loading of SCC-1 cohesin complexes onto meiotic chromosome axes. Second, we showed that WAPL-1 is required for the repair of DNA DSB breaks.

After determining that WAPL-1 did function during meiotic prophase, we performed a candidate screen to identify regulators of WAPL-1 at the mitosis-to-meiosis transition. Surprisingly, we identified the meiosis-specific kinase CHK-2 as a regulator of WAPL-1. When WAPL-1 was misregulated due to the lack of CHK-2, loading of COH-3/4 cohesin complexes onto meiotic chromosomes was defective. In conclusion, WAPL-1 plays a conserved role during mitosis through interaction with cohesin complexes. WAPL-1 also functions during meiotic prophase to antagonize cohesin complexes and regulation DNA DSB repair. WAPL-1 is regulated during meiotic prophase by the CHK-2.

C. elegans displays asymmetric chromosome nondisjunction

During Meiosis I, homologous chromosome must segregation away from one another in order to reduce the chromosome complement by half. To do this, physical linkages called chiasmata must be formed between homologous chromosomes. If a chiasma fails to form, then homologous chromosomes enter Meiosis I as separate, achiasmate chromosomes. During anaphase I, Mendelian genetics predicts that achiasmate chromosomes would nondisjoin to either meiotic spindle pole at equal probabilities. Evidence from a number of organisms suggests that

this is not the case as evidenced by unequal percentages of monosomy and trisomy (Fragouli et al., 2011; Hodgkin et al., 1979; LeMaire-Adkins and Hunt, 2000). During female meiosis, segregation to one pole means chromosomes are destined for the polar body and segregation to the other pole means chromosomes are destined for the oocyte and Meiosis II. As a result, asymmetric nondisjunction could occur if chromosomes missegregated to the polar body at a different frequency than the oocyte. Here, we explored asymmetric chromosome nondisjunction in *C. elegans.*

We hypothesized that asymmetric nondisjunction was caused by a global mechanism that would affect all achiasmate chromosomes, including autosomes. In order to test this hypothesis, we required an assay that could detect chromosome copy number of single embryos. Since the assays available at the time had a variety of limitations, we developed changes to the *r*estriction *l*ength *f*ragment *p*olymorphism first development by Severson et al. in 2009. By removing the restriction digestion step, replacing the single PCR step with nested PCR amplification, and introducing integrated DNA barcodes, we developed the *f*ragment *l*ength *p*olymorphism (FLP) assay.

Use of FLP assay to detect chromosome II nondisjunction in wildtype hermaphrodites displayed a very low nondisjunction rate. To increase the nondisjunction rate and better assay autosomal nondisjunction, we used the FLP assay on *zim-1* mutant hermaphrodites. In the *zim-1* background, the frequency of chromosome II monosomy was clearly greater than the frequency of chromosome II trisomy. Based on this, we concluded that asymmetric nondisjunction is a biological phenomenon that affects both sex chromosomes and autosomes.

Apoptosis protects *C. elegans* from the meiotic age-effect

The meiotic age-effect is a conserved biological phenomenon that describes the worsening of fertility as an organism ages. The meiotic age-effect is most commonly ascribed to the female, which is why it is also commonly referred to as the maternal age-effect. In humans, women experience a deterioration of reproductive processes throughout their reproductive lifespan (Hassold and Hunt, 2001; Hawley, 2003). Here, we explored the maternal age-effect in *C. elegans.*

We began by assaying autosomal nondisjunction using the FLP assay in wildtype hermaphrodites over the course of their reproductive lifespan. Surprisingly, wildtype hermaphrodites displayed little to no increase in chromosome nondisjunction as they aged. Considering that the nondisjunction rates in wildtype worms are very low, we utilized the *zim-1* genetic background to increase nondisjunction. In this background, hermaphrodites displayed no increase in nondisjunction over their reproductive lifespan. There are two reasons why we did not see an increase in nondisjunction. The first is that the small increase in nondisjunction in wildtype worms was due to defects in pairing, synapsis or crossover formation. Since *zim-1* abrogates these processes, no increase took place. The second is that the small increase in nondisjunction in wildtype worms is so small that it requires a much larger sample size.

We hypothesized that the lack of a robust maternal age-effect in *C. elegans* was due to a protective mechanism. Based on previous data, we suspected that the apoptotic machinery could be culling defective nuclei in the germlines of aged worms (Bhalla and Dernburg, 2005). To test this, we performed the FLP assay in *ced-4* worms. We found *ced-4* hermaphrodites displayed an

increase in nondisjunction over their reproductive lifespan suggesting that the apoptotic machinery does protect *C. elegans* from reproductive defects as they age.

4.2 Implication of findings

The function and regulation of sister chromatid cohesion in meiosis

Sister chromatid cohesion is absolutely essential for both mitosis and meiosis. Defects in cohesion can be disastrous for a developing organism and result in spontaneous abortion or a variety of developmental disorders. As a result, it is imperative that we have an understanding of the regulation and functions of sister chromatid cohesion and the proteins underlying this process.

Our work provided evidence that the cohesin-associated protein WAPL-1, previously thought to function only during mitosis in animals, also functions during meiosis. Additionally, WAPL-1 experiences specialized regulation by the meiosis-specific kinase, CHK-2, and if misregulated, negatively affects only a subset of meiotic cohesin complexes. This work has a number of implications for our understanding of sister chromatid cohesion. First, that the mitotic cohesin complex must be regulated during meiosis and that it does so through a specialized process, which suggests that its regulation is not simply a relic of its mitotic regulation. Second, that sister chromatid cohesion is mediated by an ever-growing library of cohesin complexes. During meiosis alone, multiple meiotic cohesin complexes, defined by different α-kleisins, and the mitotic cohesin complex, defined by the mitotic α-kleisin, are all present and regulated differently.

Our work on WAPL-1 in meiosis also uncovered a role for cohesin in DNA DSB repair. Immunoprecipitation of WAPL-1 identified RAD-50 and MRE-11, two components of the conserved MRN complex, which acts during DNA DSB repair to resect DNA. Additionally, *wapl-1* germlines displayed an increase in unrepaired DNA DSBs. While it has been previously known that the cohesin complex is required for proper DNA DSB repair, it was not understood mechanistically what role cohesin might play. Our work suggests that the cohesin complex acts during meiosis in the repair of programmed DNA DSBs. While little is understood of the mechanistics of this role, it is possible that cohesin is required to recruit or load the MRN complex onto DNA.

The regulation of WAPL-1 by CHK-2 is interesting due to its implications for the regulation of WAPL-1 during DNA damage. While in *C. elegans* CHK-2 is a meiotic regulator, its homologs in other organisms function in the DNA damage repair pathway to induce apoptosis and cell cycle arrest. It is tempting to theorize that Wapl is similarly regulated during the DNA damage repair pathway to mediate cohesin's role in DSB repair.

Chromosome nondisjunction and the meiotic age-effect

Chromosome nondisjunction during meiosis has terrible consequences. Chromosomal aneuploidy in gametes can result in spontaneous abortion or developmental disorders. In females, chromosome nondisjunction and the production of aneuploid gametes increases as the mother ages. This phenomenon is referred to as the meiotic age-effect or maternal age-effect. It is currently unclear why women experience the meiotic age-effect, but hypotheses range from a

loss of sister chromatid cohesion over time and/or environmental stresses on eggs over time (Hassold and Hunt, 2009; Hunt and Hassold, 2008; Nagaoka et al., 2012). Additionally, genetic recombination and the inheritance of a full genetic complement through gametes is absolutely critical as it is the first step in introducing population diversity and ensuring the perpetuation of a species. As a result, it is important that we understand the mechanisms underlying chromosome nondisjunction. Here, we studied to aspects of chromosome nondisjunction, the asymmetric nondisjunction of chromosomes to the polar body and the maternal age-effect.

We identified asymmetric autosomal nondisjunction in *C. elegans*, similar to the skewed nondisjunction of the X chromosome previously described (Hodgkin et al., 1979). Interestingly, this asymmetric nondisjunction has been described in other organisms, including mice and humans (Fragouli et al., 2011; LeMaire-Adkins and Hunt, 2000). In human and mice, however, the asymmetric nondisjunction was skewed so as to produce an excess of trisomic progeny rather than what is seen in *C. elegans,* which is an excess of monosomic progeny. This leads us to ask two questions: Why is there conservation of asymmetric nondisjunction and why is this asymmetry flipped in *C. elegans*?

In order to hypothesize why asymmetric nondisjunction has been conserved, we can look to see what benefits it provides to an organism and its species. Recent studies have suggested that asymmetric nondisjunction is a way for trisomic hermaphrodites to correct its meiosis (Cortes et al., 2015). Additionally, during female meiosis, the meiotic spindle is located close to the cell cortex and, in many species, perpendicular to the cortex. If, in the positioning of the meiotic spindle an asymmetry between the meiotic spindle poles arose, then this could bias chromosome segregation toward the dominant pole. Lastly, while it appears that asymmetric nondisjunction is present in a variety of organisms, it is flipped in *C. elegans*. It is tempting to speculate that this flip is due to the fact that sex chromosome monosomy in *C. elegans* produces males, an evolutionarily positive outcome as males can introduce genetic diversity by outcrossing and are better than hermaphrodites at withstanding starvation (Morran et al., 2009).

In addition to investigating asymmetric nondisjunction, we analyzed nondisjunction in aged hermaphrodites to test whether the maternal age-effect could be studied in the model organism, *C. elegans*. Previous work had suggested that *C. elegans* could be used to study reproductive aging and the maternal age-effect (Luo et al., 2010). Through the careful study of nondisjunction in aged hermaphrodites, we determined that, without additional genetic mutations, *C. elegans* could not be used to study the maternal age-effect as protective mechanisms are in place.

4.3 Remaining questions

How does WAPL-1 function in DNA double-strand break repair?

The cohesin complex has long been implicated in the repair of DNA double-strand (DSB) breaks, but it is unclear the mechanistic role of cohesin in repair. In this study, we presented two pieces of evidence suggesting that the cohesin complex is required for DNA DSB repair in the germline and that programmed DNA DSBs require the cohesin-associated protein, WAPL-1.

We found two roles for WAPL-1 during meiosis. The first is the antagonism of mitotic cohesin axes during meiotic prophase. The second is the repair of programmed DSBs. It is interesting to speculate that the loading of mitotic cohesin complexes somehow impairs the

repair of DSBs. Given that cohesion is established *de novo* upon DSBs in budding yeast, it is possible that mitotic cohesin complexes somehow inhibit the formation of new cohesion. Conversely, the roel of WAPL-1 in repair of DNA DSBs may be completely separate from the loading of mitotic cohesin complexes during meiosis that is seen in *wapl-1* mutants. In other organisms, Wapl has been implicated in DNA DSB repair during mitosis. In our immunoprecipitation of WAPL-1, two components of the MRN complex co-eluted with WAPL-1. Is is tempting to hypothesize that WAPL-1 and/or the cohesin complex acts to recruit or stabilize DNA DSB repair proteins on the DNA. Additional investigation will hopefully shed light on the role of WAPL-1 and the cohesin complex in DNA DSB repair during mitosis and meiosis.

How and why does WAPL-1 act specifically on some cohesin complexes, but not all, during meiosis?

It has previously been shown that, during meiosis, cohesin complexes containing REC-8, COH-3, COH-4, and SCC-1 are present and functional. It is interesting, therefore, that we have shown WAPL-1 to only affect SCC-1 and COH-3/4 cohesin complexes. During meiosis, WAPL-1 specifically antagonizes the loading of SCC-1 cohesin complexes. When WAPL-1 is misregulated in the germline, REC-8 cohesin complexes are unaffected while COH-3/4 loading is disrupted. This leads us to two questions: How can WAPL-1 selectively affect certain cohesin complexes and, considering that it appears to have no detrimental affect on meiosis, why is WAPL-1 antagonizing SCC-1 cohesin complexes during meiosis?

SCC-1, REC-8, and COH-3/4 are all members of the α-kleisin family, they can all bind to SMC-3 and HIM-1 (SMC-1), and they can all mediate cohesion. It is unclear then how WAPL-1 can selective affect a subset of the α-kleisins present in the meiotic germline. There are two, not mutually exclusive possibilities. The first is that there is a physical or structural difference between the α-kleisins that is currently unrecognized. Further research, possibly *in vitro*, could illuminate whether or not certain proteins are simply immune to WAPL-1's affect. The second possibility is that regulation and additional co-factors direct WAPL-1's affects to a subset of cohesin complexes. Considering that we identified CHK-2 as a regulator of WAPL-1 and CHK-2 is known to affect COH-3/4, but not REC-8, it is possible that WAPL-1's regulation is what is directing it to act on a subset of cohesin complexes.

Although that we described a role for WAPL-1 in antagonizing SCC-1 cohesin complexes during meiosis, it is unclear why SCC-1 cohesin complexes are present during meiosis at all. It is possible that mitotic cohesin is present in the germline simply to be deposited into the oocyte for the mitotic divisions? In this case, WAPL-1 is required to specifically inhibit the mitotic cohesin complexes during meiosis. In the absence of the meiotic cohesin complexes, WAPL-1 can then release the mitotic cohesin complexes from their inhibition so that they can partially substitute for the lost meiotic cohesins.

It is also possible that SCC-1 normally functions during meiosis. In fission yeast and *C. elegans*, it is known that mitotic cohesin complexes can function in the meiotic germline to rescue sister chromatid cohesion in the absence of the meiotic α-kleisins (Severson and Meyer, 2014; Yokobayashi et al., 2003). The role of WAPL-1 in regulation mitotic cohesin during meiosis provides further evidence that mitotic cohesin complexes are present during meiosis and that specific regulation of the mitotic cohesin complexes takes place. It is therefore possible that

mitotic cohesin complexes act during meiosis and provide some currently unknown benefit. Further research will illuminate the complex relationship between WAPL-1 and the cohesin complexes during meiosis.

How are males exhibiting asymmetric nondisjunction?

In this work and in other studies, it has been hypothesized that asymmetric nondisjunction is due to preferential segregation of chromosomes to either the polar body or the oocyte. However, it was previously shown that *C. elegans* 2X transformed males, which do not utilize polar bodies, also demonstrate asymmetric X chromosome nondisjunction (Hodgkin et al., 1979). It is interesting to hypothesize why this might be the case.

In *C. elegans* male meiosis, spermatids undergoing meiosis bud off of what is known as the residual body (L'Hernault, 2006). It is possible that, in place of polar bodies, the residual body acts as a depository for achiasmate chromosomes. As the *f*ragment *l*ength *p*olymorphism (FLP) assay is amenable to studying nondisjunction in males, nondisjunction of autosomes could be tested to ensure that the asymmetric nondisjunction in males was not due to some other affect in 2X transformed males.

Could *C. elegans* genetic mutants replicate the human meiotic age-effect?

In this work, we determined that wildtype *C. elegans* hermaphrodites could not be used to study the meiotic age-effect as protective mechanisms exist to shield meiosis from aging. It is interesting, however, to hypothesize that genetic mutants exist to allow for the study of the maternal age-effect in this model organism.

During our studies, we found that apoptosis protects oocytes from morphology defects and chromosome nondisjunction. It is possible that an apoptosis-defective mutant could be used to study reproductive aging. Additionally, in *C. elegans*, eggs are immediately fertilized by sperm. This is unlike the case in humans where eggs arrested during Meiosis II will not be fertilized for decades. Given that this arrest has been implicated in the maternal age-effect, it is possible that a similar situation could be constructed in *C. elegans* using genetic mutants. For example, there exists genetic backgrounds in which hermaphrodites do not produce their own sperm. As a result, eggs become arrested during meiosis until fertilization by a male-derived sperm. Hermaphrodites of this genetic background could be tested for chromosome nondisjunction using the FLP assay over their reproductive lifespan.

Overall, a number of interesting scientific questions remain. Future research, either from the Dernburg Lab or other labs, will further advance our understanding of meiotic prophase regulation and chromosome nondisjunction.

References

Andux, S., and R.E. Ellis. 2008. Apoptosis maintains oocyte quality in aging Caenorhabditis elegans females. *PLoS Genet*. 4:e1000295.

Bhalla, N., and A.F. Dernburg. 2005. A conserved checkpoint monitors meiotic chromosome synapsis in Caenorhabditis elegans. *Science*. 310:1683-1686.

Birkenbihl, R.P., and S. Subramani. 1992. Cloning and characterization of rad21 an essential gene of Schizosaccharomyces pombe involved in DNA double-strand-break repair. *Nucleic Acids Res*. 20:6605-6611.

Brenner, S. 1974. The genetics of Caenorhabditis elegans. *Genetics*. 77:71-94.

Chan, K.L., M.B. Roig, B. Hu, F. Beckouet, J. Metson, and K. Nasmyth. 2012. Cohesin's DNA exit gate is distinct from its entrance gate and is regulated by acetylation. *Cell*. 150:961-974.

Chiu, H., H.T. Schwartz, I. Antoshechkin, and P.W. Sternberg. 2013. Transgene-free genome editing in Caenorhabditis elegans using CRISPR-Cas. *Genetics*. 195:1167-1171.

Consortium, C.e.S. 1998. Genome sequence of the nematode C. elegans: a platform for investigating biology. *Science*. 282:2012-2018.

Cortes, D.B., K.L. McNally, P.E. Mains, and F.J. McNally. 2015. The asymmetry of female meiosis reduces the frequency of inheritance of unpaired chromosomes. *Elife*. 4.

De, K., L. Sterle, L. Krueger, X. Yang, and C.A. Makaroff. 2014. Arabidopsis thaliana WAPL is essential for the prophase removal of cohesin during meiosis. *PLoS Genet*. 10:e1004497.

Deardorff, M.A., D.M. Clark, and I.D. Krantz. 1993. Cornelia de Lange Syndrome. *In* GeneReviews(R). R.A. Pagon, M.P. Adam, H.H. Ardinger, S.E. Wallace, A. Amemiya, L.J.H. Bean, T.D. Bird, C.R. Dolan, C.T. Fong, R.J.H. Smith, and K. Stephens, editors, Seattle (WA).

Delhanty, J.D., J.C. Harper, A. Ao, A.H. Handyside, and R.M. Winston. 1997. Multicolour FISH detects frequent chromosomal mosaicism and chaotic division in normal preimplantation embryos from fertile patients. *Hum Genet*. 99:755-760.

Dickinson, D.J., J.D. Ward, D.J. Reiner, and B. Goldstein. 2013. Engineering the Caenorhabditis elegans genome using Cas9-triggered homologous recombination. *Nat Methods*. 10:1028-1034.

Fire, A., S. Xu, M.K. Montgomery, S.A. Kostas, S.E. Driver, and C.C. Mello. 1998. Potent and specific genetic interference by double-stranded RNA in Caenorhabditis elegans. *Nature*. 391:806-811.

Fragouli, E., S. Alfarawati, N.N. Goodall, J.F. Sanchez-Garcia, P. Colls, and D. Wells. 2011. The cytogenetics of polar bodies: insights into female meiosis and the diagnosis of aneuploidy. *Mol Hum Reprod*. 17:286-295.

Fragouli, E., S. Alfarawati, K. Spath, S. Jaroudi, J. Sarasa, M. Enciso, and D. Wells. 2013. The origin and impact of embryonic aneuploidy. *Hum Genet*. 132:1001-1013.

Friedland, A.E., Y.B. Tzur, K.M. Esvelt, M.P. Colaiacovo, G.M. Church, and J.A. Calarco. 2013. Heritable genome editing in C. elegans via a CRISPR-Cas9 system. *Nat Methods*. 10:741-743.

Frokjaer-Jensen, C., M.W. Davis, C.E. Hopkins, B.J. Newman, J.M. Thummel, S.P. Olesen, M. Grunnet, and E.M. Jorgensen. 2008. Single-copy insertion of transgenes in Caenorhabditis elegans. *Nat Genet*. 40:1375-1383.

Game, J.C., G.W. Birrell, J.A. Brown, T. Shibata, C. Baccari, A.M. Chu, M.S. Williamson, and J.M. Brown. 2003. Use of a genome-wide approach to identify new genes that control resistance of Saccharomyces cerevisiae to ionizing radiation. *Radiat Res*. 160:14-24.

Gandhi, R., P.J. Gillespie, and T. Hirano. 2006. Human Wapl is a cohesin-binding protein that promotes sister-chromatid resolution in mitotic prophase. *Curr Biol*. 16:2406-2417.

Gartner, A., P.R. Boag, and T.K. Blackwell. 2008. Germline survival and apoptosis. *WormBook*:1-20.

Greenstein, D. 2005. Control of oocyte meiotic maturation and fertilization. *WormBook*:1-12.

Guacci, V., D. Koshland, and A. Strunnikov. 1997. A direct link between sister chromatid cohesion and chromosome condensation revealed through the analysis of MCD1 in S. cerevisiae. *Cell*. 91:47-57.

Gutierrez-Caballero, C., Y. Herran, M. Sanchez-Martin, J.A. Suja, J.L. Barbero, E. Llano, and A.M. Pendas. 2011. Identification and molecular characterization of the mammalian alpha-kleisin RAD21L. *Cell Cycle*. 10:1477-1487.

Hassold, T., and P. Hunt. 2001. To err (meiotically) is human: the genesis of human aneuploidy. *Nat Rev Genet*. 2:280-291.

Hassold, T., and P. Hunt. 2009. Maternal age and chromosomally abnormal pregnancies: what we know and what we wish we knew. *Curr Opin Pediatr*. 21:703-708.

Hawley, R.S. 2003. Human meiosis: model organisms address the maternal age effect. *Curr Biol*. 13:R305-307.

Hodgkin, J., H.R. Horvitz, and S. Brenner. 1979. Nondisjunction Mutants of the Nematode CAENORHABDITIS ELEGANS. *Genetics*. 91:67-94.

Hopkins, J., G. Hwang, J. Jacob, N. Sapp, R. Bedigian, K. Oka, P. Overbeek, S. Murray, and P.W. Jordan. 2014. Meiosis-specific cohesin component, Stag3 is essential for maintaining centromere chromatid cohesion, and required for DNA repair and synapsis between homologous chromosomes. *PLoS Genet*. 10:e1004413.

Hunt, P.A., and T.J. Hassold. 2008. Human female meiosis: what makes a good egg go bad? *Trends Genet*. 24:86-93.

Johnson, T.D. 2007. Maternity Leave and Employment Patterns of First-Time Mothers: 1961-2003. *In* Current Population Report, U.S. Census Bureau, Washington DC. 70-113.

Keeney, S., and M.J. Neale. 2006. Initiation of meiotic recombination by formation of DNA double-strand breaks: mechanism and regulation. *Biochem Soc Trans*. 34:523-525.

Kim, Y., N. Kostow, and A. Dernburg. *Unsubmitted*.

Kueng, S., B. Hegemann, B.H. Peters, J.J. Lipp, A. Schleiffer, K. Mechtler, and J.M. Peters. 2006. Wapl controls the dynamic association of cohesin with chromatin. *Cell*. 127:955-967.

Kuroda, M., K. Oikawa, T. Ohbayashi, K. Yoshida, K. Yamada, J. Mimura, Y. Matsuda, Y. Fujii-Kuriyama, and K. Mukai. 2005. A dioxin sensitive gene, mammalian WAPL, is implicated in spermatogenesis. *FEBS Lett*. 579:167-172.

L'Hernault, S.W. 2006. Spermatogenesis. *In* WormBook.

Larionov, V.L., T.S. Karpova, N.Y. Kouprina, and G.A. Jouravleva. 1985. A mutant of Saccharomyces cerevisiae with impaired maintenance of centromeric plasmids. *Curr Genet*. 10:15-20.

Lee, J., and T. Hirano. 2011. RAD21L, a novel cohesin subunit implicated in linking homologous chromosomes in mammalian meiosis. *J Cell Biol*. 192:263-276.

LeMaire-Adkins, R., and P.A. Hunt. 2000. Nonrandom segregation of the mouse univalent X chromosome: evidence of spindle-mediated meiotic drive. *Genetics*. 156:775-783.
Lo, D.C. 2001. Neuronal transfection using particle-mediated gene transfer. *Curr Protoc Neurosci*. Chapter 3:Unit 3 15.
Lopez-Serra, L., A. Lengronne, V. Borges, G. Kelly, and F. Uhlmann. 2013. Budding yeast Wapl controls sister chromatid cohesion maintenance and chromosome condensation. *Curr Biol*. 23:64-69.
Losada, A. 2014. Cohesin in cancer: chromosome segregation and beyond. *Nat Rev Cancer*. 14:389-393.
Luo, S., G.A. Kleemann, J.M. Ashraf, W.M. Shaw, and C.T. Murphy. 2010. TGF-beta and insulin signaling regulate reproductive aging via oocyte and germline quality maintenance. *Cell*. 143:299-312.
MacQueen, A.J., C.M. Phillips, N. Bhalla, P. Weiser, A.M. Villeneuve, and A.F. Dernburg. 2005. Chromosome sites play dual roles to establish homologous synapsis during meiosis in C. elegans. *Cell*. 123:1037-1050.
Marston, A.L. 2014. Chromosome segregation in budding yeast: sister chromatid cohesion and related mechanisms. *Genetics*. 196:31-63.
Michaelis, C., R. Ciosk, and K. Nasmyth. 1997. Cohesins: chromosomal proteins that prevent premature separation of sister chromatids. *Cell*. 91:35-45.
Morran, L.T., B.J. Cappy, J.L. Anderson, and P.C. Phillips. 2009. Sexual partners for the stressed: facultative outcrossing in the self-fertilizing nematode Caenorhabditis elegans. *Evolution*. 63:1473-1482.
Nagaoka, S.I., T.J. Hassold, and P.A. Hunt. 2012. Human aneuploidy: mechanisms and new insights into an age-old problem. *Nat Rev Genet*. 13:493-504.
Nasmyth, K., and C.H. Haering. 2005. The structure and function of SMC and kleisin complexes. *Annu Rev Biochem*. 74:595-648.
Neale, M.J., and S. Keeney. 2006. Clarifying the mechanics of DNA strand exchange in meiotic recombination. *Nature*. 442:153-158.
Nishiyama, T., R. Ladurner, J. Schmitz, E. Kreidl, A. Schleiffer, V. Bhaskara, M. Bando, K. Shirahige, A.A. Hyman, K. Mechtler, and J.M. Peters. 2010. Sororin mediates sister chromatid cohesion by antagonizing Wapl. *Cell*. 143:737-749.
Nishiyama, T., M.M. Sykora, P.J. Huis in 't Veld, K. Mechtler, and J.M. Peters. 2013. Aurora B and Cdk1 mediate Wapl activation and release of acetylated cohesin from chromosomes by phosphorylating Sororin. *Proc Natl Acad Sci U S A*. 110:13404-13409.
Oikawa, K., T. Ohbayashi, T. Kiyono, H. Nishi, K. Isaka, A. Umezawa, M. Kuroda, and K. Mukai. 2004. Expression of a novel human gene, human wings apart-like (hWAPL), is associated with cervical carcinogenesis and tumor progression. *Cancer Res*. 64:3545-3549.
Onn, I., J.M. Heidinger-Pauli, V. Guacci, E. Unal, and D.E. Koshland. 2008. Sister chromatid cohesion: a simple concept with a complex reality. *Annu Rev Cell Dev Biol*. 24:105-129.
Pasierbek, P., M. Jantsch, M. Melcher, A. Schleiffer, D. Schweizer, and J. Loidl. 2001. A Caenorhabditis elegans cohesion protein with functions in meiotic chromosome pairing and disjunction. *Genes Dev*. 15:1349-1360.
Peters, J.M., A. Tedeschi, and J. Schmitz. 2008. The cohesin complex and its roles in chromosome biology. *Genes Dev*. 22:3089-3114.

Phillips, C.M., and A.F. Dernburg. 2006. A family of zinc-finger proteins is required for chromosome-specific pairing and synapsis during meiosis in C. elegans. *Dev Cell*. 11:817-829.

Phillips, C.M., C. Wong, N. Bhalla, P.M. Carlton, P. Weiser, P.M. Meneely, and A.F. Dernburg. 2005. HIM-8 binds to the X chromosome pairing center and mediates chromosome-specific meiotic synapsis. *Cell*. 123:1051-1063.

Rose, A. 2014. Replication and repair. *In* WormBook.

Rowland, B.D., M.B. Roig, T. Nishino, A. Kurze, P. Uluocak, A. Mishra, F. Beckouet, P. Underwood, J. Metson, R. Imre, K. Mechtler, V.L. Katis, and K. Nasmyth. 2009. Building sister chromatid cohesion: smc3 acetylation counteracts an antiestablishment activity. *Mol Cell*. 33:763-774.

Sato, A., B. Isaac, C.M. Phillips, R. Rillo, P.M. Carlton, D.J. Wynne, R.A. Kasad, and A.F. Dernburg. 2009. Cytoskeletal forces span the nuclear envelope to coordinate meiotic chromosome pairing and synapsis. *Cell*. 139:907-919.

Schvarzstein, M., S.M. Wignall, and A.M. Villeneuve. 2010. Coordinating cohesion, co-orientation, and congression during meiosis: lessons from holocentric chromosomes. *Genes Dev*. 24:219-228.

Severson, A.F., L. Ling, V. van Zuylen, and B.J. Meyer. 2009. The axial element protein HTP-3 promotes cohesin loading and meiotic axis assembly in C. elegans to implement the meiotic program of chromosome segregation. *Genes Dev*. 23:1763-1778.

Severson, A.F., and B.J. Meyer. 2014. Divergent kleisin subunits of cohesin specify mechanisms to tether and release meiotic chromosomes. *Elife*. 3:e03467.

Shaham, S. 2006. Methods in cell biology. *In* WormBook.

Sjogren, C., and K. Nasmyth. 2001. Sister chromatid cohesion is required for postreplicative double-strand break repair in Saccharomyces cerevisiae. *Curr Biol*. 11:991-995.

Stoop-Myer, C., and A. Amon. 1999. Meiosis: Rec8 is the reason for cohesion. *Nat Cell Biol*. 1:E125-127.

Strom, L., C. Karlsson, H.B. Lindroos, S. Wedahl, Y. Katou, K. Shirahige, and C. Sjogren. 2007. Postreplicative formation of cohesion is required for repair and induced by a single DNA break. *Science*. 317:242-245.

Sutani, T., T. Kawaguchi, R. Kanno, T. Itoh, and K. Shirahige. 2009. Budding yeast Wpl1(Rad61)-Pds5 complex counteracts sister chromatid cohesion-establishing reaction. *Curr Biol*. 19:492-497.

Tedeschi, A., G. Wutz, S. Huet, M. Jaritz, A. Wuensche, E. Schirghuber, I.F. Davidson, W. Tang, D.A. Cisneros, V. Bhaskara, T. Nishiyama, A. Vaziri, A. Wutz, J. Ellenberg, and J.M. Peters. 2013. Wapl is an essential regulator of chromatin structure and chromosome segregation. *Nature*. 501:564-568.

Unal, E., J.M. Heidinger-Pauli, and D. Koshland. 2007. DNA double-strand breaks trigger genome-wide sister-chromatid cohesion through Eco1 (Ctf7). *Science*. 317:245-248.

Vega, H., Q. Waisfisz, M. Gordillo, N. Sakai, I. Yanagihara, M. Yamada, D. van Gosliga, H. Kayserili, C. Xu, K. Ozono, E.W. Jabs, K. Inui, and H. Joenje. 2005. Roberts syndrome is caused by mutations in ESCO2, a human homolog of yeast ECO1 that is essential for the establishment of sister chromatid cohesion. *Nat Genet*. 37:468-470.

Verni, F., R. Gandhi, M.L. Goldberg, and M. Gatti. 2000. Genetic and molecular analysis of wings apart-like (wapl), a gene controlling heterochromatin organization in Drosophila melanogaster. *Genetics*. 154:1693-1710.

Walhout, A., and S. Boulton. 2006. Biochemistry and molecular biology. *In* WormBook.
Watanabe, Y., and P. Nurse. 1999. Cohesin Rec8 is required for reductional chromosome segregation at meiosis. *Nature*. 400:461-464.
Wells, D., and J.D. Delhanty. 2000. Comprehensive chromosomal analysis of human preimplantation embryos using whole genome amplification and single cell comparative genomic hybridization. *Mol Hum Reprod*. 6:1055-1062.
Yokobayashi, S., M. Yamamoto, and Y. Watanabe. 2003. Cohesins determine the attachment manner of kinetochores to spindle microtubules at meiosis I in fission yeast. *Mol Cell Biol*. 23:3965-3973.
Yuan, L., X. Yang, J.L. Ellis, N.M. Fisher, and C.A. Makaroff. 2012. The Arabidopsis SYN3 cohesin protein is important for early meiotic events. *Plant J*. 71:147-160.
Zanin, E., J. Dumont, R. Gassmann, I. Cheeseman, P. Maddox, S. Bahmanyar, A. Carvalho, S. Niessen, J.R. Yates, 3rd, K. Oegema, and A. Desai. 2011. Affinity purification of protein complexes in C. elegans. *Methods Cell Biol*. 106:289-322.
Zhang, J., H. Hakansson, M. Kuroda, and L. Yuan. 2008. Wapl localization on the synaptonemal complex, a meiosis-specific proteinaceous structure that binds homologous chromosomes, in the female mouse. *Reprod Domest Anim*. 43:124-126.

Appendix A

Table 1 List of *C. elegans* strains used and constructed during the course of this dissertation.

Strain Name	**Genotype**
N2 bristol	Laboratory wildtype
	wapl-1(tm1814)/nT1 IV
EU552	*glp-1(or178)* III
	gfp::12aalinker::wapl-1
	*ieSi?? [cb-unc-119(+) gfp::12aalinker::wapl-1(+)]*II*;wapl-1(tm1814)*IV
	ieSi?? [cb-unc-119(+) gfp::12aalinker::wapl-1(4SA)]II;wapl-1(tm1814)IV
AZ212	*ruIs32[pie-1::GFP::H2B + unc-119(+)]* III
	ruIs32[pie-1::GFP::H2B + unc-119(+)] III; *wapl-1(tm1814)/nT1* IV
AV146	*chk-2(me64)rol-9(sc148)/unc-51(e369)rol-9(sc148)*V
AV157	*spo-11(me44)/nT1[unc-?(n754)let-? qIs50]* (IV;V)
TY5038	*htp-3(tm3655)*I*/hT2*(I,III)
RB1183	*prom-1(ok1140)*I
BS3156	*unc-13(e51)gld-1(q485)/hT2* III
JK3182	*gld-3(q730)nos-3(q650)/mIn1[mIs14 dpy-10(e128)]* II
	*wapl-1(tm1814)*IV;*chk-2(me64)rol-9(sc148)/unc-51(e369)/rol-9(sc148)*V
VC666	*rec-8(ok978)IV/nT1[qIs51]IV:V*
	rec-8(ok978)/nT1IV;chk-2(me64)rol-9(sc148)/unc-51(e369)/rol-9(sc148)V
ieSi21	*sun-1::mRuby* IV
	ieSi?? [cb-unc-119(+) FLP1] II
	ieSi?? [cb-unc-119(+) FLP2] II
	ieSi?? [cb-unc-119(+) FLP3] II
	ieSi?? [cb-unc-119(+) FLP1] X
	ieSi?? [cb-unc-119(+) FLP2] X
	ieSi?? [cb-unc-119(+) FLP3] X
	ieSi?? [cb-unc-119(+) FLP1] II;*zim-1(tm1813)/mIs11* IV
	ieSi?? [cb-unc-119(+) FLP2] II;*zim-1(tm1813)/mIs11* IV
	ieSi?? [cb-unc-119(+) FLP3] II;*zim-1(tm1813)/mIs11* IV
PS2442	*dpy-20(e1282)*IV*;SyIs44[pMH86(dpy-20(+))+pPD49-78::lacI+lacO(256)]V*
	*zim-2(tm574)*IV*;SyIs44[pMH86(dpy-20(+))+pPD49-78::lacI+lacO(256)]V*
	ieSi?? [cb-unc-119(+) FLP1] II; *ced-4(n1162)* III
	ieSi?? [cb-unc-119(+) FLP3] II; *ced-4(n1162)* III
EG6699	*ttTi5605 II; unc-119(ed3) III; oxEx1578*

Table 2 List of plasmids used and constructed during the course of this dissertation.

Name	Description	Drug Resistsance	Cell Type	Designer(s)
pNIN1	FlpFrag 1 Inserted into pCFJ350[MosSci ChrII]	Carb	DH5α	Christina Glazier
pNIN3	FlpFrag 2 Inserted into pCFJ350[MosSci ChrII]	Carb	DH5α	Christina Glazier
pNIN5	FlpFrag 3 Inserted into pCFJ350[MosSci ChrII]	Carb	DH5α	Christina Glazier
pNIN12	FlpFrag 1 Inserted into pCFJ355[MosSci XChr]	Carb	DH5α	Christina Glazier
pNIN14	FlpFrag 2 Inserted into pCFJ355[MosSci XChr]	Carb	DH5α	Christina Glazier
pNIN15	FlpFrag 3 Inserted into pCFJ355[MosSci XChr]	Carb	DH5α	Christina Glazier
pNIN24	pCR-Blunt with 5' of wapl-1 ORF and surrounding sequences	Kan	DH5α	Christina Glazier
pNIN25	pCR-Blunt with 3' of wapl-1 ORF and surrounding sequences	Kan	DH5α	Christina Glazier
pNIN26	pCR-Blunt with wapl-1 ORF and surrounding sequences	Kan	DH5α	Christina Glazier
pNK08	GFP-12aalinker-WAPL-1ORF in pCFJ350 with wapl-1 surrounding sequences	Carb		Nora Kostow
pNIN32	wapl-1 cDNA with 6XHIS in pET23c	Carb	DH5α	Christina Glazier
pNIN40	pET23c with middle 544 amino acids of WAPL-1 cDNA and 6XHIS	Carb	Rosetta	Christina Glazier
pNIN41	pNK08 with S179A mutation	Carb	DH5α	Nora Kostow and Christina Glazier
pNIN42	pNK08 S179A and S323A mutations	Carb	DH5α	Nora Kostow and Christina Glazier
pNIN43	pNIN32 with S179A mutation	Carb	DH5α or XL10	Christina Glazier
pNIN44	pNIN32 with S179A S323A mutations	Carb	DH5α or XL10	Christina Glazier
pNIN45	pNK08 with S179A S323A S728A mutations	Carb	XL10-Gold	Nora Kostow and Christina Glazier
pNIN46	pNIN32 with S179A S323A S728A mutations	Carb	XL10-Gold	Christina Glazier
pNIN47	pNK08 with S179A S323A S371A S728A mutations	Carb	XL10-Gold	Nora Kostow and Christina Glazier
pNIN48	pNIN32 with S179A S323A S371A S728A mutations	Carb	XL10-Gold	Christina Glazier
pNIN39	pET23c with last 100 amino acids of WAPL-1 cDNA and 6XHIS	Carb	Rosetta	Christina Glazier
pNK13	wapl-1(N-lobe) cDNA in pET23c with 6XHIS	Carb	XL10-Gold	Nora Kostow
pNK12	wapl-1(N-extension) cDNA in pET23c with 6XHIS	Carb	XL10-Gold	Nora Kostow
pNK14	wapl-1(C-lobe) cDNA in pET23c with 6XHIS	Carb	XL10-Gold	Nora Kostow
pNK02	pNIN26 w/ gfp ORF and 12aalinker at N-terminus of wapl-1 and PAM seq mutated from 5'cca to 5'cAa	Kan		Nora Kostow
pNK07	pDD162 with wapl-1 targeting sequence ccatcagtacgcagttccgact	Carb		Jordan Ward, Yumi Kim, and Nora Kostow
C14B9.4	Ahringer plk-1 RNAi clone	Tet/Carb		Ahringer lab
R08C7.10	Ahringe wapl-1 RNAi clone	Tet/Carb		Ahringer lab

Appendix B

Table 3 List of *C. elegans* proteins identified by mass spectrometry following immunoprecipitation of endogenous WAPL-1 with affinity purified guinea pig WAPL-1 antibody. In parallel, a negative control with normal guinea pig IgG was performed. Any *C. elegans* proteins identified by mass spectrometry of the negative control were removed from this table. Any identified human proteins, for example human keratin, were also removed from this table.

Locus	Seq. count	Spectrum count	Seq. Coverage	pI	NSAF	EMPAI	Gene Ontology	Gene name
Y47D3A.26	162	1383	66.90%	6.9	0.18600494	3.666594	Cohesin	locus:smc-3
F28B3.7a	136	1454	66.10%	7.6	0.18672153	3.581419	Cohesin	locus:him-1
R08C7.10a	99	1790	60.30%	5.3	0.14123726	3.008667	Cohesin-associated	locus:wapl-1
W02D3.11a	40	279	60.30%	6.8	0.029913478	3.008667	mRNA splicing	locus:hrpf-1
C23G10.3	22	79	57.90%	9.6	0.027905107	2.7931497	Ribosome	locus:rps-3
F54C9.5	27	104	57.70%	9.8	0.030968437	2.775722	Ribosome	locus:rpl-5
Y43B11AR.4	22	99	57.50%	10.5	0.033349473	2.758374	Ribosome	locus:rps-4
Y24D9A.4c	20	85	47.80%	10.7	0.03026958	2.006076	Ribosome	locus:rpl-7A
K04D7.1	15	45	46.80%	6.9	0.012080439	1.9376497	Embryo development	locus:rack-1
F53G12.10	19	100	46.70%	10.2	0.035757218	1.9308932	Ribosome	locus:rpl-7
B0041.4	24	171	46.40%	11.2	0.043244466	1.9107172	Ribosome	locus:rpl-4
ZK1010.1	7	31	46.10%	9.8	0.02113028	1.8906798	Ubiquitn Ribosome	locus:ubq-2
T27E9.1a	22	64	46.00%	9.7	0.018612824	1.8840315	Mitochondria	locus:tag-61
Y18D10A.17	15	42	45.60%	9.2	0.010777646	1.8575904	Embryo development	locus:car-1
F46F11.2	10	28	45.30%	8.3	0.009149562	1.837919	Transcription regulation	locus:cey-2
F18E2.3	74	1002	45.00%	6.8	0.1481653	1.8183827	Cohesin-associated	locus:scc-3
Y24D9A.4a	20	85	44.20%	10.8	0.027985083	1.7669415	Ribosome	locus:rpl-7A
Y106G6H.2a	33	165	43.50%	9	0.015034412	1.7227013	Embryo/larval development	locus:pab-1
B0393.1	13	46	43.50%	5.7	0.014541269	1.7227013	Ribosome	locus:rps-0
F56F3.5	12	43	42.80%	9.6	0.014597849	1.6791685	Ribosome	locus:rps-1
T01C3.7	22	112	42.30%	10.3	0.027760603	1.6485	Embryo/larval development	locus:fib-1
K08A8.3	54	259	42.20%	4.9	0.0233823	1.6424088	Cohesin	locus:coh-1
Y71A12B.1	17	70	40.70%	10.3	0.024826556	1.5527012	Ribosome	locus:rps-6
C32E8.2a	12	26	40.60%	11.1	0.010958638	1.5468302	Ribosome	locus:rpl-13
C49H3.11	13	51	40.10%	10.1	0.016358927	1.5176768	Ribosome	locus:rps-2
M01E11.5	9	16	39.60%	8.5	0.00526778	1.4888573	Transcription regulation	locus:cey-3

Locus	Seq. count	Spectrum count	Seq. Coverage	pI	NSAF	EMPAI	Gene Ontology	Gene name
F07A5.7	30	111	37.70%	5.5	0.020629838	1.3823195	Locomotion	locus:unc-15
F43G9.1	11	22	37.40%	7.4	0.005361585	1.3659198		
F42C5.8	6	10	37.00%	10.6	0.004194597	1.3442287	Ribosome	locus:rps-8
Y69A2AR.18a	9	24	36.10%	9	0.007003153	1.2961485		
M163.3	6	13	35.60%	10.9	0.005452976	1.2698648	Histone	locus:his-24
F45E4.2	8	11	34.50%	9.3	0.004246566	1.2130947	Embryo and gut development	locus:plp-1
K07C5.4	14	49	33.50%	8.6	0.005934646	1.1627185		
B0035.9	4	8	33.00%	11.2	0.006776514	1.1379621	Histone	locus:his-46
C50F4.7	4	8	33.00%	11.2	0.006776514	1.1379621	Histone	locus:his-37
F07B7.9	4	8	33.00%	11.2	0.006776514	1.1379621	Histone	locus:his-50
F17E9.12	4	8	33.00%	11.2	0.006776514	1.1379621	Histone	locus:his-31
F22B3.1	4	8	33.00%	11.2	0.006776514	1.1379621	Histone	locus:his-64
F45F2.3	4	8	33.00%	11.2	0.006776514	1.1379621	Histone	locus:his-5
F54E12.3	4	8	33.00%	11.2	0.006776514	1.1379621	Histone	locus:his-56
F55G1.11	4	8	33.00%	11.2	0.006776514	1.1379621	Histone	locus:his-60
K03A1.6	4	8	33.00%	11.2	0.006776514	1.1379621	Histone	locus:his-38
K06C4.10	4	8	33.00%	11.2	0.006776514	1.1379621	Histone	locus:his-18
K06C4.2	4	8	33.00%	11.2	0.006776514	1.1379621	Histone	locus:his-28
T10C6.14	4	8	33.00%	11.2	0.006776514	1.1379621	Histone	locus:his-1
T23D8.5	4	8	33.00%	11.2	0.006776514	1.1379621	Histone	locus:his-67
ZK131.1	4	8	33.00%	11.2	0.006776514	1.1379621	Histone	locus:his-26
ZK131.4	4	8	33.00%	11.2	0.006776514	1.1379621	Histone	locus:his-10
ZK131.8	4	8	33.00%	11.2	0.006776514	1.1379621	Histone	locus:his-14
C04F6.1	59	308	32.80%	7	0.031139137	1.128139	Lipid transport	locus:vit-5
F01F1.12a	9	17	32.50%	7.9	0.004052485	1.1134889	Fructose-biphosphate aldolase	
Y66H1A.4	7	18	32.40%	10.9	0.0064363	1.1086283	Probable ribonucleo protein	
C26C6.2	9	13	31.40%	5.4	0.003204008	1.0606298	G-protein	locus:goa-1
D2092.4	8	33	30.60%	5.5	0.007931601	1.0230191		
C37H5.8	22	53	30.40%	6.2	0.004748381	1.0137241	Heat shock protein	locus:hsp-6
D2030.6	30	101	30.20%	8.4	0.027866315	1.004472	Argonaut/piwi proteins	locus:prg-1
B0250.1	13	98	29.60%	11.1	0.032885637	0.9769696	Ribosome	locus:rpl-2
Y54E10A.10	8	19	29.60%	9.8	0.005581497	0.9769696		
K09F5.2	57	405	28.90%	6.9	0.04061655	0.94536006	Lipid transport	locus:vit-1
W09H1.6a	7	17	28.70%	6.6	0.005316163	0.936422	Cuticle	locus:lec-1

Locus	Seq. count	Spectrum count	Seq. Coverage	pI	NSAF	EMPAI	Gene Ontology	Gene name
C27A2.2a	4	7	28.50%	9.8	0.004697948	0.9275249	Ribosome	locus:rpl-22
K11D9.2a	24	85	28.20%	5.2	0.013008053	0.914256	Calcium transport	locus:sca-1
F01G4.6a	10	22	27.60%	9	0.005645434	0.8879913	Mitochondrial	
F46E10.10a	8	13	26.80%	7.1	0.003375652	0.8535316	Carbohydrate metabolisn	
C56G2.6	8	15	26.30%	9.5	0.0041415	0.8323144	Hormone metabolism	locus:let-767
F59D8.1	48	259	26.30%	6.9	0.026185183	0.8323144	Lipid transport	locus:vit-3
F37C12.9	3	6	26.30%	10.4	0.003443985	0.8323144	Ribosome	locus:rps-14
F36A2.6	4	5	25.80%	10.3	0.002888994	0.8113401	Ribosome	locus:rps-15
Y45F10D.12	4	6	25.50%	11.4	0.002784498	0.7988709	Ribosome	locus:rpl-18
F59D8.2	46	258	25.00%	7	0.02608408	0.7782794	Lipid transport	locus:vit-4
T01B11.4	9	30	24.30%	9.8	0.008362391	0.7498466	Endocytosis	locus:tag-316
T08B2.7a	14	20	24.30%	9.4	0.00150735	0.7498466	Fatty acid metabolism	
R13A5.12	11	23	24.30%	9.4	0.002549578	0.7498466	Lipid storage	locus:lpd-7
ZK892.1a	6	9	24.20%	7.7	0.002643867	0.7458222	Carbohydrate binding	locus:lec-3
E02D9.1b	6	9	24.10%	8.5	0.002492789	0.74180686	Locomotion and larval development	
T04A8.6	11	22	24.10%	10.8	0.006252272	0.74180686	Ribosome biogenesis	
F46H5.3a	8	14	23.50%	7.3	0.003084512	0.7179084	Arginine kinase	
K11H12.2	3	6	23.50%	11.6	0.002566106	0.7179084	Ribosome	locus:rpl-15
ZC302.1	20	81	23.10%	5.6	0.025295252	0.7021586	Double-strand break repair	locus:mre-11
F23C8.5	4	6	23.10%	8.6	0.002052885	0.7021586	Electron carrier	
T07A9.11	2	2	22.90%	10.7	0.001332025	0.69433784	Ribosome	locus:rps-24
K12G11.3	9	17	22.60%	6.5	0.004249884	0.68267405	Alcohol dehydrogenase	locus:sodh-1
Y53F4B.22	8	23	22.20%	6.7	0.005365495	0.6672472	Actin-like	
Y71F9AM.6	4	10	22.20%	6.2	0.003394849	0.6672472	Embryo development	locus:trap-1
F45F2.2	3	5	22.20%	9.6	0.004039241	0.6672472	Histone	locus:his-39
F55F8.2a	12	17	22.10%	9.3	0.003693171	0.6634127	RNA helicase	
Y32H12A.3	6	8	21.90%	8.8	0.002188028	0.65576994	Metabolism	locus:dhs-9
Y53G8AR.9	4	12	21.90%	7.7	0.003323719	0.65576994	Metal ion binding	
T05G5.6	6	15	21.90%	8.4	0.004544146	0.65576994	Mitochondrial /larval development	locus:ech-6
Y71F9AL.13a	4	13	21.80%	9.9	0.005251014	0.6519618	Ribosome	locus:rpl-1

Locus	Seq. count	Spectrum count	Seq. Coverage	pI	NSAF	EMPAI	Gene Ontology	Gene name
F52D10.3a	6	11	21.40%	4.9	0.003869854	0.6368165	14-3-3 protein	locus:ftt-2
B0207.9	3	63	21.30%	9.8	0.10157967	0.633052		
C15H9.6	12	40	20.90%	5.1	0.003561997	0.61808	Heat shock protein	locus:hsp-3
R07B7.3	6	11	20.30%	12.6	0.002703447	0.5958791		locus:pqn-53
F10B5.1	6	11	20.10%	10.3	0.00448469	0.58854675	Ribosome	locus:rpl-10
T04C12.4	7	14	19.90%	5.5	0.006034337	0.58124804	Actin	locus:act-3
T04C12.5	7	14	19.90%	5.5	0.006034337	0.58124804	Actin	locus:act-2
T04C12.6	7	14	19.90%	5.5	0.006034337	0.58124804	Actin	locus:act-1
F08G2.1	3	5	19.70%	10.4	0.003575722	0.57398295	Histone	locus:his-44
F17E9.9	3	5	19.70%	10.4	0.003575722	0.57398295	Histone	locus:his-34
F35H10.11	3	5	19.70%	10.4	0.003575722	0.57398295	Histone	locus:his-29
ZK131.5	3	5	19.70%	10.4	0.003575722	0.57398295	Histone	locus:his-11
ZK131.9	3	5	19.70%	10.4	0.003575722	0.57398295	Histone	locus:his-15
W07E6.1	8	20	19.60%	9.1	0.001772952	0.5703628	Methyltransferase/larval development	locus:nol-1
B0035.8	3	5	19.50%	10.4	0.003546651	0.566751	Histone	locus:his-48
C50F4.5	3	5	19.50%	10.3	0.003546651	0.566751	Histone	locus:his-41
F45F2.12	3	5	19.50%	10.4	0.003546651	0.566751	Histone	locus:his-8
F54E12.4	3	5	19.50%	10.4	0.003546651	0.566751	Histone	locus:his-58
F55G1.3	3	5	19.50%	10.4	0.003546651	0.566751	Histone	locus:his-62
H02I12.6	3	5	19.50%	10.4	0.003546651	0.566751	Histone	locus:his-66
K06C4.12	3	5	19.50%	10.4	0.003546651	0.566751	Histone	locus:his-22
K06C4.4	3	5	19.50%	10.4	0.003546651	0.566751	Histone	locus:his-20
C34E10.6	7	16	19.10%	5.8	0.002594725	0.552387	ATP hydrolysis	locus:atp-2
C54G4.8	4	12	18.60%	8.6	0.003673584	0.53461695	ATP production	locus:cyc-1
Y38F2AL.3a	6	9	18.50%	8	0.002044866	0.5310875	ATP hydrolysis	locus:vha-11
C44B12.5	4	5	18.10%	6.7	0.001098836	0.5170504		
B0365.3	15	18	18.00%	5.5	0.004108644	0.51356125	Sodium transport	locus:eat-6
T10B5.3	6	11	18.00%	4.7	0.003253301	0.51356125		
C28H8.12	5	8	17.80%	5.2	0.002108704	0.50660706	Microtubule movement	locus:dnc-2
Y37E3.9	4	10	17.80%	7.6	0.00317264	0.50660706	Mitochondrial organization	locus:phb-1
R07H5.1	3	4	17.40%	4.9	0.001352676	0.4927944	Embryo/larval development	locus:prx-14
ZC155.1	5	10	17.40%	6.6	0.002709553	0.4927944	Engulfment of apoptotic cells	locus:nex-1
F01G4.4	10	43	17.40%	9.6	0.015062919	0.4927944		

Locus	Seq. count	Spectrum count	Seq. Coverage	pI	NSAF	EMPAI	Gene Ontology	Gene name
Y105E8B.1a	4	5	17.30%	4.7	0.00153605	0.48936105	Actin-binding	locus:lev-11
F07D10.1	3	12	17.30%	10	0.005341691	0.48936105	Ribosome	locus:rpl-11.2
T22F3.4	3	12	17.30%	10	0.005341691	0.48936105	Ribosome	locus:rpl-11.1
R05D11.8	8	16	17.30%	8.1	0.001663944	0.48936105		locus:edc-3
F33H1.2	8	18	17.00%	7.9	0.004605446	0.47910845	GAPDH Enzyme	locus:gpd-4
T09F3.3	8	18	17.00%	7.9	0.004605446	0.47910845	GAPDH Enzyme	locus:gpd-1
F07B7.11	3	5	17.00%	10.4	0.003093887	0.47910845	Histone	locus:his-54
F07B7.4	3	5	17.00%	10.4	0.003093887	0.47910845	Histone	locus:his-52
T10C6.11	3	5	17.00%	10.4	0.003093887	0.47910845	Histone	locus:his-4
D1007.12	2	6	17.00%	11.3	0.003292363	0.47910845	Ribosome	locus:rpl-24.1
K07A1.8	6	7	16.90%	6.6	0.003234583	0.47570658		locus:ile-1
C27B7.5	4	5	16.80%	9.3	0.00113015	0.47231245		Zinc
F18H3.3a	14	54	16.80%	9.1	0.004593278	0.47231245		locus:pab-2
ZK945.3	15	34	16.70%	9.3	0.010091031	0.4689263	Oviposition and embryo development	locus:puf-12
ZK909.3	2	2	16.60%	5.8	7.62E-04	0.46554792		
T04G9.3	5	28	16.40%	6.4	0.007040153	0.45881426	Oviposition and embryo development	locus:ile-2
F28D1.7	2	2	16.10%	10.5	0.001220246	0.44877183	Ribosome	locus:rps-23
R07H5.8	4	7	16.10%	6	0.00178577	0.44877183		
F43E2.8	8	32	16.00%	5.1	0.002866947	0.44543982	Heat shock protein	locus:hsp-4
ZC434.2	5	15	16.00%	9.9	0.006745949	0.44543982	Ribosome	locus:rps-7
T28D6.6	4	6	15.60%	8.9	0.001430289	0.4321879		
F11C3.3	23	39	15.30%	5.7	0.003219836	0.42232883	Myosin	locus:unc-54
C36E8.5	6	10	15.30%	4.9	0.001938836	0.42232883	Tubuline	locus:tbb-2
K12G11.4	5	8	15.10%	6.6	0.00198855	0.41579378	Oxidation-reduction	locus:sodh-2
M117.2	6	16	14.90%	4.8	0.005628878	0.40928876	14-3-3 protein	locus:par-5
T04H1.4a	16	37	14.90%	7.5	0.004619728	0.40928876	Double-strand break repair	locus:rad-50
F13B10.2a	5	9	14.70%	10.4	0.001958176	0.40281367	Ribosome	locus:rpl-3
D2013.7	2	2	14.60%	6.1	5.94E-04	0.39958727	Translation initiation	locus:eif-3.F
Y39A1C.3	4	4	14.60%	9.5	0.001187042	0.39958727		locus:cey-4
F53F4.11	6	7	14.50%	9.4	7.59E-04	0.39636838		
Y54F10AL.1a	2	4	14.50%	5.2	0.002182694	0.39636838		
R07G3.5	3	9	14.40%	8.9	0.002764889	0.39315677	Serine/threonine phosphatase	

Locus	Seq. count	Spectrum count	Seq. Coverage	pI	NSAF	EMPAI	Gene Ontology	Gene name
F53A2.4	4	4	14.40%	5.2	0.001090595	0.39315677	Synaptic transmission	locus:nud-1
R06C7.1	11	23	14.30%	8.5	0.00394444	0.38995266	Argonaut/risc protein	
H39E23.1a	10	14	14.20%	9.5	0.002670159	0.38675582	Embryonic polarity	locus:par-1
Y59A8A.3	8	10	14.20%	6.9	0.003363092	0.38675582	Endoplasmic reticulum protein	
F56F3.1	8	22	14.20%	8.8	0.006572391	0.38675582		locus:pqn-45
C03C10.1	6	8	14.10%	9.6	0.002046865	0.38356638	Casein Kinase I	locus:kin-19
C47B2.3	4	6	14.10%	5.1	0.002170514	0.38356638	Tubulin	locus:tba-2
R10E4.1	4	10	14.10%	8.5	0.00231426	0.38356638		
Y18D10A.11	2	2	14.10%	4.9	7.04E-04	0.38356638		
K01G5.7	8	43	14.00%	4.9	0.005637119	0.38038433	Tubulin	locus:tbb-1
ZK662.4	14	23	14.00%	6.9	0.003631205	0.38038433	Vulval development	locus:lin-15B
F07A5.2	4	6	13.90%	11	0.001688664	0.37720942		
F13D12.2	4	6	13.80%	6.9	0.001572029	0.37404191	Lactate dehydrogenase	locus:ldh-1
Y22F5A.4	3	6	13.80%	5.7	0.001756663	0.37404191	Putative lysozyme	locus:lys-1
VW02B12L.3	2	4	13.70%	5.1	0.001167192	0.3708818	Microtubule-binding protein	locus:ebp-2
F25H5.4	11	21	13.70%	6.5	0.003994561	0.3708818	Translation elongation	locus:eft-2
Y71H2AM.19	7	14	13.50%	6.9	0.001281599	0.36458313	RNA helicase	
Y57A10A.26	4	8	13.40%	8	0.002594725	0.3614447		
ZK795.3	3	9	13.40%	8.6	0.002689139	0.3614447		
T24H7.1	4	9	13.30%	9.7	0.002670845	0.35831344	Mitochondrial organization	locus:phb-2
JC8.3a	2	4	13.30%	9.4	0.002115094	0.35831344	Ribosome	locus:rpl-12
C15F1.6	3	4	13.00%	9.6	0.001133086	0.3489629	Lipid metabolism	locus:art-1
C01G5.2	13	34	12.70%	8.7	0.010705996	0.33967674	Argonaut/Piwi protein	locus:prg-2
F29F11.6	3	5	12.50%	6.1	0.001325952	0.3335215	Protein phosphatase I	locus:gsp-1
C17E4.9	4	8	12.50%	7.6	0.00218119	0.3335215	Sodium transport	
Y110A2AL.14	3	4	12.40%	8.2	0.001057547	0.33045447	Embryo and vulval morphogenesis	locus:sqv-2
F56H11.4	4	7	12.20%	9.7	0.002120602	0.32434154	Fatty acid biosynthesis	locus:elo-1

Locus	Seq. count	Spectrum count	Seq. Coverage	pI	NSAF	EMPAI	Gene Ontology	Gene name
F08C6.4a	3	4	12.10%	5.3	0.001057547	0.32129562		locus:sto-1
CD4.6	2	3	11.90%	7	0.001006703	0.31522477		locus:pas-6
F02E8.1	3	4	11.80%	8.7	0.001144231	0.31219995	ATP synthesis	locus:asb-2
F31E3.5	5	23	11.70%	8.9	0.004334115	0.30918193	Translation elongation	locus:eft-3
R03G5.1a	5	23	11.70%	8.9	0.004334115	0.30918193	Translation elongation	locus:eft-4
VW06B3R.1a	4	8	11.70%	8.1	0.001702393	0.30918193		locus:ucr-2.1
ZK686.3	4	10	11.50%	9.1	0.002635879	0.30316675	Magnesium transport	
ZK1248.16	4	8	11.50%	8	0.002222869	0.30316675		locus:lec-5
W02D3.6	4	8	11.30%	9.5	0.002326603	0.29717934	ATP translocase	locus:tag-194
T12F5.3	9	22	11.30%	5.4	0.004326635	0.29717934	RNA helicase	locus:glh-4
F52B5.3	12	29	11.00%	8.4	0.003298166	0.2882495	Helicase	
C08H9.2	11	20	11.00%	6.8	0.002656804	0.2882495		
W03C9.7	2	4	10.90%	7.1	4.77E-04	0.28528666	Embryonic polarity	locus:mex-1
Y23H5A.3	3	4	10.70%	8.7	0.001136777	0.27938128		
Y44E3A.6a	5	5	10.70%	5.3	0.001351635	0.27938128		
T02G5.7	3	5	10.30%	5.4	0.001118559	0.26765192		
C17H12.14	2	3	10.20%	7.2	0.001158154	0.2647363	ATP hydrolysis	locus:vha-8
C24H12.4a	6	12	10.10%	9.3	0.001114107	0.2618276	DEAD-box helicase	
Y74C10AR.1	3	5	10.10%	5.5	0.001334061	0.2618276	Serine/ threonine kinase receptor ortholog	locus:eif-3.I
F42A8.2	3	7	10.10%	8.2	0.002049441	0.2618276	Succinate dehydrogenase	locus:sdhb-1
C07D8.6	3	4	10.10%	5.7	0.001100916	0.2618276		
T04A8.9	2	3	10.00%	9.6	0.001051176	0.25892544		locus:dnj-18
T05H4.5	3	3	10.00%	8	8.47E-04	0.25892544		
Y48B6A.1	5	15	9.90%	8.3	0.001309985	0.25602996	Embryo/larval development	
T05E11.3	7	11	9.70%	5.1	0.00329052	0.25025904	ER chaperone	
K07A12.7	3	4	9.70%	9.2	0.001057547	0.25025904	Mitochondrial ribosome	
F52H3.7a	11	18	9.60%	4.4	0.001261411	0.24738348		locus:lec-2
Reverse_F45E4.1	1	1	9.50%	7.3	0.001270084	0.24451458	ADP-ribosylation	locus:arf-1.1
K04G2.3	5	8	9.40%	7.2	6.50E-04	0.24165225	Embryo/larval development	locus:cdc-48.3
D1081.7a	6	30	9.30%	5.6	0.005673222	0.23879659		
F44F4.11	3	6	9.20%	5	0.001168495	0.23594749	Tubulin	locus:tba-4

Locus	Seq. count	Spectrum count	Seq. Coverage	pI	NSAF	EMPAI	Gene Ontology	Gene name
B0303.3	4	8	9.20%	9.1	0.001557993	0.23594749		
T23G11.3	3	5	9.10%	8.2	9.42E-04	0.23310483	Mitosis-to-meiosis regulation	locus:gld-1
F26E4.8	3	6	9.10%	5.1	0.001165892	0.23310483	Tubulin	locus:tba-1
F14E5.2a	9	29	9.00%	6.1	0.004090415	0.23026884	Golgi apparatus	
C54C6.2	4	6	9.00%	4.9	0.002190068	0.23026884	Tubulin	locus:ben-1
C04F12.4	1	3	8.90%	11.3	0.001938836	0.22743917	Ribosome	locus:rpl-14
T05F1.3	1	2	8.90%	10.3	0.001195173	0.22743917	Ribosome	locus:rps-19
F13D12.7	2	3	8.80%	6	7.70E-04	0.22461617	Mitotic spindle orientation	locus:gpb-1
Y47G6A.20b	6	10	8.80%	5.7	0.001164855	0.22461617	mRNA regulation	locus:rnp-6
R12H7.2	3	8	8.80%	6.5	0.001572029	0.22461617	Necrotic cell death	locus:asp-4
K12H4.3	3	7	8.80%	9.1	0.001735038	0.22461617	Ribosome biogenesis	
H15N14.2a	6	6	8.70%	7.5	0.001655425	0.22179961	Vesicular-fusion protein	locus:nsf-1
C44B7.10	4	8	8.70%	8.6	0.001481913	0.22179961		
F54D5.8	2	9	8.50%	9.2	0.002372292	0.21618605		locus:dnj-13
Y57G7A.10a	2	4	8.50%	6	0.001187042	0.21618605		
T08G2.3	4	4	8.40%	8.2	8.37E-04	0.2133888	Oxidation-reduction	
C44B12.1	2	5	8.40%	8.5	0.002148956	0.2133888		
R74.1	8	15	8.40%	6.6	0.002049727	0.2133888		locus:lrs-1
T06D8.8	3	4	8.30%	6.8	9.02E-04	0.21059811	19S proteasome	locus:rpn-9
F08C6.2a	2	2	8.30%	6.4	4.82E-04	0.21059811	Cholinephosphate cytidylyltransferase	
C06B3.4	2	3	8.30%	7.5	8.34E-04	0.21059811	Metabolism	locus:stdh-1
F11A5.12	2	3	8.30%	8.7	8.31E-04	0.21059811	Metabolism	locus:stdh-2
F55F3.3	2	3	8.20%	7.1	8.26E-04	0.20781386	Potassium and sodium transport	
Y57G11C.11a	2	3	8.20%	7.9	9.77E-04	0.20781386	Ubiquinone biosynthesis	locus:coq-3
T13F2.8	1	2	8.10%	5.5	7.43E-04	0.20503592	Meiotic nuclear division	locus:cav-1
F56C9.1	2	3	8.10%	6.8	7.86E-04	0.20503592	Protein phosphatase I	locus:gsp-2
Y63D3A.6b	4	5	8.00%	5.2	0.001511602	0.20226443		locus:dnj-29
Y71F9AL.9	2	3	8.00%	9.8	8.34E-04	0.20226443		
D2023.2	6	12	7.90%	7	0.001655132	0.19949937	Metabolism	locus:pyc-1

Locus	Seq. count	Spectrum count	Seq. Coverage	pI	NSAF	EMPAI	Gene Ontology	Gene name
C37E2.1	3	5	7.90%	7.8	0.001151024	0.19949937	Oxidation-reduction	
T19C4.6	2	3	7.80%	7.9	7.33E-04	0.19674051	Neuronal G-protein	locus:gpa-1
W01B11.3	3	5	7.80%	7.1	8.96E-04	0.19674051	Ribonucleoprotein	locus:nol-5
K02F2.2	3	9	7.80%	6.3	0.001796862	0.19674051	S-adenosylhomocystein hydrolase	
ZK688.8	4	5	7.70%	7.7	4.81E-04	0.19398808		locus:gly-3
C16A3.3	12	37	7.60%	7.6	0.003440279	0.19124198	Programmed cell death	locus:let-716
K01G5.5	3	22	7.60%	8.6	0.004313365	0.19124198		
F42G8.11	2	4	7.50%	7.6	0.001537403	0.18850219	Synaptic vesicle transport	locus:sph-1
T05A12.3	3	3	7.50%	9.8	0.002109006	0.18850219		
F40E10.3	3	3	7.40%	4.3	6.28E-04	0.18576872	Calcium homeostasis	locus:csq-1
C18B2.4	2	3	7.40%	8.3	8.84E-04	0.18576872		
F57A8.2b	3	4	7.40%	5.9	9.18E-04	0.18576872		
F17C11.9a	2	4	7.30%	6.7	8.77E-04	0.18304157	Translation elongation	
F43D9.2	2	3	7.20%	6.5	8.53E-04	0.18032062	Protein transport	locus:rab-33
B0432.13	2	3	7.10%	9	5.80E-04	0.17760599		
Y116A8C.35	1	2	7.00%	8.6	6.12E-04	0.17489755	Embryo development	locus:uaf-2
ZK430.1	9	21	7.00%	7.6	0.002062646	0.17489755	Embryo/larval development	
F25B5.4a	7	38	7.00%	7.4	0.003956336	0.17489755	Ubiquitin	locus:ubq-1
F58F6.4	2	5	6.90%	8.6	0.001306102	0.17219532	DNA Replication	locus:rfc-2
F10G7.4	3	5	6.80%	4.7	0.003569506	0.1694994	Cohesin	locus:scc-1
C47E8.5	4	4	6.80%	5	9.23E-04	0.1694994	Heat shock protein	locus:daf-21
C39F7.4	2	4	6.80%	5.7	0.001702393	0.1694994	Ras-like Small GTPase	locus:rab-1
F33G12.5	6	9	6.80%	5.2	0.001571751	0.1694994		
Y55F3AM.13	2	3	6.80%	9.4	7.39E-04	0.1694994		
C42C1.15	2	4	6.70%	6.5	0.001118559	0.16680968	Lipid rafts	
C02E11.1a	4	11	6.70%	7.4	0.00159029	0.16680968		
F11F1.4	1	6	6.70%	4.2	0.011511656	0.16680968		
F32D1.5	2	3	6.70%	7.6	7.31E-04	0.16680968		
F57B9.6a	2	3	6.70%	5.1	6.51E-04	0.16680968		locus:inf-1
ZK593.5	7	17	6.60%	5.8	0.002077757	0.16412604	Microtubule movement	locus:dnc-1

Locus	Seq. count	Spectrum count	Seq. Coverage	pI	NSAF	EMPAI	Gene Ontology	Gene name
M01D7.2	2	2	6.60%	7.3	5.21E-04	0.16412604	Protein transport	locus:scm-1
F23B12.7	4	5	6.60%	5.6	8.50E-04	0.16412604		
C36B1.8b	4	5	6.50%	8.2	7.70E-04	0.1614486	Embryo/larval development	
T10E9.7a	2	3	6.50%	8.6	5.88E-04	0.1614486	Mitochondrial complex	locus:nuo-2
Y48G8AL.6	5	6	6.50%	7	9.10E-04	0.1614486	mRNA processing	locus:smg-2
C31C9.2	2	4	6.50%	6.8	0.001083821	0.1614486		
T07A9.9a	3	4	6.50%	9	5.12E-04	0.1614486		
Y41E3.4	5	6	6.40%	7.7	0.001735458	0.15877736	tRNA synthetase	locus:ers-1
F01G10.1	3	4	6.30%	6.6	5.65E-04	0.1561122		
W09C2.3a	6	7	6.20%	8.2	9.06E-04	0.15345323	Calcium transport	locus:mca-1
Y73B6BL.9a	1	10	6.20%	10.8	0.009433402	0.15345323	Histone	locus:hil-2
Y45G12B.1a	3	5	6.20%	6.7	4.04E-04	0.15345323	Oxidation-reduction	locus:nuo-5
ZK1248.7	2	3	6.10%	8.1	0.001339381	0.15080035	Risc component	
K01D12.12	1	2	6.10%	7.9	6.30E-04	0.15080035		locus:cdr-6
K04C2.2	4	4	6.10%	5.5	3.53E-04	0.15080035		
D2005.5	6	10	6.00%	7.1	0.001448302	0.14815366		locus:drh-3
K11H3.1a	2	3	5.90%	6.8	7.06E-04	0.14551294	Carbohydrate metabolisn	locus:gpdh-2
F28H1.3	4	7	5.90%	5.8	0.001171958	0.14551294	tRNA synthetase	locus:ars-2
B0205.7	3	3	5.80%	6.9	7.27E-04	0.1428783	Casein kinase II	locus:kin-3
Reverse_Y53F4B.25	2	6	5.80%	9.1	8.68E-04	0.1428783		
C44F1.3	1	2	5.70%	6.5	6.17E-04	0.14024973	Carbohydrate binding	locus:lec-4
T18D3.4	8	9	5.60%	6.3	4.03E-04	0.13762724	Myosin	locus:myo-2
F10G7.2	4	6	5.50%	7.8	0.001063884	0.13501084	Risc component	locus:tsn-1
F18F11.4	4	5	5.50%	7.8	7.93E-04	0.13501084		
T12D8.9a	5	6	5.50%	5.9	8.23E-04	0.13501084		
F11G11.5	1	1	5.40%	7.3	3.91E-04	0.1324004		
R06A10.2	2	3	5.30%	6.9	6.98E-04	0.12979591	G-protein signaling in oocyte development	locus:gsa-1
C18A11.7a	3	7	5.30%	8	9.54E-04	0.12979591	Muscle organization	locus:dim-1
Y48G8AL.8a	1	2	5.30%	10.3	9.33E-04	0.12979591	Ribosome	locus:rpl-17
F35H8.1	1	2	5.30%	5.6	0.00613955	0.12979591		

Locus	Seq. count	Spectrum count	Seq. Coverage	pI	NSAF	EMPAI	Gene Ontology	Gene name
T16A9.5	1	2	5.30%	5	5.42E-04	0.12979591		
W03D8.9	1	2	5.30%	5.4	5.47E-04	0.12979591		
Y69E1A.1	1	2	5.30%	5	5.42E-04	0.12979591		
F52B10.1	7	10	5.20%	5.7	8.26E-04	0.1271975		locus:nmy-1
C03B1.12	1	6	5.10%	5.4	0.0022088	0.12460494	Lysosome protein	locus:lmp-1
Y11D7A.8	1	1	5.10%	5.2	3.46E-04	0.12460494		
R186.3	1	2	5.00%	7.4	7.27E-04	0.12201846		
W05H9.4	4	4	5.00%	6	0.001165872	0.12201846		
R148.3a	3	6	4.80%	5.1	8.72E-04	0.11686325		
C36B1.4	1	2	4.70%	6.3	6.90E-04	0.11429453	20S proteasome subunit	locus:pas-4
F38H4.9	1	1	4.70%	5.3	2.74E-04	0.11429453	Protein phosphatase 2a	locus:let-92
Y67D8C.10a	4	6	4.60%	5.8	8.38E-04	0.11173177	Calcium transport	locus:mca-3
C16C10.2	1	4	4.60%	9.8	0.001332025	0.11173177		
Y37D8A.5	1	2	4.60%	8.1	4.77E-04	0.11173177		
F47B10.1	2	3	4.40%	6.4	6.02E-04	0.10662377	Metabolism	
ZK381.4a	2	7	4.40%	5	0.004415429	0.10662377	P granule formation	locus:pgl-1
F55A11.2	2	3	4.40%	6.6	6.34E-04	0.10662377	SNARE protein	locus:syn-3
H03A11.2	4	9	4.40%	7.3	0.001197525	0.10662377		
Y45G5AL.1a	1	1	4.40%	4.9	3.20E-04	0.10662377		
Y46G5A.17	4	9	4.40%	8.3	6.80E-04	0.10662377		locus:cpt-1
W02B9.1b	8	21	4.30%	5	6.27E-04	0.10407865	Cadherin	locus:hmr-1
H28O16.1a	2	7	4.30%	8.9	0.001135192	0.10407865	Mitochondrial ATP synthase	
ZC434.5	4	7	4.30%	8.7	9.87E-04	0.10407865	tRNA synthetase	locus:ers-2
H12I19.2	1	2	4.30%	9.8	0.001403364	0.10407865		locus:srz-31
T05E8.3	3	5	4.30%	9.6	9.47E-04	0.10407865		
K11C4.3b	8	9	4.20%	5.5	6.34E-04	0.101539254	Cytoskeletal protein	locus:unc-70
F26A3.3	7	12	4.20%	8.2	0.001191655	0.101539254	RNA polymerase	locus:ego-1
F59C6.5	1	1	4.20%	6.6	3.36E-04	0.101539254		
T22D1.9	3	6	4.10%	6.3	9.91E-04	0.09900582	26S proteasome subunit	locus:rpn-1
C06A1.1	2	2	4.10%	5.3	0.001138359	0.09900582	AAA ATPase/larval development	locus:cdc-48.1

Locus	Seq. count	Spectrum count	Seq. Coverage	pI	NSAF	EMPAI	Gene Ontology	Gene name
H19N07.2a	4	5	4.10%	5.7	7.15E-04	0.09900582		locus:math-33
F56D2.1	2	3	4.00%	6.5	5.56E-04	0.096478224	Mitochondrial processing	locus:ucr-1
B0348.6a	1	2	4.00%	6	7.04E-04	0.096478224	Translational initiation	locus:ife-3
M03F8.3a	3	3	4.00%	5.3	9.17E-04	0.096478224		
T20G5.1	4	7	3.80%	6	6.75E-04	0.09144032	Clathrin heavy chain	locus:chc-1
T10D4.6	3	3	3.80%	6.4	3.29E-04	0.09144032		
C41C4.8	2	3	3.70%	5.4	6.00E-04	0.08893013	AAA ATPase/larval development	locus:cdc-48.2
M106.5	1	1	3.70%	5.2	3.23E-04	0.08893013	Actin capping protein	locus:cap-2
Y23H5B.6	2	2	3.70%	6.1	0.001258105	0.08893013	DEAD-box helicase	
F45E10.1d	4	12	3.70%	9.5	6.89E-04	0.08893013	Migratory cell guidance	locus:unc-53
C01B10.11	1	2	3.60%	7.8	5.74E-04	0.08642566	Locomotion	
D1014.3	1	2	3.40%	5.5	5.92E-04	0.08143401	Endocytosis and secretion	locus:snap-1
T21C12.2	1	6	3.30%	5.7	0.003470916	0.07894671	Oxidation-reduction	locus:hpd-1
Reverse_Y48E1A.1a	5	5	3.30%	8	4.67E-04	0.07894671	RNA polymerase	
C18G1.4a	2	3	3.20%	5.2	2.55E-04	0.07646525	P granule formation	locus:pgl-3
C07D10.5	1	2	3.20%	7.4	4.59E-04	0.07646525		
ZK1320.9	1	2	3.20%	8.6	3.70E-04	0.07646525		
C02D5.2a	1	2	3.10%	8.8	5.40E-04	0.07398939		
R11A5.4a	1	1	3.10%	6.2	1.33E-04	0.07398939		
F27D4.1	1	2	3.00%	9.2	5.26E-04	0.071519256		
W08E3.3	1	4	2.80%	6.9	8.84E-04	0.06659615	Larval development	locus:tag-210
K11G12.5	1	2	2.80%	9.6	6.02E-04	0.06659615		
M88.5a	1	1	2.80%	8.2	1.96E-04	0.06659615		
C53D5.6	2	5	2.70%	4.7	7.42E-04	0.06414306	Importin beta	locus:imb-3
C39E9.13	1	2	2.50%	8.2	4.93E-04	0.059253693	DNA Replication	locus:rfc-3
K10D2.3	3	5	2.50%	8.6	5.69E-04	0.059253693	RNA poly-U polymerase	locus:cid-1
F32A7.5a	2	3	2.50%	5.1	2.98E-04	0.059253693		
C35E7.1	1	3	2.30%	5.1	6.67E-04	0.054386854		
F57C2.5	1	2	2.30%	8.3	4.51E-04	0.054386854		

Locus	Seq. count	Spectrum count	Seq. Coverage	pI	NSAF	EMPAI	Gene Ontology	Gene name
F35G12.8	3	4	2.10%	8	4.19E-04	0.049542427	Mitotic condensin	locus:smc-4
Y57A10A.18a	2	2	2.10%	6.2	2.23E-04	0.049542427		locus:pqn-87
R10E4.4	1	2	2.00%	8.8	0.00121335	0.04712856	DNA Replication	locus:mcm-5
C06C3.1a	1	1	1.50%	5.6	2.24E-04	0.035142183	Myosin-associated phosphatase	locus:mel-11
T22B11.5	1	1	1.50%	6.8	1.57E-04	0.035142183		
C46A5.9	1	1	1.40%	6.4	5.89E-04	0.032761455	Transcriptional regulator	locus:hcf-1
Y110A7A.17a	1	3	1.10%	7	0.001753044	0.025651932	APC/C subunit	locus:mat-1
K02F2.3	1	2	1.10%	5.6	2.66E-04	0.025651932	Embryo development	locus:tag-203
ZK1005.1a	2	2	1.00%	8.6	1.42E-04	0.023293018	ADP ribosylation	locus:pme-5
D2005.4	1	2	1.00%	5	2.73E-04	0.023293018		
F40H6.2	2	14	0.90%	4.7	0.003192407	0.02093947		
T21B10.3	1	1	0.90%	6.4	1.39E-04	0.02093947		
F57B9.2	2	3	0.80%	7.4	1.94E-04	0.018591404	Microtubule organization	locus:let-711

Table 4 List of phosphorylated amino acids identified by mass spectrometry following in vitro phosphorylation of recombinant WAPL-1 by enzymatically-active, recombinant CHK-2. An asterisk (*) following an amino acid denotes phosphorylation. A pound sign (#) following a methionine denotes oxidation of methionine.

Sequence	Xcorr	DeltCN	ObsM+H+	CalcM+H+	SpR	SpScore	Ion%	#
M.ASMSSDANSDDPFSKPIVR.K	4.0085	0.5005	2025.389	2025.1863	1	618.5	31.90%	1
M.ASMSSDANSDDPFSKPIVR.K	4.7768	0.2898	2026.462	2025.1863	1	1388.8	69.40%	13
M.ASM#SSDANSDDPFSKPIVR.K	4.3565	0.4189	2042.261	2041.1857	1	718.5	55.60%	5
M.ASMSSDANSDDPFSKPIVRK.R	4.2632	0.6216	2153.806	2153.3591	1	454.6	44.70%	2
A.SMSSDANSDDPFSKPIVR.K	5.496	0.5678	1955.466	1954.108	1	869.3	58.80%	7
A.SM#SSDANSDDPFSKPIVR.K	4.1555	0.6073	1970.371	1970.1074	1	923	64.70%	5
A.SM#SS*DANSDDPFSKPIVR.K	2.7049	0.071	2051.349	2050.0874	1	247.7	33.30%	1
A.SMSSDANSDDPFSKPIVRK.R	2.6853	0.3663	2081.802	2082.281	1	700.4	55.60%	1
S.MSSDANSDDPFSKPIVR.K	3.6978	0.5272	1865.819	1867.0304	1	945.6	59.40%	1
S.MS*S*DANSDDPFSKPIVR.K	3.9272	0.3095	2026.428	2026.9901	1	787.1	45.30%	1
M.SSDANSDDPFSKPIVR.K	4.2921	0.6161	1735.502	1735.8333	1	1129.6	70.00%	2
M.S*S*DANS*DDPFSKPIVR.K	2.2056	0.0778	1976.515	1975.773	1	367.6	30.70%	1
S.SDANSDDPFSKPIVR.K	3.8479	0.5483	1648.622	1648.7556	1	1595.1	78.60%	1
S.DANSDDPFSKPIVR.K	3.5784	0.5532	1561.794	1561.678	1	1648	80.80%	1

Sequence	Xcorr	DeltCN	ObsM+H+	CalcM+H+	SpR	SpScore	Ion%	#
D.ANSDDPFSKPIVR.K	2.4133	0.5201	1445.872	1446.5901	1	1240.7	79.20%	1
D.PFSKPIVR.K	2.4076	0.4078	944.131	944.1554	1	197.7	64.30%	16
D.PFSKPIVR.K	2.5944	0.5185	944.219	944.1554	1	650.4	85.70%	12
R.KRFQATLAQQGIEDDQLPSVR.S	7.2014	0.5521	2402.373	2401.6643	1	3065.6	52.50%	25
R.KRFQATLAQQGIEDDQLPSVR.S	4.935	0.5848	2402.406	2401.6643	1	1317.6	65.00%	20
K.RFQATLAQQGIEDDQLPSVR.S	5.1564	0.6338	2274.031	2273.4915	1	1030.5	63.20%	14
K.RFQATLAQQGIEDDQLPSVR.S	4.3112	0.5896	2274.354	2273.4915	1	1012.9	46.10%	3
R.FQATLAQQ.G	2.0938	0.3802	906.385	907.0057	1	954.8	85.70%	1
R.FQATLAQQGIEDD.Q	4.3485	0.6029	1437.099	1436.5057	1	1422.8	75.00%	2
R.FQATLAQQGIEDDQLPSVR.S	6.3912	0.6924	2118.38	2117.305	1	1568.5	72.20%	70
R.FQATLAQQGIEDDQLPSVR.S	5.639	0.6418	2118.695	2117.305	1	1829.4	56.90%	27
Q.ATLAQQGIEDDQLPSVR.S	2.4606	0.5251	1842.353	1842.0005	1	461.2	46.90%	1
A.TLAQQGIEDDQLPSVR.S	3.1181	0.4375	1770.422	1770.9222	1	1176.4	70.00%	1
T.LAQQGIEDDQLPSVR.S	2.2548	0.4335	1669.104	1669.818	1	1056	67.90%	1
L.AQQGIEDDQLPSVR.S	3.3668	0.5613	1556.187	1556.6598	1	740.6	65.40%	4
L.SEGNAETNLSDDSEPEMLSQSSTSSLNR.R	3.7552	0.5011	2986.87	2987.029	1	721.7	38.90%	2
L.SDDSEPEMLSQSSTSSLNR.R	2.9385	0.4693	2072.228	2071.1238	1	656.3	55.60%	1
Q.SSTS*SLNRR.M	2.0177	0.0306	1088.65	1088.0515	6	69.6	37.50%	1
R.RMEDSAIDPSRGTR.K	2.9005	0.4565	1591.435	1591.7323	1	503.9	61.50%	2
R.MEDSAIDPSR.G	3.4693	0.4695	1121.174	1121.2037	1	2050.8	94.40%	5
R.MEDSAIDPSR.G	2.4621	0.5733	1121.478	1121.2037	1	513.2	72.20%	4
R.M#EDSAIDPSR.G	3.2698	0.468	1137.156	1137.2031	1	1699.4	94.40%	2
K.SQSRGFDYDPAGERTTAPVQK.K	2.3092	0.2132	2311.489	2311.4534	2	244.5	37.50%	1
R.GFDYDPAGER.T	1.9226	0.2929	1127.492	1127.145	1	164.3	55.60%	1
R.GFDYDPAGER.T	3.3813	0.6345	1128.007	1127.145	1	1376.7	88.90%	13
R.GFDYDPAGERTTAPVQK.K	3.8484	0.5908	1853.467	1852.9818	1	622.7	65.60%	4
R.GFDYDPAGERTTAPVQKK.K	2.7517	0.5952	1980.72	1981.1548	1	423.7	55.90%	1
F.DYDPAGERT*T*APVQK.K	2.7253	0.2803	1808.512	1808.7155	3	279.4	28.60%	1
F.DYDPAGERT*TAPVQKK.K	2.2448	0.0193	1857.976	1856.9084	30	240.8	31.10%	1
K.KKKDEIDMGGAK.F	2.8959	0.5857	1320.664	1320.5411	1	660.2	68.20%	1
K.KKKDEIDMGGAK.F	3.6562	0.6632	1321.423	1320.5411	1	1637	90.90%	12
K.KKDEIDMGGAK.F	2.8291	0.5883	1192.267	1192.3683	1	1282.3	90.00%	1
K.KKDEIDMGGAKFFPK.Q	4.5019	0.514	1711.466	1712.0062	1	1242.7	78.60%	14
K.KHVYTHKWTTEEDDEDEK.T	5.0989	0.5505	2291.315	2291.3726	1	1126.8	64.70%	1
K.KHVYTHKWTTEEDDEDEKTISSSSNR.Y	6.4663	0.6546	3124.634	3124.235	1	1024.6	37.00%	4
K.HVYTHKWTTEEDDEDEKTISSS.S	2.9186	0.2746	2637.91	2638.695	1	322.9	38.10%	1
K.HVYTHKWTTEEDDEDEKTISSSSNR.Y	6.7062	0.7111	2995.897	2996.0623	1	2188.3	43.80%	2
H.KWTTEEDDEDEKTISSSSNR.Y	3.8929	0.5612	2358.338	2358.3723	1	742.2	47.40%	1
K.WTTEEDDEDEK.T	3.7441	0.4645	1398.117	1397.3368	1	950.5	85.00%	6

Sequence	Xcorr	DeltCN	ObsM+H+	CalcM+H+	SpR	SpScore	Ion%	#
K.WTTEEDDEDEK.T	3.0245	0.5731	1398.492	1397.3368	1	619.8	70.00%	3
K.WTTEEDDEDEKTI.S	3.4655	0.5622	1611.109	1611.5994	1	1541.5	87.50%	1
K.WTTEEDDEDEKTISSS.S	3.6807	0.6129	1872.223	1872.8324	1	510.8	60.00%	1
K.WTTEEDDEDEKTISSSSNR.Y	3.4582	0.4981	2230.596	2230.1995	1	665.9	52.80%	6
D.DEDEKTISS*SSNR.Y	1.9568	0.0407	1549.757	1548.4429	1	142.4	33.30%	1
R.YSSRPNQPAVSAR.P	3.5812	0.5378	1434.029	1433.5547	1	1756	56.20%	1
R.YSSRPNQPAVSAR.P	3.9779	0.5032	1434.052	1433.5547	1	752	70.80%	79
R.YSSRPNQPAVSARPR.Q	2.7355	0.2842	1685.523	1686.8567	1	197.5	50.00%	2
R.PRQPVYATTSTY.S	3.3526	0.567	1384.393	1384.5188	1	1066.4	72.70%	1
R.PRQPVYATTSTYSKPLASGYGSR.V	7.27	0.6385	2487.94	2488.7405	1	1352.6	46.60%	13
R.PRQPVYATTSTYSKPLASGYGSR.V	5.7772	0.6159	2488.771	2488.7405	1	628.6	56.80%	10
R.QPVYATTSTYSKPLA.S	2.4736	0.4603	1626.901	1627.8195	1	328.7	57.10%	1
R.QPVYATTSTYSKPLAS.G	2.8744	0.6116	1714.531	1714.8971	1	465.2	56.70%	1
R.QPVYATTSTYSKPLASG.Y	3.4568	0.4837	1771.627	1771.9487	1	534.4	56.20%	4
R.QPVYATTSTYSKPLASGY.G	3.4423	0.4472	1934.604	1935.1228	1	599.9	61.80%	2
R.QPVYATTSTYSKPLASGYGSR.V	3.9937	0.449	2234.985	2235.4382	1	791	31.20%	4
R.QPVYATTSTYSKPLASGYGSR.V	4.0947	0.7622	2236.129	2235.4382	1	335.8	52.50%	22
R.QPVYATTSTYSKPLASGYGSRV.R	2.2379	0.378	2333.815	2334.5698	1	139.2	35.70%	1
Q.PVYATTSTYSKPLASGYGSR.V	5.6042	0.6267	2106.593	2107.3086	1	1311.1	65.80%	2
Q.PVYATTSTYSKPLASGYGSR.V	3.9497	0.4834	2107.759	2107.3086	1	467.5	35.50%	1
P.VYATTSTYSKPLASGYGSR.V	4.7293	0.6368	2009.47	2010.1929	1	1462.2	72.20%	1
V.YATTSTYSKPLASGYGSR.V	4.7313	0.5899	1910.735	1911.0613	1	1353.8	73.50%	8
V.YATTSTYSKPLASGYGSR.V	4.0956	0.6641	1911.88	1911.0613	1	898.4	44.10%	1
Y.ATTSTYSKPLASGYGSR.V	4.3022	0.6276	1748.716	1747.8872	1	1081.1	75.00%	6
A.TTSTYSKPLASGYGSR.V	3.2836	0.6322	1676.366	1676.809	1	722.9	66.70%	5
A.TTSTYSKPLASGYGSR.V	2.2803	0.4736	1676.594	1676.809	1	148	46.70%	1
T.TSTYSKPLASGYGSR.V	3.9551	0.6093	1575.485	1575.7046	1	1374	82.10%	11
T.STYSKPLASGYGSR.V	2.5688	0.5314	1474.688	1474.6003	1	130.1	50.00%	1
T.STYSKPLASGYGSR.V	3.6932	0.6564	1475.429	1474.6003	1	632.2	80.80%	5
S.TYSKPLASGYGSR.V	2.1259	0.5671	1386.951	1387.5227	1	183.4	54.20%	1
S.TYSKPLASGYGSR.V	3.0356	0.6143	1387.504	1387.5227	1	698.9	70.80%	3
S.TYSKPLASGYGSRVR.H	2.5621	0.3335	1642.451	1642.8406	3	193.8	46.40%	1
T.YSKPLASGYGSR.V	2.4143	0.4269	1286.652	1286.4183	1	239.9	63.60%	1
Y.SKPLASGYGSR.V	2.4404	0.5662	1122.702	1123.2443	1	185.7	65.00%	5
S.KPLASGYGSR.V	2.0259	0.5973	1035.075	1036.1665	1	208.5	66.70%	1
K.PLASGYGSR.V	2.6895	0.4759	907.575	907.99365	1	233.4	75.00%	11
K.PLASGYGSR.V	2.8324	0.691	908.085	907.99365	1	790.3	93.80%	4
R.HIKEANELR.E	3.0504	0.5686	1111.153	1110.2487	1	1000.8	93.80%	11
K.EANELRESGEYDDFKQDLV.Y	3.0704	0.4763	2257.459	2258.3408	1	662.8	55.60%	1

Sequence	Xcorr	DeltCN	ObsM+H+	CalcM+H+	SpR	SpScore	Ion%	#
K.EANELRESGEYDDFKQDLVY.I	3.0983	0.4116	2421.688	2421.515	1	341.2	42.10%	1
K.EANELRESGEYDDFKQDLVYIL.S	3.2889	0.4971	2646.927	2647.8315	1	533.8	38.10%	4
K.EANELRESGEYDDFKQDLVYILS.S	2.3295	0.1107	2735.302	2734.9092	3	128.3	25.00%	1
R.ESGEYDDFKQDLVYIL.S	2.5807	0.3307	1935.057	1935.0764	1	255.6	46.70%	1
R.ESGEYDDFKQDLVYIL.S	2.9583	0.388	1935.24	1935.0764	1	779.3	60.00%	7
R.ESGEYDDFKQDLVYILS.S	3.805	0.5504	2022.281	2022.154	1	492.2	56.20%	1
R.ESGEYDDFKQDLVYILSSLQSSDAS*M.K	4.9066	0.1021	3009.487	3009.0957	1	556.1	22.70%	3
R.ESGEYDDFKQDLVYILSSLQSSDASMK.V	5.5781	0.6227	3057.051	3057.2888	1	1156.9	31.70%	7
R.ESGEYDDFKQDLVYILSSLQSSDASMK.V	5.2551	0.531	3057.736	3057.2888	1	490.1	38.50%	9
R.ESGEYDDFKQDLVYILSSLQSSDASMKVK.C	5.4581	0.6658	3283.868	3284.5933	1	1345	33.00%	3
K.QDLVYILSSLQSSDASMK.V	2.9307	0.4396	1986.693	1986.233	1	355.7	41.20%	1
K.VKCLSAISLAK.K	3.1354	0.5438	1190.323	1190.4518	1	857.4	85.00%	5
V.KCLSAISLAK.K	1.822	0.4826	1090.593	1091.3202	1	394.8	72.20%	1
V.KCLSAISLAK.K	2.4784	0.3899	1091.314	1091.3202	1	392.9	66.70%	3
K.CLSAISLAK.K	2.9052	0.492	963.179	963.1472	1	857.7	100.00%	8
K.CLSAISLAK.K	1.9502	0.2235	964.024	963.1472	1	281.2	68.80%	1
K.CLSAISLAKK.C	3.0182	0.3572	1091.55	1091.3202	1	649.8	77.80%	5
K.KCVSPDFR.Q	2.2415	0.5961	1009.064	1009.1346	1	229	64.30%	2
K.KCVSPDFR.Q	2.4583	0.5369	1009.602	1009.1346	1	396.9	78.60%	3
K.KCVSPDFRQFIK.S	4.4425	0.6083	1525.433	1525.7701	1	1360.3	90.90%	7
K.KCVS*PDFRQFIKS*E.N	2.2609	0.1891	1902.214	1901.9221	12	252.9	32.70%	1
K.KCVSPDFRQFIKSENMTK.S	2.2984	0.3579	2216.52	2216.5398	3	225.9	35.30%	2
K.CVSPDFRQFIK.S	2.2978	0.2694	1396.516	1397.5973	1	447.5	60.00%	1
F.IKSENMTKS*IVK.A	2.4074	0.1818	1459.29	1458.6437	1	606.6	51.50%	1
K.S*IVKALMDS*PEDDLFALAASTV.L	2.2633	0.2754	2454.852	2454.5671	8	127.2	17.90%	1
K.SIVKALMDSPEDDLFALAAST*VLYLLT*RD.F	3.6375	0.0651	3330.29	3329.5947	1	736.9	20.10%	1
K.ALMDSPEDDLFALAASTV.L	2.8615	0.5885	1866.904	1867.067	1	554.3	58.80%	1
K.ALMDSPEDDLFALAASTVLYLLTR.D	3.6358	0.6296	2625.648	2627.0066	1	1766.9	54.30%	1
K.ALM#DSPEDDLFALAASTVLYLLTR.D	3.7058	0.6203	2642.472	2643.0059	1	882.5	37.00%	2
D.SPEDDLFALAAS*TVLYLLT*R.D	2.3087	0.0591	2356.515	2356.445	25	91.3	23.70%	1
E.DDLFALAASTVLYLLT*R.D	2.247	0.2611	1963.259	1963.1572	1	345.7	35.40%	1
D.LFALAASTVLYLLTR.D	2.7872	0.2368	1654.388	1653.0016	1	760.4	53.60%	9
F.ALAASTVLYLLTR.D	2.8443	0.461	1393.893	1392.6686	1	872.5	66.70%	1
L.AASTVLYLLTR.D	3.9581	0.5698	1209.389	1208.4321	1	958.9	80.00%	5
A.STVLYLLTR.D	3.3263	0.523	1066.555	1066.2758	1	1269.6	87.50%	3
S.TVLYLLTR.D	2.8023	0.481	979.054	979.19806	1	810.4	92.90%	2

Sequence	Xcorr	DeltCN	ObsM+H+	CalcM+H+	SpR	SpScore	Ion%	#
V.LYLLTR.D	1.8765	0.3336	779.597	778.96216	1	334.6	80.00%	1
R.DFNSIKIDFPSLR.L	3.0038	0.3727	1552.265	1552.7559	1	393.3	62.50%	2
R.DFNSIKIDFPSLR.L	4.5275	0.5436	1552.4	1552.7559	1	926.1	75.00%	11
R.DFNSIKIDFPSLR.L	4.276	0.5147	1552.901	1552.7559	1	1394.7	58.30%	3
D.FNSIKIDFPSLR.L	3.3265	0.4704	1437.705	1437.668	1	1090.8	81.80%	1
R.LVSQLLR.I	2.295	0.5529	829.017	829.0227	1	502.6	91.70%	2
R.LVSQLLR.I	1.9245	0.3394	829.128	829.0227	1	145.5	66.70%	1
R.LVSQLLRIEK.F	3.3387	0.5698	1199.303	1199.4684	1	1345.2	88.90%	2
K.FEQRPEDKDKVVNMVWEVFNSYIEK.Q	7.6613	0.7198	3132.333	3131.5068	1	3181.1	44.80%	77
K.FEQRPEDKDKVVNM#VWEVFNSYIEK.Q	6.2391	0.4739	3146.923	3147.5063	1	1437.3	37.50%	16
K.DKVVNMVWEVFNSYIEK.Q	5.5286	0.6201	2100.627	2101.4106	1	2451.3	84.40%	12
K.DKVVNM#VWEVFNSYIEK.Q	2.6604	0.33	2118.461	2117.41	1	404.4	40.60%	2
K.DKVVNMVWEVFNSYIEKQEVGGQK.V	6.0181	0.5416	2828.673	2828.1921	1	1122.8	38.00%	3
K.VVNMVWEVFNSYIEK.Q	5.4399	0.6123	1858.009	1858.1498	1	3561.8	60.70%	3
K.VVNMVWEVFNSYIEK.Q	4.2453	0.5566	1858.783	1858.1498	1	469	53.60%	6
K.VVNMVWEVFNSYIEK.Q	5.5625	0.5823	1858.875	1858.1498	1	2542.3	78.60%	25
K.VVNM#VWEVFNSYIEK.Q	4.7994	0.5726	1873.475	1874.1492	1	2392.9	82.10%	4
K.VVNMVWEVFNS*YIEKQEV.G	2.2251	0.2147	2294.192	2294.5056	1	352.5	35.30%	1
K.VVNMVWEVFNSYIEKQEVGGQK.V	4.9265	0.5375	2584.654	2584.9314	1	677.8	36.90%	6
K.VVNMVWEVFNSYIEKQEVGGQK.V	5.8929	0.6239	2585.932	2584.9314	1	1533	54.80%	9
K.VVNM#VWEVFNSYIEKQEVGGQK.V	3.5678	0.5296	2600.368	2600.931	1	536.7	34.50%	2
K.VVNMVWEVFNSYIEKQEVGGQKV.S	2.3554	0.1615	2684.886	2684.063	2	213.7	25.00%	1
V.VNMVWEVFNSYIEK.Q	5.3549	0.6021	1759.856	1759.0182	1	2253.1	84.60%	2
V.NMVWEVFNSYIEK.Q	4.4511	0.5148	1659.156	1659.8866	1	2012.2	87.50%	1
N.MVWEVFNSYIEK.Q	3.1182	0.4316	1544.999	1545.7836	1	1194.7	77.30%	1
M.VWEVFNSYIEK.Q	2.3624	0.446	1413.967	1414.5864	1	831	75.00%	1
M.VWEVFNSYIEKQEVGGQK.V	3.7179	0.2609	2141.459	2141.3682	1	506.4	50.00%	1
R.KESLTPSSLIIEALVFICSR.S	4.0566	0.6578	2263.764	2264.6409	1	1083.5	57.90%	2
K.ES*LT*PS*SLIIEALVF.I	2.3749	0.0144	1859.999	1859.8201	18	238.7	24.30%	2
K.ESLTPSSLIIEALVFICSR.S	6.0353	0.6625	2137.203	2136.4678	1	1735.2	66.70%	6
L.IIEALVFICS*RSVNDDNLK.S	2.2588	0.1744	2286.715	2287.486	1	681.9	35.20%	1
R.SVNDDNLK.S	2.2351	0.5555	905.102	904.94495	1	470.2	92.90%	1
R.SVNDDNLK.S	2.0191	0.4356	905.476	904.94495	1	277	64.30%	1
R.SVNDDNLKSELLNLGIL.Q	3.9313	0.6114	1858.464	1858.083	1	1505.8	71.90%	2
R.SVNDDNLKSELLNLGILQFV.V	5.1637	0.704	2232.935	2232.519	1	1681.6	63.20%	2
R.SVNDDNLKSELLNLGILQFVVAK.I	5.859	0.5683	2531.017	2530.9019	1	2182.7	44.30%	16

Sequence	Xcorr	DeltCN	ObsM+H+	CalcM+H+	SpR	SpScore	Ion%	#
R.SVNDDNLKSELLNLGILQFVVAK.I	5.8682	0.6106	2531.988	2530.9019	1	2202.4	61.40%	33
D.DNLKSELLNLGILQFVVAK.I	3.5857	0.5396	2114.527	2115.5015	1	325.3	50.00%	1
K.SELLNLGILQF.V	2.6993	0.3853	1247.786	1247.4652	1	655.4	75.00%	1
K.SELLNLGILQFVVAK.I	3.4886	0.37	1644.908	1644.9795	1	987.7	57.10%	3
K.SELLNLGILQFVVAK.I	4.9953	0.6941	1644.957	1644.9795	1	2164.3	82.10%	25
K.SELLNLGILQFVVAK.I	5.5477	0.4956	1645.994	1644.9795	1	2290.3	58.90%	3
K.S*ELLNLGILQFVVAK.I	2.346	0.3587	1725.641	1724.9594	1	327.6	33.30%	1
N.LGILQFVVAK.I	3.9343	0.6535	1088.293	1088.3677	1	1485	88.90%	1
L.GILQFVVAK.I	2.2244	0.1513	974.784	975.2094	2	585.9	62.50%	1
K.IETNVNLI.A	1.8021	0.3154	917	916.054	3	224.2	57.10%	1
K.IETNVNLIADNADDTYSILILNR.C	5.6612	0.6103	2592.022	2591.8557	1	1549.4	40.90%	77
K.IETNVNLIADNADDTYSILILNR.C	6.6355	0.6506	2593.072	2591.8557	1	2014.6	61.40%	120
V.NLIADNADDTYSILILNR.C	5.1876	0.5694	2035.361	2035.2439	1	2653.8	73.50%	3
I.ADNADDTYSILILNR.C	2.1507	0.3072	1694.736	1694.8243	1	301.5	50.00%	2
I.ADNADDTYSILILNR.C	3.5363	0.4941	1696.073	1694.8243	1	553.2	57.10%	9
Y.SILILNR.C	2.0673	0.3685	828.659	829.0227	1	161.5	66.70%	2
R.ILESSSVFH.K	2.4343	0.5258	1018.513	1019.13275	1	715.2	87.50%	1
R.ILESSSVFHK.K	2.5185	0.2998	1147.653	1147.3057	1	339.7	72.20%	12
R.ILESSSVFHK.K	3.1835	0.4385	1148.058	1147.3057	1	861.9	88.90%	15
R.ILESSSVFHKK.N	2.4088	0.3155	1275.711	1275.4786	1	453.3	70.00%	17
R.ILESSSVFHKK.N	3.9418	0.4126	1276.474	1275.4786	1	764.9	75.00%	51
R.ILESSSVFHKKN.Q	2.3508	0.3808	1388.244	1389.5817	1	547.6	63.60%	1
R.ILESS*S*VFHKKN.Q	1.8368	0.0552	1550.627	1549.5415	1	306.1	36.40%	1
I.LESSSVFHKK.N	2.6962	0.388	1161.701	1162.3203	1	462.3	66.70%	4
K.KNQAFLISHR.S	3.7615	0.5483	1213.937	1214.4017	1	924.2	88.90%	32
K.KNQAFLISHR.S	3.9379	0.5032	1215.17	1214.4017	1	810.2	61.10%	6
K.NQAFLISH.R	2.2684	0.4366	930.061	930.0424	1	656.4	78.60%	1
K.NQAFLISHR.S	3.3101	0.5579	1086.625	1086.2288	1	280.4	81.20%	33
K.NQAFLISHR.S	3.5222	0.5312	1087.182	1086.2288	1	1477.4	93.80%	47
K.NQAFLISHRSNILIS.S	2.8598	0.1514	1714.516	1713.9619	5	273.5	42.90%	5
R.SNILISSLAK.F	2.3106	0.4499	1046.121	1046.2428	1	526	66.70%	4
R.SNILISSLAK.F	3.3292	0.4233	1046.241	1046.2428	1	1383.8	88.90%	7
I.LISSLAK.F	2.0458	0.3042	732.548	731.9038	1	698.1	83.30%	2
K.FLQVILDR.V	2.8033	0.563	1004.169	1004.2076	1	365.3	78.60%	7
K.FLQVILDR.V	3.5875	0.51	1005.121	1004.2076	1	1177.9	92.90%	12
K.FLQVILDRVHQLAEEEVKK.Y	4.4609	0.5971	2295.131	2295.6663	1	856.1	55.60%	11
K.FLQVILDRVHQLAEEEVKK.Y	6.5123	0.5381	2295.606	2295.6663	1	2332.9	47.20%	85
D.RVHQLAEEEVKK.Y	2.9532	0.5883	1466.01	1466.6677	1	1274.7	86.40%	13
R.VHQLAEEEVKK.Y	4.1339	0.6234	1311.438	1310.4813	1	1352.7	85.00%	5

Sequence	Xcorr	DeltCN	ObsM+H+	CalcM+H+	SpR	SpScore	Ion%	#
V.HQLAEEEVKK.Y	2.2291	0.532	1211.108	1211.3497	1	867	83.30%	1
K.KYISCLALMCR.L	4.5778	0.609	1416.387	1415.7141	1	1737.1	90.00%	5
K.KYISCLALM#CR.L	2.8383	0.6317	1431.224	1431.7135	1	842	85.00%	1
K.YISCLALMCR.L	3.4993	0.5515	1288.289	1287.5413	1	965.3	83.30%	13
K.YISCLALMCR.L	2.6485	0.5416	1288.599	1287.5413	1	212.9	61.10%	6
K.YISCLALM#CR.L	2.9092	0.562	1302.724	1303.5406	1	1074.5	83.30%	3
I.SCLALMCR.L	2.5281	0.5558	1010.97	1011.20886	1	1149.4	85.70%	1
I.SCLALMCR.L	1.9321	0.5055	1011.039	1011.20886	1	249.9	71.40%	4
R.LLINISHDNELCCSK.L	5.6664	0.5429	1817.685	1817.021	1	1191.4	71.40%	120
R.LLINISHDNELCCSK.L	5.4434	0.5384	1817.805	1817.021	1	542.8	60.70%	19
R.LLINISHDNELCCSK.L	4.8491	0.5137	1818.155	1817.021	1	966.7	53.60%	15
L.LINISHDNELCCSK.L	3.8053	0.5216	1704.585	1703.8628	1	415	69.20%	2
L.INISHDNELCCSK.L	4.4161	0.6772	1590.993	1590.7045	1	980.6	75.00%	2
S.KLGQIEGFLPNAITTFTYLAPK.F	4.1593	0.5163	2422.887	2423.8345	1	1197.2	38.10%	1
S.KLGQIEGFLPNAITTFTYLAPK.F	4.6353	0.5982	2423.781	2423.8345	1	1727.6	69.00%	5
K.LGQIEGFLPNAI.T	1.9189	0.4396	1271.589	1272.4747	1	661.2	68.20%	1
K.LGQIEGFLPNAITTF.T	2.525	0.4549	1621.346	1621.858	1	1202.5	75.00%	1
K.LGQIEGFLPNAITTF.T	2.3201	0.5102	1621.6	1621.858	1	801.9	57.10%	3
K.LGQIEGFLPNAITTFT.Y	2.4028	0.5196	1722.099	1722.9624	1	605.5	60.00%	1
K.LGQIEGFLPNAITTFTYLAPK.F	5.1127	0.5875	2295.988	2295.6616	1	1343.6	46.20%	7
K.LGQIEGFLPNAITTFTYLAPK.F	6.298	0.6273	2296.296	2295.6616	1	1105	67.50%	86
K.LGQIEGFLPNAIT*T*FTYLAP.K	3.2717	0.0352	2327.872	2327.4485	4	164.1	22.40%	1
K.LGQIEGFLPNAITT*FT*YLAP.K	3.6023	0.0425	2328.263	2327.4485	1	215.3	23.70%	2
K.LGQIEGFLPNAITTFTYLAPKFGK.E	2.9973	0.4984	2628.12	2628.0608	1	289	32.60%	1
K.LGQIEGFLPNAITTFTYLAPKFGK.E	4.4191	0.4716	2628.228	2628.0608	1	711.7	34.80%	2
L.GQIEGFLPNAITTFTYLAPK.F	5.2706	0.5899	2182.686	2182.5034	1	836.3	63.20%	3
G.QIEGFLPNAITTFTYLAPK.F	4.8653	0.5692	2125.72	2125.4517	1	1427.1	75.00%	2
I.EGFLPNAITTFTYLAPK.F	3.3511	0.595	1883.555	1884.1637	1	826	62.50%	3
E.GFLPNAITTFTYLAPK.F	3.6849	0.6242	1755.329	1755.0492	1	943.5	63.30%	2
G.FLPNAITTFTYLAPK.F	3.5575	0.4587	1697.639	1697.9977	1	983.4	78.60%	2
F.LPNAITTFTYLAPK.F	1.9986	0.285	1550.658	1550.823	3	231.1	38.50%	1
F.LPNAITTFTYLAPK.F	3.4918	0.4985	1550.903	1550.823	1	877.3	73.10%	1
L.PNAITTFTYLAPK.F	4.8177	0.5848	1438.013	1437.6647	1	1390.1	79.20%	4
N.AITTFTYLAPK.F	3.2724	0.4597	1227.277	1226.4459	1	1060.9	85.00%	3
I.TTFTYLAPK.F	2.9644	0.4905	1042.061	1042.2095	1	574.3	87.50%	2
I.TTFTYLAPK.F	2.1923	0.4387	1043.509	1042.2095	1	215.6	62.50%	1
T.FTYLAPK.F	1.9006	0.4675	840.45	840.0008	1	343.8	75.00%	1
K.FGKENSYDINV.M	2.9257	0.2044	1286.032	1286.372	1	1255.1	85.00%	1
K.FGKENSYDINVM#.M	3.6869	0.5844	1433.617	1433.5685	1	1229.5	77.30%	1

Sequence	Xcorr	DeltCN	ObsM+H+	CalcM+H+	SpR	SpScore	Ion%	#
K.FGKENSYDINVMMT.S	2.5828	0.5767	1649.209	1649.8705	1	990.7	69.20%	1
K.FGKENSYDINVMM#T.S	2.2059	0.0959	1665.314	1665.8699	1	423.5	46.20%	1
K.FGKENSYDINVMMTSLLTNLVER.C	6.6061	0.6685	2676.858	2676.0627	1	1768.8	38.60%	33
K.FGKENSYDINVMMTSLLTNLVER.C	7.0535	0.6236	2677.046	2676.0627	1	2073.5	61.40%	21
K.FGKENSYDINVMMTS*LLT*NLVE.R	3.0299	0.0549	2680.129	2679.8362	2	365.3	20.20%	3
K.FGKENSYDINVMM#TSLLTNLVER.C	4.7725	0.0235	2691.453	2692.062	1	613.2	50.00%	2
K.FGKENSYDINVM#MTSLLTNLVER.C	5.5527	0.0383	2691.684	2692.062	1	879.1	59.10%	2
K.FGKENSYDINVM#MTSLLTNLVER.C	6.1605	0.0303	2692.501	2692.062	1	1680.6	37.50%	3
K.FGKENSYDINVMM#TSLLTNLVER.C	6.1946	0.0642	2693.036	2692.062	1	1652.8	36.40%	4
K.FGKENSYDINVM#M#TSLLTNLVER.C	6.0249	0.4881	2706.848	2708.0615	1	2192.2	37.50%	2
K.FGKENSYDINVM#M#TSLLTNLVER.C	4.0424	0.5744	2709.091	2708.0615	1	342.5	45.50%	3
F.GKENS*YDINVM#MT*SLLTNLVER.C	3.6319	0.0215	2705.105	2704.8472	1	740.6	20.20%	1
K.ENSYDINVMMTSLLTNLVER.C	5.8127	0.6238	2344.208	2343.6636	1	1201.6	40.80%	7
K.ENSYDINVMMTSLLTNLVER.C	6.2367	0.7167	2344.473	2343.6636	1	2008.2	65.80%	21
K.ENSYDINVM#MTSLLTNLVER.C	4.6453	0.0756	2359.51	2359.663	1	1569.6	60.50%	1
K.ENSYDINVM#M#TSLLTNLVER.C	3.326	0.1213	2375.607	2375.6624	1	451.7	36.80%	1
D.INVMMTSLLTNLVER.C	4.1211	0.1514	1734.198	1735.1063	1	1408	67.90%	1
I.NVM#M#T*SLLTNLVER.C	3.3751	0.0301	1734.33	1733.9268	2	1082.7	46.20%	1
N.VMMTSLLTNLVER.C	2.0164	0.3324	1507.749	1507.845	1	113	41.70%	1
T.SLLTNLVER.C	2.3552	0.4023	1044.714	1045.2148	1	198.3	68.80%	3
T.SLLTNLVER.C	3.0839	0.2403	1044.968	1045.2148	1	913.5	81.20%	3
R.KVLIAQTVK.M	3.2078	0.653	1000.578	1000.2604	1	942	93.80%	27
R.KVLIAQTVK.M	3.6616	0.289	1000.614	1000.2604	1	1145.7	68.80%	1
R.KVLIAQTVK.M	2.7626	0.3748	1000.736	1000.2604	1	500	75.00%	18
K.VLIAQTVK.M	1.8096	0.4343	872.083	872.08746	1	115.9	64.30%	1
K.VLIAQTVK.M	3.1383	0.5333	873.252	872.08746	1	537	92.90%	9
K.VLIAQTVKMVIPGHDVEEVPALEAITR.L	5.3828	0.4871	2930.713	2930.4553	1	1044.1	33.70%	2
V.LIAQTVK.M	2.0817	0.1219	772.633	772.95593	1	413.9	83.30%	1
V.KMVIPGHDVEEVPALEAITR.L	4.2416	0.5985	2205.59	2205.5635	1	740.6	57.90%	3
K.MVIPGHDVEEVPALEAI.T	2.6617	0.3555	1820.65	1820.0999	24	123.1	34.40%	2
K.MVIPGHDVEEVPALEAI.T	3.8888	0.5646	1820.731	1820.0999	1	752.2	59.40%	2
K.MVIPGHDVEEVPALEAITR.L	4.9449	0.6369	2077.588	2077.3906	1	653.2	63.90%	22
K.MVIPGHDVEEVPALEAITR.L	4.0341	0.415	2078.133	2077.3906	1	1213.3	44.40%	5
K.M#VIPGHDVEEVPALEAITR.L	5.0828	0.6588	2094.563	2093.39	1	1436.7	77.80%	10
M.VIPGHDVEEVPALEAITR.L	2.5506	0.4585	1945.352	1946.1935	1	184.6	44.10%	1
V.IPGHDVEEVPALEAITR.L	4.6732	0.6195	1846.81	1847.0619	1	1741.8	71.90%	5

Sequence	Xcorr	DeltCN	ObsM+H+	CalcM+H+	SpR	SpScore	Ion%	#
I.PGHDVEEVPALEAITR.L	5.0032	0.6114	1733.865	1733.9037	1	1645.9	73.30%	3
I.PGHDVEEVPALEAITR.L	2.4608	0.4104	1735.152	1733.9037	1	401.8	50.00%	1
P.GHDVEEVPALEAITR.L	2.4684	0.442	1637.538	1636.788	1	299.1	57.10%	1
D.VEEVPALEAITR.L	2.5661	0.3244	1327.271	1327.5087	1	585.7	72.70%	2
V.PALEAITR.L	2.392	0.6312	870.58	871.0165	1	403.3	71.40%	7
V.PALEAITR.L	2.98	0.5593	871.232	871.0165	1	855.1	92.90%	3
I.TRLFVYHESQAQIVDADLDR.E	4.2623	0.2475	2376.523	2377.5981	1	1713.7	39.50%	1
T.RLFVYHESQAQIVDADLDR.E	4.0027	0.459	2276.138	2276.4937	1	1826.2	61.10%	2
T.RLFVYHES*QAQIVDADLDR.E	2.6947	0.3711	2357.263	2356.4736	1	1544.2	46.30%	1
R.LFVYHESQAQIV.D	2.504	0.3698	1434.148	1434.621	1	712.8	77.30%	5
R.LFVYHESQAQIV.D	2.4605	0.5374	1434.722	1434.621	2	339.1	54.50%	4
R.LFVYHESQAQIVDADLD.R	2.6969	0.4037	1965.216	1964.121	3	188.6	37.50%	1
R.LFVYHESQAQIVDADLDR.E	5.8328	0.4423	2120.765	2120.3074	1	1382	47.10%	41
R.LFVYHESQAQIVDADLDR.E	6.9715	0.6276	2121.705	2120.3074	1	2995.2	73.50%	219
R.LFVYHESQAQIVDADLDRELA.F	5.6912	0.6903	2434.565	2433.6584	1	2015.8	62.50%	1
R.LFVYHESQAQIVDADLDRELAF.D	3.9974	0.4875	2580.764	2580.833	1	750.4	50.00%	1
L.FVYHESQAQIVDADLDR.E	5.5562	0.6832	2006.878	2007.149	1	3036.4	81.20%	1
H.ESQAQIVDADLDR.E	2.8636	0.3289	1460.323	1460.5288	1	493.9	62.50%	1
R.ELAFDEGGCGDEEEEEEGGDESSDEDGVR.K	6.5641	0.4926	3149.354	3148.9663	1	2272.5	44.60%	3
R.ELAFDEGGCGDEEEEEEGGDESSDEDGVR.K	5.9961	0.6824	3150.231	3148.9663	1	1041.7	41.10%	9
R.ELAFDEGGCGDEEEEEEGGDESSDEDGVRK.D	2.9483	0.6091	3276.618	3277.1392	1	470.3	36.20%	7
R.ELAFDEGGCGDEEEEEEGGDESSDEDGVRK.D	6.5905	0.6002	3278.532	3277.1392	1	2755.1	40.50%	73
E.LAFDEGGCGDEEEEEEGGDES*S*DEDGVR.K	3.1143	0.2613	3179.522	3179.8115	11	195.8	14.80%	2
L.AFDEGGCGDEEEEEEGGDESSDEDGVRK.D	4.1234	0.4172	3034.586	3034.8665	1	1410.8	35.20%	1
A.FDEGGCGDEEEEEEGGDESSDEDGVR.K	5.1965	0.6193	2835.779	2835.6152	1	2842	45.00%	1
A.FDEGGCGDEEEEEEGGDESSDEDGVRK.D	5.5348	0.5962	2963.445	2963.788	1	1494.9	38.50%	2
A.FDEGGCGDEEEEEEGGDESSDEDGVRKDGR.L	4.2101	0.469	3291.4	3292.114	1	651.6	25.90%	1
F.DEGGCGDEEEEEEGGDESSDEDGVR.K	4.3079	0.3288	2687.827	2688.4404	1	1260.2	39.60%	1
F.DEGGCGDEEEEEEGGDESSDEDGVR.K	4.7262	0.5802	2688.318	2688.4404	1	1068.2	52.10%	1
F.DEGGCGDEEEEEEGGDESSDEDGVRK.D	2.8493	0.532	2815.406	2816.6135	1	437.3	38.00%	1
F.DEGGCGDEEEEEEGGDESSDEDGVRK.D	5.3282	0.5694	2815.885	2816.6135	1	1222.5	38.00%	1
D.EGGCGDEEEEEEGGDESSDEDGVR.K	5.8672	0.6178	2573.891	2573.3528	1	2062.2	58.70%	1
D.EGGCGDEEEEEEGGDESSDEDGVRK.D	2.5986	0.3757	2700.284	2701.5256	1	490	41.70%	1
D.EGGCGDEEEEEEGGDESSDEDGVRK.D	4.0488	0.5921	2701.162	2701.5256	1	1381.8	37.50%	1

Sequence	Xcorr	DeltCN	ObsM+H+	CalcM+H+	SpR	SpScore	Ion%	#
E.GGCGDEEEEEEGGDESSDEDGVR.K	4.7528	0.508	2444.469	2444.238	1	2566.2	61.40%	1
G.GCGDEEEEEEGGDESSDEDGVR.K	4.8589	0.5825	2386.381	2387.1865	1	2607.6	64.30%	1
G.CGDEEEEEEGGDESSDEDGVR.K	5.619	0.7185	2330.338	2330.135	1	2528.6	72.50%	1
C.GDEEEEEEGGDESSDEDGVR.K	4.9703	0.6451	2169.242	2169.9697	1	3099.8	76.30%	1
G.DEEEEEEGGDESSDEDGVR.K	4.7395	0.6018	2112.802	2112.9182	1	1448.9	72.20%	1
D.EEEEEEGGDESSDEDGVR.K	4.1006	0.5586	1997.021	1997.8304	1	1869.6	73.50%	1
D.EEEEEEGGDESSDEDGVRK.D	2.2782	0.3582	2126.256	2126.0034	1	166.1	44.40%	1
E.EEEEGGDESSDEDGVR.K	3.3221	0.4589	1739.699	1739.6013	1	785.2	56.70%	2
E.GGDESSDEDGVR.K	2.7707	0.4985	1223.116	1223.1432	1	1428.2	81.80%	1
G.GDESSDEDGVR.K	2.8676	0.5761	1165.88	1166.0916	1	1088	90.00%	1
G.DESSDEDGVR.K	2.3696	0.4218	1108.436	1109.04	1	910.4	83.30%	1
R.NKMDRMDQVDVVHALQQVMNK.A	3.1056	0.478	2500.457	2500.9077	1	471.8	45.00%	1
R.NKMDRMDQVDVVHALQQVMNK.A	5.1371	0.5372	2501.6	2500.9077	1	2202.8	43.80%	1
K.MDRMDQVDVVHALQQV.M	3.4114	0.5536	1885.699	1885.1587	1	849.6	73.30%	1
K.MDRMDQVDVVHALQQVMNK.A	6.4793	0.682	2259.434	2258.6318	1	3005.9	54.20%	9
K.MDRMDQVDVVHALQQVMNK.A	6.0265	0.6959	2259.786	2258.6318	1	2541.1	75.00%	7
R.MDQVDVVHAL.Q	2.3745	0.3926	1127.301	1127.2963	1	661	77.80%	2
R.MDQVDVVHALQ.Q	2.1637	0.4916	1255.294	1255.426	1	396.5	60.00%	1
R.MDQVDVVHALQQV.M	2.9157	0.5042	1481.935	1482.6874	1	1211.9	79.20%	1
R.MDQVDVVHALQQVMNK.A	5.6593	0.6106	1856.458	1856.1605	1	1644.9	73.30%	16
R.MDQVDVVHALQQVMNK.A	4.5212	0.557	1856.652	1856.1605	1	2006.4	56.70%	8
R.MDQVDVVHALQQVMNK.A	4.9629	0.5745	1856.763	1856.1605	1	811	63.30%	8
R.M#DQVDVVHALQQVMNK.A	5.1342	0.6402	1871.738	1872.1599	1	1204.8	76.70%	2
R.MDQVDVVHALQQVM#NK.A	5.1269	0.6449	1872.684	1872.1599	1	1246.9	73.30%	4
R.MDQVDVVHALQQVM#NK.A	2.6561	0.4863	1873.206	1872.1599	1	166.2	43.30%	1
R.M#DQVDVVHALQQVM#NK.A	4.1537	0.6177	1888.275	1888.1593	1	607.6	70.00%	2
R.MDQVDVVHALQQVMNKA.S	5.1971	0.6708	1926.676	1927.2388	1	2420.9	75.00%	2
M.DQVDVVHALQQVMNK.A	4.6374	0.6314	1724.748	1724.9634	1	1882.6	78.60%	1
V.DVVHALQQVMNK.A	3.4372	0.5663	1382.452	1382.6143	1	1325.8	77.30%	1
D.VVHALQQVMNK.A	3.8581	0.4898	1268.329	1267.5264	1	934.6	80.00%	6
V.HALQQVMNK.A	2.7572	0.5614	1069.534	1069.2632	1	369.6	75.00%	7
V.HALQQVMNK.A	3.5431	0.5831	1069.997	1069.2632	1	1106.1	87.50%	9
K.ASAHMEGSVIASYHAL.L	3.1519	0.5073	1644.098	1644.8336	1	909.5	60.00%	4
K.ASAHM#EGS*VIAS*YHALLVGFV.L	2.28	0.1969	2336.412	2336.4404	21	61.1	17.50%	1
S.YHALLVGFVLQQNEDHLDEVRK.H	2.3723	0.3373	2623.712	2624.9355	22	94.9	23.80%	1
Y.HALLVGFVLQQNEDHLDEVRK.H	3.2797	0.587	2461.937	2461.7612	1	592.6	47.50%	3
Y.HALLVGFVLQQNEDHLDEVRK.H	3.689	0.2186	2462.079	2461.7612	2	738.7	32.50%	1

Sequence	Xcorr	DeltCN	ObsM+H+	CalcM+H+	SpR	SpScore	Ion%	#
H.ALLVGFVLQQNEDHLDEVRK.H	4.7701	0.5407	2325.232	2324.6213	1	892.4	38.20%	3
L.LVGFVLQQNEDHLDEVRK.H	4.2235	0.4769	2140.222	2140.385	1	1003.1	48.50%	1
L.LVGFVLQQNEDHLDEVRK.H	4.9112	0.4729	2140.714	2140.385	1	1373.4	70.60%	3
V.GFVLQQNEDHLDEVR.K	5.3725	0.4715	1799.507	1799.9222	1	1786.9	78.60%	1
K.HLPGKNFQNMISQLK.R	2.2082	0.1904	1755.888	1756.0654	1	249.3	50.00%	1
K.NFQNMISQLK.R	2.9951	0.426	1224.01	1223.4272	1	501.3	77.80%	6
K.NFQNMISQLK.R	3.7435	0.3838	1224.405	1223.4272	1	1531.3	83.30%	6
K.NFQNM#ISQLK.R	2.9789	0.4762	1239.31	1239.4266	1	966	83.30%	6
K.NFQNMIS*QLK.R	2.6442	0.312	1303.26	1303.4071	1	348.6	59.30%	1
K.NFQNMISQLKR.L	2.8172	0.4277	1379.291	1379.6135	1	161	65.00%	12
K.NFQNMISQLKR.L	4.1277	0.5498	1380.851	1379.6135	1	1555	85.00%	34
K.NFQNM#ISQLKR.L	4.0905	0.5961	1397.008	1395.6129	1	560.1	80.00%	29
K.NFQNMISQLKRLYD.F	2.271	0.0709	1771.992	1771.0338	1	346.8	53.80%	1
Q.NMISQLKR.L	2.2372	0.5106	989.693	990.206	1	213.1	78.60%	2
M.ISQLKR.L	1.8031	0.3847	744.528	744.90576	1	115.9	70.00%	1
K.RLYDFTK.A	2.316	0.4842	943.256	943.0811	1	622.4	100.00%	1
R.LYDFTK.A	2.1732	0.5492	786.904	786.8948	1	522.5	80.00%	37
R.LYDFTKATMAK.R	2.4577	0.5237	1289.718	1289.5255	1	486.4	70.00%	1
R.LYDFTKATMAK.R	2.5922	0.5048	1289.955	1289.5255	1	788.5	75.00%	1
R.LYDFTKATMAKR.V	3.1831	0.6094	1445.416	1445.7119	1	1024.8	77.30%	3
K.RVESNSGFR.A	3.3991	0.5899	1052.596	1052.1261	1	448.2	87.50%	5
R.VIEYLER.L	2.2544	0.4148	922.036	922.06024	1	296	75.00%	35
R.VIEYLER.L	2.9832	0.5593	922.421	922.06024	1	514.7	91.70%	30
M.ASMSSDANSDDPFSKPIVR.K	4.8174	0.7376	2025.395	2025.1863	1	589.5	55.60%	16
M.ASM#SSDANSDDPFSKPIVR.K	3.8564	0.3742	2041.981	2041.1857	1	736	58.30%	18
A.SMSSDANSDDPFSKPIVR.K	4.5898	0.5849	1954.294	1954.108	1	707.5	64.70%	11
A.SM#SSDANSDDPFSKPIVR.K	3.3892	0.5278	1970.068	1970.1074	1	398.2	58.80%	9
S.MS*SDANSDDPFSKPIVR.K	2.3142	0.0517	1948.307	1947.0103	1	261.1	35.40%	1
M.SSDANSDDPFSKPIVR.K	3.4146	0.6197	1736.33	1735.8333	1	680.2	63.30%	8
D.PFSKPIVR.K	2.3044	0.4896	944.923	944.1554	1	217.2	71.40%	2
R.FQATLAQQGIEDD.Q	4.1594	0.6253	1437.044	1436.5057	1	2187.1	87.50%	1
R.FQATLAQQGIEDDQLPSVR.S	5.2852	0.5649	2118.265	2117.305	1	1447	51.40%	15
R.FQATLAQQGIEDDQLPSVR.S	5.7186	0.7178	2118.385	2117.305	1	1778.3	72.20%	77
F.QATLAQQGIEDDQLPSVR.S	3.7093	0.4225	1971.304	1970.1302	1	606.6	47.10%	3
Q.ATLAQQGIEDDQLPSVR.S	2.493	0.5093	1842.697	1842.0005	1	335.4	50.00%	1
A.TLAQQGIEDDQLPSVR.S	2.6136	0.4158	1771.392	1770.9222	1	538.6	50.00%	1
T.LAQQGIEDDQLPSVR.S	2.2754	0.4184	1670.153	1669.818	1	183.6	35.70%	1
T.LAQQGIEDDQLPSVR.S	3.4651	0.6362	1670.379	1669.818	1	1043.2	67.90%	2
L.AQQGIEDDQLPSVR.S	3.9458	0.6229	1557.306	1556.6598	1	1192.7	76.90%	7
A.QQGIEDDQLPSVR.S	2.3353	0.4469	1486.311	1485.5815	1	346.7	58.30%	1

Sequence	Xcorr	DeltCN	ObsM+H+	CalcM+H+	SpR	SpScore	Ion%	#
Q.GIEDDQLPSVR.S	3.8737	0.5232	1229.666	1229.3219	1	1036.6	85.00%	1
G.IEDDQLPSVR.S	3.1407	0.4947	1172.408	1172.2704	1	1014.5	77.80%	2
R.SSDSPDVPDTPD.V	1.9964	0.4861	1231.785	1232.19	1	492.1	59.10%	1
L.SEGNAETNLSDDSEPEMLSQSSTSSLNR.R	3.3296	0.5936	2987.355	2987.029	1	389.1	33.30%	5
N.AETNLSDDSEPEMLSQSSTSSLNR.R	4.0832	0.6128	2600.45	2599.6821	1	935	52.20%	1
N.LSDDSEPEMLSQSSTSSLNR.R	3.6708	0.6014	2185.048	2184.282	1	633.5	52.60%	2
N.LSDDSEPEM#LSQSSTSSLNR.R	4.7238	0.6344	2200.184	2200.2815	1	1312.1	68.40%	2
L.SDDSEPEMLSQSSTSSLNR.R	4.3756	0.6743	2070.906	2071.1238	1	1621.6	66.70%	1
D.DSEPEMLSQSSTSSLNR.R	4.3189	0.624	1869.088	1868.9583	1	1919	75.00%	2
D.DSEPEM#LSQSSTSSLNR.R	4.1425	0.62	1885.265	1884.9576	1	1007	71.90%	4
D.SEPEMLSQSSTSSLNR.R	4.6613	0.6027	1754.26	1753.8704	1	1616.1	80.00%	3
D.SEPEM#LSQSSTSSLNR.R	4.4381	0.6968	1770.039	1769.8699	1	722	76.70%	5
E.PEMLSQSSTSSLNR.R	3.0478	0.4551	1537.253	1537.6782	1	249	61.50%	3
E.PEMLSQSSTSSLNR.R	4.4484	0.6794	1538.296	1537.6782	1	1461.6	80.80%	1
E.PEM#LSQSSTSSLNR.R	3.5168	0.5701	1554.845	1553.6776	1	1059.5	73.10%	2
E.M#LSQSSTSSLNR.R	3.5448	0.6722	1327.994	1327.4474	1	1586.6	81.80%	2
R.GFDYDPAGER.T	1.8097	0.2728	1127.068	1127.145	1	154.8	50.00%	1
R.GFDYDPAGER.T	3.2881	0.625	1128.117	1127.145	1	1377.2	88.90%	15
K.WTTEEDDEDEKTISSSSNR.Y	4.7504	0.6629	2230.311	2230.1995	1	1359.7	58.30%	2
R.QPVYATTSTYSKPLAS.G	2.4179	0.4748	1715.286	1714.8971	1	198.2	40.00%	1
Q.PVYATTSTYSKPLASGYGSR.V	3.4719	0.6088	2107.458	2107.3086	1	704.9	50.00%	1
V.YATTSTYSKPLASGYGSR.V	2.5563	0.4836	1911.466	1911.0613	1	450.9	47.10%	1
Y.ATTSTYSKPLASGYGSR.V	2.7417	0.4796	1748.639	1747.8872	1	512.3	50.00%	3
A.TTSTYSKPLASGYGSR.V	2.6985	0.5831	1678.105	1676.809	1	422.6	53.30%	1
Y.SKPLASGYGSR.V	1.8515	0.4723	1122.492	1123.2443	2	115.6	50.00%	1
K.PLASGYGSR.V	2.1621	0.3053	908.01	907.99365	1	193.1	68.80%	5
K.PLASGYGSR.V	2.7449	0.6587	908.734	907.99365	1	627.4	87.50%	4
R.ESGEYDDFKQDLV.Y	2.8017	0.5756	1546.135	1545.5858	1	718.1	66.70%	1
R.ESGEYDDFKQDLVYILS.S	2.4881	0.4459	2022.939	2022.154	1	439.5	50.00%	2
K.QDLVYILSSLQSSDASMK.V	5.1311	0.7161	1986.596	1986.233	1	1746.2	70.60%	3
Q.DLVYILSSLQSSDASMK.V	2.6999	0.4174	1858.56	1858.1033	1	607.2	50.00%	1
D.LVYILSSLQSSDASMK.V	3.982	0.6027	1742.944	1743.0154	1	1481	70.00%	3
Y.ILSSLQSSDASMK.V	2.6197	0.5777	1367.828	1367.5515	1	509.3	66.70%	1
Y.ILSSLQSSDASMK.V	3.709	0.7321	1368.715	1367.5515	1	1271.3	79.20%	2
K.CLSAISLAK.K	2.9459	0.554	963.719	963.1472	1	453.2	81.20%	16
K.CLSAISLAK.K	1.8367	0.2923	964.007	963.1472	1	216.3	62.50%	1
K.CVSPDFR.Q	2.2093	0.6059	882.153	880.9617	1	460.4	83.30%	1
R.QFIKSENMT*KSIVKALM#DS*P.E	2.2823	0.0172	2443.337	2444.642	7	217.2	22.40%	1
K.ALMDSPED.D	2.0257	0.2951	878.917	877.93976	1	359.8	64.30%	1

Sequence	Xcorr	DeltCN	ObsM+H+	CalcM+H+	SpR	SpScore	Ion%	#
K.ALM#DSPEDDLFALAA.S	2.5404	0.6999	1596.247	1595.7529	1	527.6	71.40%	1
K.ALMDSPEDDLFALAASTV.L	4.1308	0.5553	1868.439	1867.067	1	708.6	38.20%	1
D.LFALAASTVLYLLTR.D	2.6452	0.327	1654.066	1653.0016	1	637	53.60%	9
L.AASTVLYLLTR.D	2.9275	0.5669	1209.062	1208.4321	1	1043.5	75.00%	3
A.STVLYLLTR.D	3.276	0.5055	1067.344	1066.2758	1	1324.1	87.50%	2
R.LVSQLLR.I	2.3683	0.4908	830.028	829.0227	1	403.3	91.70%	12
K.VVNM#VWEVFNSYIEK.Q	5.2035	0.5272	1874.337	1874.1492	1	2036.8	82.10%	5
M.VWEVFNSYIEK.Q	2.2769	0.4335	1415.738	1414.5864	1	476.1	65.00%	1
V.WEVFNSYIEK.Q	2.3689	0.4045	1316.273	1315.455	1	493.7	61.10%	1
K.VSFDMRK.E	2.4613	0.4989	883.997	883.0507	1	536.3	83.30%	1
K.ESLTPSSLIIEAL.V	3.0004	0.5212	1374.364	1373.5741	1	1569.4	75.00%	1
R.SVNDDNLKSELLNLGILQF.V	4.3326	0.6281	2134.272	2133.3875	1	1521	61.10%	5
K.SELLNLGILQF.V	3.5545	0.6284	1247.268	1247.4652	1	1440.1	80.00%	2
K.SELLNLGILQFVVAK.I	5.1234	0.7221	1646.33	1644.9795	1	1614	78.60%	21
K.IETNVNLIADNAD.D	2.6887	0.4488	1402.637	1402.4893	1	999.9	75.00%	1
K.IETNVNLIADNADD.T	3.5032	0.7079	1518.295	1517.5771	1	1461.6	80.80%	1
K.IETNVNLIADNADDTYSILILNR.C	5.5412	0.6641	2592.167	2591.8557	1	1417.2	38.60%	37
K.IETNVNLIADNADDTYSILILNR.C	5.4154	0.6958	2592.319	2591.8557	1	1643.7	59.10%	25
V.NLIADNADDTYSILILNR.C	4.9925	0.518	2036.478	2035.2439	1	2125.8	70.60%	1
N.LIADNADDTYSILILNR.C	2.3566	0.2924	1922.441	1921.1407	1	482.3	43.80%	1
I.ADNADDTYSILILNR.C	4.3084	0.6032	1695.48	1694.8243	1	2148	78.60%	16
A.DNADDTYSILILNR.C	2.812	0.4437	1624.65	1623.7461	1	822.7	65.40%	1
D.DTYSILILNR.C	3.053	0.579	1209.119	1208.389	1	809.4	66.70%	1
K.NQAFLISHR.S	2.312	0.3808	1087.107	1086.2288	1	1434.4	93.80%	4
R.SNILISSLAK.F	2.6557	0.236	1047.081	1046.2428	2	749.8	72.20%	23
R.SNILISSLAK.F	3.4274	0.5071	1047.516	1046.2428	1	1172.5	83.30%	98
L.ISSLAK.F	1.8261	0.2902	619.09	618.74554	1	466.2	80.00%	1
K.FLQVILDR.V	2.6945	0.5018	1004.515	1004.2076	2	273.6	71.40%	49
K.FLQVILDR.V	3.5576	0.562	1005.048	1004.2076	1	1152.2	92.90%	236
F.LQVILDR.V	1.9473	0.4664	857.212	857.0329	1	295.4	75.00%	1
R.VHQLAEEEVKK.Y	3.8798	0.6717	1311.214	1310.4813	1	1579.7	90.00%	2
K.YISCLALMCR.L	1.9604	0.4124	1286.821	1287.5413	1	219.3	61.10%	2
K.YISCLALMCR.L	3.6703	0.5716	1287.952	1287.5413	1	1128.4	88.90%	210
K.YISCLALM#CR.L	3.752	0.6593	1304.366	1303.5406	1	1116.4	83.30%	148
R.LLINISHD.N	2.2532	0.5152	926.257	925.0641	1	677.3	78.60%	1
R.LLINISHDNELCCSK.L	3.8707	0.512	1816.463	1817.021	1	773.4	60.70%	16
K.LGQIEGFLPNAI.T	2.7134	0.5675	1271.885	1272.4747	1	851.7	68.20%	1
K.LGQIEGFLPNAI.T	3.696	0.4595	1273.406	1272.4747	1	1135.7	77.30%	1
K.LGQIEGFLPNAITTF.T	2.7001	0.6196	1621.139	1621.858	1	933.1	57.10%	1

Sequence	Xcorr	DeltCN	ObsM+H+	CalcM+H+	SpR	SpScore	Ion%	#
K.LGQIEGFLPNAITTF.T	2.2232	0.3397	1621.889	1621.858	1	341.9	53.60%	1
K.LGQIEGFLPNAITTFT.Y	3.1052	0.5702	1723.028	1722.9624	1	589.5	60.00%	1
K.LGQIEGFLPNAITTFTYLAPK.F	5.5739	0.661	2296.486	2295.6616	1	908.4	65.00%	73
K.LGQIEGFLPNAITTFTYLAPK.F	5.7058	0.6153	2296.948	2295.6616	1	1786.9	46.20%	17
L.GQIEGFLPNAITTFTYLAPK.F	3.3464	0.5123	2182.317	2182.5034	1	458.7	50.00%	2
I.EGFLPNAITTFTYLAPK.F	4.1956	0.6067	1885.242	1884.1637	1	883.5	65.60%	2
E.GFLPNAITTFTYLAPK.F	2.768	0.5983	1755.017	1755.0492	1	659.3	56.70%	1
G.FLPNAITTFTYLAPK.F	3.2858	0.5326	1698.166	1697.9977	1	581.3	64.30%	2
F.LPNAITTFTYLAPK.F	2.2889	0.5443	1549.906	1550.823	1	552.5	61.50%	1
P.NAIT*T*FT*YLAPK.F	2.3301	0.3595	1579.471	1580.4888	2	305.7	29.10%	1
N.AITTFTYLAPK.F	3.853	0.573	1226.989	1226.4459	1	1524.2	85.00%	11
I.TTFTYLAPK.F	2.9026	0.5438	1043.159	1042.2095	1	673.4	87.50%	3
T.FTYLAPK.F	2.205	0.5995	841.12	840.0008	1	764.4	91.70%	1
K.ENSYDINVM#M#T.S	2.6802	0.4159	1349.128	1349.4701	1	553.1	65.00%	1
K.ENSYDINVMMTSLLTNLVER.C	5.3877	0.5996	2344.14	2343.6636	1	1198	57.90%	33
K.ENSYDINVMMTSLLTNLVER.C	5.1751	0.5829	2344.498	2343.6636	1	1284.8	36.80%	10
K.ENSYDINVM#MTSLLTNLVER.C	4.417	0.0464	2359.671	2359.663	1	1236.3	40.80%	4
K.ENSYDINVMM#TSLLTNLVER.C	4.7881	0.0567	2360.109	2359.663	1	1285.6	36.80%	2
K.ENSYDINVMM#TSLLTNLVER.C	4.6173	0.0937	2360.171	2359.663	1	1956.2	68.40%	12
K.ENSYDINVM#MTSLLTNLVER.C	4.5678	0.094	2360.207	2359.663	1	1170.6	55.30%	11
K.ENSYDINVM#M#TSLLTNLVER.C	4.3677	0.5714	2375.52	2375.6624	1	1157.6	55.30%	5
K.ENSYDINVM#M#TSLLTNLVER.C	3.7737	0.5123	2376.415	2375.6624	6	908.9	32.90%	1
N.SYDINVMM#TSLLTNLVER.C	3.3962	0.0969	2117.749	2116.4453	1	769.4	55.90%	1
N.VMMTSLLTNLVER.C	3.9199	0.4467	1509.111	1507.845	1	1584.4	75.00%	3
V.MMTSLLTNLVER.C	2.3978	0.235	1409.302	1408.7134	2	446.3	59.10%	1
M.MTSLLTNLVER.C	4.0634	0.5916	1278.092	1277.5164	1	1256.4	85.00%	16
M.M#TSLLTNLVER.C	3.1597	0.4476	1294.487	1293.5157	1	675.8	80.00%	4
M.TSLLTNLVER.C	3.2363	0.4478	1147.186	1146.3192	1	1524.3	88.90%	3
M.T*S*LLTNLVER.C	2.2528	0.0556	1306.408	1306.279	3	659.7	47.20%	1
T.SLLTNLVER.C	3.2157	0.2213	1046.012	1045.2148	1	940.5	81.20%	29
R.CNANRKVLIAQT*VKM#V.I	2.5016	0.2021	1943.425	1942.2043	23	170.4	26.70%	1
K.VLIAQTVK.M	3.0186	0.5832	873.11	872.08746	1	518.2	92.90%	27
K.MVIPGHDVEEVPALEAI.T	3.1668	0.4872	1820.843	1820.0999	1	462.4	56.20%	11
K.MVIPGHDVEEVPALEAITR.L	4.0672	0.6192	2076.433	2077.3906	1	779.1	61.10%	7
H.DVEEVPALEAITR.L	2.9755	0.1991	1442.976	1442.5966	1	705.7	70.80%	2
D.VEEVPALEAITR.L	3.6928	0.5992	1328.031	1327.5087	1	1130.1	90.90%	5
R.LFVYHESQAQIV.D	3.5676	0.518	1434.757	1434.621	1	708	77.30%	34
R.LFVYHESQAQIVD.A	2.2679	0.1922	1549.546	1549.7087	1	785	70.80%	2
R.LFVYHESQAQIVDA.D	2.5459	0.466	1621.039	1620.787	1	609.3	61.50%	4
R.LFVYHESQAQIVDADLD.R	3.3387	0.5466	1965.287	1964.121	1	884.7	59.40%	10

Sequence	Xcorr	DeltCN	ObsM+H+	CalcM+H+	SpR	SpScore	Ion%	#
H.ESQAQIVDADLLDR.E	2.7297	0.4898	1461.519	1460.5288	1	347.2	66.70%	1
R.ELAFDEGGCGDEEEEEEGGD.E	3.3192	0.5398	2173.906	2174.0366	1	2741.7	71.10%	1
R.ELAFDEGGCGDEEEEEEGGDESS DED.G	4.772	0.5539	2837.711	2836.5967	1	1034.4	35.00%	1
R.ELAFDEGGCGDEEEEEEGGDESS DEDGVR.K	2.9376	0.2672	3148.834	3148.9663	1	839.2	39.30%	1
R.ELAFDEGGCGDEEEEEEGGDESS DEDGVR.K	6.3849	0.6301	3150.009	3148.9663	1	2516.9	43.80%	5
R.ELAFDEGGCGDEEEEEEGGDES*S DEDGVR.K	3.89	0.0385	3230.079	3228.946	1	695	25.00%	1
K.MDRMDQVDVV.H	2.3359	0.2372	1209.084	1208.3912	1	472.7	83.30%	1
R.MDQVDVVHAL.Q	3.62	0.5572	1128.196	1127.2963	1	1471.5	88.90%	2
R.M#DQVDVVHAL.Q	2.2176	0.1182	1144.091	1143.2957	1	1041.7	83.30%	1
R.MDQVDVVHALQ.Q	3.3522	0.4766	1256.406	1255.426	1	892.6	80.00%	2
R.MDQVDVVHALQQV.M	3.5535	0.5107	1483.383	1482.6874	1	1610.8	83.30%	8
R.M#DQVDVVHALQQV.M	3.3248	0.5727	1499.195	1498.6868	1	1170.4	75.00%	3
R.MDQVDVVHALQQVM.N	3.3516	0.5042	1614.463	1613.8845	1	519.3	69.20%	10
R.MDQVDVVHALQQVMNK.A	4.2809	0.6717	1856.237	1856.1605	1	1499.8	70.00%	9
R.MDQVDVVHALQQVM#NK.A	3.6789	0.6164	1873.201	1872.1599	1	625.9	56.70%	3
R.M#DQVDVVHALQQVM#NK.A	4.2984	0.6406	1889.114	1888.1593	1	805.7	70.00%	8
K.NFQNMISQLK.R	2.7622	0.3876	1223.047	1223.4272	1	516.5	72.20%	12
K.NFQNMISQLK.R	4.0043	0.4896	1224.755	1223.4272	1	1468.4	83.30%	113
K.NFQNM#ISQLK.R	3.6967	0.4821	1240.321	1239.4266	1	1514.2	83.30%	24
R.LYDFTK.A	1.9028	0.5687	786.225	786.8948	1	431.7	80.00%	14
R.VIEYLER.L	1.8801	0.4762	922.091	922.06024	1	294.5	75.00%	6
R.VIEYLER.L	3.0524	0.555	923.125	922.06024	1	453.9	91.70%	16
V.IEYLER.L	1.8138	0.4512	823.039	822.92865	1	239.4	80.00%	1
M.ASMSSDANSDDPFSKPIVR.K	4.0729	0.5642	2024.766	2025.1863	1	757.5	40.30%	10
M.ASMSSDANSDDPFSKPIVR.K	6.1087	0.4008	2026.452	2025.1863	1	1084.1	63.90%	46
M.ASM#SSDANSDDPFSKPIVR.K	4.8598	0.4355	2042.51	2041.1857	1	784.6	63.90%	3
M.ASMSSDANSDDPFSKPIVRK.R	3.1976	0.4682	2152.98	2153.3591	1	384.9	36.80%	2
A.SMSSDANSDDPFSKPIVR.K	2.461	0.4403	1953.894	1954.108	1	253.7	44.10%	2
A.SMSSDANSDDPFSKPIVR.K	5.8018	0.6351	1955.434	1954.108	1	753.1	61.80%	77
A.SM#SSDANSDDPFSKPIVR.K	3.7837	0.5544	1970.389	1970.1074	1	548.9	52.90%	5
A.S*M#SSDANSDDPFSKPIVR.K	2.2894	0.0423	2050.393	2050.0874	1	525.6	39.20%	1
A.SM#SS*DANSDDPFSKPIVR.K	2.2894	0.0423	2050.393	2050.0874	2	472.8	37.30%	1
A.SMSSDANSDDPFSKPIVRK.R	3.1152	0.4852	2081.408	2082.281	1	274	41.70%	4
A.S*MS*SDANSDDPFSKPIVR.K	2.662	0.0295	2113.677	2114.0679	2	214.7	25.00%	1
A.SMS*S*DANSDDPFSKPIVR.K	3.0654	0.0326	2115.436	2114.0679	2	201.1	30.90%	1
S.MSSDANSDDPFSKPIVR.K	3.7184	0.3982	1866.171	1867.0304	1	585.2	56.20%	1
S.MS*S*DANSDDPFSKPIVR.K	4.4366	0.262	2028.369	2026.9901	1	1010.8	42.20%	5
M.SSDANSDDPFSKPIVR.K	4.2298	0.628	1735.484	1735.8333	1	711.1	70.00%	2

Sequence	Xcorr	DeltCN	ObsM+H+	CalcM+H+	SpR	SpScore	Ion%	#
S.SDANSDDPFSKPIVR.K	3.3234	0.4884	1648.078	1648.7556	1	1398.8	78.60%	1
S.DANSDDPFSKPIVR.K	3.9762	0.573	1560.8	1561.678	1	1243.4	80.80%	2
D.ANSDDPFSKPIVR.K	3.6203	0.374	1446.57	1446.5901	1	1189.3	79.20%	9
A.NSDDPFSKPIVR.K	2.2168	0.4914	1376.703	1375.5118	1	413.1	68.20%	1
D.PFSKPIVR.K	2.5398	0.4617	943.67	944.1554	1	326.5	71.40%	56
D.PFSKPIVR.K	2.7513	0.4168	945.074	944.1554	1	631.1	85.70%	5
R.KRFQATLAQQGIEDDQLPSVR.S	4.9528	0.6283	2401.666	2401.6643	1	1155.9	57.50%	32
R.KRFQATLAQQGIEDDQLPSVR.S	7.3909	0.5906	2402.84	2401.6643	1	1948.8	47.50%	27
K.RFQATLAQQGIEDDQLPSVR.S	4.0331	0.5158	2273.661	2273.4915	1	1434.9	53.90%	2
K.RFQATLAQQGIEDDQLPSVR.S	4.9535	0.5578	2273.854	2273.4915	1	1177.4	65.80%	9
R.FQATLAQQGIEDDQLPSVR.S	5.3965	0.6535	2118.205	2117.305	1	1695.4	58.30%	11
R.FQATLAQQGIEDDQLPSVR.S	6.2296	0.668	2118.589	2117.305	1	1453.4	69.40%	58
F.QATLAQQGIEDDQLPSVR.S	2.463	0.3379	1969.676	1970.1302	1	358.1	38.20%	1
Q.ATLAQQGIEDDQLPSVR.S	4.2282	0.5707	1841.471	1842.0005	1	1126.1	68.80%	1
A.TLAQQGIEDDQLPSVR.S	4.1914	0.5746	1770.41	1770.9222	1	1493.4	76.70%	1
T.LAQQGIEDDQLPSVR.S	4.0664	0.5449	1669.558	1669.818	1	1638.7	82.10%	1
L.AQQGIEDDQLPSVR.S	3.4728	0.5482	1556.382	1556.6598	1	1299.2	80.80%	5
Q.GIEDDQLPSVR.S	2.3327	0.383	1229.004	1229.3219	1	430.6	65.00%	1
G.IEDDQLPSVR.S	1.8673	0.1488	1172.245	1172.2704	2	288.7	55.60%	1
A.ETNLSDDS*EPEM#LSQSST*SSLNR.R	2.4355	0.0338	2703.718	2704.5632	20	200.9	20.50%	1
D.SEPEMLSQSSTSSLNR.R	3.8326	0.6142	1752.981	1753.8704	1	1705.5	80.00%	2
E.PEMLSQSSTSSLNR.R	3.0695	0.4266	1536.67	1537.6782	1	1119.9	73.10%	1
E.MLSQSSTSSLNR.R	2.3842	0.4481	1311.04	1311.448	1	480.7	63.60%	1
R.RMEDSAIDPSR.G	2.2372	0.4481	1276.672	1277.3901	1	413.6	70.00%	1
R.RMEDSAIDPSRGTR.K	3.312	0.4602	1591.455	1591.7323	1	704.9	73.10%	6
R.RMEDSAIDPSRGTR.K	2.5953	0.5238	1591.697	1591.7323	1	177.9	53.80%	1
R.RM#EDSAIDPSRGTR.K	2.6675	0.2977	1607.401	1607.7317	1	335.7	57.70%	4
R.RMEDSAIDPSRGTRK.S	2.5285	0.4305	1720.028	1719.9053	1	403.9	57.10%	4
R.RM#EDSAIDPSRGTRK.S	2.2437	0.4122	1736.991	1735.9047	1	289.1	53.60%	1
R.MEDSAIDPSR.G	2.2738	0.4494	1120.58	1121.2037	1	389.3	61.10%	1
R.MEDSAIDPSR.G	3.8938	0.4701	1122.205	1121.2037	1	1983.8	94.40%	5
R.M#EDSAIDPSR.G	2.4386	0.464	1137.585	1137.2031	1	1010.4	83.30%	2
K.SQSRGFDYDPAGER.T	2.5028	0.3278	1585.267	1585.6165	1	308.4	57.70%	2
K.SQSRGFDYDPAGERTTAPVQK.K	3.3347	0.5037	2311.666	2311.4534	1	436.5	50.00%	2
K.SQSRGFDYDPAGERTTAPVQKK.K	2.2505	0.1117	2440.223	2439.6262	55	72.9	19.00%	1
S.QS*RGFDYDPAGERTTAPVQK.K	2.2226	0.2007	2304.36	2304.3555	1	123.6	24.60%	1
R.GFDYDPAGER.T	3.2842	0.648	1128.132	1127.145	1	1416.9	88.90%	13
R.GFDYDPAGER.T	2.421	0.3453	1128.529	1127.145	1	178.7	55.60%	4
R.GFDYDPAGERTTAPVQK.K	4.1792	0.6206	1853.612	1852.9818	1	844.8	75.00%	8

Sequence	Xcorr	DeltCN	ObsM+H+	CalcM+H+	SpR	SpScore	Ion%	#
R.GFDYDPAGERTTAPVQKK.K	3.0501	0.5682	1980.762	1981.1548	1	900.9	67.60%	27
D.PAGERTTAPVQK.K	2.9074	0.3835	1255.361	1255.4058	1	1213.9	81.80%	6
P.AGERT*TAPVQK.K	1.8638	0.1739	1237.17	1238.27	1	182.8	46.70%	1
K.KKKDEIDMGGAK.F	4.0121	0.6496	1321.447	1320.5411	1	1712.7	86.40%	17
K.KKKDEIDM#GGAK.F	3.0593	0.4862	1336.556	1336.5405	1	753.7	72.70%	7
K.KKDEIDMGGAK.F	2.7054	0.5586	1192.269	1192.3683	1	1587.5	90.00%	1
K.KKDEIDMGGAKFFPK.Q	4.5423	0.5725	1711.768	1712.0062	1	1925.8	58.90%	2
K.KKDEIDMGGAKFFPK.Q	5.6559	0.4702	1712.529	1712.0062	1	1281	78.60%	38
K.KKDEIDM#GGAKFFPK.Q	3.3693	0.4333	1727.857	1728.0056	1	369.2	53.60%	5
K.KDEIDMGGAKFFPKQEK.K	3.0064	0.4855	1970.324	1969.2506	1	415.3	50.00%	2
K.DEIDMGGAKFFPK.Q	3.2532	0.5254	1456.064	1455.6604	1	1693.8	79.20%	1
M.GGAKFFPKQEK.K	2.6834	0.2603	1237.915	1237.432	1	448.4	65.00%	3
K.KHVYTHKWTTEEDDEDEK.T	4.6023	0.5984	2290.769	2291.3726	1	1258.2	67.60%	2
K.KHVYTHKWTTEEDDEDEK.T	3.8754	0.4463	2291.383	2291.3726	1	1209.4	45.60%	1
K.KHVYTHKWTTEEDDEDEKTISSSSNR.Y	6.9685	0.6297	3124.19	3124.235	1	1155.8	39.00%	6
K.HVYTHKWTTEEDDEDEK.T	2.2723	0.4968	2163.733	2163.1995	1	460.3	50.00%	1
K.HVYTHKWTT*EEDDEDEK.T	2.3202	0.0189	2242.982	2243.1794	15	166.5	25.00%	2
K.HVYTHKWTTEEDDEDEKTISSSSNR.Y	3.9107	0.6027	2994.719	2996.0623	1	885.4	45.80%	2
K.HVYTHKWTTEEDDEDEKTISSSSNR.Y	8.9459	0.6418	2997.189	2996.0623	1	3056.7	47.90%	3
H.VYTHKWTTEEDDEDEKTISSSSNR.Y	6.2187	0.5783	2858.539	2858.9224	1	1462.7	37.00%	1
V.YTHKWTTEEDDEDEKTISSSSNR.Y	6.2617	0.6726	2759.129	2759.7908	1	2222.2	47.70%	2
K.WTTEEDDEDEK.T	2.2063	0.4491	1397.381	1397.3368	1	500.7	70.00%	1
W.T*TEEDDEDEKTISSSSNR.Y	2.2114	0.0603	2123.368	2123.9685	15	113.7	25.50%	1
R.YSSRPNQPAVSAR.P	3.7424	0.5139	1433.268	1433.5547	1	1452.1	54.20%	1
R.YSSRPNQPAVSAR.P	3.2804	0.3965	1434.393	1433.5547	1	444	62.50%	8
R.YSSRPNQPAVSARPR.Q	4.1103	0.3488	1687.029	1686.8567	1	1325	51.80%	4
R.YSSRPNQPAVSARPR.Q	2.2082	0.3928	1687.758	1686.8567	2	142.3	42.90%	1
R.PRQPVYATTSTYSKPLASGYGSR.V	5.4888	0.6376	2487.749	2488.7405	1	689.1	56.80%	4
R.PRQPVYATTSTYSKPLASGYGSR.V	6.7705	0.6704	2489.054	2488.7405	1	1249.5	42.00%	2
R.QPVYATTSTYSKPLASGYG.S	2.2374	0.4316	1991.139	1992.1743	1	423.5	38.90%	1
R.QPVYATTSTYSKPLASGYGSR.V	3.9922	0.6897	2235.593	2235.4382	1	319.1	55.00%	12
R.QPVYATTSTYSKPLASGYGSR.V	3.8059	0.4991	2235.848	2235.4382	1	793.3	30.00%	1
Q.PVYATTSTYSKPLASGYGSR.V	6.0901	0.7107	2106.676	2107.3086	1	1537.9	65.80%	4
P.VYATTSTYSKPLASGYGSR.V	6.126	0.6787	2011.538	2010.1929	1	1579.3	72.20%	8
V.YATTSTYSKPLASGYGSR.V	3.8329	0.6554	1910.832	1911.0613	1	804.4	61.80%	2
Y.ATTSTYSKPLASGYGSR.V	4.5601	0.5901	1747.56	1747.8872	1	786.4	65.60%	7
A.TTSTYSKPLASGYGSR.V	3.1691	0.5707	1676.958	1676.809	1	492.8	60.00%	5

Sequence	Xcorr	DeltCN	ObsM+H+	CalcM+H+	SpR	SpScore	Ion%	#
T.TSTYSKPLASGYGSR.V	3.8763	0.6106	1575.296	1575.7046	1	977.2	78.60%	5
T.STYSKPLASGYGSR.V	3.3999	0.6925	1475.382	1474.6003	1	656.5	80.80%	5
S.TYSKPLASGYGSR.V	3.0362	0.6554	1387.288	1387.5227	1	604.3	70.80%	4
T.YSKPLASGYGSR.V	2.6077	0.4486	1286.446	1286.4183	1	417.2	72.70%	2
K.PLASGYGSR.V	2.4713	0.6514	907.467	907.99365	1	222.4	75.00%	4
R.VRHIKEANELRESGEYD.D	2.3573	0.3233	2046.035	2046.1869	2	202.1	40.60%	1
R.VRHIKEANELRESGEYDD.F	3.6235	0.5618	2161.668	2161.2747	1	602.5	38.20%	1
R.HIKEANELR.E	3.1455	0.5878	1110.454	1110.2487	1	647.3	87.50%	13
R.HIKEANELRESGEYD.D	2.5861	0.3625	1790.282	1790.8689	1	455.4	60.70%	1
R.HIKEANELRESGEYDDFKQD.L	3.6241	0.4514	2424.23	2424.522	1	1175	38.20%	1
K.EANELRESGEYDDFKQDLVYIL.S	4.063	0.3353	2648.307	2647.8315	1	468.1	38.10%	3
R.ESGEYDDFKQDLVYILSSLQSSDA SMK.V	4.7062	0.5839	3056.721	3057.2888	1	455.2	38.50%	4
R.ESGEYDDFKQDLVYILSSLQSSDA SMK.V	4.957	0.6655	3057.893	3057.2888	1	1422.6	33.70%	3
R.ESGEYDDFKQDLVYILSSLQSSDA SMKVK.C	6.0036	0.57	3284.243	3284.5933	1	1566.2	33.00%	1
K.VKCLSAISLAK.K	3.1187	0.4832	1191.427	1190.4518	1	665.7	80.00%	4
K.VKCLSAISLAKK.C	3.4885	0.42	1318.613	1318.6246	1	1058.8	77.30%	3
K.CLSAISLAK.K	2.9505	0.514	963.132	963.1472	1	708.8	93.80%	7
K.CLSAISLAK.K	1.8425	0.142	964.53	963.1472	1	193.1	56.20%	1
K.CLSAISLAKK.C	3.029	0.5388	1092.284	1091.3202	1	702.7	83.30%	10
K.CLSAISLAKKCVSPDFR.Q	4.3812	0.0631	1952.392	1953.2592	1	1293.6	65.60%	2
K.CLSAISLAKKCVSPDFRQFIK.S	4.8356	0.5407	2468.876	2469.8948	1	1306.1	45.00%	3
K.KCVSPDFR.Q	2.0326	0.5406	1008.519	1009.1346	1	285.4	64.30%	8
K.KCVSPDFR.Q	2.237	0.4832	1010.112	1009.1346	1	460.5	78.60%	2
K.KCVSPDFRQFIK.S	4.642	0.5287	1526.235	1525.7701	1	1104.2	86.40%	8
K.KCVSPDFRQFIKSENMT*.K	3.2308	0.201	2167.648	2168.3467	1	320.7	37.50%	1
K.KCVSPDFRQFIKSENMTK.S	4.4161	0.5842	2216.416	2216.5398	1	914	47.10%	4
K.KCVSPDFRQFIKSENMTK.S	5.6475	0.6979	2217.169	2216.5398	1	880.4	61.80%	12
K.KCVSPDFRQFIKSENM#TK.S	2.9764	0.3193	2232.746	2232.5393	1	183.5	47.10%	1
K.CVSPDFRQFIK.S	1.8397	0.314	1397.845	1397.5973	1	162.6	50.00%	1
K.CVSPDFRQFIK.S	3.2731	0.4754	1398.345	1397.5973	1	828	70.00%	7
K.CVSPDFRQFIKSENMTK.S	4.2546	0.654	2088.57	2088.367	1	617.5	65.60%	3
K.SENMTKSIVK.A	2.354	0.4174	1137.211	1137.3326	1	563.1	72.20%	1
K.ALMDSPEDDLFALAASTVLYLLT R.D	4.0557	0.5412	2627.293	2627.0066	1	787.8	35.90%	1
K.ALMDSPEDDLFALAASTVLYLLT R.D	6.3783	0.6763	2627.702	2627.0066	1	1585.3	50.00%	6
K.ALMDSPEDDLFALAAST*VLYLL T*.R	2.3141	0.0891	2629.596	2630.78	3	225.4	18.20%	1
K.ALM#DSPEDDLFALAASTVLYLL TR.D	3.9072	0.6302	2641.794	2643.0059	1	1416.5	52.20%	1
K.ALM#DSPEDDLFALAASTVLYLL TR.D	3.7787	0.4401	2642.703	2643.0059	1	615.1	32.60%	2

Sequence	Xcorr	DeltCN	ObsM+H+	CalcM+H+	SpR	SpScore	Ion%	#
K.ALMDSPEDDLFALAASTVLYLLTRDFNSIK.I	3.9701	0.3508	3331.97	3331.781	1	381.9	26.70%	1
D.SPEDDLFALAASTVLYLLTR.D	4.1854	0.5254	2195.448	2196.485	1	3040.7	65.80%	1
D.LFALAASTVLYLLTR.D	2.6134	0.2658	1653.708	1653.0016	1	894.7	57.10%	7
A.LAAS*T*VLYLLTR.D	2.2119	0.2575	1482.639	1481.5502	3	300	38.60%	1
R.DFNSIKIDFPSLR.L	3.8154	0.5294	1553.862	1552.7559	1	460.1	66.70%	3
R.DFNSIKIDFPSLR.L	4.5332	0.5441	1553.922	1552.7559	1	1945.5	60.40%	4
R.DFNSIKIDFPSLR.L	4.9628	0.6406	1554.088	1552.7559	1	1109.3	83.30%	15
D.FNSIKIDFPSLR.L	3.4058	0.4721	1437.399	1437.668	1	1305.3	86.40%	2
R.LVSQLLR.I	2.405	0.6014	829.371	829.0227	1	509.3	91.70%	3
R.LVSQLLR.I	1.8074	0.1613	829.522	829.0227	1	162.8	66.70%	1
R.LVSQLLRI.E	1.8882	0.3836	941.722	942.18097	1	267.4	64.30%	1
R.LVSQLLRIEK.F	3.676	0.4655	1200.362	1199.4684	1	1276.6	88.90%	19
K.FEQRPEDKDKVVNMVWEVFNSYIEK.Q	6.1066	0.477	3131.285	3131.5068	1	1931.4	36.50%	10
K.VVNMVWEVFNSYIEK.Q	3.4714	0.5294	1858.038	1858.1498	1	962.7	64.30%	1
K.VVNMVWEVFNSYIEKQEVGG.Q	2.5373	0.0401	2327.741	2328.629	1	231.8	31.60%	1
K.VVNMVWEVFNS*YIEKQEVG.G	2.2971	0.1801	2352.889	2351.5571	5	103.9	24.10%	1
K.VVNMVWEVFNSYIEKQEVGGQK.V	4.7769	0.5224	2584.228	2584.9314	1	1190.5	39.30%	1
K.VVNMVWEVFNSYIEKQEVGGQK.V	5.3747	0.6874	2584.663	2584.9314	1	2001.3	59.50%	1
E.VFNSYIEKQEVGGQK.V	3.3133	0.3614	1726.474	1726.9111	4	237.5	42.90%	1
K.QEVGGQKVS*FDMRKESLTPS.S	2.2884	0.2572	2304.468	2304.4604	125	73.4	21.10%	3
K.VSFDMRK.E	2.5367	0.5203	883.158	883.0507	1	370.4	75.00%	2
K.VS*FDM#RKES*LTPSSLII.E	2.351	0.1476	2101.088	2100.2104	25	135.8	20.30%	1
R.KESLTPSSLIIEALVFICSR.S	6.0136	0.6557	2265.016	2264.6409	1	1577.4	68.40%	3
K.ESLTPSSLIIEALVFICSR.S	3.5243	0.5519	2136.877	2136.4678	1	1132	44.40%	1
K.ESLTPSSLIIEALVFICSR.S	5.7116	0.6981	2137.091	2136.4678	1	1613.4	63.90%	16
R.SVNDDNLKSELLNLGILQFVVAK.I	5.5728	0.5777	2531.552	2530.9019	1	1701.3	44.30%	10
R.SVNDDNLKSELLNLGILQFVVAK.I	5.8092	0.6061	2531.844	2530.9019	1	2230.4	56.80%	29
K.SELLNLGILQFVVAK.I	5.8349	0.6925	1645.774	1644.9795	1	2108.2	82.10%	3
K.IETNVNLIADNADDTYSILILNR.C	5.518	0.6595	2592.688	2591.8557	1	1625.5	42.00%	17
K.IETNVNLIADNADDTYSILILNR.C	6.0134	0.7107	2593.017	2591.8557	1	2077.7	61.40%	81
R.ILESSSVFHK.K	2.837	0.4782	1147.566	1147.3057	1	799.5	83.30%	6
R.ILESSSVFHKK.N	3.7932	0.3958	1276.334	1275.4786	1	732.1	80.00%	25
R.ILESSSVFHKKNQAFLISHR.S	4.8017	0.647	2343.486	2342.6848	1	953.7	52.60%	3
K.KNQAFLISHR.S	3.5083	0.5617	1214.394	1214.4017	1	1051.9	94.40%	2
K.KNQAFLIS*HRSNILISS*LA.K	2.2361	0.0456	2273.874	2273.4087	44	154	20.80%	1
K.NQAFLISHR.S	3.0335	0.5159	1086.157	1086.2288	1	208.6	81.20%	12
K.NQAFLISHR.S	3.3242	0.5151	1087.05	1086.2288	1	1481.1	93.80%	28

Sequence	Xcorr	DeltCN	ObsM+H+	CalcM+H+	SpR	SpScore	Ion%	#
K.NQAFLISHRSNILIS.S	2.3057	0.0418	1714.358	1713.9619	4	180.1	42.90%	2
R.SNILISSLAK.F	3.2368	0.4806	1046.505	1046.2428	1	1342.5	88.90%	7
R.SNILISSLAK.F	2.649	0.3991	1047.629	1046.2428	2	477.5	61.10%	5
K.FLQVILDR.V	3.2041	0.5389	1003.635	1004.2076	1	1132.1	92.90%	5
K.FLQVILDR.V	2.6237	0.5647	1004.155	1004.2076	1	499.1	78.60%	3
K.FLQVILDRVHQLAEEEVKK.Y	5.305	0.5035	2295.018	2295.6663	1	1516.5	66.70%	13
K.FLQVILDRVHQLAEEEVKK.Y	6.2847	0.4429	2295.421	2295.6663	1	3042.2	50.00%	45
D.RVHQLAEEEVKK.Y	3.0701	0.5232	1466.86	1466.6677	1	939.3	72.70%	12
R.VHQLAEEEVKK.Y	3.2471	0.6292	1310.471	1310.4813	1	1493.5	85.00%	2
R.VHQLAEEEVKKYISCLALMCR.L	2.4698	0.41	2579.367	2579	65	72.8	25.00%	1
K.KYISCLALMCR.L	3.6416	0.4912	1416.692	1415.7141	1	1411.3	85.00%	1
K.YISCLALMCR.L	2.0332	0.5024	1287.024	1287.5413	1	202.2	61.10%	1
K.YISCLALMCR.L	3.6375	0.5305	1288.222	1287.5413	1	944.4	83.30%	8
K.YISCLALM#CR.L	2.5229	0.5027	1303.261	1303.5406	1	1228.3	83.30%	1
R.LLINISHD.N	2.29	0.641	924.68	925.0641	1	533.1	78.60%	1
R.LLINISHDNELCCSK.L	4.2435	0.4792	1816.777	1817.021	1	466.8	57.10%	5
R.LLINISHDNELCCSK.L	5.7325	0.5265	1817.48	1817.021	1	1299.1	71.40%	67
R.LLINISHDNELCCSK.L	4.752	0.4319	1818.244	1817.021	1	1292.5	58.90%	6
S.KLGQIEGFLPNAITTFTYLAPK.F	3.2332	0.5164	2425.047	2423.8345	1	740.1	47.60%	2
K.LGQIEGFLPNAITTF.T	2.6778	0.3916	1621.77	1621.858	1	654.3	60.70%	1
K.LGQIEGFLPNAITTFTYLAPK.F	6.1497	0.629	2295.901	2295.6616	1	838.5	62.50%	21
K.LGQIEGFLPNAITTFTYLAPK.F	5.4842	0.6495	2296.208	2295.6616	1	1216.8	45.00%	8
K.LGQIEGFLPNAITT*FT*YLAP.K	3.5156	0.0152	2328.494	2327.4485	1	290	26.30%	1
K.LGQIEGFLPNAIT*T*FTYLAP.K	3.1459	0.0604	2328.767	2327.4485	3	225.5	23.70%	4
K.LGQIEGFLPNAITTFTYLAPKFGK.E	4.5256	0.4181	2628.189	2628.0608	1	452.9	30.40%	1
G.FLPNAITTFTYLAPK.F	3.4839	0.4873	1698.672	1697.9977	1	719.5	67.90%	3
F.LPNAITTFTYLAPK.F	3.0474	0.5489	1550.692	1550.823	1	1102.6	73.10%	1
L.PNAITTFTYLAPK.F	1.8012	0.1353	1437.717	1437.6647	3	214.4	45.80%	1
K.FGKENSYDINVMMTSLLTNLVER.C	7.1561	0.6625	2675.927	2676.0627	1	2134.1	61.40%	35
K.FGKENSYDINVMMTSLLTNLVER.C	5.9749	0.6856	2677.097	2676.0627	1	1214.5	36.40%	41
K.FGKENSYDINVMMT*S*LLTNLVE.R	2.9739	0.0321	2680.226	2679.8362	3	261	17.90%	1
K.FGKENSYDINVM#MTSLLTNLVER.C	4.1016	0.0325	2690.982	2692.062	1	421.6	40.90%	2
K.FGKENSYDINVMM#TSLLTNLVER.C	5.5105	0.0609	2691.253	2692.062	1	1525.8	37.50%	4
K.FGKENSYDINVM#MTSLLTNLVER.C	4.9018	0.0794	2691.268	2692.062	1	1560.8	35.20%	3
K.FGKENSYDINVMM#TSLLTNLVER.C	5.1177	0.0307	2691.492	2692.062	1	878.5	56.80%	3
K.FGKENSYDINVM#M#TSLLTNLVER.C	6.6084	0.5063	2707.768	2708.0615	1	2005.3	39.80%	1

Sequence	Xcorr	DeltCN	ObsM+H+	CalcM+H+	SpR	SpScore	Ion%	#
K.FGKENSYDINVM#M#TSLLTNLVER.C	4.5495	0.6644	2708.35	2708.0615	1	269.3	43.20%	6
K.FGKENSYDINVMMTSLLTNLVERCNANR.K	4.6318	0.4256	3290.863	3291.6987	1	594.3	27.80%	3
K.FGKENSYDINVMMTSLLTNLVERCNANRK.V	4.5822	0.6021	3418.715	3419.8716	3	556.7	23.20%	1
F.GKENS*YDINVM#MTS*LLTNLVER.C	3.5323	0.0152	2703.978	2704.8472	1	799.2	19.60%	1
F.GKENS*YDINVM#MT*SLLTNLVER.C	3.5638	0.0107	2704.42	2704.8472	1	843	21.40%	1
F.GKENS*YDINVM#MT*SLLTNLVER.C	2.9693	0.0533	2705.286	2704.8472	3	312.1	21.40%	1
F.GKENSYDINVM#MT*S*LLTNLVER.C	3.8354	0.0994	2706.116	2704.8472	4	624	19.00%	3
F.GKENSYDINVM#MT*S*LLTNLVER.C	3.1192	0.1387	2706.234	2704.8472	3	363.3	23.80%	12
K.ENSYDINVMMTSLLTNLVER.C	4.97	0.5711	2343.932	2343.6636	1	1222.2	36.80%	3
K.ENSYDINVMMTSLLTNLVER.C	5.6362	0.652	2344.648	2343.6636	1	1754	63.20%	7
D.INVMMTSLLTNLVER.C	5.1692	0.6459	1735.618	1735.1063	1	3117.7	85.70%	1
I.NVM#M#T*SLLTNLVER.C	2.9521	0.0112	1733.999	1733.9268	2	1128.7	48.70%	1
M.MTSLLTNLVER.C	3.1791	0.6439	1277.456	1277.5164	1	899.1	85.00%	1
T.SLLTNLVER.C	2.8489	0.2481	1045.457	1045.2148	1	822.7	81.20%	1
S.LLTNLVER.C	2.1147	0.4175	956.84	958.13727	1	264.3	78.60%	1
L.LTNLVER.C	2.2622	0.4886	845.031	844.979	1	550.9	91.70%	1
R.CNANRKVLIAQTVK.M	2.5732	0.2184	1615.357	1615.8964	2	143.5	46.20%	1
R.KVLIAQTVK.M	2.6604	0.5223	1000.097	1000.2604	1	425.3	68.80%	3
R.KVLIAQTVK.M	3.1214	0.5653	1001.152	1000.2604	1	952.3	93.80%	11
R.KVLIAQTVKMVIPGHDVEEVPALEAITR.L	4.6568	0.3905	3058.265	3058.6284	1	1261	34.30%	2
K.VLIAQTVK.M	1.959	0.3991	871.497	872.08746	1	494	71.40%	2
K.VLIAQTVK.M	3.0367	0.5487	873.141	872.08746	1	541.4	92.90%	10
K.VLIAQTVKMVIPGHDVEEVPALEAITR.L	5.7013	0.6006	2930.933	2930.4553	1	902.9	32.70%	10
V.KMVIPGHDVEEVPALEAITR.L	3.1366	0.4852	2205.92	2205.5635	1	308.1	39.50%	2
K.MVIPGHDVEEVPALEAI.T	2.4471	0.471	1820.702	1820.0999	1	398.2	50.00%	1
K.MVIPGHDVEEVPALEAITR.L	5.7672	0.6708	2077.686	2077.3906	1	1056.8	72.20%	24
K.MVIPGHDVEEVPALEAITR.L	4.2397	0.4151	2078.161	2077.3906	1	1029	40.30%	4
K.M#VIPGHDVEEVPALEAITR.L	5.166	0.704	2094.585	2093.39	1	1362.2	75.00%	6
V.IPGHDVEEVPALEAITR.L	4.3621	0.4334	1846.764	1847.0619	1	905.1	59.40%	2
I.PGHDVEEVPALEAITR.L	4.5644	0.6342	1733.701	1733.9037	1	1792.8	76.70%	3
G.HDVEEVPALEAITR.L	3.3295	0.6213	1579.661	1579.7365	1	1218.7	80.80%	1
D.VEEVPALEAITR.L	2.9007	0.474	1327.763	1327.5087	1	927.1	77.30%	2
V.PALEAITR.L	2.3017	0.5551	870.588	871.0165	1	415.9	71.40%	6
V.PALEAITR.L	3.1386	0.561	871.189	871.0165	1	918.6	92.90%	2
R.LFVYHESQAQIVDADLD.R	2.3884	0.3612	1963.933	1964.121	1	696.6	46.90%	1
R.LFVYHESQAQIVDADLDR.E	3.869	0.4606	2120.257	2120.3074	1	1024	41.20%	1

Sequence	Xcorr	DeltCN	ObsM+H+	CalcM+H+	SpR	SpScore	Ion%	#
R.LFVYHESQAQIVDADLDR.E	6.2714	0.611	2120.543	2120.3074	1	2844.8	73.50%	45
R.LDRNKMDRMDQVDVVHALQQVMNK.A	5.2992	0.6626	2885.211	2885.3403	1	617.9	32.60%	13
R.LDRNKMDRMDQVDVVHALQQVMNK.A	3.1171	0.4408	2885.724	2885.3403	1	138.3	30.40%	2
R.LDRNKM#DRMDQVDVVHALQQVMNK.A	3.5478	0.1117	2900.455	2901.3396	1	372.1	28.30%	1
R.LDRNKMDRM#DQVDVVHALQQVMNK.A	4.1448	0.0365	2900.944	2901.3396	2	256	27.20%	2
R.NKMDRMDQVDVV.H	2.963	0.4998	1450.152	1450.6672	1	377.7	68.20%	1
R.NKMDRMDQVDVVHALQQVMNK.A	7.5706	0.6787	2500.709	2500.9077	1	3966.2	51.20%	53
R.NKMDRMDQVDVVHALQQVMNK.A	5.912	0.7065	2501.646	2500.9077	1	1223.7	62.50%	36
R.NKMDRM#DQVDVVHALQQVMNK.A	6.0235	0.023	2516.042	2516.9072	2	1757.8	43.80%	17
R.NKMDRM#DQVDVVHALQQVMNK.A	3.4779	0.0793	2516.158	2516.9072	1	304.7	40.00%	3
R.NKM#DRMDQVDVVHALQQVMNK.A	5.8151	0.0239	2516.369	2516.9072	1	2011	47.50%	3
R.NKMDRMDQVDVVHALQQVM#NK.A	2.839	0.0441	2516.461	2516.9072	1	226.3	37.50%	1
R.NKMDRMDQVDVVHALQQVM#NK.A	5.8184	0.3475	2516.473	2516.9072	1	1193.4	41.20%	5
R.NKM#DRMDQVDVVHALQQVMNK.A	3.5798	0.0635	2516.915	2516.9072	1	233.1	37.50%	8
R.NKMDRM#DQVDVVHALQQVM#NK.A	3.7305	0.0123	2532.619	2532.9065	2	434.6	33.80%	1
R.NKM#DRM#DQVDVVHALQQVMNK.A	3.7103	0.0813	2533.143	2532.9065	13	204.4	27.50%	2
R.NKM#DRMDQVDVVHALQQVM#NK.A	5.1349	0.083	2534.258	2532.9065	1	718	41.20%	3
R.NKM#DRM#DQVDVVHALQQVM#NK.A	3.7014	0.3984	2550.039	2548.906	1	658.3	41.20%	1
K.MDRMDQVDVVHALQQVMNK.A	5.8903	0.6515	2258.632	2258.6318	1	2423.1	75.00%	23
K.MDRMDQVDVVHALQQVMNK.A	7.1262	0.6497	2260.007	2258.6318	1	3285.9	52.80%	22
R.MDQVDVVHALQQVMNK.A	4.7351	0.5815	1856.313	1856.1605	1	602.6	56.70%	4
R.MDQVDVVHALQQVMNK.A	4.857	0.5425	1856.33	1856.1605	1	1521.3	53.30%	6
R.MDQVDVVHALQQVMNK.A	5.6003	0.65	1857.081	1856.1605	1	1632.6	73.30%	16
R.MDQVDVVHALQQVM#NK.A	4.7048	0.647	1872.375	1872.1599	1	933.1	70.00%	7
R.M#DQVDVVHALQQVMNK.A	4.7733	0.6037	1872.521	1872.1599	1	1359.7	76.70%	5
R.MDQVDVVHALQQVM#NK.A	3.9015	0.433	1873.062	1872.1599	1	1109	43.30%	1
M.DQVDVVHALQQVMNK.A	3.4462	0.5191	1725.521	1724.9634	1	519.3	53.60%	1
D.VVHALQQVMNK.A	3.2429	0.5663	1267.164	1267.5264	1	1134.9	85.00%	4
S.AHMEGS*VIAS*YHALLVGFVLQQNEDHLDEVR.K	5.3021	0.4655	3639.054	3639.827	1	1571.7	22.10%	6
K.HLPGKNFQNMISQLK.R	3.5969	0.4893	1756.318	1756.0654	1	302.8	57.10%	2
L.PGKNFQNMISQLKR.L	2.2787	0.2085	1660.613	1661.9537	1	262	50.00%	1
K.NFQNMISQLK.R	1.9473	0.2102	1222.559	1223.4272	1	422.4	72.20%	1
K.NFQNMISQLK.R	3.3898	0.3644	1224.279	1223.4272	1	1492.4	83.30%	1
K.NFQNMISQLKR.L	4.2793	0.5434	1380.403	1379.6135	1	1269	85.00%	12

Sequence	Xcorr	DeltCN	ObsM+H+	CalcM+H+	SpR	SpScore	Ion%	#
K.NFQNM#ISQLKR.L	3.4724	0.4092	1395.273	1395.6129	1	326.2	75.00%	12
N.M#IS*QLKRLYDFT*K.A	2.2401	0.1759	1820.213	1819.9342	2	292.2	33.30%	1
K.RLYDFTK.A	2.3446	0.5993	943.192	943.0811	1	683.2	100.00%	4
K.RLYDFTKATMAK.R	2.7192	0.1304	1446.038	1445.7119	2	407.6	68.20%	2
R.LYDFTK.A	2.1261	0.4615	786.956	786.8948	1	522.7	80.00%	4
R.LYDFTKATMAK.R	3.3562	0.5776	1289.216	1289.5255	1	997	80.00%	11
R.LYDFTKATMAK.R	2.7809	0.4973	1289.481	1289.5255	1	592.3	70.00%	4
R.LYDFTKATM#AK.R	2.728	0.5677	1305.516	1305.5249	1	499.5	75.00%	1
R.LYDFTKATMAKR.V	3.6881	0.6745	1446.448	1445.7119	1	933.3	77.30%	11
K.RVESNSGFR.A	3.2659	0.574	1053.403	1052.1261	1	667.4	87.50%	10
K.RVESNSGFRAIER.V	2.9193	0.3975	1521.554	1521.6635	1	165	54.20%	12
R.VESNSGFRAIER.V	2.2727	0.3376	1365.545	1365.477	11	139.8	50.00%	1
R.VIEYLER.L	2.3016	0.4906	922.191	922.06024	1	275.8	75.00%	13
R.VIEYLER.L	3.1424	0.5267	922.995	922.06024	1	474.4	91.70%	13

Table 5 List of phosphorylated amino acids identified by mass spectrometry following purification of WAPL-1 from wildtype *C. elegans* lysate. An amino acid followed by 79.9663 denotes phosphorylation. A methionine followed by 15.9994 denotes oxidation of methionine. These numbers correspond to the mass change of the amino acid due to the post-translational modification.

Sequence	Xcorr	Delt CN	Conf %	Obs M+H+	Calc M+H+	PPM	Prob Score	pI	Ion%	#
R.FQATLAQQGIEDDQLPSVR.S	7.14	0.59	100%	2117.5	2116.1	199.5	11.12	4.14	90%	48
R.FQATLAQQGIEDDQLPSVR.S	4.50	0.39	100%	2117.4	2116.1	139.4	8.18	4.14	79%	44
R.RMEDSAIDPSR.G	2.91	0.14	99%	1276.6	1276.6	29.5	5.32	4.72	83%	3
R.MEDSAIDPSR.G	3.63	0.48	100%	1121.2	1120.5	-307.3	7.97	4.14	94%	22
R.M(15.9949)EDSAIDPSR.G	3.69	0.44	100%	1136.8	1136.5	285.0	9.31	4.14	94%	7
R.GFDYDPAGER.T	1.98	0.28	100%	1126.4	1126.5	-79.9	6.40	4.14	79%	5
R.GFDYDPAGER.T	3.46	0.52	100%	1128.0	1126.5	-420.2	10.58	4.14	94%	50
R.TTAPVQK.K	1.60	0.19	98%	744.4	744.4	-6.8	4.11	9.08	100%	24
R.TTAPVQK.K	1.97	0.22	98%	745.2	744.4	-289.4	5.44	9.08	100%	26
K.KKDEIDMGGAK.F	3.41	0.49	100%	1192.4	1191.6	-213.4	7.39	6.56	94%	11
K.KKDEIDM(15.9949)GGAK.F	2.97	0.40	100%	1207.9	1207.6	260.0	6.36	6.56	94%	3
K.KDEIDM(15.9949)GGAK.F	2.29	0.36	100%	1080.0	1079.5	452.8	6.24	4.72	75%	5
K.DEIDMGGAK.F	1.86	0.40	100%	935.4	935.4	-36.2	6.43	4.14	100%	1
K.DEIDMGGAK.F	1.95	0.07	84%	936.1	935.4	-325.3	4.45	4.14	93%	3
K.DEIDM(15.9949)GGAK.F	1.13	0.45	100%	951.4	951.4	11.8	6.92	4.14	92%	1
K.DEIDM(15.9949)GGAK.F	2.20	0.13	95%	952.0	951.4	-419.5	5.34	4.14	100%	2
K.KHVY(79.9663)T(79.9663)HKWT(79.9663)TEEDDEDEKTISSSSNR.Y	3.10	0.42	100%	3364.0	3362.3	-104.0	6.80	5.17	29%	1

Sequence	Xcorr	Delt CN	Conf %	Obs M+H+	Calc M+H+	PPM	Prob Score	pI	Ion%	#
K.HVYTHK.W	1.56	0.15	95%	784.5	784.4	51.0	4.43	8.8	100%	5
K.HVYTHK.W	1.39	0.15	76%	785.0	784.4	-561.4	4.42	8.8	90%	5
K.WTTEEDDEDEK.T	4.20	0.45	100%	1397.0	1396.5	310.8	7.06	3.69	94%	4
K.WTTEEDDEDEKTISSSSNR.Y	5.84	0.48	100%	2229.3	2228.9	175.0	11.43	4.03	77%	4
K.WTTEEDDEDEKTISSSSNR.Y	2.05	0.25	66%	2229.2	2228.9	118.0	4.55	4.03	40%	1
K.TISSSSNR.Y	1.55	0.32	100%	851.4	851.4	21.4	5.82	10.06	82%	8
K.TISSSSNR.Y	2.22	0.27	100%	851.8	851.4	435.5	6.62	10.06	92%	18
R.YSSRPNQPAVSAR.P	1.06	0.12	52%	1432.8	1432.7	21.6	3.69	10.88	46%	1
R.YSSRPNQPAVSAR.P	4.01	0.49	100%	1433.0	1432.7	156.1	8.04	10.88	77%	105
R.YSSRPNQPAVSAR.P	2.90	0.25	99%	1433.6	1432.7	-88.6	5.41	10.88	51%	48
R.PNQPAVSAR.P	3.06	0.36	100%	939.7	939.5	246.9	7.70	10.06	100%	16
R.PNQPAVSARPR.Q	1.48	0.16	77%	1193.5	1192.7	-104.9	4.31	12	59%	1
R.QPVYATTSTYSK.P	3.08	0.45	100%	1346.5	1345.7	-99.6	8.97	8.64	85%	12
K.PLASGYGSR.V	2.43	0.33	100%	907.4	907.5	-58.7	6.77	9.08	100%	3
K.PLASGYGSR.V	3.26	0.38	100%	908.2	907.5	-323.5	9.91	9.08	93%	36
K.EANELR.E	1.44	0.07	71%	731.4	731.4	98.1	2.80	4.46	100%	25
K.EANELR.E	1.44	0.02	60%	731.9	731.4	-681.6	2.60	4.46	90%	11
R.ESGEYDDFK.Q	2.13	0.47	100%	1090.7	1089.4	212.9	6.79	3.96	79%	3
K.QDLVYILSSLQSSDASMK.V	5.09	0.56	100%	1985.5	1985.0	233.3	10.96	4.46	79%	8
K.QDLVYILSSLQSSDASM(15.9949)K.V	6.32	0.58	100%	2001.6	2001.0	-217.4	11.49	4.46	100%	6
K.QDLVYILSSLQSSDASM(15.9949)K.V	2.64	0.28	96%	2001.5	2001.0	245.3	5.57	4.46	42%	2
K.CLSAISLAK.K	1.79	0.31	100%	962.4	962.5	-139.1	4.80	8.26	85%	5
K.CLSAISLAK.K	2.97	0.31	100%	962.9	962.5	393.4	6.32	8.26	88%	7
K.KCVSPDFR.Q	2.52	0.42	100%	1009.0	1008.5	-459.6	6.15	8.26	100%	81
K.KCVSPDFR.Q	1.37	0.16	12%	1009.8	1008.5	266.4	3.41	8.26	55%	1
K.CVSPDFR.Q	2.26	0.20	99%	880.7	880.4	379.9	5.74	6.56	100%	8
K.SENMTK.S	1.73	0.03	76%	709.3	709.3	-12.0	5.23	6.56	100%	2
K.SENMTK.S	1.93	0.05	88%	709.7	709.3	555.5	4.61	6.56	100%	2
R.DFNSIK.I	1.56	0.20	97%	723.3	723.4	-92.9	5.59	6.56	100%	10
R.DFNSIK.I	1.56	0.11	79%	724.1	723.4	-356.0	3.50	6.56	90%	3
K.IDFPSLR.L	1.01	0.02	26%	847.5	847.5	62.3	2.86	6.56	67%	1
K.IDFPSLR.L	2.12	0.29	100%	848.0	847.5	-516.3	4.98	6.56	100%	25
R.LVSQLLR.I	1.71	0.16	97%	829.5	828.5	7.8	3.84	10.06	100%	26
R.LVSQLLR.I	2.41	0.16	99%	829.2	828.5	-362.7	4.82	10.06	100%	40
K.FEQRPEDK.D	1.37	0.11	72%	1048.5	1048.5	-15.0	4.41	4.72	80%	1
K.FEQRPEDK.D	2.22	0.13	96%	1048.6	1048.5	102.0	5.20	4.72	75%	3
K.FEQRPEDK.D	1.80	0.16	41%	1049.0	1048.5	476.4	3.76	4.72	71%	1
K.FEQRPEDKDK.V	2.72	0.16	99%	1293.2	1291.6	-357.0	3.98	4.89	88%	4

Sequence	Xcorr	Delt CN	Conf %	Obs M+H+	Calc M+H+	PPM	Prob Score	pI	Ion%	#
K.FEQRPEDKDK.V	1.98	0.23	71%	1292.6	1291.6	3.4	3.99	4.89	79%	2
K.VVNM(15.9949)VWEVFNSYIEK.Q	3.12	0.16	99%	1874.3	1872.9	186.4	5.72	4.46	33%	2
K.QEVGGQK.V	1.61	0.08	78%	745.3	745.4	-58.8	3.48	6.56	80%	2
K.VSFDMR.K	1.42	0.22	98%	754.4	754.4	46.1	4.75	6.56	100%	3
K.VSFDMR.K	1.79	0.30	99%	754.8	754.4	526.7	6.37	6.56	100%	26
K.VSFDM(15.9949)R.K	1.81	0.36	100%	771.1	770.4	-390.1	6.57	6.56	89%	39
R.SVNDDNLK.S	1.81	0.27	100%	904.5	904.4	14.4	4.61	4.46	100%	5
R.SVNDDNLK.S	2.25	0.12	96%	904.9	904.4	525.7	5.27	4.46	100%	8
R.ILESSSVFHK.K	1.73	0.17	97%	1146.7	1146.6	30.2	4.70	7.33	93%	8
R.ILESSSVFHK.K	3.05	0.22	100%	1147.2	1146.6	-371.3	6.18	7.33	100%	119
R.ILESSSVFHK.K	1.97	0.13	40%	1147.6	1146.6	23.3	4.10	7.33	67%	14
K.NQAFLISHR.S	3.56	0.31	100%	1085.9	1085.6	246.4	7.04	10.06	100%	93
K.NQAFLISHR.S	2.22	0.20	83%	1088.0	1085.6	380.2	5.06	10.06	72%	4
R.SNILISSLAK.F	2.75	0.29	100%	1046.6	1045.6	-46.4	5.85	9.08	100%	24
R.SNILISSLAK.F	3.37	0.39	100%	1046.1	1045.6	427.9	7.29	9.08	100%	63
R.S(79.9663)NILISSLAK.F	1.07	0.02	36%	1127.6	1125.6	-40.3	2.85	9.08	31%	1
K.FLQVILDR.V	2.06	0.09	94%	1003.8	1003.6	185.8	5.94	6.56	73%	6
K.FLQVILDR.V	3.39	0.18	100%	1005.1	1003.6	-485.0	5.17	6.56	100%	36
R.VHQLAEEEVK.K	2.98	0.52	100%	1182.4	1181.6	-225.6	8.85	4.72	94%	10
R.VHQLAEEEVKK.Y	4.30	0.57	100%	1310.2	1309.7	-382.9	10.37	5.8	100%	27
R.VHQLAEEEVKK.Y	3.20	0.43	100%	1310.6	1309.7	-60.2	6.93	5.8	93%	4
K.YISCLALM(15.9949)CR.L	2.43	0.46	100%	1304.2	1302.6	-348.3	7.89	8.04	73%	6
R.LLINISHDNELCCSK.L	3.02	0.43	100%	1817.3	1815.9	251.3	7.29	5.63	40%	1
K.ENSYDINVMM(15.9949)TSLLTNLVER.C	3.75	0.60	100%	2359.3	2358.1	49.9	11.86	4.14	50%	3
K.ENSYDINVM(15.9949)M(15.9949)TSLLTNLVER.C	6.60	0.65	100%	2375.5	2374.1	161.2	12.52	4.14	93%	10
K.ENSYDINVM(15.9949)M(15.9949)TSLLTNLVER.C	3.55	0.42	100%	2375.5	2374.1	149.7	7.42	4.14	43%	2
R.KVLIAQTVK.M	3.05	0.26	100%	1000.2	999.7	-446.6	6.11	10.04	100%	113
R.KVLIAQTVK.M	2.18	0.16	72%	1000.5	999.7	-133.9	4.44	10.04	67%	1
K.VLIAQTVK.M	1.85	0.30	100%	871.6	871.6	-12.7	4.90	9.08	100%	12
K.VLIAQTVK.M	2.77	0.28	100%	872.1	871.6	-540.9	6.00	9.08	100%	27
R.LDRNKMDRM(15.9949)DQVDVVHALQQVM(15.9949)NK.A	1.46	0.14	12%	2912.5	2915.4	-1000.2	3.09	7.33	22%	1
R.MDQVDVVHALQQVM(15.9949)NK.A	2.11	0.07	82%	1870.3	1870.9	-311.3	3.76	5.63	46%	1
R.M(15.9949)DQVDVVHALQQVM(15.9949)NK.A	5.50	0.55	100%	1887.7	1886.9	-106.1	10.49	5.63	92%	65
R.M(15.9949)DQVDVVHALQQVM(15.9949)NK.A	4.60	0.56	100%	1887.5	1886.9	-216.0	8.64	5.63	80%	13
K.NFQNMISQLK.R	1.33	0.13	75%	1222.6	1222.6	-61.2	3.70	9.08	50%	1
K.NFQNMISQLK.R	3.74	0.23	100%	1225.1	1222.6	376.4	5.34	9.08	88%	51

Sequence	Xcorr	Delt CN	Conf %	Obs M+H+	Calc M+H+	PPM	Prob Score	pI	Ion%	#
K.NFQNM(15.9949)ISQLK.R	1.08	0.18	71%	1238.5	1238.6	-80.5	3.51	9.08	50%	1
K.NFQNM(15.9949)ISQLK.R	3.86	0.26	100%	1238.6	1238.6	-21.8	6.59	9.08	100%	65
K.RLYDFTK.A	2.26	0.16	98%	942.5	942.5	-12.3	3.95	8.8	75%	7
R.LYDFTK.A	1.81	0.03	80%	786.4	786.4	-4.0	4.19	6.56	100%	12
R.LYDFTK.A	1.15	0.02	41%	786.7	786.4	342.6	3.65	6.56	90%	4
K.RVESNSGFR.A	1.59	0.21	98%	1051.5	1051.5	-26.6	5.23	10.06	58%	4
K.RVESNSGFR.A	3.74	0.41	100%	1051.5	1051.5	4.5	8.15	10.06	100%	57
R.VESNSGFR.A	1.90	0.19	98%	895.4	895.4	-41.1	4.70	6.56	82%	4
R.VESNSGFR.A	2.86	0.47	100%	896.3	895.4	-198.0	9.05	6.56	100%	9
R.VIEYLERLE.-	2.09	0.35	100%	1163.5	1163.6	-86.4	5.60	4.14	82%	7
R.VIEYLERLE.-	4.06	0.43	100%	1164.3	1163.6	-310.3	8.09	4.14	100%	17
R.FQATLAQQGIEDDQLPSVR.S	7.49	0.61	100%	2117.5	2116.1	190.0	11.27	4.14	93%	31
R.FQATLAQQGIEDDQLPSVR.S	4.58	0.48	100%	2118.8	2116.1	-142.3	9.60	4.14	85%	13
R.FQAT(79.9663)LAQQGIEDDQLPSVR.S	2.11	0.31	97%	2198.8	2196.0	-132.2	5.75	4.14	39%	1
R.RMEDSAIDPSR.G	2.71	0.14	96%	1277.1	1276.6	358.5	6.17	4.72	94%	2
R.M(15.9949)EDSAIDPSR.G	3.61	0.46	100%	1137.1	1136.5	-351.2	8.59	4.14	100%	1
R.GFDYDPAGER.T	3.02	0.57	100%	1127.8	1126.5	274.3	10.02	4.14	94%	18
R.TTAPVQK.K	1.48	0.07	63%	744.4	744.4	-33.6	3.15	9.08	89%	1
R.TTAPVQK.K	1.66	0.15	76%	744.5	744.4	64.0	3.97	9.08	91%	1
K.KKKDEIDM(15.9949)GGAK.F	3.21	0.39	100%	1335.6	1335.7	-105.5	7.10	8.7	90%	1
K.KKDEIDM(15.9949)GGAK.F	2.97	0.40	100%	1207.8	1207.6	144.1	6.64	6.56	100%	1
K.TISSSSNR.Y	1.79	0.37	100%	851.5	851.4	56.6	6.11	10.06	82%	5
K.TISSSSNR.Y	2.00	0.37	100%	851.8	851.4	412.0	6.58	10.06	100%	4
R.YSSRPNQPAVSAR.P	3.98	0.29	100%	1433.4	1432.7	-251.0	7.21	10.88	82%	54
R.QPVYATTSTYSK.P	2.78	0.56	100%	1347.2	1345.7	-354.4	8.93	8.64	75%	7
R.QPVYATTSTYSKPLASGYGSR.V	3.77	0.31	100%	2234.9	2234.1	-80.3	5.66	9.53	53%	10
R.QPVYATTSTYSKPLASGYGSR.V	2.54	0.25	78%	2234.3	2234.1	101.5	4.19	9.53	50%	1
K.PLASGYGSR.V	2.62	0.35	100%	908.5	907.5	36.8	7.31	9.08	100%	13
K.PLASGYGSR.V	3.31	0.36	100%	907.6	907.5	164.8	8.77	9.08	100%	18
K.EANELR.E	1.82	0.11	91%	732.4	731.4	79.8	3.35	4.46	100%	2
K.QDLVYILSSLQSSDASMK.V	5.79	0.63	100%	1987.2	1985.0	109.0	11.65	4.46	67%	1
K.QDLVYILSSLQSSDASM(15.9949)K.V	4.36	0.53	100%	2000.8	2001.0	-115.9	10.34	4.46	90%	1
K.KCVSPDFR.Q	2.08	0.36	100%	1008.2	1008.5	-310.6	6.15	8.26	83%	1
K.KCVSPDFR.Q	2.34	0.27	100%	1008.4	1008.5	-139.2	5.58	8.26	85%	8
K.SENMTK.S	1.82	0.11	91%	710.3	709.3	-73.0	4.62	6.56	100%	2
R.DFNSIK.I	1.54	0.19	93%	723.3	723.4	-92.9	4.71	6.56	100%	3
K.IDFPSLR.L	1.06	0.05	20%	849.5	847.5	54.2	3.65	6.56	100%	1
K.IDFPSLR.L	2.24	0.31	100%	849.0	847.5	-519.7	5.54	6.56	100%	17

Sequence	Xcorr	Delt CN	Conf %	Obs M+H+	Calc M+H+	PPM	Prob Score	pI	Ion%	#
R.LVSQLLR.I	1.85	0.15	95%	829.4	828.5	-112.7	4.14	10.06	100%	41
R.LVSQLLR.I	2.57	0.17	99%	830.1	828.5	-535.1	4.39	10.06	100%	45
K.FEQRPEDKDK.V	2.48	0.13	93%	1292.1	1291.6	344.5	3.88	4.89	81%	4
K.QEVGGQK.V	1.36	0.06	43%	745.3	745.4	-152.7	2.78	6.56	80%	1
K.VSFDMR.K	1.70	0.29	98%	755.3	754.4	-37.8	5.35	6.56	86%	8
K.VSFDMR.K	1.86	0.32	99%	754.7	754.4	500.2	5.96	6.56	100%	1
K.VSFDM(15.9949)R.K	1.43	0.15	62%	771.2	770.4	-234.4	3.87	6.56	78%	1
R.SVNDDNLK.S	1.89	0.29	98%	904.4	904.4	-7.8	4.51	4.46	91%	2
R.SVNDDNLK.S	2.04	0.07	78%	905.0	904.4	-494.6	4.07	4.46	85%	1
K.IETNVNLIADNADDTYSILILNR.C	3.60	0.32	100%	2590.9	2590.3	-152.0	5.02	3.96	45%	1
R.ILESSSVFHK.K	2.33	0.14	93%	1147.6	1146.6	-59.8	4.71	7.33	79%	36
R.ILESSSVFHK.K	3.53	0.22	100%	1148.4	1146.6	-182.3	5.59	7.33	100%	260
R.ILESSSVFHK.K	1.86	0.26	48%	1147.6	1146.6	-55.2	4.16	7.33	56%	1
K.NQAFLISHR.S	1.59	0.20	91%	1087.2	1085.6	-342.0	4.65	10.06	46%	1
K.NQAFLISHR.S	2.67	0.25	100%	1087.6	1085.6	-35.9	4.83	10.06	73%	27
R.SNILISSLAK.F	2.61	0.24	100%	1046.6	1045.6	-27.2	5.22	9.08	93%	23
R.SNILISSLAK.F	3.51	0.45	100%	1046.5	1045.6	-110.6	7.52	9.08	100%	109
K.FLQVILDR.V	2.41	0.12	92%	1003.6	1003.6	36.4	5.90	6.56	100%	8
K.FLQVILDR.V	3.39	0.18	100%	1005.2	1003.6	-405.4	5.35	6.56	100%	41
K.YISCLALMCR.L	2.64	0.31	100%	1288.8	1286.6	124.7	6.38	8.04	75%	1
R.LLINISHDNELCCSK.L	2.95	0.43	100%	1815.8	1815.9	-66.2	7.66	5.63	57%	6
K.ENSYDINVMM(15.9949)TSLLTNLVER.C	6.22	0.68	100%	2359.6	2358.1	202.5	13.22	4.14	93%	2
K.ENSYDINVMM(15.9949)TSLLTNLVER.C	2.39	0.23	51%	2358.3	2358.1	82.2	5.08	4.14	38%	1
K.ENSYDINVM(15.9949)M(15.9949)TSLLTNLVER.C	5.29	0.58	100%	2376.6	2374.1	193.4	11.71	4.14	71%	8
K.ENSYDINVM(15.9949)M(15.9949)TSLLTNLVER.C	4.66	0.54	100%	2375.4	2374.1	99.2	8.15	4.14	58%	2
R.KVLIAQTVK.M	2.52	0.16	97%	1000.5	999.7	-126.6	5.56	10.04	86%	41
R.KVLIAQT(79.9663)VKMVIPGHDVEEVPALEAITR.L	2.22	0.25	42%	3139.4	3136.7	-82.3	4.20	5.74	27%	2
R.KVLIAQT(79.9663)VKM(15.9949)VIPGHDVEEVPALEAITR.L	2.34	0.14	10%	3155.1	3152.7	130.0	3.80	5.74	23%	1
K.VLIAQTVK.M	2.06	0.26	98%	872.5	871.6	-73.9	4.92	9.08	100%	28
K.VLIAQTVK.M	3.07	0.20	100%	873.7	871.6	143.0	5.68	9.08	100%	15
K.MVIPGHDVEEVPALEAITR.L	2.26	0.24	95%	2075.8	2076.1	-118.8	5.72	4.4	50%	3
K.M(15.9949)VIPGHDVEEVPALEAITR.L	4.66	0.54	100%	2093.3	2092.1	102.8	9.44	4.4	71%	20
K.M(15.9949)VIPGHDVEEVPALEAITR.L	2.25	0.17	21%	2092.6	2092.1	-206.5	3.16	4.4	33%	1
R.LFVYHESQAQIVDADLDR.E	7.55	0.56	100%	2120.6	2119.0	-197.7	10.50	4.4	93%	43
R.LFVYHESQAQIVDADLDR.E	3.79	0.39	100%	2120.3	2119.0	121.0	5.94	4.4	53%	8
R.MDQVDVVHALQQVM(15.9949)NK.A	4.80	0.46	100%	1871.4	1870.9	255.3	8.47	5.63	84%	17

Sequence	Xcorr	Delt CN	Conf %	Obs M+H+	Calc M+H+	PPM	Prob Score	pI	Ion%	#
R.M(15.9949)DQVDVVHALQQVM(15.9949)NK.A	6.18	0.57	100%	1888.2	1886.9	158.7	9.94	5.63	81%	75
R.M(15.9949)DQVDVVHALQQVM(15.9949)NK.A	4.88	0.48	100%	1887.6	1886.9	-168.3	8.03	5.63	76%	15
K.NFQNMISQLK.R	3.26	0.22	100%	1223.5	1222.6	-145.7	5.02	9.08	100%	5
K.NFQNMISQLK.R	3.99	0.29	100%	1225.3	1222.6	-295.6	5.40	9.08	94%	71
K.NFQNM(15.9949)ISQLK.R	1.72	0.09	76%	1238.9	1238.6	185.8	3.60	9.08	64%	2
K.NFQNM(15.9949)ISQLK.R	3.90	0.26	100%	1240.1	1238.6	346.5	6.35	9.08	94%	45
R.LYDFTK.A	1.72	0.06	80%	786.3	786.4	-131.3	3.97	6.56	100%	2
K.RVESNSGFR.A	3.72	0.40	100%	1051.6	1051.5	61.6	8.08	10.06	100%	27
R.VESNSGFR.A	2.29	0.43	100%	896.4	895.4	-33.6	6.79	6.56	91%	4
R.VESNSGFR.A	3.02	0.47	100%	897.0	895.4	-513.7	7.85	6.56	100%	8
R.VIEYLERLE.-	3.34	0.29	100%	1164.5	1163.6	-97.9	6.05	4.14	100%	8
R.VIEYLERLE.-	4.01	0.44	100%	1164.2	1163.6	-361.8	8.28	4.14	100%	13
K.RFQATLAQQGIEDDQLPSVR.S	4.02	0.35	100%	2273.3	2272.2	35.8	5.66	4.72	68%	2
R.FQATLAQQGIEDDQLPSVR.S	7.09	0.57	100%	2117.1	2116.1	-8.3	10.81	4.14	87%	9
R.FQATLAQQGIEDDQLPSVR.S	4.46	0.46	100%	2117.2	2116.1	68.5	9.10	4.14	89%	3
R.RMEDSAIDPSR.G	2.25	0.03	61%	1277.5	1276.6	-98.3	4.79	4.72	72%	2
R.RM(15.9949)EDSAIDPSR.G	1.65	0.32	85%	1292.5	1292.6	-75.2	5.35	4.72	72%	3
R.MEDSAIDPSR.G	2.29	0.21	88%	1122.0	1120.5	-437.2	5.17	4.14	71%	4
R.MEDSAIDPSR.G	3.11	0.48	100%	1121.0	1120.5	-432.2	8.16	4.14	94%	1
R.M(15.9949)EDSAIDPSR.G	3.48	0.46	100%	1137.2	1136.5	-298.5	8.79	4.14	100%	2
R.GFDYDPAGER.T	1.52	0.34	88%	1126.2	1126.5	-257.5	5.58	4.14	62%	2
R.GFDYDPAGER.T	3.28	0.54	100%	1127.6	1126.5	114.7	10.85	4.14	100%	6
R.TTAPVQK.K	1.45	0.13	56%	744.4	744.4	-100.9	3.84	9.08	89%	1
R.TTAPVQK.K	1.88	0.21	85%	744.9	744.4	627.8	5.31	9.08	73%	2
R.TTAPVQKK.K	1.86	0.10	64%	872.6	872.5	60.4	3.38	10.04	85%	1
K.KKKDEIDMGGAK.F	4.14	0.32	100%	1321.4	1319.7	-267.0	6.54	8.7	95%	2
K.KKDEIDMGGAK.F	3.31	0.45	100%	1193.2	1191.6	-350.1	7.56	6.56	100%	3
K.KKDEIDM(15.9949)GGAK.F	3.32	0.44	100%	1208.0	1207.6	342.8	6.08	6.56	89%	1
K.KDEIDMGGAK.F	2.11	0.25	92%	1063.3	1063.5	-184.4	4.99	4.72	100%	1
K.DEIDMGGAK.F	2.20	0.32	100%	935.7	935.4	252.4	5.99	4.14	100%	1
K.HVYTHK.W	1.00	0.02	14%	784.7	784.4	344.0	2.95	8.8	57%	1
R.YSSRPNQPAVSAR.P	3.47	0.38	100%	1434.2	1432.7	334.9	7.50	10.88	73%	8
R.PNQPAVSAR.P	2.21	0.23	93%	939.3	939.5	-178.8	5.00	10.06	80%	1
R.QPVYATTSTYSKPLASGYGSR.V	4.32	0.64	100%	2235.1	2234.1	-8.6	11.42	9.53	58%	3
R.QPVYATTSTYSKPLASGYGSR.V	3.43	0.46	100%	2235.3	2234.1	95.5	7.14	9.53	48%	1
K.PLASGYGSR.V	1.94	0.06	58%	907.2	907.5	-342.3	2.78	9.08	93%	1
K.EANELR.E	1.71	0.12	63%	732.4	731.4	52.4	2.94	4.46	100%	5
R.ESGEYDDFKQDLVYILSSLQSSDASM(15.9949)K.V	3.65	0.24	95%	3072.3	3071.4	-26.6	6.36	4.12	35%	2

Sequence	Xcorr	Delt CN	Conf %	Obs M+H+	Calc M+H+	PPM	Prob Score	pI	Ion%	#
K.KCVSPDFR.Q	1.85	0.22	83%	1009.1	1008.5	-420.0	4.09	8.26	85%	3
K.SENMTK.S	1.33	0.14	52%	711.0	709.3	-429.2	3.70	6.56	100%	1
R.DFNSIK.I	1.84	0.20	82%	724.3	723.4	-97.4	5.28	6.56	100%	1
K.IDFPSLR.L	1.85	0.30	94%	848.0	847.5	-587.1	5.30	6.56	82%	2
R.LVSQLLR.I	1.71	0.09	57%	828.6	828.5	48.1	3.91	10.06	89%	3
R.LVSQLLR.I	1.90	0.18	82%	828.5	828.5	-93.5	4.40	10.06	100%	2
K.VSFDMR.K	1.25	0.14	42%	754.4	754.4	46.1	3.86	6.56	86%	2
K.VSFDMR.K	1.78	0.29	93%	754.7	754.4	500.2	7.33	6.56	100%	2
R.SVNDDNLK.S	1.79	0.27	85%	903.9	904.4	-616.2	4.98	4.46	91%	2
K.IETNVNLIADNADDTYSILILNR.C	4.59	0.47	100%	2591.1	2590.3	-79.7	8.78	3.96	83%	3
K.IETNVNLIADNADDTYSILILNR.C	2.47	0.34	95%	2591.2	2590.3	-59.3	4.91	3.96	39%	2
R.ILESSSVFHK.K	3.18	0.22	99%	1147.1	1146.6	416.2	6.03	7.33	100%	15
R.ILESSSVFHK.K	2.10	0.17	21%	1147.8	1146.6	127.9	4.08	7.33	89%	1
K.NQAFLISHR.S	3.59	0.34	100%	1086.1	1085.6	-419.6	7.80	10.06	100%	21
K.NQAFLISHR.S	2.43	0.25	89%	1087.2	1085.6	-364.6	5.11	10.06	84%	2
R.SNILISSLAK.F	2.16	0.20	83%	1045.5	1045.6	-91.0	4.99	9.08	100%	2
R.SNILISSLAK.F	2.96	0.40	100%	1045.8	1045.6	122.0	7.63	9.08	94%	15
K.FLQVILDR.V	2.47	0.10	76%	1003.7	1003.6	86.2	6.04	6.56	100%	4
K.FLQVILDR.V	3.15	0.21	100%	1004.1	1003.6	477.2	5.59	6.56	100%	15
R.VHQLAEEEVKK.Y	4.25	0.44	100%	1312.2	1309.7	346.7	8.08	5.8	100%	1
K.ENSYDINVMM(15.9949)TSLLTNLVER.C	6.61	0.64	100%	2359.5	2358.1	151.6	13.87	4.14	89%	3
K.ENSYDINVM(15.9949)M(15.9949)TSLLTNLVER.C	5.73	0.61	100%	2375.4	2374.1	93.9	11.10	4.14	89%	3
K.ENSYDINVM(15.9949)M(15.9949)TSLLTNLVER.C	3.80	0.34	100%	2375.3	2374.1	86.6	6.49	4.14	38%	3
R.KVLIAQTVK.M	2.89	0.18	98%	999.7	999.7	-3.4	6.99	10.04	100%	14
R.KVLIAQT(79.9663)VKMVIPGHDVEEVPALEAITR.L	2.37	0.24	46%	3137.2	3136.7	-140.8	4.59	5.74	28%	1
R.KVLIAQT(79.9663)VKM(15.9949)VIPGHDVEEVPALEAITR.L	2.32	0.27	57%	3155.3	3152.7	-112.0	4.80	5.74	24%	1
K.VLIAQTVK.M	1.45	0.17	60%	871.6	871.6	21.7	3.61	9.08	100%	2
K.VLIAQTVK.M	2.83	0.29	100%	872.0	871.6	495.0	6.07	9.08	100%	3
K.M(15.9949)VIPGHDVEEVPALEAITR.L	6.35	0.61	100%	2093.6	2092.1	227.0	10.60	4.4	77%	5
R.LFVYHESQAQIVDADLDR.E	6.87	0.56	100%	2121.0	2119.0	-28.0	10.15	4.4	83%	5
R.LFVYHESQAQIVDADLDR.E	3.78	0.35	100%	2119.2	2119.0	56.7	5.56	4.4	65%	2
R.M(15.9949)DQVDVVHALQQVM(15.9949)NK.A	5.17	0.57	100%	1888.2	1886.9	126.9	10.39	5.63	88%	1
K.NFQNMISQLK.R	3.26	0.30	100%	1222.8	1222.6	104.5	6.47	9.08	94%	8
K.NFQNM(15.9949)ISQLK.R	3.56	0.22	100%	1239.3	1238.6	-266.6	5.81	9.08	94%	3
K.NFQNM(15.9949)ISQLKR.L	3.34	0.22	100%	1395.8	1394.7	63.4	5.58	10.99	78%	10
R.LYDFTK.A	1.91	0.03	42%	787.3	786.4	-186.1	4.21	6.56	100%	1

Sequence	Xcorr	Delt CN	Conf %	Obs M+H+	Calc M+H+	PPM	Prob Score	pI	Ion%	#
K.RVESNSGFR.A	3.54	0.38	100%	1051.5	1051.5	4.5	7.28	10.06	100%	4
R.VESNSGFR.A	1.76	0.11	60%	896.2	895.4	-309.6	5.02	6.56	92%	1
R.VIEYLERLE.-	2.03	0.15	76%	1163.5	1163.6	-103.7	4.47	4.14	92%	2
R.VIEYLERLE.-	3.82	0.46	100%	1163.7	1163.6	19.0	7.70	4.14	100%	5
R.FQATLAQQGIEDDQLPSVR.S	6.77	0.56	100%	2116.9	2116.1	-83.8	10.92	4.14	83%	5
R.FQATLAQQGIEDDQLPSVR.S	3.37	0.33	100%	2116.1	2116.1	18.2	6.58	4.14	66%	2
R.RMEDSAIDPSR.G	3.11	0.05	95%	1278.3	1276.6	-226.0	5.75	4.72	94%	5
R.RM(15.9949)EDSAIDPSR.G	1.89	0.17	78%	1294.0	1292.6	308.7	4.03	4.72	78%	3
R.MEDSAIDPSR.G	2.14	0.46	100%	1120.2	1120.5	-235.6	7.05	4.14	86%	3
R.MEDSAIDPSR.G	3.63	0.26	99%	1123.0	1120.5	420.5	6.18	4.14	88%	16
R.M(15.9949)EDSAIDPSR.G	3.24	0.45	99%	1137.0	1136.5	-421.7	7.40	4.14	100%	2
R.GFDYDPAGER.T	2.11	0.46	100%	1127.4	1126.5	-38.5	7.70	4.14	93%	3
R.GFDYDPAGER.T	3.34	0.60	100%	1127.9	1126.5	327.5	9.78	4.14	100%	1
R.TTAPVQK.K	1.68	0.17	95%	744.5	744.4	114.1	3.33	9.08	89%	7
R.TTAPVQK.K	1.90	0.27	95%	744.9	744.4	-665.4	5.42	9.08	82%	3
K.KKKDEIDM(15.9949)GGAK.F	1.69	0.21	75%	1336.4	1335.7	-227.7	5.48	8.7	42%	1
K.KKDEIDMGGAK.F	2.79	0.39	99%	1191.4	1191.6	-210.8	7.03	6.56	94%	2
K.KKDEIDM(15.9949)GGAK.F	2.81	0.31	99%	1209.1	1207.6	-407.5	5.73	6.56	83%	3
K.DEIDMGGAK.F	2.17	0.42	100%	935.3	935.4	-89.7	7.83	4.14	92%	3
K.FFPKQEK.K	1.54	0.06	53%	923.0	923.5	-548.0	3.78	8.8	75%	2
K.TISSSSNR.Y	1.57	0.27	98%	851.2	851.4	-260.5	4.44	10.06	91%	2
K.TISSSSNR.Y	1.76	0.19	81%	851.7	851.4	365.1	4.33	10.06	75%	1
R.YSSRPNQPAVSAR.P	3.83	0.39	99%	1433.1	1432.7	239.8	7.88	10.88	73%	108
R.YSSRPNQPAVSAR.P	2.27	0.09	25%	1433.1	1432.7	276.6	4.00	10.88	66%	5
R.YSSRPNQPAVSARPR.Q	1.77	0.04	52%	1685.9	1685.9	5.7	3.99	11.72	44%	1
R.YSSRPNQPAVSARPR.Q	3.54	0.27	100%	1687.4	1685.9	289.8	5.40	11.72	62%	1
R.PNQPAVSAR.P	2.76	0.19	98%	939.7	939.5	204.4	7.81	10.06	100%	2
R.QPVYATTSTYSK.P	2.31	0.32	98%	1346.9	1345.7	167.7	6.43	8.64	60%	2
R.QPVYATTSTYSKPLASGYGSR.V	5.16	0.64	100%	2234.5	2234.1	162.9	12.44	9.53	55%	15
R.QPVYATTSTYSKPLASGYGSR.V	2.29	0.11	22%	2234.8	2234.1	-119.3	3.54	9.53	42%	2
K.PLASGYGSR.V	1.94	0.32	100%	907.5	907.5	-14.5	6.21	9.08	85%	3
K.PLASGYGSR.V	3.32	0.37	99%	907.7	907.5	230.8	8.65	9.08	100%	8
K.EANELR.E	1.45	0.09	79%	731.3	731.4	-79.6	2.80	4.46	100%	2
R.ESGEYDDFK.Q	2.46	0.31	100%	1090.4	1089.4	-46.3	6.50	3.96	82%	2
K.KCVSPDFR.Q	2.31	0.32	98%	1008.9	1008.5	396.1	5.13	8.26	92%	15
K.KCVSPDFRQFIKS(79.9663)ENMTKS(79.9663)IVK.A	2.49	0.19	58%	2801.5	2802.3	-273.5	4.34	9.6	32%	1
K.SENMTK.S	1.78	0.01	88%	709.3	709.3	-82.4	5.57	6.56	100%	2
K.SENMTK.S	2.26	0.06	91%	709.8	709.3	640.0	4.65	6.56	100%	2

Sequence	Xcorr	Delt CN	Conf %	Obs M+H+	Calc M+H+	PPM	Prob Score	pI	Ion%	#
R.DFNSIK.I	1.80	0.22	100%	724.3	723.4	-69.8	4.68	6.56	100%	7
K.IDFPSLR.L	1.96	0.24	94%	847.8	847.5	431.1	5.47	6.56	100%	15
R.LVSQLLR.I	1.73	0.11	91%	829.6	828.5	56.1	3.44	10.06	100%	20
R.LVSQLLR.I	2.61	0.19	98%	829.1	828.5	-483.4	4.44	10.06	100%	32
R.IEKFEQRPEDKDK.V	4.37	0.25	99%	1663.5	1661.8	-242.4	5.44	5.02	90%	2
K.FEQRPEDK.D	1.51	0.12	81%	1048.8	1048.5	280.6	3.51	4.72	80%	2
K.FEQRPEDK.D	2.09	0.09	82%	1050.4	1048.5	-133.1	3.96	4.72	100%	2
K.FEQRPEDKDK.V	2.53	0.16	95%	1292.0	1291.6	267.1	3.94	4.89	88%	8
K.VVNMVWEVFNSYIEK.Q	1.92	0.17	76%	1857.0	1856.9	57.9	4.23	4.46	52%	1
K.VVNM(15.9949)VWEVFNSYIEK.Q	5.28	0.40	100%	1874.5	1872.9	-242.2	7.75	4.46	64%	6
K.VSFDMR.K	1.59	0.24	99%	755.3	754.4	-24.6	5.07	6.56	100%	4
K.VSFDMR.K	1.80	0.31	96%	754.7	754.4	394.2	6.54	6.56	100%	2
K.VSFDM(15.9949)R.K	1.76	0.35	97%	770.7	770.4	470.4	7.39	6.56	100%	10
R.SVNDDNLK.S	1.85	0.12	94%	906.4	904.4	-15.1	3.82	4.46	80%	4
R.SVNDDNLK.S	2.20	0.10	87%	904.8	904.4	437.3	5.02	4.46	92%	1
K.SELLNLGILQFVVAK.I	1.56	0.09	50%	1644.6	1644.0	-257.6	3.39	6.56	42%	1
K.IETNVNLIADNADDTYSILILNR.C	1.13	0.11	38%	2590.0	2590.3	-148.0	3.59	3.96	26%	1
K.IETNVNLIADNADDTYSILILNR.C	3.29	0.31	100%	2591.1	2590.3	-105.7	5.83	3.96	44%	9
R.ILESSSVFHK.K	2.23	0.13	99%	1146.5	1146.6	-91.9	4.72	7.33	93%	4
R.ILESSSVFHK.K	3.42	0.26	99%	1148.2	1146.6	-391.3	5.29	7.33	94%	218
K.NQAFLISHR.S	3.30	0.28	100%	1085.6	1085.6	-4.7	5.69	10.06	100%	12
K.NQAFLISHR.S	3.61	0.32	99%	1085.5	1085.6	-48.2	7.12	10.06	93%	173
K.NQAFLISHR.S	2.93	0.31	100%	1086.7	1085.6	116.9	5.61	10.06	92%	4
R.SNILISSLAK.F	2.43	0.29	100%	1045.4	1045.6	-253.6	5.62	9.08	100%	9
R.SNILISSLAK.F	3.76	0.39	99%	1048.1	1045.6	439.8	6.86	9.08	94%	79
K.FLQVILDR.V	2.71	0.12	100%	1003.6	1003.6	-3.5	6.40	6.56	100%	14
K.FLQVILDR.V	3.49	0.26	99%	1003.5	1003.6	-80.5	5.05	6.56	100%	116
R.VHQLAEEEVK.K	3.34	0.56	100%	1181.9	1181.6	200.2	10.72	4.72	100%	4
R.VHQLAEEEVKK.Y	3.40	0.34	100%	1310.6	1309.7	-64.4	6.03	5.8	94%	4
R.VHQLAEEEVKK.Y	4.43	0.47	100%	1311.3	1309.7	-308.9	8.61	5.8	100%	28
K.YISCLALMCR.L	2.68	0.29	99%	1286.3	1286.6	-243.0	6.44	8.04	88%	2
K.YISCLALM(15.9949)CR.L	1.40	0.15	54%	1303.6	1302.6	22.3	3.82	8.04	75%	1
R.LLINISHDNELCCSK.L	4.93	0.50	100%	1817.3	1815.9	207.2	8.78	5.63	71%	27
K.LGQIEGFLPNAITTFTYLAPK.F	3.49	0.36	99%	2296.9	2294.2	-165.6	6.20	6.56	45%	3
K.ENSYDINVMM(15.9949)TSLLTNLVER.C	6.40	0.62	100%	2359.8	2358.1	-129.5	11.79	4.14	86%	8
K.ENSYDINVM(15.9949)MTSLLTNLVER.C	4.12	0.54	100%	2359.0	2358.1	-77.3	9.30	4.14	71%	2
K.ENSYDINVM(15.9949)MTSLLTNLVER.C	4.28	0.39	100%	2360.0	2358.1	-56.3	6.94	4.14	47%	1

Sequence	Xcorr	Delt CN	Conf %	Obs M+H+	Calc M+H+	PPM	Prob Score	pI	Ion%	#
K.ENSYDINVMM(15.9949)TSLLTNLVER.C	3.73	0.43	100%	2358.6	2358.1	196.7	6.70	4.14	59%	2
K.ENSYDINVM(15.9949)M(15.9949)TSLLTNLVER.C	6.88	0.67	100%	2374.0	2374.1	-56.4	11.98	4.14	96%	10
K.ENSYDINVM(15.9949)M(15.9949)TSLLTNLVER.C	4.72	0.39	100%	2374.3	2374.1	92.2	9.02	4.14	54%	4
R.KVLIAQTVK.M	2.65	0.42	100%	1000.5	999.7	-119.4	7.47	10.04	83%	9
R.KVLIAQTVK.M	3.26	0.36	99%	1001.2	999.7	-449.5	6.41	10.04	100%	75
R.KVLIAQT(79.9663)VKMVIPGHDVEEVPALEAITR.L	2.97	0.29	96%	3139.3	3136.7	-111.0	4.97	5.74	31%	28
K.VLIAQTVK.M	1.75	0.20	98%	870.8	871.6	-885.5	4.25	9.08	100%	7
K.VLIAQTVK.M	2.83	0.28	99%	871.9	871.6	380.3	5.74	9.08	100%	7
K.MVIPGHDVEEVPALEAITR.L	2.61	0.45	99%	2076.8	2076.1	-120.3	7.32	4.4	44%	4
K.MVIPGHDVEEVPALEAITR.L	2.16	0.06	11%	2078.7	2076.1	-189.5	3.10	4.4	50%	1
K.M(15.9949)VIPGHDVEEVPALEAITR.L	5.92	0.59	100%	2093.4	2092.1	141.0	11.05	4.4	93%	54
K.M(15.9949)VIPGHDVEEVPALEAITR.L	3.24	0.37	100%	2094.7	2092.1	-176.1	6.07	4.4	57%	45
R.LFVYHESQAQIVDADLDR.E	6.08	0.54	100%	2120.0	2119.0	-7.6	9.82	4.4	86%	10
R.MDQVDVVHALQQVM(15.9949)NK.A	5.84	0.48	100%	1871.7	1870.9	-141.9	9.76	5.63	88%	55
R.MDQVDVVHALQQVM(15.9949)NK.A	4.00	0.49	100%	1872.7	1870.9	-94.1	8.63	5.63	67%	4
R.M(15.9949)DQVDVVHALQQVM(15.9949)NK.A	5.25	0.54	100%	1888.3	1886.9	211.6	9.94	5.63	85%	52
R.M(15.9949)DQVDVVHALQQVM(15.9949)NK.A	3.63	0.32	100%	1888.0	1886.9	70.1	6.67	5.63	63%	8
K.NFQNMISQLK.R	2.91	0.28	100%	1222.3	1222.6	-257.6	4.85	9.08	86%	4
K.NFQNMISQLK.R	3.95	0.29	99%	1224.1	1222.6	379.5	5.84	9.08	94%	98
K.NFQNM(15.9949)ISQLK.R	3.82	0.20	99%	1239.1	1238.6	349.4	5.75	9.08	94%	47
K.NFQNMISQLKR.L	2.26	0.03	73%	1380.3	1378.7	-304.2	3.01	10.99	59%	1
K.NFQNM(15.9949)ISQLKR.L	3.93	0.28	99%	1396.3	1394.7	-282.7	6.08	10.99	89%	16
K.RLYDFTK.A	1.33	0.23	89%	942.5	942.5	6.0	5.61	8.8	100%	2
K.RLYDFTK.A	2.21	0.29	98%	942.4	942.5	-118.5	6.11	8.8	92%	19
R.LYDFTK.A	1.64	0.03	83%	786.2	786.4	-233.0	4.35	6.56	100%	2
K.RVESNSGFR.A	3.66	0.41	99%	1051.5	1051.5	-14.5	7.65	10.06	100%	37
R.VESNSGFR.A	2.40	0.48	100%	895.4	895.4	-63.5	7.11	6.56	100%	8
R.VESNSGFR.A	2.83	0.49	99%	896.9	895.4	493.5	8.84	6.56	100%	8
R.VIEYLERLE.-	2.99	0.23	100%	1164.4	1163.6	-192.3	5.65	4.14	92%	4
R.VIEYLERLE.-	3.97	0.44	100%	1164.2	1163.6	-361.8	8.07	4.14	100%	80